Coating Engineering of Composite Materials for Organic Field-Effect Transistors

by

Freddy G Del Pozo León

Doctoral Thesis
PhD programme in Materials Science
Physics Department

Directors

Marta Mas-Torrent and Concepció Rovira
Institut de Ciència de Materials de Barcelona

Tutor

Dolors Baró
Physics Department,Universitat Autònoma de Barcelona

October 2014

Memória presentada per aspirar al Grau de Doctor per:

Freddy G Del Pozo León

Vist i plau,

Els directors:

Marta Mas-Torrent	Concepció Rovira
Research Scientist	Research Professor

a Bellaterra, September 23, 2014

DECLARATION

I hereby declare that the work carried out in this Doctoral Thesis has not been previously submitted for any degree and is no currently being submitted in candidature for any other degree.

Signed ....
Freddy G Del Pozo León
Candidate

The work of this Doctoral Thesis was carried out by the candidate at the Institut de Ciéncia de Materials de Barcelona under our supervision. Also, we certify that we have read this Doctoral Thesis and that, in our opinion, it is fully adequate in scope and quality as a Doctoral Thesis for the degree of Doctor of Philosophy.

Signed ....
Marta Mas-Torrent
Research Scientist
Institut de Ciència de Materials de Barcelona

Signed ....
Concepció Rovira
Research Professor
Institut de Ciència de Materials de Barcelona

Signed ....
Dolors Baró
Professor - Applied Physics
Universitat Autònoma de Barcelona

Nothing in life is to be feared. It is only to be understood.

Marie Curie

Only those who will risk going too far can possibly find out how far one can go.

T.S. Eliot

Success comes from knowing that you did your best to become the best that you are capable of becoming.

John Wooden

ACKNOWLEDGMENTS

I would like to first thank Marta Mas-Torrent for being an exceptional advisor. Definitely, I am lucky to have her as an advisor and a mentor. Under her guidance I understood how to pursue a well-developed and well-documented research agenda, conduct independent research, but more importantly, she is an understanding teacher, great scientist with a kind caring demeanor. Always thankful to Dr Imma Ratera who made everything possible by making the right connections at the right time. After connections were made, I deeply thank Prof. Jaume Veciana and Prof. Concepció Rovira for accepting me to be a member of the Molecular Nanoscience and Organic Materials (NANOMOL) Family at Institut de Ciencia de Materials de Barcelona (ICMAB). Also like to thank to everybody for all the help given. I like to thank deeply Dr. Raphael Pfattner, postdoctoral fellow, who have taught me a lot about the field of organic electronics, and all the intricacies of the daily life in a lab, as well as about being a good researcher. His kindness and patient teaching helped me understand how to plan all experiments, also always setting the bar high while programming in MATLAB was required. I like to extend my deepest appreciation and thankfulness to Prof. Magnus Berggren for accepting my internship at his lab, that time was highly productive and rewarding. Also, I like to thank Dr. Simone Fabiano, postdoctoral fellow at Linköping University, who help me out from day one through my last day at Norrköping, his kindness and patience in teaching definitely help me out to better understand fundamental concepts and to plan experiments well and efficiently. His eagerness to get experiments well done and on time despite his own duties at the lab will be always appreciated. Thank you very much Simone. Additionally, I like to thank all the LOE members at Linköping for all the help given. Here I like to thank all my family. My gratitude and admiration to both of my parents Estuardo and Martha, for all their work as parents. A thought experiment, if one works during the time that takes to go

through the entire universe is not enough to pay for everything they gave me. But I like to say **Thank you** Dad and Mom for everything. Huge appreciation and love to my whole family: Carlos, Carla, Nicolas, and Emily. Marcelo, Anita, Andrea, and Daniela, Daisy and Alejandro. I like to ∞-thank my brother-in-law Marcelo Fabricio Villafuerte for his support and his trust on me to ask his father Marcelo Villafuerte to sign the scholarship guarantee that finally impelled this 4 year adventure. To both my aunts Ketty and Carmita for all your support during this time. Always thankful to a great man my uncle Gustavo and his wife Maggie, both helped me out during my time at USA, without you this will not exist, I thank you both for everything you did actually you adopted me for a while, thank you. Thank you very much uncle for all the time, and for everything you gave me, I learned a lot from you. My gratitude also goes to Franklyn Leon my cousin for all the wonderful time that he made me live, from that small concert down in NY to a big show upstate NY, a time that I really cherish with all my heart, also I like to thank Alex Leon for being nice to me and caring when I really needed - thank you. To my wife Dayana for her understanding and support during this entire process. Finally, I like to thank Hari, Paramatma, Allah, Ahuramazda, God, Yezdan, and Hu for the life given.

Research funded by:

senescyt
Secretaría Nacional de Educación Superior, Ciencia, Tecnología e Innovación

NANOMOL
CENTRE OF NANOTECHNOLOGY
AND MOLECULAR MATERIALS

ciber-bbn
Centro Investigación Biomédica en Red
Bioingeniería, Biomateriales y Nanomedicina

Contents

List of Figures

List of Tables

List of Abbreviations

Abbreviations

OE Organic Electronics

TFT Thin-Film Transistor

OLAE Organic Large Area Electronics

OLED Organic Light Emitting Diode

OFET Organic Field-Effect Transistor

SC Single Crystal

SC-OFETs Single crystal organic field-effect transistors

OTFT Organic Thin-Film Transistor

OSC Organic Semiconductor

LEFET Light Emitting Field-Effect Transistor

RFID Radio Frequency Identification

OPV Organic Photovoltaic

HOMO Highest Occupied Molecular Orbital

LUMO Lowest Unoccupied Molecular Orbital

$\boldsymbol{\rho}$ electrical resistivity [Ωm], [Ωcm]

$\boldsymbol{\sigma}$ electrical conductivity [S/m], [S/cm]

λ_{reorg} reorganization energy [eV]

J transfer integral [eV]

IRS Ion-Radical Salt

CTC Charge Transfer Complex

MTR Multiple Trapping and Release

DOS Density Of States

DFT Density Functional Theory

VRH Variable Range Hopping

FET Field-Effect Transistor

MOSFET Metal-Oxide-Semiconductor Field-Effect-Transistor

$\mathbf{E}_a$ activation energy of the conductivity [eV]

$\mathbf{E}_F$ Fermi energy [eV]

Φ work function [eV]

$\mathbf{I}_{SD}$ source-drain current [A], [nA], [μA]

$\mathbf{I}_{SD}^{sat}$ source-drain current at the saturation regime [A], [nA], [μA]

$\mathbf{I}_{SD}^{lin}$ source-drain current at the linear regime [A], [nA], [μA]

$\mathbf{V}_{SD}$ source-drain voltage [V]

$\mathbf{V}_{SG}$ source-gate voltage [V]

$\mathbf{I}_{SG}$ source-gate current [A]

μ_{FE} field-effect mobility [$^{cm^2}/_{Vs}$]

$\mathbf{V}_{TH}$ threshold voltage [V]

$\mathbf{V}_{SO}$ switch-on voltage [V]

$\mathbf{I}_{OFF}$ off-current [A], [nA]

$\mathbf{I}_{ON}$ on-current [A], [nA], [μA]

$\mathbf{I}_{ON}/\mathbf{I}_{OFF}$ on/off current ratio [ ]

S Subthreshold swing

$\mathbf{C}_i$ gate-dielectric capacitance [$^{nF}/_{cm^2}$]

ϵ_r relative permittivity [ ]

BGBC Bottom-Gate Bottom-Contact

BGTC Bottom-Gate Top-Contact

$\mathbf{R}_C$ contact resistance [Ω]

$\mathbf{R}_S$ contact resistance at source [Ω]

$\mathbf{R}_D$ contact resistance at drain [Ω]

$\mathbf{R}_{CH}$ channel resistance [Ω]

TLM Transfer Line Method

MTLM Modified Transfer Line Method

POM Polarized Optical Microscopy

AFM Atomic Force Microscopy

RMS	Root mean square
SEM	Scanning Electron Microscopy
FIB-SEM	Focused Ion Beam - Scanning Electron Microscopy
EDX	Energy-Dispersive X-ray spectroscopy
XRD	X-ray diffraction
ToF-SIMS	Secondary ion mass spectroscopy with time of flight detection
EToF	Electrical Time of Flight
BAMs	Bar Assisted Meniscus Sheering
MATLAB	Matrix Laboratory
R	GNU language and environment for statistical computing and graphics

List of Compounds

Compounds

TTF tetrathiafulvalene

TTF-TCNQ tetrathiafulvalene-tetracyanoquinodimethane

DT-TTF dithiophene-tetrathiafulvalene

DB-TTF dibenzo-tetrathiafulvalene

BET-TTF bis(ethylenethio)tetrathiafulvalene

P3HT poly(3-hexylthiophene)

PTAA Poly (bis(4-phenyl) (2,4,6-trimethylphenyl)amine)

OTS n-octadecyltrichlorosilane

iPS Isotactic Polystyrene

PS280k Atactic Polystyrene

PS10000 polystyrene for GPC 10000

PS3000 polystyrene for GPC 3000

PS1000 Polystyrene for GPC 1000

PAMS Poly-(α methyl styrene)

PMMA Poly-(methyl methacrylate)

Chapter 1

A Primer in Organic Electronics

Introduction

Silicon and gallium arsenide, inorganic semiconductors, have led and fuelled the computer revolution over the past five decades. Our modern life is assisted or even controlled in every facet (i.e. healthcare, energy, entertainment, transport, communications) by devices containing semiconductors processors, memory elements, detectors, sensors, circuitry, light emitting diodes, photodiodes, etc. However, many of this high-technology essentials are deliberately designed to be obsolete a few years after purchase, with no plans of being recycled, leading to an undesired and unfortunate outcome, massive amounts of often toxic electronics waste, becoming unsustainable. Energy consumption is another issue to be addressed, since the energy expended in manufacturing just one chip processor exceeds the total energy consumed over a 3 year period in the lifespam of a modern laptop. There is no doubt that the "silicon age" had improved our daily life, but how much longer can it last, and what is next?[1].

The term "organic" was introduced in the 19th century, when it was believed that organic compounds could only be formed by living organisms[2,3]. Nowadays it is known that organic molecules can also be synthesized in a laboratory. The common characteristic of organic materials, either natural or synthetic, is that they consist of carbon atoms in combination with other elements such as hydrogen (H), nitrogen (N), sulfur (S), phosphor (P), oxygen (O) as well as halogens or metals. Within this definition there is a plethora of possible variations in organic molecules and, in fact, more than 90% of known matter is of organic nature[2,3].

The mechanical, electrical and optical properties of organic materials are attractive to the industry and have found numerous applications. In particular, some of these materials are also applicable in technologies based on semiconductors and have been topic of research since the late 1940's[2,4]. Important breakthroughs were achieved when back in 1973[5,6] the first organic metal (tetrathiafulvalene-tetracyanoquinodimethane (TTF-TCNQ)), and in 1977 the first highly conducting polymer, chemically doped polyacetylene[7–9], were discovered demonstrating that both organic molecular materials and organic conjugated polymers could be used as electrically active materials. These achievements led to a huge research interest opening a new field called Organic Electronics (OE).

Micro- and nano- electronics based on organic materials show some advantages like mechanical flexibility over traditional silicon electronics counterparts. Further, organic electronic devices have key manufacturing advantages including solution processing and large-scale fabrication at low cost. Moreover, organic devices can be made on polymeric substrates, which are suitable for flexible devices and show potential to be fabricated using roll-to-roll technologies. Also, green organic electronic devices have been thought of in the literature to create organic devices that are sustainable, biodegradable, biocompatible, bioresorbable, or even metabolizable. Organic devices have been made for applications ranging from displays to sensors. So, organic electronics in the future may help to solve the issue of the electronic waste, which has become a concern due to the high volumes in which it is generated, and the hazardous constituents it often contains (lead, mercury, and chromium)[10–13].

Imagine patterned wallpapers that can be controlled by the flick of a switch, smart drug release strips that can monitor child's temperature and give a dose of a fever relieve medication, electronic newspapers and electronic books whose contents can be downloaded upon request, but still feels like a traditional newspaper or a traditional paper-based book; perhaps interactive and smart. The core of such dream-like applications are organic molecules and polymers[12]. However, it is not only a matter of devising a new set of smart, light weight, nature-inspired gadgets; it is to design alternative electronics at low-cost with features impossible to match by traditional crystalline silicon architectures.

In 2006 a study carried out by the US marketing research institute IDTechEX, predicted that the global market of organic and printed electronics would grow economically in a period of 10 years by a factor of forty, from its 1.18 billion US dollars to 48.18 billion US dollars; therefore, due to the perspective of producing considerable revenues in the near future, organic and printed electronics had drawn the attention of money investors as well[16]. Perhaps, swapping the electronics industry interests from silicon-based electronics to organic molecules and polymers based electronics is highly influenced by thermal management and power consumption as well (Fig.1.1)[14,17–22], because if organic and printed electronics are low power consuming devices, this will result in a smaller energy bill; which may reduce the overall cost of the gadgets. In consequence, organic electronics became a rapid evolving research field, with a solid foundation in multidisciplinary

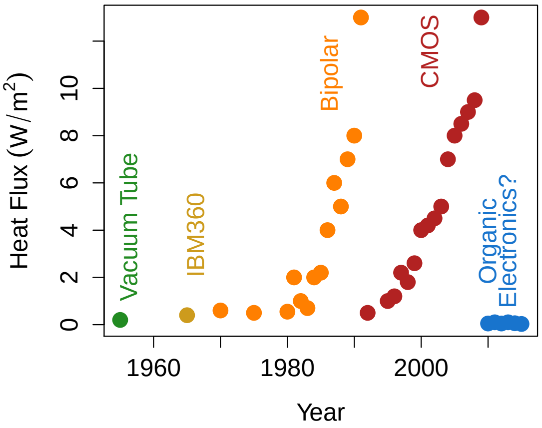

Figure 1.1 *Thermal management of electronics adapted from references*[14,15].

teams[12]. In this chapter the background and various applications of organic and printed electronics will be reviewed, as well as, the charge transport mechanisms that take place and the basics of organic field-effect transistors.

1.1 Organic Electronics

Currently, most of the electronic devices that we use in our daily life are based on inorganic materials, especially on silicon (Si). Since both the mobility of charge carriers and the conductivity in organic materials are orders of magnitude lower[23] than in their inorganic counterparts (*i.e.* Si, Ge and GaAs)[24], they will not be useful to fabricate high-speed switching devices. However, organic materials offer great potential for applications where low-cost, light weight and flexibility are required. In addition, the low temperature processability that they require compared to the techniques employed for inorganic materials[25] opens the opportunity to fabricate devices on flexible plastics. Organic materials are also compatible with solution processability, which is a very important issue, since it allows to apply simple and low-cost fabrication techniques[26] on large areas such as spin coating, ink-jet printing[27–30] or roll-to-roll printing[31]. The transfer of the outstanding properties of organic active materials to device fabrication and technology are reflected in the recent appearance of the term "OLAE" - Organic Large Area Electronics[32,33].

Organic materials have been implemented in devices, for a wide range of potential applications during the last decade. For instance, Organic Light Emitting Diodes (OLEDs)[34–37], which are, generally speaking, based on the recombination of charges (holes and electrons) to emit light, are raising great perspectives. Depending on which active material is chosen one can tune the emitted color, or even manage to obtain "white" light emitting devices[38]. Organic Field-Effect Transistors (OFETs) are a second possible application, where active Organic Semiconductors (OSCs) can be implemented leading to p (*i.e.* hole conduction) or n (*i.e.* electron conduction) device operation depending on the particular composition of the device[39–43]. Devices exhibiting ambipolar[44] characteristics (*i.e.* hole and electron conduction) have also been reported, as well as ambipolar Light Emitting Field-Effect Transistors (LEFETs)[45–48]. OFETs have a high potential to be applied in flat panel displays based on flexible matrix elements and complementary circuits[33,49–51] where large area coverage and low-cost production plays an increasing important role. There are a large number of other promising applications that OFETs can offer, such as small integrated circuits[52], Radio Frequency Identification (RFID) tags[53,54], electronic paper[49,55–57] or chemical and pressure sensing devices[58–62]. Figures 1.2(a) and 1.2(b) show digital displays devices products, which include OSCs developed by Plastic Logic[57]. A third group of devices where organic active materials can be found are organic photovoltaics (OPV), that consist in converting the electromagnetic waves emitted from the sun to an electrical current. Traditional photovoltaic devices based on silicon show high energy conversion efficiency (single crystalline Si $\eta_{c-Si} = 41.6\,\%$, poly crystalline Si $\eta_{pc-Si} = 20\,\%$ or amorphous Si $\eta_{a-Si} = 12.5\,\%$)[63], but their production is extremely costly[64]. One possible

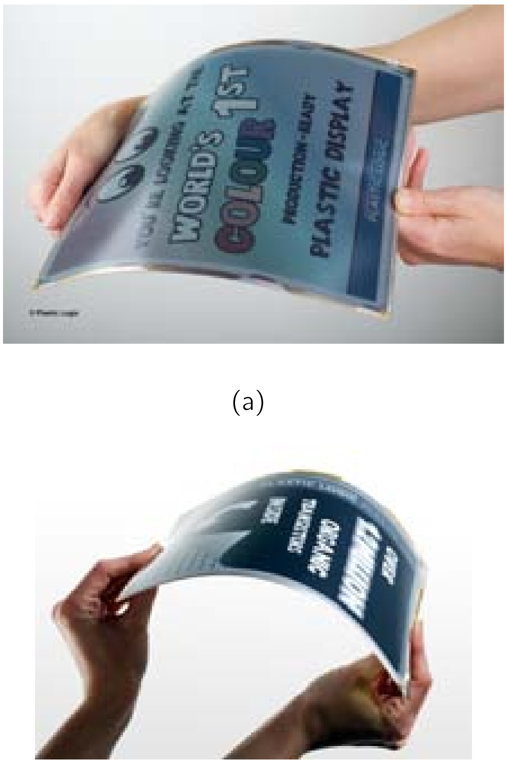

(a)

(b)

Figure 1.2 *Plastic Logic flexible displays (a) Flexible Colour Plastic Display, and (b) Flexible Monochrome Plastic Display.Images taken from PlasticLogic.com media center.*

improvement is therefore to look for low-cost materials which have lower performance, but due to their low production cost, devices covering larger areas[65] can be fabricated. However improvements in the performance is desired and subject of a current vast of research. For low-cost dye sensitized and OPV cells, efficiencies up to $\eta_{dye-sensitized} = 11.4\,\%$[66] and $\eta_{organic-cells} = 12\,\%$ were reported, respectively. Another potential application of organic active materials that have emerged are Lasers, which can either be optically or electrically pumped[67].

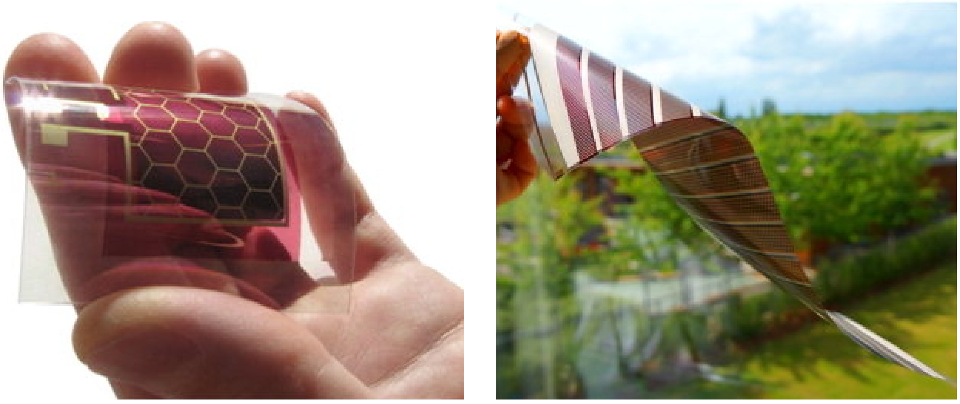

(a) (b)

Figure 1.3 *Typical pictures of flexible Organic Solar Cells. (a) screen printed Ag grid and (b) a large area highly flexible modules completely processed by vacuum-free Roll-to-Roll printing and coating. Both from reference[68].*

1.2 Charge Transport Mechanisms in Organic Semiconductors

As previously mentioned, charge carrier mobilities found in organic devices are generally by far lower compared to their inorganic counterparts, since in organic materials the intermolecular interaction forces are van der Waals forces, which means that their bonding energy is significantly lower ($E_{vdW} = 0\ 05 - 40 kJ\ mol$) compared to convalent interatomic bonds present in silicon or germanium ($E_{cov} = 150 - 1100 kJ\ mol$)[69]. Several groups have studied the transport mechanisms of both organic thin-film (amorphous and polycrystalline) as well as organic single crystal OFETs. In both these systems the charge carriers interact strongly with the molecules forming molecular polarons*. As a consequence, the charge transport in organic semiconductors is most likely associated to hopping motion of molecular polarons through the system, in contrast to in inorganic semiconductors where the transport follows the band theory due to the delocalization of the charges. However, we would like to point out here that a full, comprehensive theory to describe the charge transport completely in these systems is still lacking. Below a few widely used ideas of charge transport models are briefly discussed.

1.2.1 Band Transport in Organic Crystals

The theory for fundamental charge transport in high quality crystals is well established, where charge carriers are highly delocalized and travel in extended Bloch-waves through the periodic lattice structure[70]. The electronic structure for crystalline solids is characterized by its band structure, which is strongly related to the crystal lattice parameters. It is generally true that the periodic translation symmetry is a necessary condition for the application of band models, however it is not a sufficient condition. Another important requirement is that the interaction of the atoms or molecules sitting at the lattice sites has to be sufficiently strong[71]. For highly purified single crystals of naphtalene[72] the fundamental transport was previously ascribed to band formation. Upon decreasing temperature, an increase of both the hole and electron mobility was observed, which stays in agreement with the assumed band-like transport. At low temperatures, however, charge scattering

---

*A polaron is a quasi particle composed of a charge and its accompanying polarization field, which results in a lattice polarization and a lattice distortion.

mechanisms lead to a mobility saturation. Also, it should be highlighted that, a band-like temperature dependence of mobility, (i.e. negative temperature coefficient ($-\frac{\mu}{T} < 0$)), in solution-processed TIPS-pentacene OFETs was reported[73]. This, however, is not the general case in organic single crystals, which even though single crystals, may include a significant number of structural and chemical defects.

1.2.2 Hopping Transport

A theory involving electron transfer based on oxidation-reduction reactions was introduced by Marcus in 1956[74], assuming very little spacial overlap of the electronic orbitals of two reacting molecules, as it is the general case in solutions. The charge transport at this microscopic level can be described as involving a self-exchange electron (hole) transfer from a charged molecule to an adjacent neutral one, *i.e.* hopping of charges. According to this theory[75,76], two major parameters determine self-exchange rates and, thus, the charge carrier mobility: (i) the electronic coupling or J between adjacent molecules, which needs to be maximized, and (ii) the reorganization energy (λ_{reorg}), which needs to be small for efficient charge transport[77,78] (see also Figure 1.4). Here the reorganization energy essentially corresponds to the sum of geometry relaxation energies switching from the neutral state (1) to the charged state (2) and vice versa. This theory is also applied to describe hopping transport in solid organic semiconductors. All this elucidates the strong importance of intermolecular interactions on the efficiency of charge carrier hopping and their related mobility since they are directly related to transfer integral (J). Furthermore, it has even been shown that local intermolecular interactions can also have a strong influence on λ_{reorg}[79,80].

Thermally activated transport, which is often observed, stays in agreement with the hopping model, where the activation energy arises from the binding energy of the polaron to the molecule. Hopping is assisted by phonons, and thus the

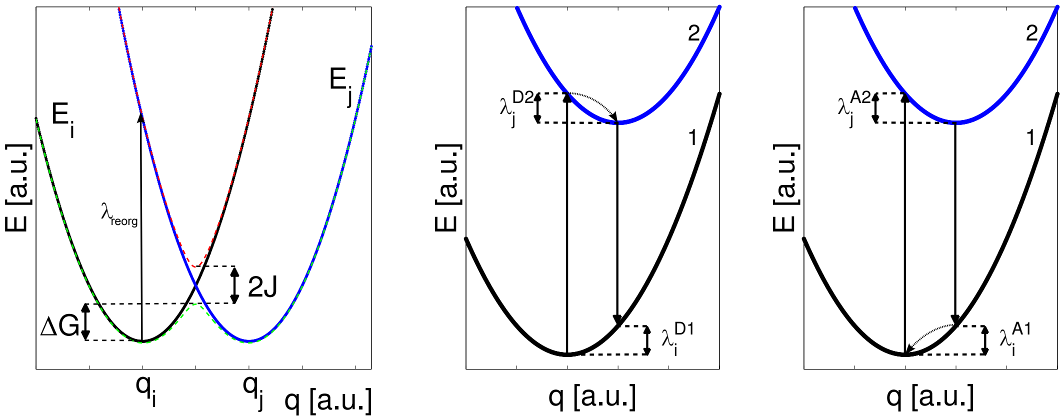

Figure 1.4 *Potential energy E of a charge transfer reaction shown with respect to generalized coordinates q. J is the transfer integral,* ΔG *the energy barrier height and* $\lambda_{reorg} = \lambda_i^{A1} + \lambda_j^{D2}$ *is the reorganization energy with neutral state (1) and charged molecule state (2).*

charge carrier mobility (μ) increases with temperature (T) following:

$$\mu = \mu_0 \, exp \left[\left(\frac{T_0}{T} \right)^{\frac{1}{\alpha}} \right] \tag{1.1}$$

where α is an integer ranging from 1 to 4, T the absolute temperature, T_0 a constant and μ_0 the trap-free mobility. It is very important to note that trapping attributed to grain boundaries and many other structural defects in polycrystalline films will significantly influence the temperature dependence of the charge carrier mobility[16,81,82].

1.2.3 Multiple Trapping and Release Model

Introduced originally to account for the low mobility of hydrogenated amorphous silicon devices[83], in the Multiple Trapping and Release (MTR) model the charge carriers are assumed to travel in narrow, delocalized bands and interact with a high concentration of localized trap levels. This model was further adapted by Horowitz et al.[84,85]. In the decentralized band the charge carriers have a band mobility μ_0, but interact further by trapping and detrapping with localized states. The trapping and release mechanisms determines thermally activated behavior and overall mobility. The trap distribution (Density Of States (DOS) within the gap) is believed to be exponentially shaped. Also, the often observed gate voltage, *i.e.* electric field, dependence of the charge carrier mobility can be described with this model. The temperature mobility dependence in highly ordered molecular crystals is still controversial, whether the electron is delocalized or localized. The model for multiple trapping and releasing (see Equation(1.2)) can better describe this phenomena rather than the model in Equation(1.1), where charge carriers transit within the delocalized levels, interacting with traps through trapping and releasing with the assistance of a phonon by thermal energy. The effective mobility μ can be related to the trap-free mobility μ_0 by

$$\mu_{eff} = \mu_0 \, \alpha \, exp\left(-\frac{E_t}{kT}\right) \tag{1.2}$$

where E_t corresponds to the trap depth (energy difference between trap level and the delocalized band) and α is the ratio of density of energy states in the delocalized band edge to the trap density.Traps inside a crystal arise mostly as a result of structural defects and impurities[16,81,82].

1.2.4 Variable Range Hopping in Disordered Systems

For the description of organic thin-films, the lack of long range order confine the application of more elaborated while elegant theories. A theory based on hopping was first introduced by Miller and Abrahams[86] based on a random-resistor network. The idea was further amplified by Mott[87] assuming that the hopping occurs around the Fermi level within a range of k$_B$T. A new perspective was introduced by the pioneering work of Bässler[88] which is based on the same idea of Miller and Abrahams, but on a Gaussian distribution of energy states (DOS). The Variable

Range Hopping (VRH) was then further developed by Vissenberg and Matters[89] using the approximation of an exponentially shaped DOS. In combination with the Fermi-Dirac occupation function the latter model describes also the thermally activated transport behavior. The basic difference here is the hopping of charge carriers between localized states in contrast to the above described model where charge carriers are activated to a transport level. The exponential DOS combined with percolation theory explains the temperature and gate field dependence of the mobility found for amorphous pentacene OFETs[90].

1.3 Organic Field Effect Transistor

Julius Lilienfield in 1930 in his patent described the idea of unipolar solid devices in which current is modulated between two electrodes by an electric field generated from a third electrode. Johan Bardeen, William Schockley and Walter Brattain invented the three-terminal germanium transistor that successfully demonstrated large current gain, field-effect transistors (FETs)[91]. The metal-oxide-semiconductor capacitor using organic semiconductors was demonstrated by Ebisawa et all in 1982, using polyacetylene as semiconductor on a polysiloxane gate dielectric. The next significant milestone was consolidated by Tsumura et al in 1986 by the development of the first organic field effect transistor with recognizable current gain by an in-situ polymerized polythiophene[92].

A field-effect transistor is a device with three terminals, in which a channel is constructed between two contacts, namely source and drain. In an OFET such channel is formed inside an organic material, more precisely, inside an organic semiconductor. The current in the channel is modulated by the third terminal (the gate) by a voltage that generates an electric field through the dielectric, which is sandwiched between the gate and the semiconductor[42].

There are different architectures of OFETs, the most common are depicted in Figure 1.5. The architecture called Bottom-Gate Bottom-Contact (BGBC, see Figure 1.5(a)) is one of the most widely used, in which on the gate electrode the dielectric is deposited, and on top contacts are constructed; and on top of the previous structure the active material (semiconductor) is deposited.Alternatively, in the bottom-gate top contact (BGBC) configuration (Figure 1.5(b)) the source and drain electrodes are deposited on top of the organic semiconductor.

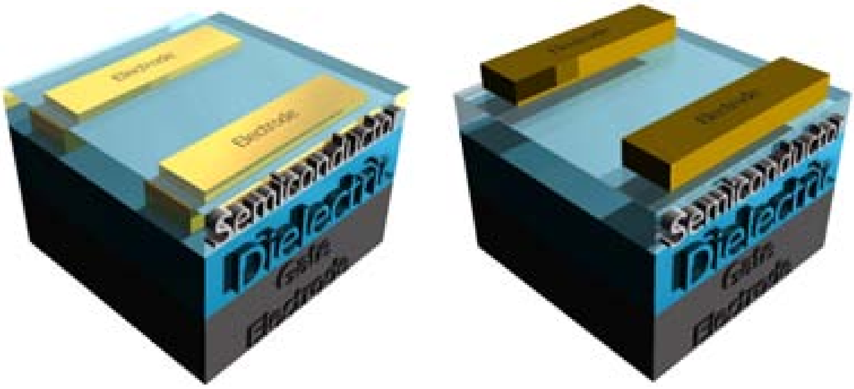

(a) (b)

Figure 1.5 *(a) Bottom-Gate Bottom-Contact (BGBC) and (b) Bottom-Gate Top-Contact (BGTC) architectures of an OFET.*

1.3.1 Operation Principle and Main Device Characteristics

To discuss the operation principle of an OFET a very simplified electronic energy level diagram is shown in Figure 1.6(a), which reflects the HOMO and the LUMO of an OSC relative to the Fermi levels of the source and drain contacts[93]. Since there is no V_{SG} applied in this case, there are no mobile charges, and in an ideal device there will be no charge transport upon applying a V_{SD}. Now considering a p-channel active material, where holes are the majority charge carriers, accumulation of holes at the very semiconductor/insulator interface is then produced by applying a negative V_{SG}. Due to the negative V_{SG} the HOMO/LUMO energy levels shift upwards in energy, so the HOMO becomes resonant with the Fermi energy (E_F) of the injecting source electrode, which remains fixed as its potential is externally controlled, and holes accumulate at the OSC/dielectric interface. Upon applying a negative V_{SD}, holes start to move from source to drain. Contrary, for n-type transport, a positive V_{SG} has to be applied to reach the resonance of the LUMO with E_F. Thus, one can easily see that the matching of the E_F of the source and drain electrodes with the HOMO (p-channel) or LUMO (n-channel) is a crucial issue to obtain efficient carrier injection in high performing devices.

This very simplified description visualizes the basic mechanisms of charge transport in OFETs. To study real devices in a quantitative way, however, the model is by far too simple, and one has to take into account additional effects such as charge trapping which can be caused by chemical or structural defects in the OSC, at the dielectric/OSC interface or within the dielectric layer. Also this model neglects the effect of band bending[96], which appears in metal/semiconductor junctions where the E_F (*i.e.* the work function (Φ) of the metal) differs from the energy levels of the semiconductor. As one may expect, all OSCs can potentially behave both as p- and n-channel materials (ambipolar) depending on the polarity of the gate. This is in principle true, although typically poor HOMO-HOMO overlap for hole conduction or LUMO-LUMO overlap for n-channel operation, as well as high injection barriers at the contacts for either p- or n-channel operation tend to give unipolar devices[44,97,98].

To describe the current voltage characteristics of an OFET mathematically, Horowitz et al.[99] developed a simple comprehensive model taking some assumptions and hence it can be, applied only to particular cases and inside its validity. First of all, the charge carrier mobility is assumed to be constant[99], while it has been shown for many OFETs that this may not be the general case[84,100], since the

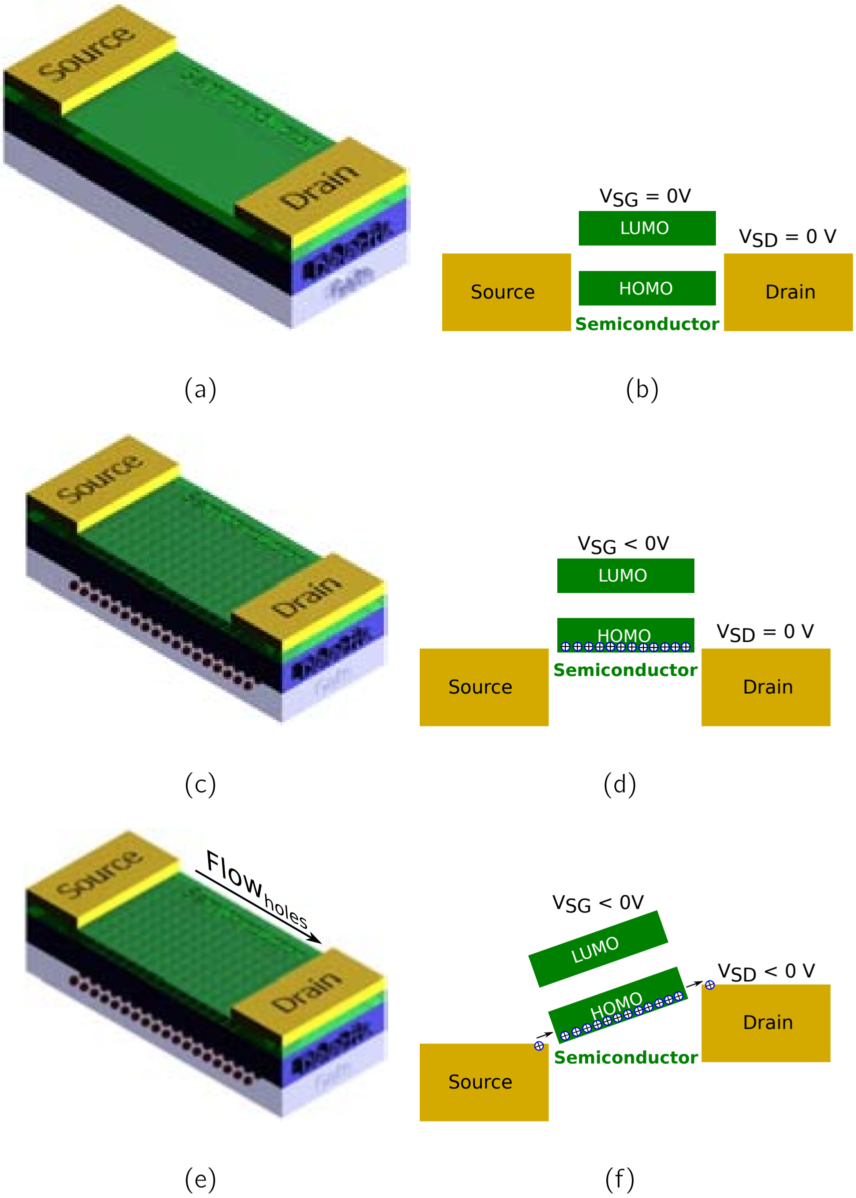

Figure 1.6 *Schematic showing p-channel operation of an OFET. (a) and (b)Ideal device in off-state, no V_{SD} and no V_{SG} applied. (c) and (d) shift of the HOMO-LUMO, due to negative V_{SG} and accumulation of holes near the OSC/insulator interface. (e) and (f) hole transport upon applying a negative V_{SD}. (a), (c), and (e) adapted from Reference*[94]*. (b), (d), and (f) adapted from References*[94,95]

field-effect mobility (μ_{FE}) does in fact often depend on the applied electric field. Secondly, parasitic contact resistances are not taken into account in this model[99]. Also, the gradual channel approximation ($|\frac{\partial E_x}{\partial x}| << |\frac{\partial E_y}{\partial y}|$) is assumed as well, which suggests that the electric field perpendicular to the channel is significantly higher than the electric field parallel to the channel. This assumption is fulfilled only for devices with long channels and thin dielectrics. In this model the OFET operates in two distinct regimes. In the so called linear regime, $V_{SD} << V_{SG} - V_{TH}$, the source-drain current at the linear regime (I_{SD}^{lin}) increases linearly with V_{SD} and the following relation can be derived:

$$I_{SD}^{lin} = \frac{W}{L}\mu_{FE}C_i\left[(V_{SG} - V_{TH})V_{SD} - \frac{{V_{SD}}^2}{2}\right] \tag{1.3}$$

where I_{SD}^{lin} is the source-drain current in the linear regime; W, L the channel width and length, respectively; μ_{FE} is the field-effect mobility; C_i the gate capacitance per unit area; V_{SG} and V_{TH} are the source-gate and threshold voltage, respectively, and V_{SD} the source-drain voltage.
In the so called saturation regime, $V_{SD} >> V_{SG} - V_{TH}$, I_{SD}^{lin} starts to saturate at a point where the channel is pinched-off and one can derive:

$$I_{SD}^{sat} = \frac{W}{2L}\mu_{FE}C_i(V_{SG} - V_{TH})^2 \tag{1.4}$$

with I_{SD}^{sat} source-drain current in the saturation regime.

In an OFET basically two different device characteristics are measured. The output characteristics are obtained when the I_{SD}^{lin} is measured sweeping the source-drain voltage at constant gate voltages. Further, the transfer characteristics, are obtained when I_{SD}^{lin} is measured as function of the source-gate voltage at constant V_{SD}. Figure 1.7(b) shows the simulated device characteristics for a p-type device.

Following, the most important OFET parameters that determine the device performance are described.

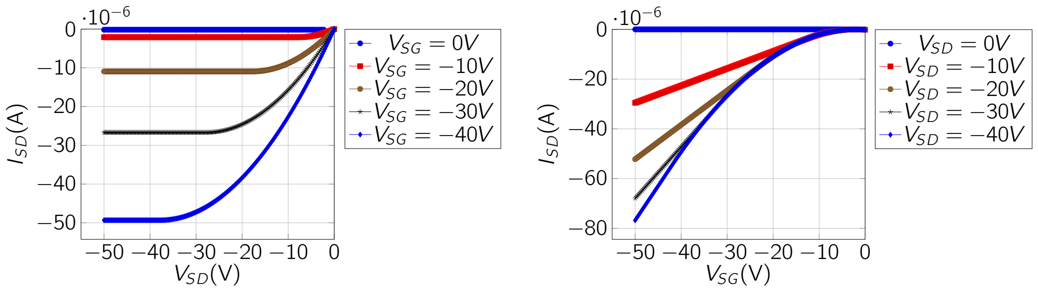

(a) (b)

Figure 1.7 *Simulated characteristics for a p-type OFET (a) Output characteristics, (b) Transfer characteristics.* W = 2000 μm, L = 50 μm, μ_{FE} = 0.1 $cm^2V^{-1}s^{-1}$, C_i = 17.26 nF/cm^2 and V_{TH} = 0 V.

1.3.2 Field-Effect Mobility

At low applied electric fields, the charge carrier mobility μ is given by:

$$\mu = \frac{\nu}{E} \tag{1.5}$$

where ν is the average drift velocity of charge carriers and E is the applied electric field.

In equation (1.5) μ can be seen as a quantitative term of how facile charge carriers can move under an applied electric field. It is important to note that at high electric fields, the linear relationship between drift velocity and applied electric field is no more valid. The increase of an electric field leads to higher drift velocity values and higher charge carrier energy.

Equation (1.6) shows that μ while applying Newton's law and considering the fact that a charge carrier with charge q and effective mass m^* is scattered after time τ, can be expressed in a new form:

$$\mu = \frac{q \cdot \tau}{m^*} \tag{1.6}$$

The field-effect mobility μ_{FE} is the key parameter in OFETs, and this value is close to the intrinsic mobility μ only for the ideal device. However, in real devices this is a rare case, because parasitic contact resistance (R_C) and structural defects are always present. Thus the field-effect mobility is a device parameter instead of a material intrinsic property. The field-effect mobility can be extracted from equations (1.7) and (1.8). The field-effect mobility in the linear regime of an OFET can be extracted using:

$$\mu_{FE}^{lin} = \frac{L}{W\,C_i\;V_{SD}}\left(\frac{I_{SD\;lin}}{V_{SG}}\right)_{V_{SD}=const} \tag{1.7}$$

where μ_{FE}^{lin} is the field-effect mobility in the linear regime, L the channel length, W the channel width, C_i the insulator capacitance per unit area, V_{SD} the source-drain voltage, $I_{SD\;lin}$ the source-drain current in the linear regime, and V_{SG} the source-gate voltage. Plotting I_{SD} versus V_{SG} a linear fit can be done and the obtained slope is then introduced in the Equation (1.7), leading to an average value for the device mobility in the linear regime. Also, the mobility can be extracted calculating the derivative of the curve obtained by plotting I_{SD} versus V_{SG} and then calculating the mobility according to Equation(1.7). The before mentioned method gives additional information about the field dependence, like gate voltage dependence of μ_{FE}.

In the saturation regime Equation (1.8) must be used instead.

$$\mu_{FE}^{sat} = \left(\frac{\sqrt{I_{SD\;sat}}}{V_{SG}}\right)^2_{V_{SD}=const}\frac{2L}{WC_i} \tag{1.8}$$

where μ_{FE}^{sat} field-effect mobility in the saturation regime, and $I_{SD\;sat}$ the source-drain current in the saturation regime.

In this case, a plot is prepared locating data as follows: in the y-axis the values of the square root of the absolute value of I_{SD} and on the x-axis the values of V_{SG}, so by performing a linear fit and introducing the slope in Equation (1.8) the mean value for μ_{FE} is estimated. Also, by calculating the derivative of $\sqrt{|\mu^{sat}_{FE}|}$ with respect to V_{SG} the mobility can be extracted as a function of V_{SG}.

It is important to keep in mind that in devices based on single crystals, the field-effect mobility is normally not dependent on the gate bias, which asseverates that the gate bias dependency originates on the localised levels attributed to structural defects and grain boundaries[16,95].

1.3.3 Threshold Voltage

Measuring the threshold voltage is somewhat difficult by the relatively gradual turn-on of the device, and as in c-Si in OFETs there is no a single definition that is universally accepted [†]. For c-Si the threshold voltage is the voltage at which inversion is achieved, but organic semiconductors properly speaking never achieve inversion so there is no definite threshold voltage, only a voltage at which the devices start to accumulate charge. However, the term threshold voltage is generally used in the community to specify the gate voltage at which current begins to flow[92], in OFETs at the onset of strong accumulation in the channel, determining the operating voltage of the transistor[101]. It is common in experimental endeavours to use the threshold voltage as a parameter for quality control in device fabrication, and is often used to get information about impurities concentrations, traps and interface states. So, in a transistor made of a pure material without traps and not doped the threshold voltage should be close to zero. However, it has to be taken into account that organic materials have a large density of traps, which means that not all charge induced by the gate contributes to the current. A widely used method to calculate the threshold voltage (V_{TH}) is to plot

---

[†] The threshold voltage can be defined as a value that measures the divergence from an ideal state which is assumed as threshold voltage equals to zero Volts. For a p type semiconductor, if the value of threshold voltage is negative, the divergence is ascribed to defects on the semiconductor/dielectric interface and if it is positive it is due to a doped semiconductor.

the square root of the absolute value of the saturation current as a function of the gate voltage. The resulting straight line for an ideal device can be used to find the intercept point with the x-axis (in this case V_{SG}), where V_{TH} can be determined (see Figure 1.8). Care must be taken while extracting the threshold voltage value, because the plot of the square root of I_{SD} not always produces a straight line, where the R-square parameter may reflect dependencies from other sources. Also, the threshold voltage can be extracted by the transconductance change method (TC). In this method the threshold voltage value is equal to the maximum of the derivative of the transconductance. The difficulty of defining a threshold voltage in disordered organic transistors was highlighted first by Horowitz et al, therefore instead of only reporting the threshold voltage as characterization parameter it is also important to use the gate voltage at which these is no band-bending in the semiconductor and such parameter is defined as switch-on voltage V_{SO}.[102]

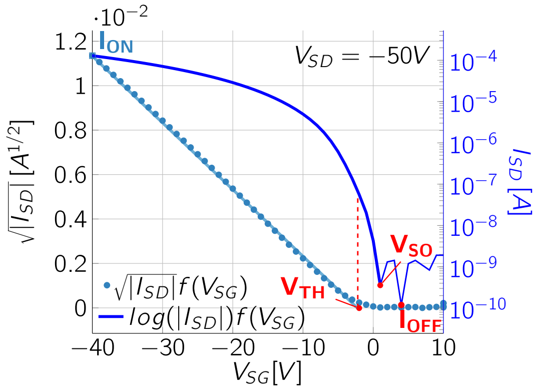

Figure 1.8 *OFET parameter extraction shown in a typical transfer curve measured in the saturation regime at* V_{SD} = *-50 V. Threshold voltage* V_{TH}, *switch-on Voltage* V_{SO}, *on-current* I_{ON}, *off-current* I_{OFF}.

1.3.4 On-,Off-currents and On/Off Current Ratio

In high performing devices the on-current (I_{ON}) must have a high value, as high as possible. This parameter is directly proportional to the device geometry, so by increasing the channel width, I_{ON} will increase as well. The off-current (I_{OFF})

The transconductance (g_m) is the derivative of I_{SD} with respect to V_{SG} calculated from the transfer characteristics, so: $g_m = \frac{\partial I_{SD}}{\partial V_{SG}}$

should be as low as possible since it reflects the quality, and the purity of the active material. In all engineered devices, it is desired that the device switches off, when zero gate voltage is applied. A parameter that gives information about the switching efficiency of the OFET is the on/off current ratio (I_{ON} I_{OFF}), and values of such parameter must be compared at the same sets of V_{SG} and V_{SD} (see Figure 1.8)[95,103].

1.3.5 Subthreshold Region

The subthreshold current is the drain current when the gate bias is below the threshold voltage. This region is of extremely importance when low-voltage, and low-power applications are needed because this region gives information about how sharply the current drops with gate bias. The subthreshold swing is the parameter that quantifies how sharply the transistor is turned off by the gate voltage. The subthreshold swing (S) (inverse of subthreshold slope see Equation 1.9) is defined as the gate voltage change needed to induce a drain-current change of one order of magnitude[104]. It is important to keep in mind that minimizing the subthreshold swing value will minimize the power consumption of the actual device.

$$S = \left(\frac{d\,(log_{10} I_{SD})}{dV_{SG}} \right)^{-1} \tag{1.9}$$

1.3.6 Trapping of Charge Carriers and Hysteresis Effects

It was mentioned before that even the purest organic single crystals have a number of structural defects. To obtain high performing devices it is very important to have well formed interfaces between the organic semiconductor and the insulator as well as the organic semiconductor and metal contacts interfaces. Such well formed interfaces will prevent hysteresis effects to appear in the I_{SD} f(V_{SD}) and I_{SD} f(V_{SG}) curves between forward and reverse swept voltages. Defects present at the interfaces can lead to trap sites, where charges are highly localized and are available as free charge carriers only after releasing them again. Organic materials are often not stable under ambient conditions, where moisture and oxygen act as dopants increasing the number of charges within the active material observing an increasing current in time or as electron traps which leads to a hysteresis in the I_{SD} curves[95,103].

1.3.7 Contact Resistance

Under a given bias condition contacts can inject and retrieve all the charge carriers through the channel only if the source and drain contacts are ohmic, which means that the value of the contact resistance is negligible compared with the channel resistance. Contacts are ohmic when the work function of the metal is close to the highest occupied molecular orbital (HOMO) or to the lowest unoccupied molecular orbital (LUMO) level of the semiconductor, for p- and n- type, respectively, following the Mott-Schottky model. Otherwise, an energy barrier will form at the metal/semiconductor interface preventing charge injection. However, many metal/organic-semiconductor interfaces do not follow Mott-Schottky model, in such cases additional barriers will arise. Also, the channel dimension is another critical issue concerning contact resistance. Figure 1.9 depicts a very simple schematic of contact and channel resistances. In such case, parasitic series resistances at the contacts of the organic semiconductor can have a detrimental impact on the device performance. Contact resistance measurements

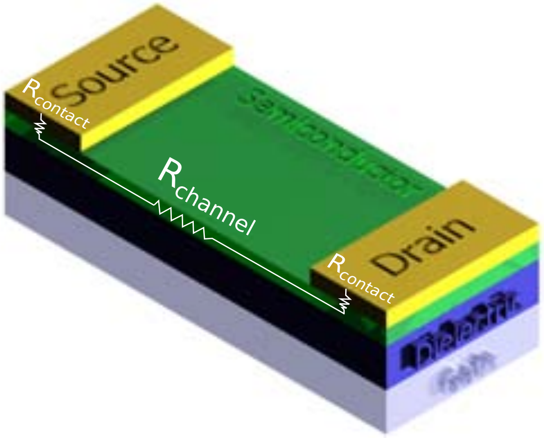

Figure 1.9 *Simple schematic of contact resistances in an OFET.*

are not straightforward extracted from current-voltage curve, however, different methods are developed and shown in literature in order to estimate the contact resistances values[105].

The contact resistance can be extracted using the I-V characteristics from different-length transistors. The channel can be assumed as a simple resistor, and as the length of the channel increases, the resistance increases linearly. Then, the measured resistance multiplied by W to normalize the resistance is plotted as a function of the channel length. From the linear fit equation the intercept with the y-axis at L = 0 μm produces the contact resistance, (see Eq. 1.12) assuming that the resistance at the source and drain contacts is independent of the potential drop across the contacts[106]. Therefore, the device resistance can be expressed as:

$$R_{total} = R_{channel} + R_{SD} \tag{1.10}$$

$$R_{total} = R^{sheet}_{channel}\frac{L}{W} + R_{SD} \tag{1.11}$$

where $R^{sheet}_{channel}$ is the channel sheet resistance, R_{SD} is the normalized contact resistance and L and W are the channel length and channel width of the device, respectively[16,95]. Subsequently, normalizing with the device dimensions:

$$R_{total}W = \frac{L}{\mu C_i(V_{SG}-V_{TH})} + R_{SD}W \tag{1.12}$$

$$\frac{R_{total}W}{L} = \frac{1}{\mu C_i(V_{SG}-V_{TH})} + (R_{SD}W)\frac{1}{L} \tag{1.13}$$

In the linear regime, the channel could be approximated as a uniform resistance controlled by the gate voltage. Equation 1.12 represents the conventional Transfer Line Method, while Equation 1.13 represents a modified version of Equation 1.12. Using equation 1.11, the channel resistance reads $R_{channel} = L \quad W\mu C_i(V_{SG}-V_{TH})$, where W is the channel width, L is the channel length, μ_{FE} is the mobility, C_i is the unit area capacitance of the dielectric, V_{SG} is the gate voltage and V_{TH} is the threshold voltage. It is well known that the parameter variation in organic transistors is very large, μ_{FE} and V_{TH},so in order to reduce scattering and uncertainty of data a modification in the traditional TLM method is introduced, simply by plotting $(R_{total}W)\ L$ with respect to $1\ L$ (see Eq. 1.13), then the slope is now controlled by the contact resistance contribution $R_{SD}W$ which will manifest small variations from device to device[107–109].

1.4 Organic Semiconductors

The active materials in OFETs can be divided into two main groups: (i) small conjugated molecules with low molecular weight (Figure 1.10)[42] and (ii) conjugated polymers (Figure 1.11). In both cases, the conductivity is mainly determined by the relative position of the π-π orbitals, and thus the molecular ordering is very important to achieve OFETs with high performance.

1.4.1 Small Molecules

Small molecules, which had been more commonly deposited employing vacuum deposition techniques due to their lower solubility in organic solvents, can form films with a variety of crystallinity degrees and even exhibit different solid-state structures. For instance, Dimitrakopoulos and Mascaro demonstrated that films of pentacene, evaporated at different temperatures show a range of crystallinity that correlate with the resulting OFET performance[110]. The influence of the substrate temperature was also investigated in thin-films of copper phthalocyanine (CuPc), see Figure 1.10, where a strong impact on the film morphology was observed, which went from grains to rod-like and large flat crystals with increasing temperature[111].

On the other hand, Salleo and coworkers reported that the device performance can be optimized by controlling the grain boundary orientation or reducing

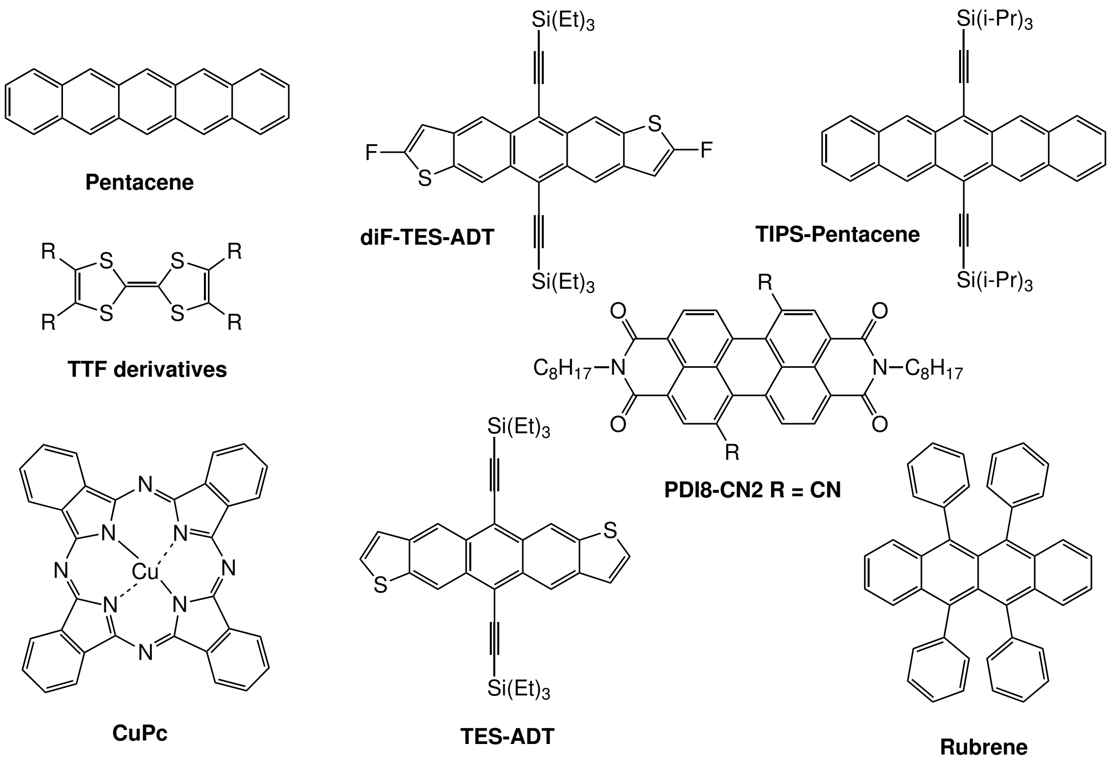

Figure 1.10 *Small conjugated molecules employed as active material for the fabrication of OFETs.*

the energetic barrier associated with transport across less favorable boundaries[112]. They found that in films based on the perylenediimide PDI8-CN2 semiconductor (Figure 1.10), the grain-boundary orientation modulates by about two orders of magnitude the charge mobility and also that the molecular packing motif is crucial in the grain-boundary-induced anisotropy. There are other parameters during the evaporation of the OSC that also affect the molecular solid-state structure and, hence, the device performance. For example, the deposition rate affects the nucleation density[113]. Preferably and in general a slower deposition rate results in a lower nucleation density and large grains, which are favorable for charge transport. However, the investigation of the molecular beam deposition of pentacene, Figure 1.10, revealed that this material show higher OFET mobility when it is deposited at high rate due to the presence of mixed phases at low deposition rate[114,115].

Recently, one of the routes followed to impart solubility to organic semiconductors is to prepare structurally modified molecules by functionalisation with solubilising side groups able not only to induce solubility but also crystallinity to the material (i.e. bis (triethylsilylethynyl) anthradithiophene (TES - ADT) and bis (triisopropylsilylethynyl) pentacene (TIPS - PEN))[42]. These materials can be processed from solution and exhibit very high mobilities due to an enhanced π-π interaction.

For achieving higher field-effect performance, single crystals are most suitable due to their high molecular order and the absence of grain boundaries[72]. In the development of single crystal OFETs, π conjugated small molecules like rubrene[116], pentacene[117], phthalocyanine[118] (Figure 1.10), for instance, have shown attractive results with mobilities of the order of 10 $\mathrm{cm^2/Vs}$. Tetrathiafulvalenes (TTFs) have also been shown to be promising organic semiconductors due to their high performance and processability[119–124]. The technologies applied to grow organic single crystals are based on solution and vapor deposition techniques. The physical vapor transport method is widely used to purify and grow high quality single crystals[125,126] like, for example, platelike rubrene and pentacene single crystals[127] and micro and nanometer sized single crystals of copper phthalocyanine (CuPc)[128]. Solution based methods basically includes recrystallization[129], solvent exchange[130] and dropcasting[131,132] which are applicable to well soluble organic materials. Although impressive progress have been shown for organic single crystals, there are still many challenging questions to solve, where the understanding of the structure-mobility relation and the transfer of organic single crystals OFETs to real applications are still open. So, the device fabrication processes must be further improved to control the quality and size of organic single crystals, and to obtain single crystal arrays over large areas from solution, which will enable the transfer to applications and is desired for low-cost production[129,133].

1.4.2 Polymers

Solution processed polymers are in most cases amorphous or form complex microstructures, where microcrystalline domains are embedded in an amorphous matrix. High disorder limits the charge transport resulting in low field-effect mobilities[134]. The most studied polymer for OFETs is regioregular poly(3-hexylthiophene) (P3HT) shown in Figure 1.11, which was the first polymer giving a high mobility of the order of 0.1 cm^2/Vs[135–142]. This high mobility is ascribed to structural order in the polymer film induced by the regioregular head-to-tail coupling of the hexyl side chains[143]. Additionally, depending on the solvent employed to solubilize this polymer, P3HT can form fibers in solution, which can then be deposited on the substrate[144]. Hole mobilities in the range of 0.02 - 0.06 cm^2/Vs have been reported for single nanofibers and films of aligned fibers[145–147]. The formation of similar fibers has also been observed in other conjugated polymers and is believed to be governed by the π-stacking of the conjugated chains[148]. Polymers with elevated molecular weight have also been proved to generally reveal higher molecular order reducing the number of trapping or scattering sites such as cyclopentadithiophenebenzothiadiazole copolymer (CDT-BTZ, Figure 1.11), which reached a mobility of up to 0.67 cm^2/Vs[149].

A different strategy followed recently to obtain polymers with increased structural order has been the use of polymer liquid crystals. OFETs based on the liquid crystal poly(2,5 - bis(3 - alkylthiophene - 2 - yl) thieno [3,2-b] thiophene) (PBTTT), Figure 1.11, have led to mobilities as high as 0.7 $cm^2V^{-1}s^{-1}$ in its mesophase[150].

All the previously mentioned polymers belong to p-channel semiconductors, since the progress in OFETs using n-channel semiconductors is still far from the performance achieved with p-channel materials. However, a new n-channel polymer based on a naphatelene - bis (dicarboximide) (P(NDI2OD-T2), Figure 1.11) has

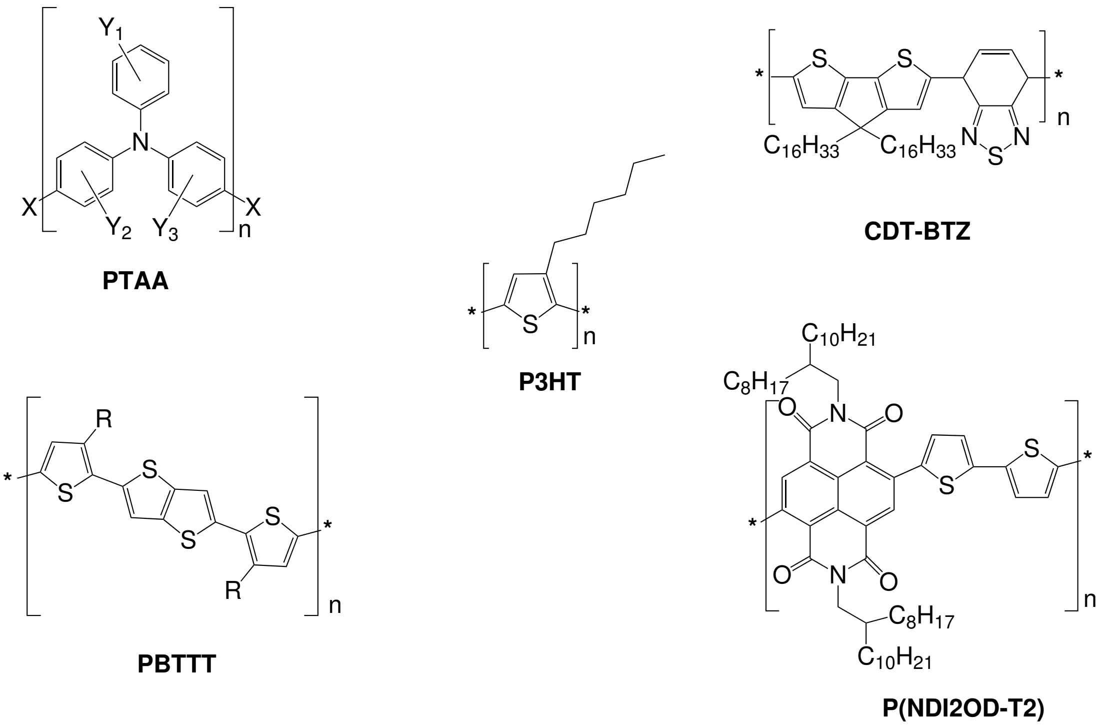

Figure 1.11 *Conjugated polymers used as active material for the fabrication of solution processed thin-film OFETs.*

been reported to show a very high electron mobility (0.45 - 0.85 cm^2/Vs) together with solution processability and air stability, surprisingly, in amorphous films[151,152].

1.4.3 Composite Materials

Composite materials are multiphase materials obtained by combining different materials to attain properties that the individual component cannot exhibit. Composite materials can be tailored to achieve a distinctive property or properties by appropriately choosing their components, their proportions, their distributions, their morphologies, and engineering the interfaces between components. The structure of a composite is such that one of the components is the matrix while the other component or components are fillers bound by the matrix, which is often called the binder[153,154]. The technique of blending organic semiconductors with polymers either insulating or semiconducting for tuning the solution processability and thin film properties, is now commonly employed in organic electronics and thin film transistors alike[155]. When a thin film is composed of two or more components, there is highly likely to have wide range of microstructural variations and phase separation. Therefore, in OSC/binder polymer composites, there can be several factors that finally determine the overall phase behaviour, like the kinetics of solvent evaporation and changes that this induces in the solution, such as viscosity variations and phase separation within the solution. Also, the thermodynamics of mixing between components and the balance in contributions by entropy and enthalpy to the free energy of mixing, ΔG_{mix} is an important factor. This energy, ΔG_{mix}, in a two-component system varies with composition leading to three well-defined regions: complete solution, metastable region and an unstable region. For polymer/polymer composites, especially for high molecular weights and amorphous systems, the entropy change on mixing is usually negligible. So, phase separation is common, since mixing is only favourable when a strong enthalpic interaction between components is present, this holds even for polymer solutions with relatively low concentrations.

Small-molecule/polymer and polymer/polymer blends where the semiconducting component is either p- or n-type are commonly used to enhance processability in organic electronics as stated before, and it was also found that the weight ratio of components in composites drastically affects the mobility for both holes and electrons[156]. The small molecule crystals will inherently possess high charge carrier mobility (i.e. acenes or oligothiophenes), and can be blended with polymers (i.e. insulating or semiconducting) that are easy to process and/or have a low-cost to manufacture (i.e. polystyrene (PS), or poly(methyl methacrylate) (PMMA))[157]. There are copious examples of composite materials used as active layers in OFETs, here only a few typical examples are highlighted. Soluble acenes/insulating polymer blends are interesting composites and deeply studied in the literature. For example, 5,11 - bis (triethylsilylethynyl) anthradithiophene (TES - ADT, Figure 1.10) with PMMA as binder, where the low surface energy TES - ADT is deposited on the air - film interface and the PMMA with high surface energy is deposited on the film-substrate interface during spin-coating. In such films the average field-effect mobility increases from 10^{-3} to 0.5 $cm^2V^{-1}s^{-1}$ after solvent vapor annealing[158]. Systems comprised by 6,13 - bis (triisopropylsilylethynyl) pentacene (TIPS-pentacene, Figure 1.10) are also deeply studied to better understand the acene/polymer system interactions. One key feature in these composites, is the high mobility obtained even with significant concentration of an insulating polymer, and is ascribed to vertical phase separation (i.e. TIPS-pentacene blended with poly(α - methylstyrene) shows a mobility of 0.7 $cm^2V^{-1}s^{-1}$)[157,159].

Another tendency is to blend small-molecules with polymeric semiconductors which possesses mobilities much lower than the crystals of the small-molecule but could be enhanced by blending, such as polytriarylamines (PTAA, Figure 1.11) and polythiophenes. One example, is a blend of TIPS-pentacene with PTAA which shows a mobility of 1.1 $cm^2V^{-1}s^{-1}$. Using this approach mobilities as high as 2.4 $cm^2V^{-1}s^{-1}$ were found for systems small-molecule/polytriarylamine composites (i.e. DiF-TESADT/PTAA composite)[157].

Also polymer/polymer composites have been studied, in which poly (3 - hexylthiophene) (P3HT) has been by far the most studied. For instance, Goffri et al have analysed different combinations of insulators and the semiconductor P3HT, and shown that the crystallisation sequence is controlled by the selection of deposition temperature[160]. Also, Babel et al[161] studied blends of P3HT with a polymeric semiconductor, poly[2 - methoxy - 5 - (2-ethylhexoxy)-1,4-phenylenevinylene] (MEH-PPV), and polystyrene as binder, exhibiting relatively high field effect hole mobility ((0.1-6)x10^{-3} $cm^2V^{-1}s^{-1}$) for these type of composites.

Also, amorphous poly(triarylamines), poly(4,4-diphenyl-(4-methoxy-2-methylphenyl)amine) with selected amorphous and semi-crystalline polymeric binders, like: poly(α-methylstyrene) (PAMS), amorphous polystyrene (PS), isotactic polystyrene (iPS), amorphous poly(methylmethacrylate) (PMMA) have been either deposited by drop casting or inkjet printing giving mobilities in the range $10^{-5} - 10^{-3}$ $cm^2V^{-1}s^{-1}$ where the maximum values for mobility were observed in the drop casted samples[162]. Despite the myriad of possibilities in blending and composite forming, common binders are: polystyrene either atactic or isotactic, poly(αmethyl styrene), poly(methylmethacrylate) and polyethylene.

1.5 Organic Semiconductor Deposition Techniques

The organic semiconductor deposition techniques can be subdivided into two main categories, namely vapor phase deposition and liquid phase deposition.

1.5.1 Vapor Phase Deposition

The vapor phase deposition of organic semiconductors is a thermal evaporation in vacuum, which is used not only for the deposition of the semiconductor but also for the purification of the material (see Figure 1.12). For the deposition, the material is located in vacuum and heated. Once the vapor pressure of the heated material exceeds the pressure inside the vacuum chamber, the material evaporates and condenses on cooler surfaces where it lands on. It is worth noting that deposition of organic semiconductors is typically performed under high vacuum conditions (10^{-6} - 10^{-8} mbar)[92], and the control of the substrate temperature or the deposition rate can have an impact on the film morphology and crystallinity.

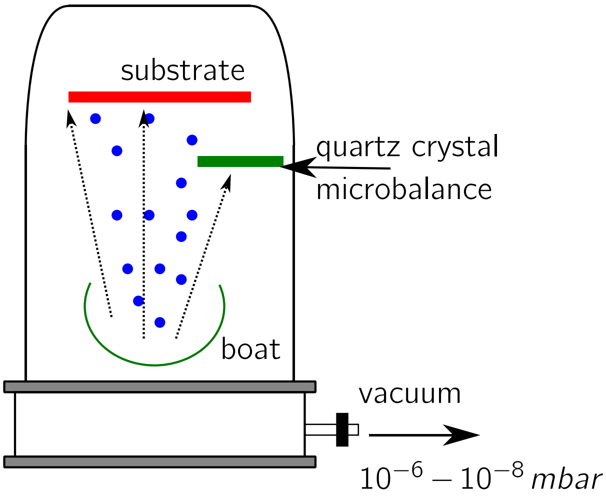

Figure 1.12 *Thermal evaporation system for thin film deposition.*

1.5.2 Liquid Phase Deposition

Solution processability is generally preferred for low cost fabrication. Although the first studied OSCs such as pentacene or sexithiophene suffered from poor solubility, many organic semiconductors materials are now engineered to be soluble or dispersible from solution.

The most common deposition strategies include:

- *Drop-casting*, is probably the simplest technique available to form a film. The procedure is to drop an OSC solution on a substrate followed by spontaneous solvent evaporation. Although it is possible the preparation of films with good quality, the method suffers from a lack of control over the film thickness, reproducibility and compatibility with upscaling[163,164].

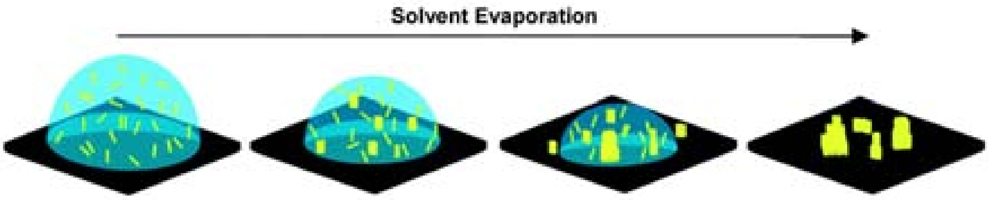

Figure 1.13 *Schematic for a typical drop casting process, taken from reference*[165].

- *Spin-coating*, is one of the most commonly used techniques for preparing thin films of OSCs[166]. A small quantity of an OSC solution, typically in some volatile solvent, is dispensed on a clean substrate. Then the substrate is rotationally accelerated to high speed, while the spinning causes most of the solution to be ejected from the substrate immediately, leaving a thin film flowing outwards from the center of the substrate under centrifugal force. Finally the solvent evaporates and a thin solid film is formed[167]. This is a simple and fast technique but not suitable for covering large areas.

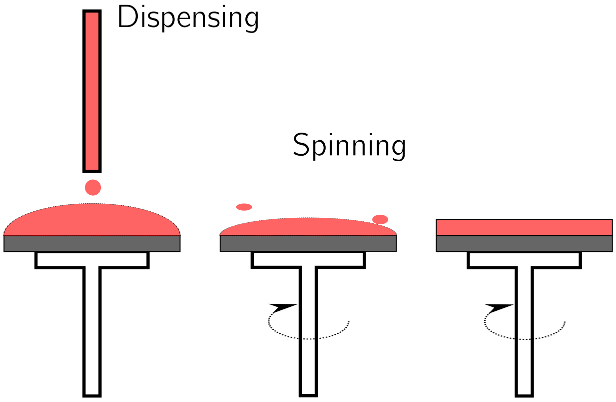

Figure 1.14 *Spin coating Scheme.*

- *Dip coating*, is a coating technique in which a substrate is dipped in a sufficiently large beaker to permit the immersion of the whole substrate in the host OSC solution and then vertically withdrew. The thickness of the film can be controlled by choosing an appropriate combination of withdrawal speed and solute concentration[168].

- *Spray coating* consists of supplying the OSC solution by a spraying nozzle, which traverses over the whole the substrate. During the dispensing phase the substrate rotates at slow speed. Then, the substrate rotates at high speed for the thinning phase[169].

- *Blade coating*, is the simplest example of a self-metered coating process in

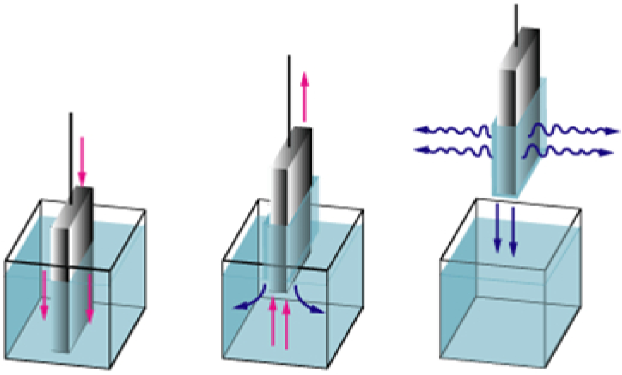

Figure 1.15 *Schematic for a typical dip coating process. Image from www.ahk-service.de*

Figure 1.16 *Spray coating scheme. Image from www.elveflow.com*

which a fluid is applied on a moving substrate and the excess of fluid is removed by dragging the substrate under a fixed blade. Similarly, in the *Wire coater* technique a wire in direct contact with the substrate spreads a thin film. Both, processes relies on the basics of the lubrication theory[170].

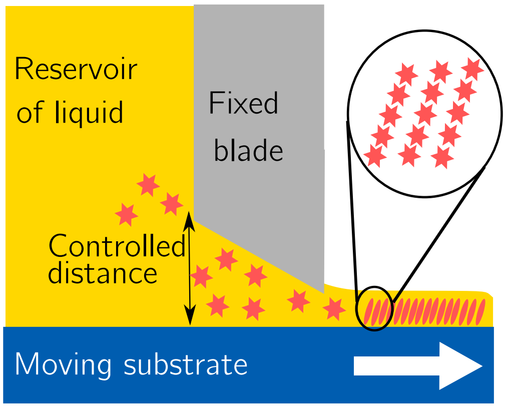

Figure 1.17 *Scheme of a typical blade coating process.*

- *Zone casting*, consist in continuously deposit a material from solution by a flat nozzle on a moving substrate where the solvent evaporates from the meniscus zone, while controlling the temperature of the solution and the substrate[118,171,172]. This technique gives rise to highly crystalline anisotropic films. A main drawback is that it is a very slow technique.

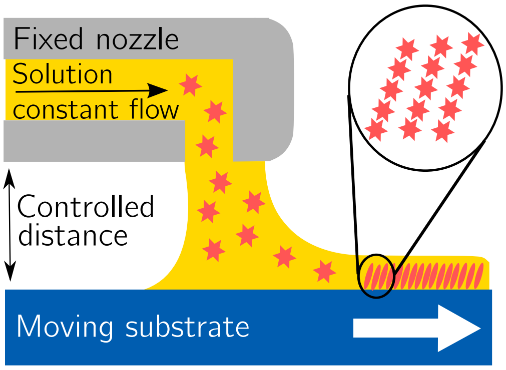

Figure 1.18 *Zone casting scheme adapted from Miskiewicz et al.*[124].

Printing of the semiconductor can also be classified as a liquid phase deposition, since the starting materials are in liquid form, however printing comprises a family of operations that simultaneously deposit and pattern a target material[92].

1.6 Tetrathiafulvalene (TTF)

A huge interest in tetrathiafulvalene (TTF)-derivatives started to appear after the discovery of the first organic metal TTF-TCNQ back in 1973[5]. Since then a vast number of metallic and even superconducting charge transfer salts based on TTFs have been reported[173]. The possibility to apply TTF-derivatives as active materials in high performing field-effect transistors, however, was initiated by Mas-Torrent at al. in 2004[131,174]. The basic characteristics that makes TTF-derivatives attractive for a number of potential applications in organic electronics are discussed next.

1.6.1 Electronic and Supramolecular Properties

Each dithiolylidene ring of the neutral TTF has 7 π electrons: 2 for each sulphur atom and 1 for each sp^2 carbon atom. Removing one of these electrons (*i.e.* oxidation) from the neutral TTF leads to the formation of a radical cation where one of the two rings becomes aromatic with a delocalization of the remaining electron system in the fulvalene moiety. Similarly, when a second electron is removed from the TTF rings, the radical dication consisting of 6 π electrons per ring is formed. Figure 1.19 shows the redox processes of TTFs. These redox processes are characterized by cyclic voltametry that is a widely used technique to characterize the redox reactions of electro-active species[175]. The π-electron rich TTF-derivatives leads to two reversible oxidation processes at positive voltages[176]. Furthermore, the redox potentials, and thus, the HOMO and LUMO levels, can be tuned modifying the substituents (R) by adding electron withdrawing or electron donating groups.

TTF-derivatives are generally soluble in conventional organic solvents and stable, avoiding strong acid conditions or strong oxidants, to a large number of synthetic transformations, which are important features for their implementation as active materials in potential devices.

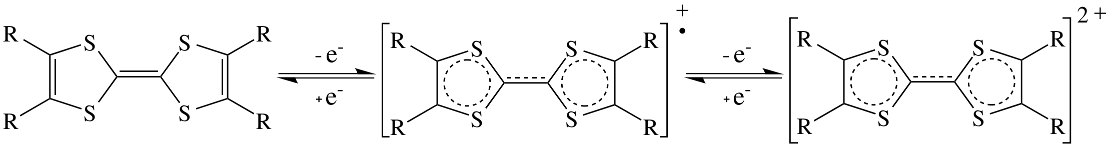

Figure 1.19 *Oxidation processes of tetrathiafulvalene (TTF) to radical-cation and di-cation species.*

The strong intermolecular interactions due to the π - π electrons as well as the S···S interactions of the sulphur atoms determine the supramolecular organization in these materials[176]. A close molecular packing and a strong overlap of the π-electrons are crucial issues for intermolecular charge transport. Figure 1.20 shows schematically a 1D stacking of TTF molecules and the overlap of the π-electrons, as well as the close S$\cdots$S interactions.

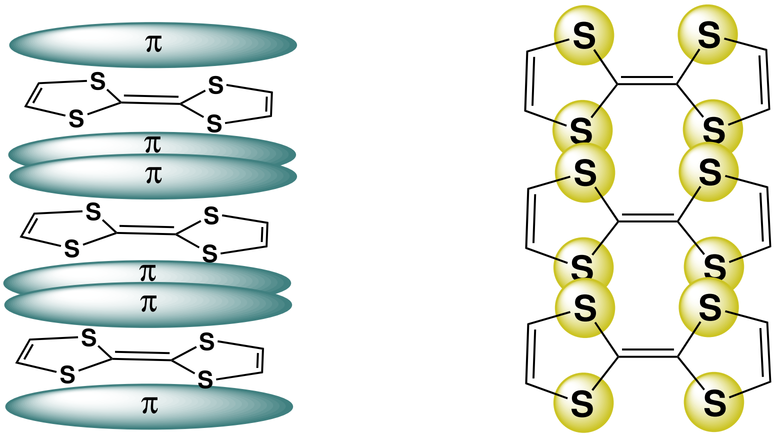

Figure 1.20 *Schematic representation of the main intermolecular interactions, π - π-orbital overlap and S$\cdots$S-interactions, that govern the electronically relevant supramolecular organization of TTF-based crystals. π-orbitals above and below the molecular plane and sulfur (S) atoms are shown in light blue and red, respectively.*

1.6.2 Organic Field-Effect Transistors based on Tetrathiafulvalene derivatives

Since 2004, TTF-derivatives were found to be potential candidates for active materials in OFETs[131,174]. A large number of compounds have been studied since then[119,177]. A short summary of the most interesting TTF-derivatives used in OFETs, which have been processed employing vacuum and solution based techniques is presented in the following.

The group of TTFs shown in Figure 1.21 were used in thin-film OFETs by thermally evaporating the organic material. Bis(bisphenyl)-tetrathiafulvalene (DBP-TTF) and dipyrazine-TTF (DPy-TTF), for example, were successfully used as p-channel material and exhibited mobilities up to $\mu = 0.11\ cm^2V^{-1}s^{-1}$ and $\mu = 0.64\ cm^2V^{-1}s^{-1}$, respectively[178]. For dinaphtho-tetrathiafulvalene (DN-TTF)[179], a mobility up to $\mu = 0.42 cm^2V^{-1}s^{-1}$ was reported. Diquinoxalino-TTF

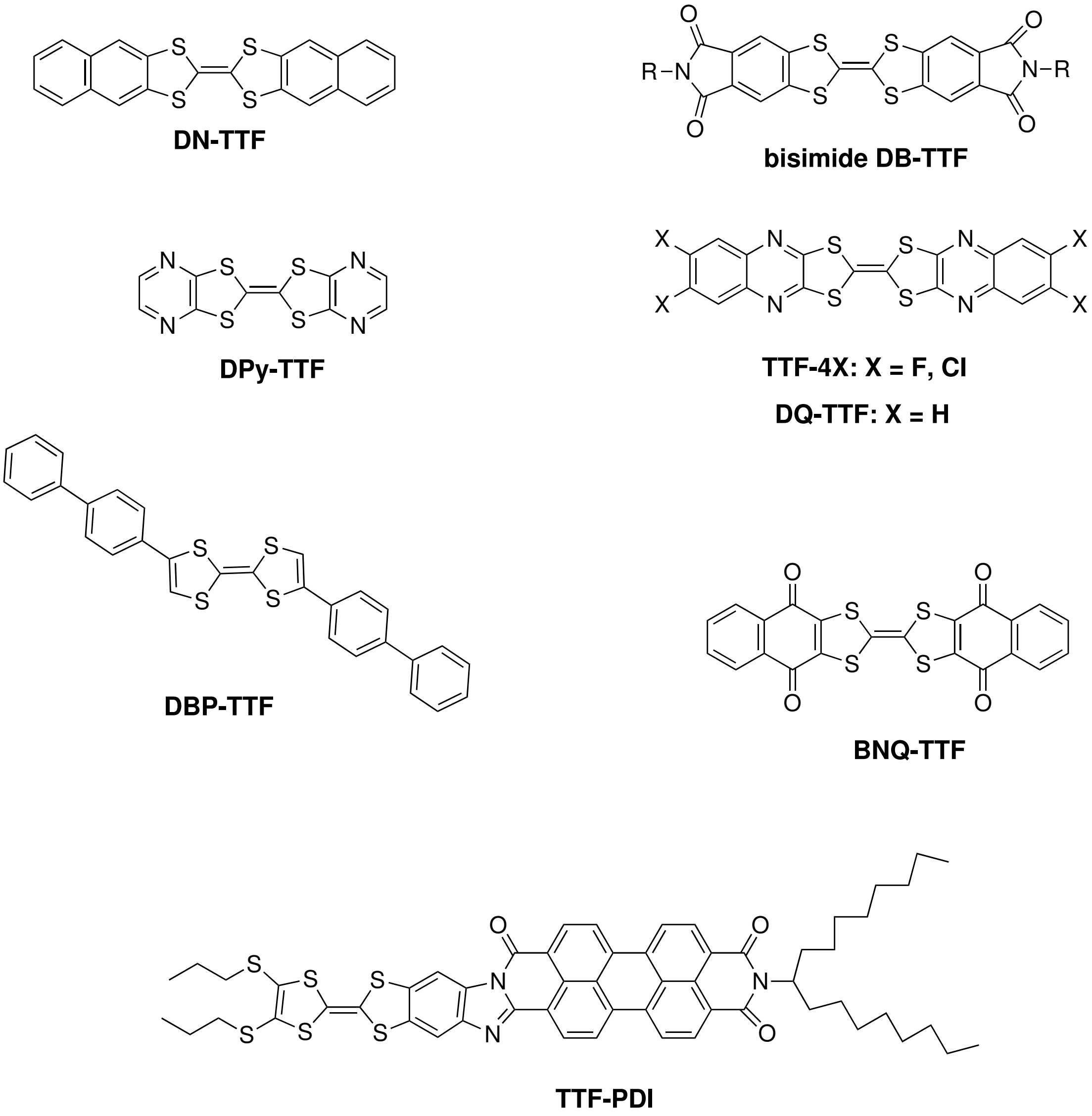

Figure 1.21 *Molecular structure of a small selection of TTF-derivatives applied in OFETs by thermal evaporation.*

(DQ-TTF) exhibited a mobility up to $\mu = 0.2cm^2V^{-1}s^{-1}$[179]. The introduction of imide groups in TTFs leads to a lowering of the HOMO and makes materials more stable under ambient conditions with respect to H_2O and O_2[123,180–182] as in the case of bisimide DB-TTF (Figure 1.21). Introducing electron withdrawing groups (*e.g.* halogens or quinones) to the TTF has also been a successful route to achieve, n-channel behavior, as it was observed in thin-film OFETs with electron mobilities up to $\mu = 0.11cm^2V^{-1}s^{-1}$ for the TTF-tetrahalogen (TTF-4X, with X

= F)[122,182]. A donor-acceptor dyad formed by TTF and a perylenediimide (TTF-PDI, Figure 1.21) derivative and the biquinone functionalized TTF (BNQ-TTF, Figure 1.21) have also been reported to show ambipolar transport[48].

Many of the TTF-derivatives are soluble in common used organic solvents which makes them interesting for low-cost applications. Single crystal TTF OFETs have been prepared from solution by drop casting (Figure 1.22). The method consists in dissolving the TTF in an organic solvent, and drop casting the solution onto a substrate. The solvent is then allowed to evaporate slowly (typically in a timescale of hours) so that TTF crystals have time to grow. In this way, single crystals of dithiophene-tetrathiafulvalene (DT-TTF) and dibenzo-tetrathiafulvalene (DB-TTF) with mobilities of up to 6.2 and 1.0 $cm^2V^{-1}s^{-1}$, respectively, have been reported[171,183,184]. Correlation studies regarding the influence of crystal structure and polymorphism on the charge transport (*i.e.* field-effect mobility) in different sets of TTFs were studied previously[131,171,174].

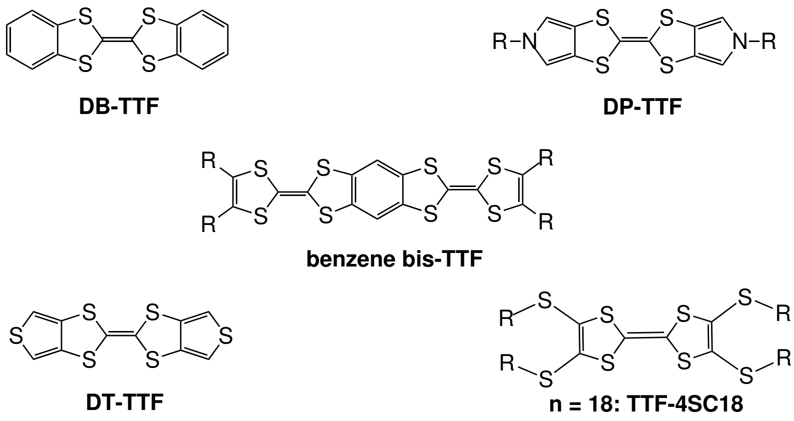

DB-TTF

DP-TTF

benzene bis-TTF

DT-TTF

n = 18: TTF-4SC18

Figure 1.22 *Molecular structure of different TTF-derivatives applied in solution processed OFETs*[185].

Large area TTF-films processed from spin coating have also been reported, for benzene bis-tetrathiafulvalene[186] and for bis(pyrrolo[3,4-d])-tetrathiafulvalene (DP-TTF)[185] giving mobilities of the order of $\mu_{FE} = 10^{-2}$ cm²/Vs. Another technique used to produce solution processed large area TTF films is the zone casting technique, which has led to large arrays of crystalline DT-TTF and TTF-SC18 with a maximum mobility of about $\mu = 0.17 cm^2 V^{-1} s^{-1}$ and $\mu = 0.25 cm^2 V^{-1} s^{-1}$, respectively[95,172,187].

Bibliography

[1] P. Meredith, C. J. Bettinger, M. Irimia-Vladu, a. B. Mostert and P. E. Schwenn. "Electronic and optoelectronic materials and devices inspired by nature." *Reports on progress in physics. Physical Society (Great Britain)*, **2013**, 76, 034501.

[2] M. Pope and C. E. Swenberg. *Electronic Processes in Organic Crystals and Polymers*. Oxford University Press, **1999**.

[3] J. Clayden, N. Greeves and S. Warren. *Organic Chemistry*. Oxford University Press, **2012**.

[4] T. Grasser. *Organic Electronics*, volume 223 of *Advances in Polymer Science*. Springer Berlin Heidelberg, Berlin, Heidelberg, **2010**.

[5] J. Ferraris, D. O. Cowan, V. Walatka and J. H. Perlstein. "Electron transfer in a new highly conducting donor-acceptor complex". *Journal of the American Chemical Society*, **1973**, 95, 948.

[6] L. B. Coleman, M. J. Cohen, D. J. Sandman, F. G. Yamagishi, A. F. Garito and A. J. Heeger. "Superconducting fluctuations and the peierls instability in an organic solid". *Solid State Communications*, **1973**, 12, 1125.

[7] A. Heeger, A. G. MacDiarmid and H. Shirakawa. "http://nobelprize.org/nobel_prizes/chemistry/laureates/2000/press.html". Nobel Prize in Chemistry 2000.

[8] H. Shirakawa, E. J. Louis, A. G. MacDiarmid, C. K. Chiang and A. J. Heeger. "Synthesis Of Electrically Conducting Organic Polymers - Halogen Derivatives Of Polyacetylene, $(Ch)_X$". *Journal of The Chemical Society-Chemical Communications*, **1977**, 16, 578.

[9] C. K. Chiang, C. R. Fincher, Y. W. Park, A. J. Heeger, H. Shirakawa, E. J. Louis, S. C. Gau and A. G. MacDiarmid. "Electrical Conductivity in Doped Polyacetylene". *Physical Review Letters*, **1977**, 39, 1098.

[10] C. J. Bettinger and Z. Bao. "Organic Thin-Film Transistors Fabricated on Resorbable Biomaterial Substrates". *Advanced Materials*, **2010**, 22, 651.

[11] M. Irimia-Vladu, N. S. Sariciftci and S. Bauer. "Exotic materials for bio-organic electronics". *J. Mater. Chem.*, **2011**, 21, 1350.

[12] Y.-L. L. Loo. "Solution-processable organic semiconductors for thin-film transistors: Opportunities for chemical engineers". *AIChE Journal*, **2007**, 53, 1066.

[13] L. Luther. "Managing Electronic Waste: Issues with Exporting E-Waste". CRS Report for Congress: Prepared for Members and Committees of Congress 7-5700, Congressional Research Service, **2010**.

[14] M. A. Alam. "ECE 606: Principles of Semiconductor Devices". Purdue University, **2008**.

[15] B. Meyerson. "Design Automation Conference 2010: Echoes of DACs Past: From Prediction to Realization, and Watts Next?" http://electronics.wesrch.com/paper-details/pdf-EL1SE1UFQOXDD-dacs-past-from-prediction-to-realization#page1, **2010**.

[16] Y. Yun. *Pentacene Based Organic Electronic Devices*. Ph.D. thesis, Durham University, **2010**.

[17] J. Calame, R. Myers, S. Binari, F. Wood and M. Garven. "Experimental investigation of microchannel coolers for the high heat flux thermal management of GaN-on-SiC semiconductor devices". *International Journal of Heat and Mass Transfer*, **2007**, 50, 4767 .

[18] S. Russo, L. L. Spina, V. Alessandro, N. Rinaldi and L. K. Nanver. "Influence of layout design and on-wafer heatspreaders on the thermal behavior of fully-isolated bipolar transistors: Part I , Static analysis". *Solid-State Electronics*, **2010**, 54, 745 .

[19] H. Yin, X. Gao, J. Ding, Z. Zhang and Y. Fang. "Thermal management of electronic components with thermal adaptation composite material". *Applied Energy*, **2010**, 87, 3784 .

[20] M. Jaworski. "Thermal performance of heat spreader for electronics cooling with incorporated phase change material". *Applied Thermal Engineering*, **2012**, 35, 212 .

[21] M. Ekpu, R. Bhatti, M. Okereke, S. Mallik and K. Otiaba. "The effect of thermal constriction on heat management in a microelectronic application". *Microelectronics Journal*, **2014**, 45, 159 .

[22] A. L. Moore and L. Shi. "Emerging challenges and materials for thermal management of electronics". *Materials Today*, **2014**, 17, 163 .

[23] Y. Yuan, G. Giri, A. L. Ayzner, A. P. Zoombelt, S. C. B. Mannsfeld, J. Chen, D. Nordlund, M. F. Toney, J. Huang and Z. Bao. "Ultra-high mobility transparent organic thin film transistors grown by an off-centre spin-coating method." *Nature communications*, **2014**, 5, 3005.

[24] Y. Taur and T. H. Ning. *Fundamentals of Modern VLSI Devices*. Cambridge University Press, **2000**.

[25] S. R. Forrest. "The path to ubiquitous and low-cost organic electronic appliances on plastic". *Nature*, **2004**, 428, 911.

[26] B. D. Gates, Q. Xu, M. Stewart, D. Ryan, C. G. Willson and G. M. Whitesides. "New Approaches to Nanofabrication: Molding, Printing, and Other Techniques". *Chemical Reviews*, **2005**, 105, 1171.

[27] T. Kawase, T. Shimoda, C. Newsome, H. Sirringhaus and R. H. Friend. "Inkjet printing of polymer thin film transistors". *Thin Solid Films*, **2003**, 438-439, 279.

[28] H. Sirringhaus, T. Kawase, R. H. Friend, T. Shimoda, M. Inbasekaran, W. Wu and E. P. Woo. "High-Resolution Inkjet Printing of All-Polymer Transistor Circuits". *Science*, **2000**, 290, 2123.

[29] A. C. Arias, S. E. Ready, R. Lujan, W. S. Wong, K. E. Paul, A. Salleo, M. L. Chabinyc, R. Apte, R. A. Street, Y. Wu, P. Liu and B. Ong. "All jet-printed polymer thin-film transistor active-matrix backplanes". *Applied Physics Letters*, **2004**, 85, 3304.

[30] M. L. Chabinyc and A. Salleo. "Materials Requirements and Fabrication of Active Matrix Arrays of Organic Thin-Film Transistors for Displays". *Chemistry of Materials*, **2004**, 16, 4509.

[31] F. Zhu, X.-T. Hao, O. K. Soo, Y. Li and L.-W. Tan. "Toward Novel Flexible Display - Top-Emitting OLEDs on Al-Laminated PET Substrates". *Proceedings of the IEEE*, **2005**, 93, 1440.

[32] C. Dimitrakopoulos and P. Malenfant. "Organic Thin Film Transistors for Large Area Electronics". *Advanced Materials*, **2002**, 14, 99.

[33] G. Gelinck, P. Heremans, K. Nomoto and T. D. Anthopoulos. "Organic

Transistors in Optical Displays and Microelectronic Applications". *Advanced Materials*, **2010**, 22, 3778.

[34] M. T. Bernius, M. Inbasekaran, J. O'Brien and W. Wu. "Progress with Light-Emitting Polymers". *Advanced Materials*, **2000**, 12, 1737.

[35] R. H. Friend, R. W. Gymer, A. B. Holmes, J. H. Burroughes, R. N. Marks, C. Taliani, D. D. C. Bradley, D. A. D. Santos, J. L. Bredas, M. Logdlund and W. R. Salaneck. "Electroluminescence in conjugated polymers". *Nature*, **1999**, 397, 121.

[36] C. W. Tang and S. A. VanSlyke. "Organic electroluminescent diodes". *Applied Physics Letters*, **1987**, 51, 913.

[37] J. H. Burroughes, D. D. C. Bradley, A. R. Brown, R. N. Marks, K. Mackay, R. H. Friend, P. L. Burns and A. B. Holmes. "Light-emitting diodes based on conjugated polymers". *Nature*, **1990**, 347, 539.

[38] O. Fadhel, M. Gras, N. Lemaitre, V. Deborde, M. Hissler, B. Geffroy and R. Rau. "Tunable Organophosphorus Dopants for Bright White Organic Light-Emitting Diodes with Simple Structures". *Advanced Materials*, **2009**, 21, 1261.

[39] G. H. Heilmeier and L. A. Zanoni. "Surface studies of α-copper phthalocyanine films". *Journal of Physics and Chemistry of Solids*, **1964**, 25, 603.

[40] J. H. Burroughes, C. A. Jones and R. H. Friend. "New semiconductor device physics in polymer diodes and transistors". *Nature*, **1988**, 335, 137.

[41] G. Horowitz, D. Fichou, X. Peng, Z. Xu and F. Garnier. "A field-effect transistor based on conjugated alpha-sexithienyl". *Solid State Communications*, **1989**, 72, 381.

[42] M. Mas-Torrent and C. Rovira. “Novel small molecules for organic field-effect transistors: towards processability and high performance.” *Chemical Society Reviews*, **2008**, 37, 827.

[43] D. Braga and G. Horowitz. “High-Performance Organic Field-Effect Transistors”. *Advanced Materials*, **2009**, 21, 1473.

[44] E. J. Meijer, D. M. de Leeuw, S. Setayesh, E. van Veenendaal, B. H. Huisman, P. W. M. Blom, J. C. Hummelen, U. Scherf and T. M. Klapwijk. “Solution-processed ambipolar organic field-effect transistors and inverters”. *Nature Materials*, **2003**, 2, 678.

[45] J. Zaumseil, R. H. Friend and H. Sirringhaus. “Spatial control of the recombination zone in an ambipolar light-emitting organic transistor”. *Nature Materials*, **2006**, 5, 69.

[46] M. Muccini. “A bright future for organic field-effect transistors”. *Nature Materials*, **2006**, 5, 605.

[47] M. C. Gwinner, S. Khodabakhsh, M. H. Song, H. Schweizer, H. Giessen and H. Sirringhaus. “Integration of a Rib Waveguide Distributed Feedback Structure into a Light-Emitting Polymer Field-Effect Transistor”. *Advanced Functional Materials*, **2009**, 19, 1360.

[48] R. Pfattner, E. Pavlica, M. Jaggi, S.-X. Liu, S. Decurtins, G. Bratina, J. Veciana, M. Mas-Torrent and C. Rovira. “Photo-induced intramolecular charge transfer in an ambipolar field-effect transistor based on a [small pi]-conjugated donor-acceptor dyad”. *J. Mater. Chem. C*, **2013**, 1, 3985.

[49] G. H. Gelinck, H. E. A. Huitema, E. van Veenendaal, E. Cantatore, L. Schrijnemakers, J. B. P. H. van der Putten, T. C. T. Geuns, M. Beenhakkers, J. B. Giesbers, B.-H. Huisman, E. J. Meijer, E. M. Benito, F. J. Touwslager, A. W.

Marsman, B. J. E. van Rens and D. M. de Leeuw. "Flexible active-matrix displays and shift registers based on solution-processed organic transistors". *Nature Materials*, **2004**, 3, 106.

[50] B. K. Crone, A. Dodabalapur, R. Sarpeshkar, R. W. Filas, Y.-Y. Lin, Z. Bao, J. H. O'Neill, W. Li and H. E. Katz. "Design and fabrication of organic complementary circuits". *Journal of Applied Physics*, **2001**, 89, 5125.

[51] C. J. Drury, C. M. J. Mutsaers, C. M. Hart, M. Matters and D. M. de Leeuw. "Low-cost all-polymer integrated circuits". *Applied Physics Letters*, **1998**, 73, 108.

[52] A. Dodabalapur, J. Laquindanum, H. E. Katz and Z. Bao. "Complementary circuits with organic transistors". *Applied Physics Letters*, **1996**, 69, 4227.

[53] W. Clemens, I. Fix, J. Ficker, A. Knobloch and A. Ullmann. "From polymer transistors toward printed electronics". *Journal of Materials Research*, **2004**, 19, 1963.

[54] P. F. Baude, D. A. Ender, M. A. Haase, T. W. Kelley, D. V. Muyres and S. D. Theiss. "Pentacene-based radio-frequency identification circuitry". *Applied Physics Letters*, **2003**, 82, 3964.

[55] B. Comiskey, J. D. Albert, H. Yoshizawa and J. Jacobson. "An electrophoretic ink for all-printed reflective electronic displays". *Nature*, **1998**, 394, 253.

[56] R. Wisnieff. "Display technology: Printing screens". *Nature*, **1998**, 394, 225.

[57] "http://www.plasticlogic.com". Plastic logic was founded in 2000 by researchers out of the Cambridge University Cavendish Laboratory.

[58] I. Manunza, A. Sulis and A. Bonfiglio. "Pressure sensing by flexible, organic, field effect transistors". *Applied Physics Letters*, **2006**, 89, 143502.

[59] P. Pacher, A. Lex, V. Proschek, H. Etschmaier, E. Tchernychova, M. Sezen, U. Scherf, W. Grogger, G. Trimmel, C. Slugovc and E. Zojer. "Chemical Control of Local Doping in Organic Thin-Film Transistors: From Depletion to Enhancement". *Advanced Materials*, **2008**, 20, 3143.

[60] L. Torsi, G. M. Farinola, F. Marinelli, M. C. Tanese, O. H. Omar, L. Valli, F. Babudri, F. Palmisano, P. G. Zambonin and F. Naso. "A sensitivity-enhanced field-effect chiral sensor". *Nature Materials*, **2008**, 7, 412.

[61] P. Stoliar, E. Bystrenova, S. Quiroga, P. Annibale, M. Facchini, M. Spijkman, S. Setayesh, D. de Leeuw and F. Biscarini. "DNA adsorption measured with ultra-thin film organic field effect transistors". *Biosensors and Bioelectronics*, **2009**, 24, 2935.

[62] S. C. B. Mannsfeld, B. C.-K. Tee, R. M. Stoltenberg, C. V. H.-H. Chen, S. Barman, B. V. O. Muir, A. N. Sokolov, C. Reese and Z. Bao. "Highly sensitive flexible pressure sensors with microstructured rubber dielectric layers". *Nature Materials*, **2010**, 9, 859.

[63] NREL. "Best Reserach-Cell Efficiencies". Technical report, National Renewable Energy Laboratory (NREL) Photovoltaic (PV) http://www.nrel.gov/pv, **2010**.

[64] T. Nohira, K. Yasuda and Y. Ito. "Pinpoint and bulk electrochemical reduction of insulating silicon dioxide to silicon". *Nature Materials*, **2003**, 2, 397.

[65] G. Yu, J. Gao, J. C. Hummelen, F. Wudl and A. J. Heeger. "Polymer Photovoltaic Cells: Enhanced Efficiencies via a Network of Internal Donor-Acceptor Heterojunctions". *Science*, **1995**, 270, 1789.

[66] M. Gratzel. "Photoelectrochemical cells". *Nature*, **2001**, 414, 338.

[67] N. Tessler, D. J. Pinner, V. Cleave, D. S. Thomas, G. Yahioglu, P. Le Barny and R. H. Friend. “Pulsed excitation of low-mobility light-emitting diodes: Implication for organic lasers”. *Applied Physics Letters*, **1999**, 74, 2764.

[68] D. Angmo and F. C. Krebs. “Flexible ITO-free polymer solar cells”. *Journal of Applied Polymer Science*, **2013**, 129, 1.

[69] P. Atkins and J. de Paula. *Physical Chemistry*. Oxford University Press, 8th edition, **2006**.

[70] C. Weißmantel and C. Hamann. *Grundlagen der Festkörperphysik*. Johann Ambrosius Barth Verlag, Heidelberg-Leipzig, **1995**.

[71] E. A. Slilinsh and V. Čápek. *Organic Molecular Crystals*. American Institut of Physics Press, New York, **1994**.

[72] W. Warta and N. Karl. “Hot holes in naphthalene: High, electric-field-dependent mobilities”. *Physical Review B*, **1985**, 32, 1172.

[73] T. Sakanoue and H. Sirringhaus. “Band-like temperature dependence of mobility in a solution-processed organic semiconductor”. *Nature Materials*, **2010**, 9, 736.

[74] R. A. Marcus. “On the Theory of Oxidation-Reduction Reactions Involving Electron Transfer”. *Journal of Chemical Physics*, **1956**, 24, 966.

[75] R. A. Marcus. “Electron transfer reactions in chemistry. Theory and experiment”. *Reviews of Modern Physics*, **1993**, 65, 599.

[76] N. E. Gruhn, D. A. da Silva Filho, T. G. Bill, M. Malagoli, V. Coropceanu, A. Kahn and J.-L. Bréas. “The Vibrational Reorganization Energy in Pentacene: Molecular Influences on Charge Transport”. *Journal of the American Chemical Society*, **2002**, 124, 7918.

[77] J.-L. Brédas, D. Beljonne, V. Coropceanu and J. Cornil. "Charge-Transfer and Energy-Transfer Processes in π-Conjugated Oligomers and Ploymers: A Molecular Picture". *Chemical Reviews*, **2004**, 104, 4971.

[78] V. Coropceanu, J. Cornil, D. A. da Silva Filho, Y. Olivier, R. Silbey and J.-L. Brédas. "Charge Transport in Organic Semiconductors". *Chemical Reviews*, **2007**, 107, 926.

[79] S. T. Bromley, M. Mas-Torrent, P. Hadley and C. Rovira. "Importance of Intermolecular Interactions in Assessing Hopping Mobilities in Organic Field Effect Transistors: Pentacene versus Dithiophene-tetrathiafulvalene". *Journal of the American Chemical Society*, **2004**, 126, 6544.

[80] S. T. Bromley, F. Illas and M. Mas-Torrent. "Dependence of charge transfer reorganization energy on carrier localisation in organic molecular crystals". *Physical Chemistry Chemical Physics*, **2008**, 10, 121.

[81] R. Pfattner. *Stability Studies on Air-Stable Organic Field-Effect Transistors with Poly(triphenylamines) as Active Layer Materials*. Master's thesis, Graz University of Technology, **2007**.

[82] J. Chen. *Novel Patterning Techniques for Manufacturing Organic and Nanostructured Electronics*. Ph.D. thesis, Massachusetts Institute of Technology, **2007**.

[83] P. G. Le Comber and W. E. Spear. "Electronic Transport in Amorphous Silicon Films". *Physical Review Letters*, **1970**, 25, 509.

[84] G. Horowitz, R. Hajlaoui and P. Delannoy. "Temperature Dependence of the Field-Effect Mobility of Sexithiophene. Determination of the Density of Traps". *Journal de Physique III France*, **1995**, 5, 355.

[85] G. Horowitz, M. E. Hajlaoui and R. Hajlaoui. "Temperature and gate voltage dependence of hole mobility in polycrystalline oligothiophene thin film transistors". *Journal of Applied Physics*, **2000**, 87, 4456.

[86] A. Miller and E. Abrahams. "Impurity Conduction at Low Concentrations". *Physical Review*, **1960**, 120, 745.

[87] N. F. Mott. "Conduction in non-crystalline materials III. Localized states in a pseudogap and near extremities of conduction and valence bands". *Philosophical Magazine*, **1969**, 19, 835.

[88] H. Bässler. "Charge Transport in Disordered Organic Photoconductors a Monte Carlo Simulation Study". *physica status solidi (b)*, **1993**, 175, 15.

[89] M. C. J. M. Vissenberg and M. Matters. "Theory of the field-effect mobility in amorphous organic transistors". *Physical Review B*, **1998**, 57, 12964.

[90] A. Schoonveld. *Transistors based on ordered organic semiconductors*. Ph.D. thesis, Department of Applied Physics of the University of Groningen, **1999**.

[91] M. Chen. *Electrochemical and Electronic Devices based on Low Bandgap Polymers*. Ph.D. thesis, Linköping University, **2005**.

[92] I. Kymissis. *Organic Field Effect Transistors: Theory, Fabrication and Characterization*. Integrated Circuits and Systems. Springer, **2008**.

[93] C. R. Newman, C. D. Frisbie, D. A. da Silva Filho, J.-L. Bredas, P. C. Ewbank and K. R. Mann. "Introduction to Organic Thin Film Transistors and Design of n-Channel Organic Semiconductors". *Chemistry of Materials*, **2004**, 16, 4436.

[94] A. Virkar. *Investigating the Nucleation, Growth, and Energy Levels of Or-*

ganic Semiconductors for High Performance Plastic Electronics. Ph.D. thesis, Stanford, **2012**.

[95] R. Pfattner. *Organic Electronics based on Tetrathiafulvalene-Derivatives: Organic Field-Effect Transistors and Sensors*. Ph.D. thesis, Universitat Autónoma de Barcelona, **2011**.

[96] V. Heine. “Theory of Surface States”. *Physical Review*, **1965**, 138, A1689.

[97] H. Sirringhaus. “Organic semiconductors: An equal-opportunity conductor”. *Nature Materials*, **2003**, 2, 641.

[98] C. Moreno, R. Pfattner, M. Mas-Torrent, J. Puigdollers, S. T. Bromley, C. Rovira, J. Veciana and R. Alcubilla. “Evidence of intrinsic ambipolar charge transport in a high band gap organic semiconductor”. *Journal of Materials Chemistry*, **2012**, 22, 345.

[99] G. Horowitz, R. Hajlaoui, H. Bouchriha, R. Bourguiga and M. Hajlaoui. “The Concept of ”Threshold Voltage” in Organic Field-Effect Transistors”. *Advanced Materials*, **1998**, 10, 923.

[100] A. R. Völkel, R. A. Street and D. Knipp. “Carrier transport and density of state distributions in pentacene transistors”. *Physical Review B*, **2002**, 66, 195336.

[101] V. Kumar Singh and B. Mazhari. “Measurement of threshold voltage in organic thin film transistors”. *Applied Physics Letters*, **2013**, 102 253304.

[102] E. J. Meijer. *Charge transport in disordered organic field-effect transistors*. Ph.D. thesis, Delft University of Technology, **2003**.

[103] P. Stallinga. *Electrical Characterization of Organic Electronic Materials and Devices*. John Wiley & Sons, **2009**.

[104] S. Sze and K. Ng. *Physics of Semiconductor Devices*. Wiley, **2006**.

[105] K. Shibata, K. Ishikawa, H. Takezoe, H. Wada and T. Mori. "Contact resistance of dibenzotetrathiafulvalene-based organic transistors with metal and organic electrodes". *Applied Physics Letters*, **2008**, 92, 023305.

[106] H. Klauk, G. Schmid, W. Radlik, W. Weber, L. Zhou, C. D. Sheraw, J. a. Nichols and T. N. Jackson. "Contact resistance in organic thin film transistors". *Solid-State Electronics*, **2003**, 47, 297.

[107] Y. Xu, T. Minari, K. Tsukagoshi, R. Gwoziecki, R. Coppard, F. Balestra and G. Ghibaudo. "Power transfer-length method for full biasing contact resistance evaluation of organic field-effect transistors". *Organic Electronics*, **2011**, 12, 2019.

[108] M. Marinkovic, D. Belaineh, V. Wagner and D. Knipp. "On the Origin of Contact Resistances of Organic Thin Film Transistors". *Advanced Materials*, **2012**, 24, 4005.

[109] Y. Xu, R. Gwoziecki, I. Chartier, R. Coppard, F. Balestra and G. Ghibaudo. "Modified transmission-line method for contact resistance extraction in organic field-effect transistors". *Applied Physics Letters*, **2010**, 97, .

[110] C. D. Dimitrakopoulos and D. J. Mascaro. "Organic thin-film transistors: A review of recent advances". *IBM Journal of Research and Development*, **2001**, 45, 11 .

[111] K. Xiao, Y. Liu, G. Yu and D. Zhu. "Influence of the substrate temperature during deposition on film characteristics of copper phthalocyanine and field-effect transistor properties". *Applied Physics A: Materials Science & Processing*, **2003**, 77, 367.

[112] J. Rivnay, L. H. Jimison, J. E. Northrup, M. F. Toney, R. Noriega, S. Lu, T. J. Marks, A. Facchetti and A. Salleo. "Large modulation of carrier transport by grain-boundary molecular packing and microstructure in organic thin films". *Nature Materials*, **2009**, 8, 952.

[113] M. M. Ling and Z. Bao. "Thin Film Deposition, Patterning, and Printing in Organic Thin Film Transistors". *Chemistry of Materials*, **2004**, 16, 4824.

[114] C. D. Dimitrakopoulos, A. R. Brown and A. Pomp. "Molecular beam deposited thin films of pentacene for organic field effect transistor applications". *Journal of Applied Physics*, **1996**, 80, 2501.

[115] J. Xue and S. R. Forrest. "Organic thin-film transistors based on bis(1,2,5-thiadiazolo)-p-quinobis (1,3-dithiole)". *Applied Physics Letters*, **2001**, 79, 3714.

[116] V. Podzorov, S. E. Sysoev, E. Loginova, V. M. Pudalov and M. E. Gershenson. "Single-crystal organic field effect transistors with the hole mobility $\sim$ 8 cm^2/Vs". *Applied Physics Letters*, **2003**, 83, 3504.

[117] L. B. Roberson, J. Kowalik, L. M. Tolbert, C. Kloc, R. Zeis, X. Chi, R. Fleming and C. Wilkins. "Pentacene Disproportionation during Sublimation for Field-Effect Transistors". *Journal of the American Chemical Society*, **2005**, 127, 3069.

[118] Y. Wen, Y. Liu, Y. Guo, G. Yu and W. Hu. "Experimental Techniques for the Fabrication and Characterization of Organic Thin Films for Field-Effect Transistors". *Chemical Reviews*, **2011**, 111, 3358.

[119] M. Mas-Torrent and C. Rovira. "Tetrathiafulvalene derivatives for organic field effect transistors". *Journal of Materials Chemistry*, **2006**, 16, 433.

[120] M.-S. Nam, A. Ardavan, R. J. Cava and P. M. Chaikin. “Intrinsic electronic transport properties of organic field-effect transitors based on single crystalline tetramethyltetraselenafulvalene”. *Applied Physics Letters*, **2003**, 83, 4782.

[121] Y. Takahashi, T. Hasegawa, S. Horiuchi, R. Kumai, Y. Tokura and G. Saito. “High Mobility Organic Field-Effect Transistor Based on Hexamethylenetetrathiafulvalene with Organic Metal Electrodes”. *Chemistry of Materials*, **2007**, 19, 6382.

[122] Naraso, J.-i. Nishida, D. Kumaki, S. Tokito and Y. Yamashita. “High Performance n- and p-Type Field-Effect Transistors Based on Tetrathiafulvalene Derivatives”. *Journal of the American Chemical Society*, **2006**, 128, 9598.

[123] X. Gao, Y. Wang, X. Yang, Y. Liu, W. Qiu, W. Wu, H. Zhang, T. Qi, Y. Liu, K. Lu, C. Du, Z. Shuai, G. Yu and D. Zhu. “Dibenzotetrathiafulvalene Bisimides: New Building Blocks for Organic Electronic Materials”. *Advanced Materials*, **2007**, 19, 3037.

[124] P. Miskiewicz, M. Mas-Torrent, J. Jung, S. Kotarba, I. Glowacki, E. Gomar-Nadal, D. B. Amabilino, J. Veciana, B. Krause, D. Carbone, C. Rovira and J. Ulanski. “Efficient High Area OFETs by Solution Based Processing of a π-Electron Rich Donor”. *Chemistry of Materials*, **2006**, 18, 4724.

[125] C. Kloc, P. G. Simpkins, T. Siegrist and R. A. Laudise. “Physical vapor growth of centimeter-sized crystals of α-hexathiophene”. *Journal of Crystal Growth*, **1997**, 182, 416.

[126] R. A. Laudise, C. Kloc, P. G. Simpkins and T. Siegrist. “Physical vapor growth of organic semiconductors”. *Journal of Crystal Growth*, **1998**, 187, 449.

[127] R. W. I. de Boer, M. E. Gershenson, A. F. Morpurgo and V. Podzorov. "Organic single-crystal field-effect transistors". *physica status solidi (a)*, **2004**, 201, 1302.

[128] Q. Tang, H. Li, M. He, W. Hu, C. Liu, K. Chen, C. Wang, Y. Liu and D. Zhu. "Low Threshold Voltage Transistors Based on Individual Single-Crystalline Submicrometer-Sized Ribbons of Copper Phthalocyanine". *Advanced Materials*, **2006**, 18, 65.

[129] A. L. Briseno, S. C. B. Mannsfeld, X. Lu, Y. Xiong, S. A. Jenekhe, Z. Bao and Y. Xia. "Fabrication of Field-Effect Transistors from Hexathiapentacene Single-Crystal Nanowires". *Nano Letters*, **2007**, 7, 668.

[130] D. Kim, D. Lee, H. Lee, W. Lee, Y. Kim, J. Han and K. Cho. "High-Mobility Organic Transistors Based on Single-Crystalline Microribbons of Triisopropylsilylethynyl Pentacene via Solution-Phase Self-Assembly". *Advanced Materials*, **2007**, 19, 678.

[131] M. Mas-Torrent, M. Durkut, P. Hadley, X. Ribas and C. Rovira. "High Mobility of Dithiophene-Tetrathiafulvalene Single-Crystal Organic Field Effect Transistors". *Journal of the American Chemical Society*, **2004**, 126, 984.

[132] L. Jiang, Y. Fu, H. Li and W. Hu. "Single-Crystalline, Size, and Orientation Controllable Nanowires and Ultralong Microwires of Organic Semiconductor with Strong Photoswitching Property". *Journal of the American Chemical Society*, **2008**, 130, 3937.

[133] L. Jiang, H. Dong and W. Hu. "Organic single crystal field-effect transistors: advances and perspectives". *Journal of Materials Chemistry*, **2010**, 20, 4994.

[134] R. D. McCullough. "The Chemistry of Conducting Polythiophenes". *Advanced Materials*, **1998**, 10, 93.

[135] H. Sirringhaus, P. J. Brown, R. H. Friend, M. M. Nielsen, K. Bechgaard, B. M. W. Langeveld-Voss, A. J. H. Spiering, R. A. J. Janssen, E. W. Meijer, P. Herwig and D. M. de Leeuw. "Two-dimensional charge transport in self-organized, high-mobility conjugated polymers". *Nature*, **1999**, 401, 685.

[136] S. Allard, M. Forster, B. Souharce, H. Thiem and U. Scherf. "Organic Semiconductors for Solution-Processable Field-Effect Transistors (OFETs)". *Angewandte Chemie International Edition*, **2008**, 47, 4070.

[137] G. Wang, J. Swensen, D. Moses and A. J. Heeger. "Increased mobility from regioregular poly(3-hexylthiophene) field-effect transistors". *Journal of Applied Physics*, **2003**, 93, 6137.

[138] H. Chang, P. Wang, H. Li, J. Zhang and D. Yan. "Solvent vapor assisted spin-coating: A simple method to directly achieve high mobility from P3HT based thin film transistors". *Synthetic Metals*, **2013**, 184, 1.

[139] J.-F. Chang, B. Sun, D. W. Breiby, M. M. Nielsen, T. I. Sölling, M. Giles, I. McCulloch and H. Sirringhaus. "Enhanced Mobility of Poly(3-hexylthiophene) Transistors by Spin-Coating from High-Boiling-Point Solvents". *Chemistry of Materials*, **2004**, 16, 4772.

[140] L. Fumagalli, M. Binda, D. Natali, M. Sampietro, E. Salmoiraghi and P. Di Gianvincenzo. "Dependence of the mobility on charge carrier density and electric field in poly(3-hexylthiophene) based thin film transistors: Effect of the molecular weight". *Journal of Applied Physics*, **2008**, 104 084513.

[141] J. Jaczewska, A. Budkowski, A. Bernasik, E. Moons and J. Rysz. "Polymer vs Solvent Diagram of Film Structures Formed in Spin-Cast Poly(3-alkylthiophene) Blends". *Macromolecules*, **2008**, 41, 4802.

[142] R. Winter, M. S. Hammer, C. Deibel and J. Pflaum. "Improvement of the poly-3-hexylthiophene transistor performance using small molecule contact functionalization". *Applied Physics Letters*, **2009**, 95 263313.

[143] E. Mena-Osteritz, A. Meyer, B. M. W. Langeveld-Voss, R. A. J. Janssen, E. W. Meijer and P. Bäuerle. "Two-Dimensional Crystals of Poly(3-Alkyl-thiophene)s: Direct Visualization of Polymer Folds in Submolecular Resolution". *Angewandte Chemie International Edition*, **2000**, 39, 2679.

[144] K. J. Ihn, J. Moulton and P. Smith. "Whiskers of poly(3-alkylthiophene)s". *Journal of Polymer Science Part B: Polymer Physics*, **1993**, 31, 735.

[145] J. A. Merlo and C. D. Frisbie. "Field effect conductance of conducting polymer nanofibers". *Journal of Polymer Science Part B: Polymer Physics*, **2003**, 41, 2674.

[146] J. A. Merlo and C. D. Frisbie. "Field Effect Transport and Trapping in Regioregular Polythiophene Nanofibers". *The Journal of Physical Chemistry B*, **2004**, 108, 19169.

[147] M. Mas-Torrent, D. Den Boer, M. Durkut, P. Hadley and A. Schenning. "Field effect transistors based on poly(3-hexylthiophene) at different length scales". *Nanotechnology*, **2004**, 15, S265.

[148] P. Leclère, E. Hennebicq, A. Calderone, P. Brocorens, A. Grimsdale, K. Müllen, J. Brédas and R. Lazzaroni. "Supramolecular organization in block copolymers containing a conjugated segment: a joint AFM/molecular modeling study". *Progress in Polymer Science*, **2003**, 28, 55.

[149] H. N. Tsao, D. Cho, J. W. Andreasen, A. Rouhanipour, D. W. Breiby, W. Pisula and K. Müllen. "The Influence of Morphology on High-Performance Polymer Field-Effect Transistors". *Advanced Materials*, **2009**, 21, 209.

[150] I. McCulloch, M. Heeney, C. Bailey, K. Genevicius, I. MacDonald, M. Shkunov, D. Sparrowe, S. Tierney, R. Wagner, W. Zhang, M. L. Chabinyc, R. J. Kline, M. D. McGehee and M. F. Toney. "Liquid-crystalline semiconducting polymers with high charge-carrier mobility". *Nature Materials*, **2006**, 5, 328.

[151] A. Facchetti. "Semiconductors for organic transistors". *materialstoday*, **2007**, 10, 28.

[152] D. Natali and M. Caironi. "Charge injection in solution-processed organic field-effect transistors: physics, models and characterization methods." *Advanced materials (Deerfield Beach, Fla.)*, **2012**, 24, 1357.

[153] J. Shackelford. *Introduction to materials science for engineers*. Pearson Prentice Hall, **2009**.

[154] D. Chung. *Composite Materials: Science and Applications*. Engineering Materials and Processes. Springer, **2010**.

[155] J. Smith, R. Hamilton, I. McCulloch, N. Stingelin-Stutzmann, M. Heeney, D. D. C. Bradley and T. D. Anthopoulos. "Solution-processed organic transistors based on semiconducting blends". *J. Mater. Chem.*, **2010**, 20, 2562.

[156] H. Hoppe and N. S. Sariciftci. "Organic solar cells: An overview". *Journal of Materials Research*, **2004**, 19, 1924.

[157] J. N. Smith, J. G. Labram and T. D. Anthopoulos. *Semiconducting Organic Molecule/Polymer Composites for Thin-Film Transistors*, pages 219 249. Wiley-VCH Verlag GmbH & Co. KGaA, **2012**.

[158] W. H. Lee and Y. D. Park. "Organic Semiconductor/Insulator Polymer Blends for High-Performance Organic Transistors". *Polymers*, **2014**, 6, 1057.

[159] Y.-H. Kim, J. E. Anthony and S. K. Park. "Polymer blended small molecule organic field effect transistors with improved device-to-device uniformity and operational stability". *Organic Electronics*, **2012**, 13, 1152.

[160] A. D. Scaccabarozzi and N. Stingelin. "Semiconducting:insulating polymer blends for optoelectronic applications - A review of recent advances". *Journal of Materials Chemistry A*, **2014**, 2, 10818.

[161] A. Babel and S. A. Jenekhe. "Morphology and Field-Effect Mobility of Charge Carriers in Binary Blends of Poly(3-hexylthiophene) with Poly[2-methoxy-5-(2-ethylhexoxy)-1,4-phenylenevinylene] and Polystyrene". *Macromolecules*, **2004**, 37, 9835.

[162] M.-B. Madec, J. J. Morrison, V. Sanchez-Romaguera, M. L. Turner and S. G. Yeates. "Organic field effect transistors from ambient solution processed poly(triarylamine)-insulator blends". *J. Mater. Chem.*, **2009**, 19, 6750.

[163] J. Park, S. Lee and H. H. Lee. "High-mobility polymer thin-film transistors fabricated by solvent-assisted drop-casting". *Organic Electronics*, **2006**, 7, 256 .

[164] F. C. Krebs. "Fabrication and processing of polymer solar cells: A review of printing and coating techniques". *Solar Energy Materials and Solar Cells*, **2009**, 93, 394 . Processing and Preparation of Polymer and Organic Solar Cells.

[165] S.-Y. Zhang, M. D. Regulacio and M.-Y. Han. "Self-assembly of colloidal one-dimensional nanocrystals." *Chemical Society reviews*, **2014**, 43, 2301.

[166] C. Liu, Y. Li, M. V. Lee, A. Kumatani and K. Tsukagoshi. "Self-assembly of semiconductor/insulator interfaces in one-step spin-coating: a versatile

approach for organic field-effect transistors". *Phys. Chem. Chem. Phys.*, **2013**, 15, 7917.

[167] C. Lawrence. "The mechanics of spin coating of polymer films". *Physics of Fluids (1958-1988)*, **1988**, 31, 2786.

[168] C.-C. Yang, J. Y. Josefowicz and L. Alexandru. "Deposition of ultrathin films by a withdrawal method". *Thin Solid Films*, **1980**, 74, 117 .

[169] J. Koo, J. Lee and C. Jung. "Planarization during spray coating: numerical study". *Journal of Micromechanics and Microengineering*, **2008**, 18, 1.

[170] A. B. Ross, S. K. Wilson and B. R. Duffy. "Blade coating of a power-law fluid". *Physics of Fluids*, **1999**, 11, 958.

[171] R. Pfattner, M. Mas-Torrent, I. Bilotti, A. Brillante, S. Milita, F. Liscio, F. Biscarini, T. Marszalek, J. Ulanski, A. Nosal, M. Gazicki-Lipman, M. Leufgen, G. Schmidt, L. W. Molenkamp, V. Laukhin, J. Veciana and C. Rovira. "High-Performance Single Crystal Organic Field-Effect Transistors Based on Two Dithiophene-Tetrathiafulvalene (DT-TTF) Polymorphs". *Advanced Materials*, **2010**, 22, 4198.

[172] M. Mas-Torrent, S. Masirek, P. Hadley, N. Crivillers, N. Oxtoby, P. Reuter, J. Veciana, C. Rovira and A. Tracz. "Organic field-effect transistors (OFETs) of highly oriented films of dithiophene-tetrathiafulvalene prepared by zone casting". *Organic Electronics*, **2008**, 9, 143.

[173] J. M. Williams, J. R. Ferraro, R. J. Thorn, K. D. Carlson, U. Geiser, H. H. Wang, A. M. Kini and M. H. Wangbo. *Organic Superconductors (Including Fullerenes) : Synthesis, Structure, Properties, and Theory*. Prentice Hall, Englewood Cliffs, New Jersey, **1992**.

[174] M. Mas-Torrent, P. Hadley, S. T. Bromley, X. Ribas, J. Tarrés, M. Mas, E. Molins, J. Veciana and C. Rovira. "Correlation between Crystal Structure and Mobility in Organic Field-Effect Transistors Based on Single Crystals of Tetrathiafulvalene Derivatives". *Journal of the American Chemical Society*, **2004**, 126, 8546.

[175] P. T. Kissinger and W. R. Heineman. "Cyclic voltammetry". *Journal of Chemical Education*, **1983**, 60, 702.

[176] J. Yamada and T. Sugimoto (Eds.). *TTF Chemistry. Fundamentals and Applications of Tetrathiafulvalene*. Kodansha Springer, **2004**.

[177] X. Gao, W. Qiu, Y. Liu, G. Yu and D. Zhu. "Organic field-effect transistors based on tetrathiafulvalene derivatives". *Pure and Applied Chemistry*, **2008**, 80, 2405.

[178] B. Noda, M. Katsuhara, I. Aoyagi, T. Mori, T. Taguchi, T. Kambayashi, K. Ishikawa and H. Takezoe. "Organic Field-effect Transistor Based on Biphenyl Substituted TTF". *Chemistry Letters*, **2005**, 34, 392.

[179] Naraso, J.-i. Nishida, S. Ando, J. Yamaguchi, K. Itaka, H. Koinuma, H. Tada, S. Tokito and Y. Yamashita. "High-Performance Organic Field-Effect Transistors Based on π-Extended Tetrathiafulvalene Derivatives". *Journal of the American Chemical Society*, **2005**, 127, 10142.

[180] F. Otón, R. Pfattner, N. S. Oxtoby, M. Mas-Torrent, K. Wurst, X. Fontrodona, Y. Olivier, J. Cornil, J. Veciana and C. Rovira. "Benzodicarbomethoxytetrathiafulvalene derivatives as soluble organic semiconductors". *Journal of Organic Chemistry*, **2011**, 76, 154.

[181] F. Otón, V. Lloveras, M. Mas-Torrent, J. Vidal-Gancedo, J. Veciana and C. Rovira. "Coupling tetracyanoquinodimethane to tetrathiafulvalene: A

fused TCNQ-TTF-TCNQ triad". *Angewandte Chemie - International Edition*, **2011**, 50, 10902.

[182] F. Otón, R. Pfattner, E. Pavlica, Y. Olivier, E. Moreno, J. Puigdollers, G. Bratina, J. Cornil, X. Fontrodona, M. Mas-Torrent, J. Veciana and C. Rovira. "Electron-withdrawing substituted tetrathiafulvalenes as ambipolar semiconductors". *Chemistry of Materials*, **2011**, 23, 851.

[183] M. Mas-Torrent, P. Hadley, S. T. Bromley, N. Crivillers, J. Veciana and C. Rovira. "Single-crystal organic field-effect transistors based on dibenzo-tetrathiafulvalene". *Applied Physics Letters*, **2005**, 86, 012110.

[184] R. Pfattner, M. Mas-Torrent, C. Moreno, J. Puigdollers, R. Alcubilla, I. Bilotti, E. Venuti, A. Brillante, V. Laukhin, J. Veciana and C. Rovira. "Organic metal-organic semiconductor blended contacts in single crystal field-effect transistors". *Journal of Materials Chemistry*, **2012**, 22, 16011.

[185] I. Doi, E. Miyazaki, K. Takimiya and Y. Kunugi. "Development of N-Alkyl-Substituted Bis(pyrrolo[3,4-d])tetrathiafulvalenes as Organic Semiconductors for Solution-Processible Field-Effect Transistors". *Chemistry of Materials*, **2007**, 19, 5230.

[186] X. Gao, W. Wu, Y. Liu, W. Qiu, X. Sun, G. Yu and D. Zhu. "A facile synthesis of linear benzene-fused bis(tetrathiafulvalene) compounds and their application for organic field-effect transistors". *Chemical Communications*, **2006**, 26, 2750.

[187] T. Marszalek, A. Nosal, R. Pfattner, J. Jung, S. Kotarba, M. Mas-Torrent, B. Krause, J. Veciana, M. Gazicki-Lipman, C. Crickert, G. Schmidt, C. Rovira and J. Ulanski. "Role of geometry, substrate and atmosphere on

performance of OFETs based on TTF derivatives". *Organic Electronics: physics, materials, applications*, **2012**, 13, 121.

Chapter 2

Statement of Problem and Objectives

Currently, there is a myriad of organic semiconductors (OSC) applied in organic field-effect transistors (OFETs), but commonly they lack stability and processability into large areas. Semiconductors based on tetrathiafulvalene (TTF) derivatives and polymeric semiconductors like poly-(3-hexyl-thiophene) (P3HT) are very attractive candidates to OFETs, yet often very susceptible to degradation as semiconductor by oxygen and water. Occluding them from beyond-the-lab applications, and devoid methods of fabrication primarily one-step procedures, that append stability and processability over large areas to the attractiveness that TTF derivatives and P3HT possess as OSC. The semiconductors may be shut down as potential candidates for OFETs, then semiconductors deprecated, with their full potential unexplored. Semiconductors do not posses intrinsic barriers to environmental agents which affect their performance. Also, actual fabrication technologies lacks the option to allow the organic semiconductor to self-encapsulate into a protective host.

The main objective of this Thesis is to fabricate organic field-effect transistors using as an active material a blend of a high performing organic semiconductor within a polymeric matrix. The motivation is to invigorate the processability in solution, and lower the cost of the device. Additionally, the matrix might provide an enhanced stability of the device in air and moisture.

As organic semiconductors were chosen poly - (3 hexylthiophene) and tetrathiafulvalene derivatives. These materials are known to have high performance as active material in OFETs, although often they can be easily doped.

As polymeric matrices we choose low molecular weight atactic polystyrenes, isotactic polystyrene, poly-(α-methyl-styrene), and poly-(methyl-methacrylate) which are commercially available and are low cost insulating polymers.
In particular, the following goals have been pursued:

- Develop an easy yet robust coating technique to successfully deposit polymeric and composite nanofilms on bare $Si\ SO_x$ substrates and $Si\ SO_x$ substrates with gold electrodes.

- Fabrication and characterisation of OFETs using different blends compositions of organic semiconductor/insulating polymer with different proportions to optimise the most suitable formulation.

- With the most promising blend, an in-depth study of the electrical properties and an exploration of the potential for OFET applications has been carried out.

Chapter 3

Experimental Methods and Materials

3.1 Materials

- **Dibenzo-Tetrathiafulvalene (DB-TTF)** was purchased from Sigma-Aldrich and used as received.
- **Dithiophene-Tetrathiafulvalene (DT-TTF)** was synthesized in our group as described in reference[1].
- **Bis(ethylenethio) - Tetrathiafulvalene (BET-TTF)** was synthesized in our group as previously reported[2] .
- **Poly (bis(4-phenyl) (2,4,6-trimethylphenyl)amine) (PTAA)** was purchased from Sigma-Aldrich and used as received.
- **Poly-(3-hexyl thiophene-2,5-diyl) (P3HT)** was purchased from BASF * and used as received without further purification.
- **Poly (α methyl styrene) (PAMS)** M_w = 10000 g/mol was purchased from Sigma-Aldrich and used as received.

---

*BASF sells this type of P3HT under the brand Sepiolid P200.

- **Isotactic Polystyrene (iPS)** M_w = 400000 g/mol was purchased from Sigma-Aldrich and used as received.

- **Atactic Polystyrene (PS280k)** M_w = 280000 g/mol was purchased from Sigma-Aldrich and used as received.

- **Polystyrene for GPC 10000 (PS10000)** was purchased from Sigma-Aldrich and used as received.

- **Polystyrene for GPC 3000 (PS3000)** was purchased from Sigma-Aldrich and used as received.

- **Polystyrene for GPC 1000 (PS1000)** was purchased from Sigma-Aldrich and used as received.

- **Poly-(methyl-methacrylate) (PMMA)** M_w = 100000 g/mol purchased from Polysciences and used as received.

- **Shipley Microposit S1813** Microposit S1800 Series Photo Resists were purchased from Shipley.

- **Shipley Microposit MF-319 Developer** for use with S1400 and S1800 Series photo resists was purchased from Shipley.

- **Silicon substrates** with 200 nm SiO_x dielectric were purchased from Si-mat Germany.

- **Fraunhofer substrates** were purchased from Fraunhofer Institute, Germany. Each chip has 4 transistors L = 2.5 μm, W = 10 mm, 4 transistors L = 5 μm, W = 10 mm, 4 transistors L = 10 μm, W = 10 mm, and 4 transistors L = 20 μm, W = 10 mm. Gate Oxide: 230 ± 10 nm SiO_2 made by thermal oxidation, and source drain electrodes are composed of ITO/Au 10/30 nm.

- **Shadow Mask E2011 and stack E191** for deposition of top contact electrodes were purchased from Ossila. This mask includes channel lengths of 30 μm, 40 μm, 50 μm, 60 μm, 80 μm and 100 μm. The W is equal to 4 mm and it is constant.

3.2 Instrumentation

- **Viscosity measurements**. All viscosity measurements were carried out using a Haake rheostress RS600 from Thermo Electron Corporation.

- **Atomic force microscopy (AFM).** Images were recorded using an 5500LS SPM system from Agilent Technologies. All samples were analysed in tapping mode.

- **Contact angle.** All contact angle measurements were carried out at room temperature by the sessile drop method. Typically 5 μl mili-q was used, using a DSA 100 from Krüss.

- **Optic microscopy.** Polarized optical microscopy images were taken with an Olympus BX51 (Japan), which includes filters to polarize the incident light and an analyser to study the crystalline nature of samples.

- **X-Ray diffraction.** X-ray diffraction measurements were carried out with a diffractometer equipped with a rotating anode source from Rigaku Company. A focus line X-ray beam (Cu Kα) was collimated by a parabolic graded multilayer mirror placed in front of the sample and a double slits were mounted before the detector to achieve the required angular resolution.

- **Scanning electron microscopy (SEM) and energy dispersive x-ray analysis (EDX).** Imaging of the composites were performed on a SEM FEI

QUANTA 200 FEG-ESEM equipped with a dispersive energy spectrometer EDX-LINK ISIS 200, system from Oxford Instruments, Bucks, England.

- **Secondary ion mass spectroscopy with time of flight detection (ToF-SIMS)[†].** Sputter etching of the surface was accomplished with the Cs^+ beam, using the 2 keV and 1keV energy settings raster over a $300\mu m$ x $300\mu m$ area. A pulsed beam of 25 keV Bi1 ions scanned over a $50\mu m$ x $50\mu m$ region centred within the sputtered area was used to generate secondary ions for analysis in positive ion mode. Analysis cycle time was $100\mu s$ and sputtering cycle was 1s and 1000ms flood gun compensation. A high current beam of low energy (<20 eV) electrons was employed for charge compensation. Negative ions were analysed.

- **Focused ion beam scanning electron microscopy (FIB-SEM).** Imaging and cross section cut were performed in a Focused Ion Beam Zeiss Neon40 .

- **Metal Evaporators.** All metal evaporations were carried out using an auto 306 from Boc Edwards.

- **Laser micro-writer.** MicroWriter ML from Durham Magneto Optics LTD. which is a direct-write laser photolithography machine was used for patterning electrodes.

- **Organic Evaporators.** An Univex 350 system designed for organic semiconductors and mounted inside a Glove Box from Jacomex was employed. Also a house-made evaporator designed for organic semiconductors was used at Universitat Politècnica de Catalunya.

[†] Analysis made at Plataforma de Nanotecnología Institut de Bioenginyeria de Catalunya (IBEC).

Analysis performed at Centre de Recerca en Nanoenginyeria (CRnE) @ Universitat Politècnica de Catalunya.

[§] O_2 and H_2O below 2 and 3 ppm respectively.

- **Spin Coater.** Spin coating was carried out using a Laurell Technologies model WS-650SZ-6NPP/LITE, located in a 10000 class clean room.

- **Bar coater.** All solution shearing was carried out with a custom RK101 applicator from RK print coat applications.

3.3 Electrode Fabrication and Sample Preparation

- **Electrode fabrication of bottom contact OFETs.** Laser lithography was carried out in a clean room class 10000 (see Figure 3.1). Pristine Wafers straight from its box were used. A flux of nitrogen was used to remove any possible particle. Then the wafer was carefully placed on a hot plate held at 95 ^oC for at least ≈ 15 min. Then, the wafer was removed from the hot plate and placed in the spin coater, where another flux of nitrogen was applied in order to remove any possible residual particle. Immediately the resist at room temperature was carefully poured on the substrate in order to evade bubble formation. Then, resist spun casted at velocity: 83.33 %, acceleration: 0.7, and time: 25 s. After spin coating, the substrate was removed and placed on a hot plate at 95 ^oC for 60 seconds. Further, the substrate was removed from the hot plate and transferred to the MicroWriter machine. All motifs were previously drawn using CleWin Software. The substrate was manually aligned using as reference the vacuum chuck and the holder itself. The first step was to focus the substrate, to do so the wafer chuck was switched on and microscope lamp switched on. An approximated value for the wafer thickness was given, such value took care of both the substrate thickness and the resist thickness. Then the autofocus option was selected. When the autofocus optimisation algorithm finished, autofocus results were checked, and observed a curve with a single local maximum. The next step was the sample alignment, three corners were chosen. The value for angle correction was observed which had to be close to zero. The writing of the electrode pattern were performed with the dose value (135 - 150 mJ/cm^2). Sample development was carried out filling a beaker with developer and immersing substrates immersed for 45 s. Subsequently, the substrates were loaded in the metal evaporator and 4 nm of Cr and 40 nm of Au at deposition rates of 0.1-0.5 Å/s and 2-5 Å/s respectively, were thermally evaporated.

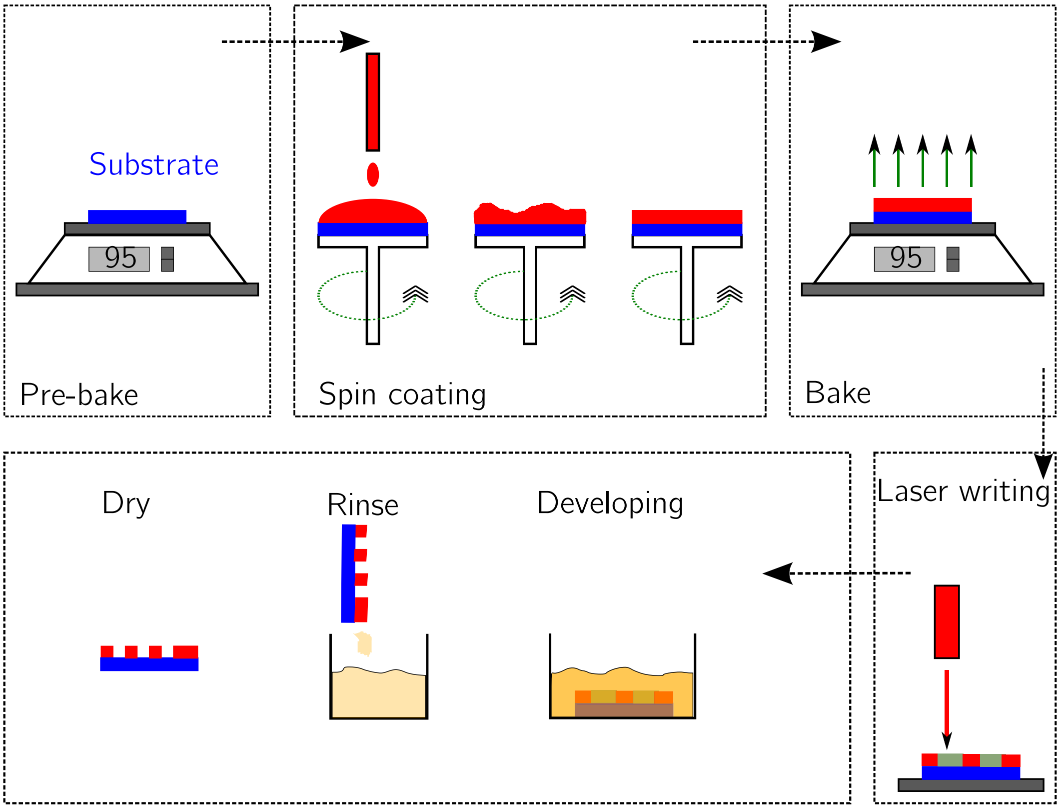

Figure 3.1 *Lithography experimental procedure scheme.*

- **Electrode fabrication of top contact OFETs.** Metal electrodes on organic thin films were deposited through a shadow mask from Ossila at a pressure less than 10^{-6} mbar. The film thickness and evaporation rate were monitored by a quartz crystal microbalance. For source/drain contacts, 50-80 nm of gold were deposited through a shadow mask.

- **Substrate Cleaning.** Substrates were used immediately after gold lift off, and flushed with acetone and isopropanol, both HPLC grade. However, if the substrates were left much time in ambient conditions, then they were cleaned with a sequence of solvents (chloroform, dichloromethane, toluene, acetone, ethanol and isopropanol) and subsequently placed in an ozone cleaner for 20-30 min, left to passivate, and used. Another possible case scenario was when substrates were re-used. In such case the same sequence of solvents than before was used. After isopropanol rinsing, substrates were dried under nitrogen and immediately dipped in nitric acid for 5-10 min. If the nitric acid could not remove the material deposited, piranha solutions were used, but in such case the dipping time did never exceed 5 min. After, acid treatment the substrates were flushed with plenty of water, dried with N_2 and left to passivate.

- **Preparation of an octadecyltrichlorosilane (OTS) self-assembled monolayer.** Substrates were first pre-cleaned in a series of solvents: chloroform, dichloromethane, toluene, acetone, ethanol and isopropanol, then cleaned by UV/ozone for 30 minutes, next immersed in $H_2SO_4 : H_2O_2$ (3:1, 15 minutes). When the substrate had gold electrodes and the sticking layer was not strong enough, this step was reduced in time or avoided. When the previous step was avoided, then after the UV/Ozone cleaning/activation was made, the substrates were removed and immersed in vials containing ethanol HPLC grade. Then the substrates were flushed with isopropanol HPLC grade, and finally dried with nitrogen and immediately loaded in a vacuum/hot plate. Along with substrates (see Figure 3.2), a crucible or watch glass with a 100 -200 μl of OTS were also loaded to the chamber. Vacuum were applied ($< -70\,cmHg$) and samples were heated to 120^oC. When the first bubbles of OTS were observed, the vacuum line was closed and the pump switched off. The samples were left at this temperature for 2 hours. Afterwards, samples left to cool down to room temperature. When room temperature was reached, samples were immersed in vials with toluene HPLC grade, and sonicated for at least 15 minutes. Then, the substrates were flushed with copious acetone, isopropanol and finally dried under a flux of nitrogen.

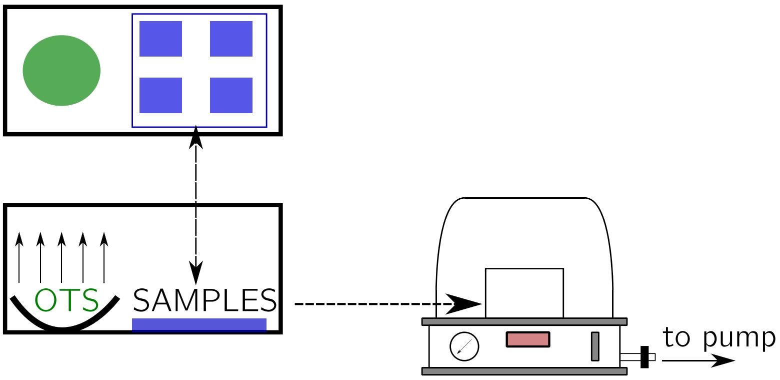

Figure 3.2 *Experimental setup for vapor phase deposition of octadecyltrichlorosilane (OTS).*

- **Materials solutions.** All polymeric solutions were prepared the day before coating and left stirring overnight, unless is stated. All solutions of semiconductors were prepared before each coating procedure, unless is stated, and bubbled a few seconds with Ar.

- **Solution deposition of polymers or organic semiconductors.**

  Spin coating. First a volume of chloroform was dropped on the substrate and spun coated, to remove any residue. Then the desired solution was spun coated. Specific details about speed and time will be given at the respective section or chapter.

  Solution sheering. Solutions were prepared typically at a concentration of 2 %wt in chlorobenzene ¶. Both the substrate and the shearing bar were held in place by respective height positioners while the substrate placed by

---

¶If concentration or solvent changes will be clearly stated in the respective section or chapter.

manual alignment on a heating stage. The gap distance between the device substrate and the sheering bar was fixed at $\approx 300\ \mu m$. The shearing bar was moved at constant velocity of 1 cm/s, unless otherwise is clearly stated. The resulting sheared film was immediately removed, and placed in a desiccator at P < -50 cm Hg and 60 ^oC for at least 2 hours, to remove residual solvent.

- **Evaporated thin films of DB-TTF and BET-TTF.** DB-TTF was evaporated at Institut de Ciencia de Materials de Barcelona at a rate of 1 Å/s, at 105 ^oC and Pressure P = 1x10^{-6} mbar using an Univex 350 G, while BET-TTF was evaporated at Universitat Politècnica de Catalunya using an house-made thermal evaporator at a rate of 0.5 Å/s and at 120 ^oC while the pressure wast kept at $1x10^{-6}$ mbar.

3.4 Electrical characterization

- **Organic Field-Effect Transistor (OFET).** The electrical characterization of samples was carried out inside a Süss probe station using a Keithley 2612A two channel source meter. Micro manipulators for easy contacting small electrode pads, were connected via BCN to the Keithley. The Keithley is finally controlled by a PC, with an interface written in MATLAB [†]. All measurements were carried out in ambient conditions.

- **OFETs Temperature dependence measurements [**].** Measurements were carried out inside a cryogenic vacuum probe station with optical port from Lakeshore for optical device characterization. Temperature were controlled by a Lakeshore temperature controller through a LabView interface. Electrical characteristics were recorded using a Keithley semiconductor parameter

---

[†] Software written by Dr. Raphael Pfattner

[**] Measurements carried out at Linköping University, at Prof. Magnus Berggren laboratory in close collaboration with Dr. Simone Fabiano.

analyser. After loading samples inside the cryogenic probe station. Vacuum was applied using a turbo molecular pump. Both temperatures, substrate and chamber, were left to stabilise to room temperature. Then, allowing a flux of nitrogen the temperature of the sample and chamber were allow to gradually decrease to 85 K at steps of 10 K. Important, at each step was procured to record a transfer characteristics at saturation an linear regimes when substrate and chamber temperatures were close enough to each other.

- **Mesurements of inverters.** For inverters measurements a Keithley 2400 was used to supply the voltage V_{DD} while the voltages V_{in} and V_{out} were measured using a Keithley 2612A. Both controlled by a MATLAB code.

3.5 Extraction of device parameters

- **Mobility.** The mobility was extracted from the linealized curve $\sqrt{I_{SD}}$ versus V_{SG} at saturation regimes by a linear fit from which the slope is equal to $\sqrt{W\ 2L C_i \mu_{FE}}$.

- **Threshold Voltage.** The threshold voltage was extracted from the same fit than the mobility, using the intercept of the straight line, which is equal to $-\sqrt{W\ 2L C_i \mu_{FE}} V_{TH}$.

- **Mobility profiles.** The mobility profiles as a function of the gate were extracted using numerical derivatives by finite differences, detailed equations at Appendix E.

- **Gain.** The gain for inverters was calculated using numerical finite differences using equations E.1 E.2.

Bibliography

[1] N. Crivillers, N. S. Oxtoby, M. Mas-Torrent, J. Veciana and C. Rovira. “Improved synthesis of the high-mobility organic semiconductor dithiophene-tetrathiafulvalene”. *Synthesis*, **2007**, 1, 1621.

[2] C. Rovira, J. Veciana, N. Santalo, J. Tarres, J. Cirujeda, E. Molins, J. Llorca and E. Espinosa. “Synthesis of Several Isomeric Tetrathiafulvalene .pi.-Electron Donors with Peripheral Sulfur Atoms. A Study of Their Radical Cations”. *The Journal of Organic Chemistry*, **1994**, 59, 3307.

Chapter 4

Development of a solution deposition technique for insulating and semiconducting polymers

4.1 Introduction

There is on going interest in reproducible fabrication techniques of nano- and micro-scale films for their use in photonic crystals, optoelectronic devices, sensors, coatings, organic field-effect transistors and other applications. A vast top-down techniques involving vacuum-based vapor deposition, lithographic etching, or chemical etching are used to make such materials. In such processes the use of large, energy intensive machinery (vacuum chambers, electron guns, ion sources, etc.) in order to make very small features is mandatory. Polymer solutions are often coated. The dominant microstructural features of a solution of a linear polymer are the length and stiffness of the polymer chain, these features control the degree of molecular entanglement. The degree of stiffness of the polymer dissolved in the solvent ranges from low, as in aqueous solutions of polyethylene oxide, to high, as in solutions of xanthan, and will depend on the nature of solvent surrounding the molecules, on the concentration and molecular weight of polymer. The concentrations range from few parts per million, as in some specialised precision coating operations, to almost pure polymer, as in hot-melt coating of low-molecular weight adhesives[1,2]. Similarly, the viscosity (η) of many polymeric solutions is located over a wide range of values ($\eta < 10mPas$ and $10mPas < \eta < 100000mPas$), and is strongly dependent on molecular weight, and concentration. The viscosity should be tuned to match the technological requirements of the desired deposition method (i.e. inkjet printing $\eta < 10mPas$)[3].

In the field of organic electronics, insulating and semiconducting films are mainly deposited on substrates by spin coating, drop casting or bar coating. Insulating organic polymers such as polystyrene (PS), poly(methyl methacrylate) (PMMA), poly(vinyl phenol) (PVP), and poly(vinyl alcohol) (PVA), to name a few, are spin-coated on substrates and have been employed as dielectrics in organic devices[4–7]. Also, organic semiconducting polymers have been deposited from solution. In particular Organic Field-Effect Transistors (OFETs) based on poly(3-hexylthiophene) (P3HT), which is a well known semiconducting material which has been deeply studied, were fabricated and reported in the literature using a vast number of techniques[8–17]. The mobility of P3HT OFETs processed from a chloroform solution has been reported as high as 0.1 $cm^2V^{-1}s^{-1}$[18]. Such high mobility value was attributed to the high molecular ordering in the polymer films due to the preferred orientation of regioregular P3HT chains. Based on x-ray analysis, it was attributed that the backbone of regioregular P3HT was parallel to the substrate while the hexyl side chains were normal to the substrate. This preferred orientation allows high mobility in this direction to occur.

In this chapter, a novel method was developed to deposit high quality thin films of insulating and semiconducting polymers. This method is driven by solvent evaporation, and a moving bar over a fixed substrate and it is shown to be simple, yet robust. First, the technique is demonstrated using solutions of polystyrene on

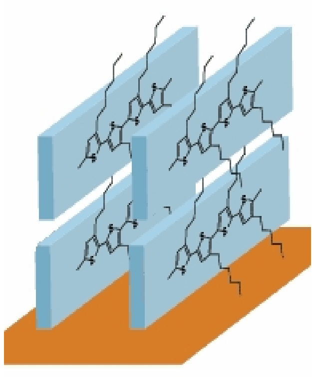

Figure 4.1 *Lamellar of a poly(3-hexylthiophene) film on a substrate. Image taken from SigmaAldrich website.*

Si SiO_x. Secondly, the technique is applied to form semiconducting films of P3HT blended with polystyrene, which are characterized as organic field-effect transistors. We demonstrate that the devices fabricated show excellent performance.

4.2 Convective deposition

Deposition of micro- and nano-particles on substrates is relevant in the manufacture of many appliances, i.e. conductive and antireflective functional coatings, surface-enhanced Raman scattering substrate, photolithography, among many others[19]. Several techniques have been developed to fabricate particle coatings and thin films, among those convective deposition is probably the most convenient and efficient if compared with dip-coating, or spin coating[20]. Convective deposition is a typical multiphysics transport process which is driven by the solvent evaporation of a restricted meniscus, so fluid dynamics, mass and heat transfer come into play in a small while deforming domain. The deposition is governed by an inward flux from a dragged evaporating meniscus which compensates the evaporation at the boundary when solidification occurs. Molecules transported towards the liquid-solid interface feed the growth of a continuous crack-free homogeneous film. In other words, particles move to the meniscus veil periphery due to the horizontal dragging movement accumulating themselves as a well packed nano film[19,21–24]. The convective self-assembly occurs due to evaporation from a wetting film, from a Newtonian liquid, and the thickness of the resulting film is a function of fluid properties (i.e. surface tension σ, viscosity μ, and density ρ), gravity g, withdrawal velocity U and meniscus radius of curvature r.

$$\frac{h}{l} = f(Ca\ Re\ Go) \tag{4.1}$$

where $l = \sqrt{\sigma\ \ \rho g}$ is the capillary length, $Ca = \mu U\ \ \sigma$ is the capillary number, $Re = \rho U h\ \ \mu$ is the Reynold number, and Go = r/l is the Goucher number[25]. Despite the process can be described by two different regimes: i) evaporative and ii) wetting film (Landau regime). Both regimes can occur in a very short time span, suggesting an unsteady multiphysics process.

Here, a novel convective deposition technique, namely Bar Assisted Meniscus Shearing (BAMs) has been developed. This work is based in pure experimental research, because the theoretical and numerical study to investigate the flow field within the fluid domain by which particles/molecules are transported to receding line is out of the scope of this thesis work. It is noticeable that the method here described is altered from the traditional convective (or evaporation-induced) self-assembly since instead of using a blade, a rod (bar) is used. Further, other parameters such as temperature, velocity, bar height, and concentration have been optimised. A very simple scheme of the BAMs process is depicted in Figures 4.2, and 4.3. The substrate is placed on a heated stage below a bar, which is located at a distance H from the bed surface, and a small volume of solution is placed in the space formed by the substrate top surface and the nadir of the bar depicted in Figure 4.2 (left). Capillary forces held the solution in place until the bar is moved. Then, the bar is withdrawn at a constant velocity v_w, dragging the solution while forming a thin wetting film attached to the solution still confined between the moving bar and the static substrate (see Figure 4.3).

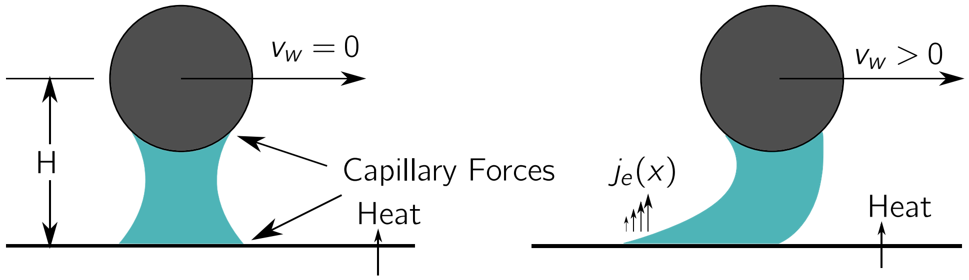

Figure 4.2 *Illustration of how the solution is held together between the substrate and the bar (left) and how the process starts to form the film (right). H: height,* v_w *withdrawing velocity and* $je(x)$ *rate of solvent evaporation.*

Evaporation mainly produced by the heat exchanged between the heating bed and the substrate and the mass transfer between solution and air, induces a flow of solvent (J_w) toward the interface substrate solution.

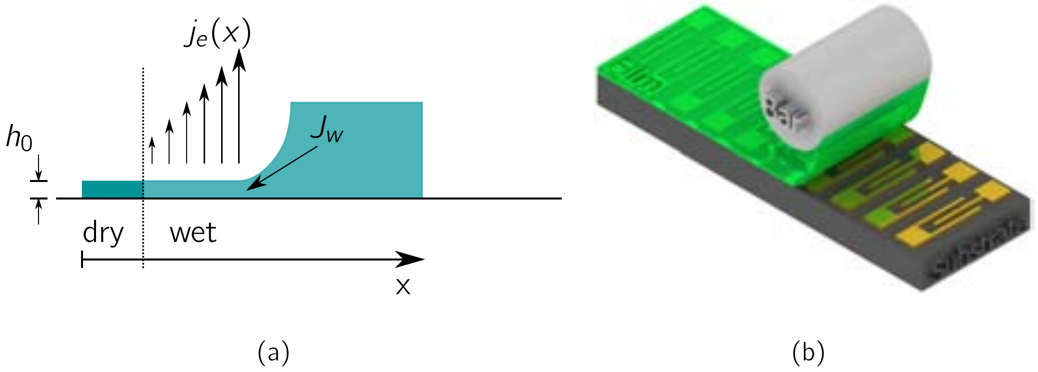

(a) (b)

Figure 4.3 *(a) Illustration of how the restricted meniscus moves forming a film, and how a thin wet film is produced before a dried thin solid film is finally produced in one step, and (b) 3D representation of the coating process.*

Molecules are pulled with the flow, which drives the growth of a thin polymeric layer[20,26–34]. The meniscus is restricted between the bar and the substrate, so the contact line of the fluid meniscus provokes a convective self-assembly of a film that forms as the bar moves and can range from a few nanometers to few microns thick depending on the film viscosity selected according to the desired application.

Using a simple abstraction based on the concept of a mass balance (Equation 4.2) and assuming steady state[29] where solvent evaporates from the film at a rate

$j_e(x)$ while a mass flux of molecules that grow $\dot{m}_{mol}^{surf}$ on the surface is giving the thickness h_0 in the dried film, it can be deduced:

$$\cancelto{0}{\frac{dM}{dt}} = \dot{m}_{in} - \dot{m}_{out} + \cancelto{0}{\dot{m}_{generation}} - \cancelto{0}{\dot{m}_{consumption}} \tag{4.2}$$

$$\dot{m}_{out} = j_e(x) + \dot{m}_{mol}^{surf} \tag{4.3}$$

$$\dot{m}_{in} = J_W \tag{4.4}$$

Equating equations 4.4 and 4.3 one can end with equation 4.5

$$J_W = j_e(x) + \dot{m}_{mol}^{surf} \tag{4.5}$$

Deposition of films has been carried out using a bar coater film applicator the basic scheme of which is depicted in Figure 4.4.

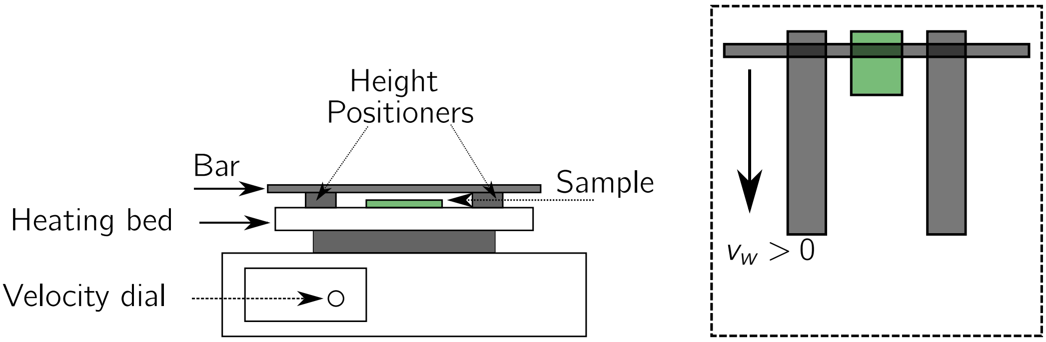

(a) (b)

Figure 4.4 *Machine scheme (a) front view and (b) top view.*

4.3 Deposition of Insulating Polymers

In this section, using substrates of Si/SiO_x previously cleaned using a sequence of solvents (chloroform, dichloromethane, toluene, acetone, ethanol and isopropanol) were carefully placed on the heated bed of the bar coater machine as depicted in Figure 4.4. Solutions of Polystyrene (PS10000 see Materials in Chapter 3) at 3% wt and 4% wt in chlorobenzene were prepared the day before the deposition, leaving to dissolve overnight. The machine was set at 105 ^{o}C and left to stabilize for at least 15 minutes. The substrates were blown with nitrogen right before the deposition, and manually aligned with the bar until the edge of the substrate was right below the lowest part of the bar. Immediately, with a micropipette $\approx 50\mu l$ of the PS10000 solution previously held at $105^{o}C$ were dispensed and the bar was withdrawn at 1 cm/s. The film was immediately formed below the bar and behind it. The coated substrate was removed immediately after deposition. Since chlorobenzene has a high boiling point, substrates were placed in a vacuum/hot plate at 60 ^{o}C and $P_{vac} = 93kPa$ in order to remove residual solvent for at least 1 hour. The withdrawal velocity was chosen as the highest possible without having problems of film adhesion to the surface in order to form homogeneous and continuous film. Further, the temperature was selected to allow fast evaporation without provoking pinholes or surface damage. These two parameters are crucial in order to produce high quality nanofilms. The thickness of the films was mainly controlled by the solution viscosity.

4.3.1 Surface Morphology

Uniform, pinhole and crack free films of polystyrene could be deposited by BAMs using a restricted continuously deforming meniscus. Tapping mode atomic force microscope (AFM) images of the surface of polystyrene film from starting concentrations of 3 % wt and 4 % wt in chlorobenzene both deposited at $105^{o}C$ on $Si\ \ SiO_x$ substrates are shown in Figures 4.5(a) and 4.5(b), respectively. Thickness equal to: $49 \pm 0\ 8nm$ for solution of polystyrene at 3% wt and $78 \pm 1nm$ for solutions of polystyrene at 4 % wt, are depicted in Figure 4.6.

Very smooth surfaces are evident for both concentrations of polystyrene, be-

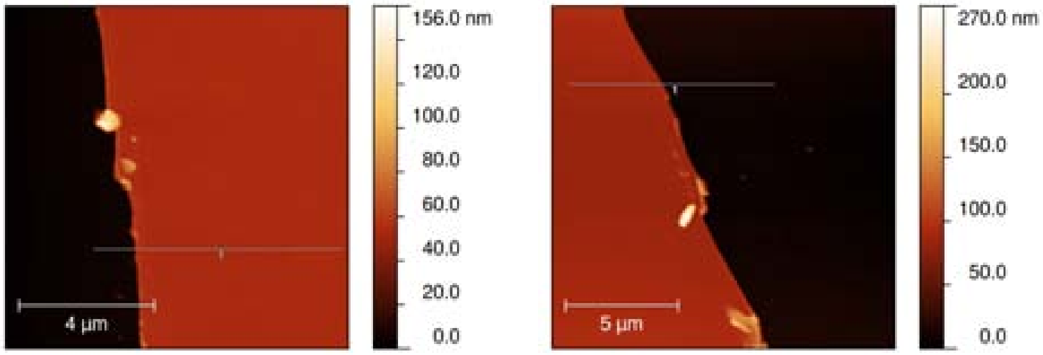

(a) (b)

Figure 4.5 *Atomic Force Microscope (AFM) images, for films of polystyrene (MW = 10000 g/mol) in chlorobenzene at different concentrations casted at 105 °C and ≈ 1 cm/s deposition velocity. (a) Solution of polystyrene at 3 wt%, (b) Solution of polystyrene at 4 wt%.RMS = 0.6 nm for 3% PS and 0.5 nm for 4% PS*

ing the root mean square (RMS) 0.6 nm for 3 % wt PS and 0.5 nm for 4 % wt PS. These very low values of RMS fall into agreement with films deposited by spin coating[35]. Also these RMS values are comparable to Poly(methyl-methacrylate) (PMMA) spin coated films which are widely used as dielectrics in OFETs, as reported by Shin et al.[36] and Young et al.[37]. Spin coated films of polystyrene are also studied as dielectric in OFETs and capacitance values of PS films are widely available in bibliography (i.e. Nunes et al.[38]). However, it should be highlighted that the films here presented have the potential to cover large areas versus spin coated films, also the scalability compatibility of BAMs is a strong feature versus spin coated films[39].

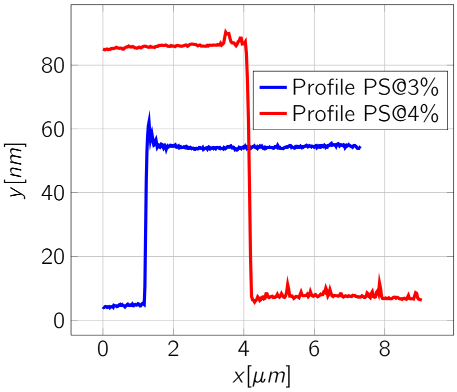

Figure 4.6 *Extracted profiles from Fig. 4.5(a) and 4.5(b), Profiles are extracted between the substrate and the polymeric film in order to evaluate the thickness of each polymeric film.*

4.4 Deposition of Blends of Semiconducting and Insulating Polymers

Organic thin-film transistors based on solution-processed semiconducting conjugated polymers have important attributes to be highlighted such as compatibility with simple direct write printing techniques, general low-cost manufacturing approaches, and compatibility with flexible plastic substrates. Only a few materials out of the immense library up-to-date of soluble materials have reached the high enough mobilities required for organic circuits for applications such as active matrix displays or low-cost intelligent labels. Poly(3-hexylthiophene) (P3HT) is the most studied organic semiconductor polymer and is of particular interest due to its self-organizing properties to form a microcrystalline structure[10]. Intensive research towards improving its mobility has shown that the microstructure in P3HT is critically affected by regioregularity (RR) and molecular weight (MW), resulting in variations of the field-effect mobilities by several orders of magnitude[8,10,12–14,18,40]. High field-effect mobilities of 0.1 $cm^2V^{-1}s^{-1}$ have been demonstrated through the optimization of device preparation, such as choosing appropriate solvents, dielectric treatments, deposition methods and post-deposition methods[8,10]. Despite the vast research carried out for the preparation of P3HT OFETs, this section is devoted to prepare field-effect transistors based on this polymer, minimizing the P3HT amount used, while matching the highest mobilities reported, as well maintaing a fairly competitive threshold voltage and on/off ratio with those reported in the literature. Further, the technique used consists of using simple steps avoiding convoluted manufacturing processes, and could be scaled up.

Blends of materials were produced by preparing a dilute, homogeneous solution of the RR-P3HT and PS3000 both 2% wt in dichlorobenzene (from Sigma-Aldrich). Each component was weight and placed in separate vials, with a stirrer in it. Organic solvent was poured and let stir overnight. Amber vials were used for P3HT solutions to avoid photo-decomposition. Substrates with pre-evaporated gold contacts defined by photolithography (4 nm/40 nm - Cr/Au) were cleaned with a series of solvents (chloroform, toluene, acetone, ethanol and isopropanol) and then dried under a flux of nitrogen. Substrates were placed carefully and aligned with the bar, and the temperature was set at $147 \pm 3^{o}C$. Blends were prepared right before the coating process, from the vials with stirrers small aliquots ($\approx$ 200 - 400 μl) were taken, and placed in one vial. So, right after the blend was prepared the vial was placed on the heated bed, in order to even temperatures with substrates. Afterwards, 50 -100 μl were dispensed between the bar and the substrate and the solution was casted. Immediately the substrate was removed from the coating machine and placed in a Petri dish covered with aluminium foil. Then the substrate was located in an oven for 15 minutes at 180 ^{o}C. After baking, the substrate was placed in a vacuum/hot plate at $120^{o}C$ with a vacuum pressure less than 90 kPa, for five minutes. After this time temperature was set to ambient temperature and left to cool down until ambient temperature was reached, subsequently the vacuum was slowly broken and the sample was ready to be characterized in air.

Figure 4.7 depicts an scheme of the deposition of the P3HT and PS3000 blend, in which a solution with P3HT and PS3000 molecules, and an inward flux J_w to a solvent depleted region in which solvent evaporation occurs $j_e(x)$ is observed.

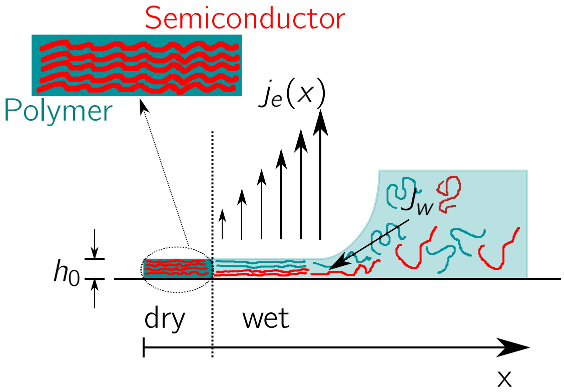

Figure 4.7 *Illustration of thin film deposition of a composite material based on P3HT and polystyrene.* $j_e(x)$ *is produced at* 147 ± 3^oC

4.4.1 Surface Morphology

In order to gather some information about the film morphology Atomic Force Microscope was employed. As shown in Figure 4.8(a) wide phase separated domains are formed. Figure 4.8(b) depicts two height profiles of the AFM image. Following profile one, the roughness is extracted using Gwyddion software giving a value of 0.9 nm, and the root mean square roughness is extracted as well with a value of 1.2 nm suggesting the formation of a smooth homogeneous film comprised between electrodes. Profile two gives a rough estimate of the height comprising film and electrode, which is $\approx 45nm$ and gives an approximation of the film thickness.

4.4.2 Electrical Characterization

The electrical characterization was carried out, in air and darkness. Before electrical characterization is carried out, each device is isolated from each other using a tip from the probe station while applying a gently pressure just to scratch

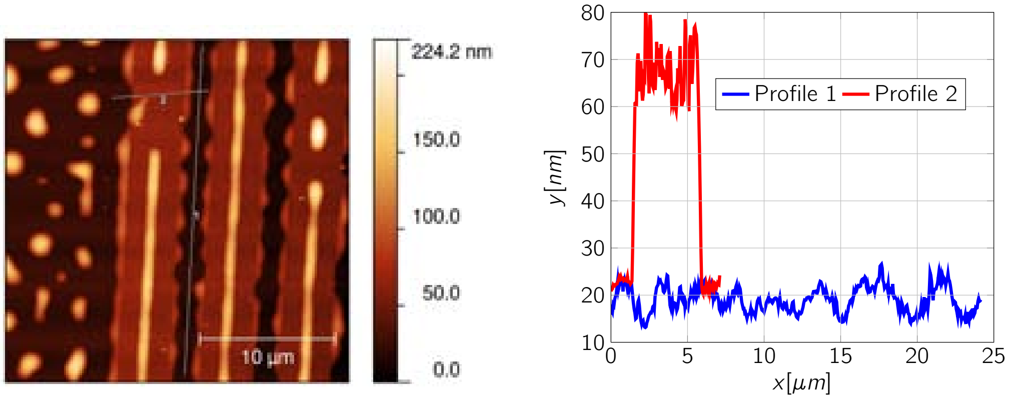

(a) (b)

Figure 4.8 *(a) Atomic force microscopy image for P3HT:PS3000 (10:90 m/m ratio) deposited on substrates with pre-patterned gold electrodes. (b) Height profiles for two different zones on the film.*

the film. For output characteristics, the gate voltage was swept from positive 10V down to $-40V$ each $-10V$, while the source-drain voltage was swept in forward and reverse fashion from positive $+10V$ down to negative $-40V$ with a step size of negative $-1V$. During this measurement the current source-drain was measured as well as the leakage source gate current. For transfer characteristics, the source-drain voltage applied was zero volts, then negative $-5V$ and finally negative $-40V$, while at each voltage a forward and reverse sweep in gate voltage was applied, from positive $+10V$ down to negative $-40V$ with a step size equal to negative $-1V$. In this fashion linear and saturation regimes were both recorded.

A screening of the best P3HT:PS3000 ratio was carried out evaluating the field-effect mobility (see Figure 4.9). Interestingly, the mobility found in all the devices using the blend is higher than when only P3HT is used, indicating that PS helps the film formation. A clear mobility peak using only 10 % of weight of the semiconductor was observed, suggesting that using this fabrication method the cost in the semiconductor used per chip is going to be reduced dramatically by 90%.

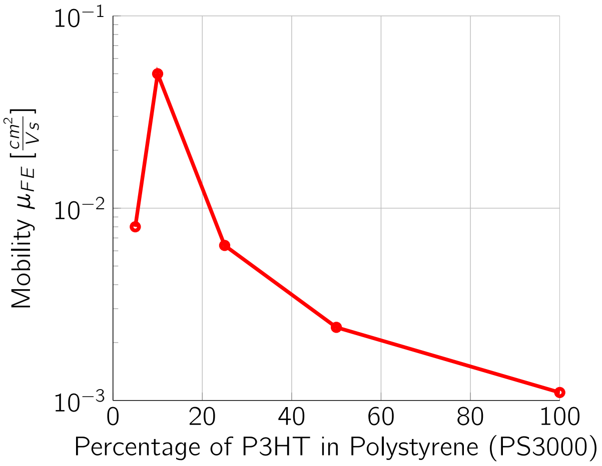

Figure 4.9 *Mobility as a function of percentage of P3HT in PS3000.*

Figures 4.10(a) and 4.10(b) show the output and transfer for a typical OFET based on P3HT:PS3000 blend (10:90 weight ratio). It can be seen that the device characteristics are very ideal for a p-type semiconductor, with low hysteresis, good saturation and low V_{TH} and V_{SO} close to 0 V. In the Logarithmic transfer plot one can see a very steep sub-threshold region suggesting a fast increase in current versus the respective variation in gate voltage, with a subthreshold-swing equals to $\approx$ 285 mV/decade.

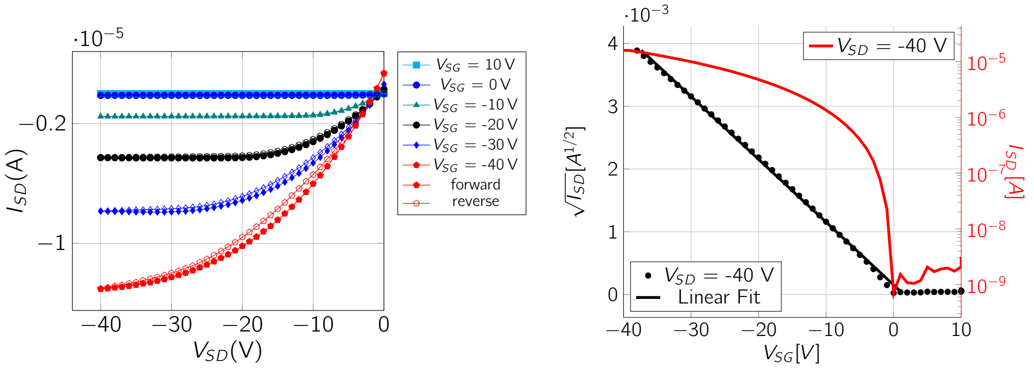

(a) (b)

Figure 4.10 *Electrical Characteristics for typical devices: (a) Output Characteristics, and (b) Log-transfer and square root plot at saturation regime ($V_{SD} = -40V$). Device with L = 100 µm and W = 2000 µm. $\mu_{FE} = 0\ 09 \frac{cm^2}{Vs}$, $V_{TH} = 1\ 5V$ and $V_{SO} \approx 0V$.*

Figures 4.11(a) and 4.11(b) shows typical output and transfer characteristics for the highest mobility device found with a short channel length L = 1.5 *μm* * in which contact resistances and short channel effects start to be noticeable an S shape at low V_{SD}.

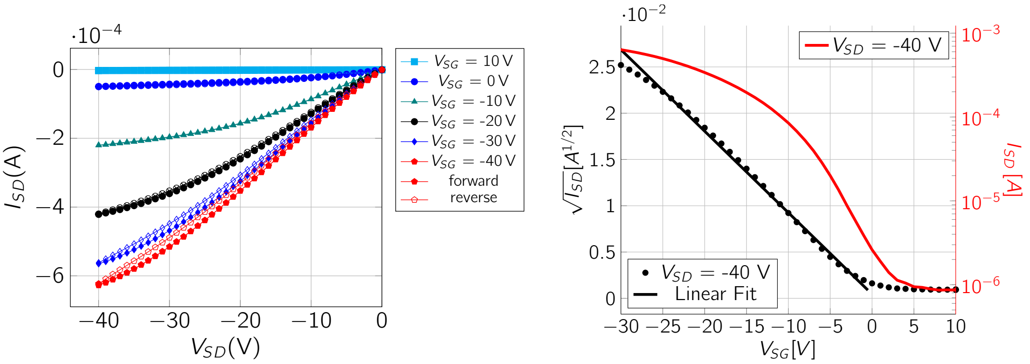

(a) (b)

Figure 4.11 *Electrical Characteristics for typical devices: (a) Output Characteristics,(b) Log-transfer and square root plot at saturation regime* ($V_{SD} = -40V$). *Device with L = 1.5 μm, W = 1000 μm.* $\mu_{FE} = 0\ 17\frac{cm^2}{V s}$ *and* $V_{TH} = 0\ 5V$.

The electrical parameters of the optimum P3HT:PS3000 ratio, like mobility, threshold voltage and on/off ratios are collected in Table 4.1. Four devices per each channel length with channel width equal to 2000 *μm* and L = 10 - 100 *μm* were analysed, while devices with channel width equal to 1000 *μm* and L = 1.5 -8 *μm* six devices were studied per channel length.

In all cases, the average mobility found is in the range 0.04-0.14 $cm^2V^{-1}s^{-1}$, while V_{TH} is very close to 0 V in devices with L > 8 *μm*, but always lower than 6 V. As mentioned before, there are several papers on P3HT, like Sirringhaus et al.[18], Yifan et al.[41] , Goffri et al.[10] and Murphy et al.[11] in which they report several techniques of preparing films for OFETs. Recently in a *Synthetic Metals* paper

---

*Devices with channel lengths lower than 10 microns were fabricated in close collaboration with Dr. Simone Fabiano at Linköping University using traditional optical lithography and lift-off procedures.

Chang et al.[40] also reported a solvent vapor assisted spin coating technique in order to achieve high mobility for P3HT based thin film transistors. In the majority of reports mobilities of the order of $10^{-2}\, cm^2 V^{-1} s^{-1}$ are described, and only in a few cases the highest mobilities reported for P3HT has been 0.1 $cm^2 V^{-1} s^{-1}$. There is another paper which reports high mobility values, using solvent treatments, the reported values are around 0.041 $cm^2 V^{-1} s^{-1}$[40]. One should also note that Goffri et al.[10] in a *Nature Materials* paper report that blends of P3HT and atactic polystyrene, at 10% wt concentration, give a mobility value lower than $10^{-6}\, cm^2 V^{-1} s^{-1}$. So here it can be noted that the mobility in the prepared blends has been improved by at least five orders of magnitude, and reaches state-of-the-art values. One key parameter related to the device performance is the dependency of the mobility as a function of gate voltage. In Figure 4.12 the mobility was calculated numerically in the linear and saturation regime using Equation 1.8 and plotted as a function of gate voltage in a log-scale y-axis. One can see its weak dependence on gate voltage using this scale. Another parameter to highlight is that mobilities at both regimes, linear and saturation, tend to overlap suggesting low contact resistance.

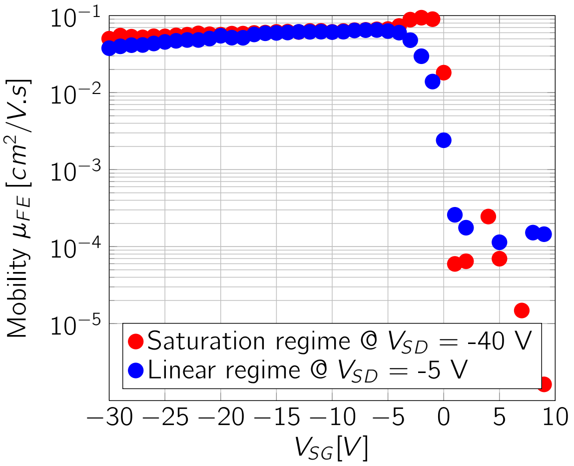

Figure 4.12 *Mobility as a function of gate voltage for saturation and linear regimes, for an OFET with a semiconductor layer composed of 10 % P3HT and 90 % PS3000, in a device with L = 100 µm and W = 2000 µm.*

Table 4.1 *Summary of channel dimensions, field-effect mobility, threshold voltage and on/off ratios for P3HT:PS3000 10:90 ratio.* $\mu_{avg}^{sat} = 0\ 08 \pm 0\ 008 \frac{cm^2}{V s}$ and $V_{TH} = 2\ 0 \pm 0\ 5V$.

Channel length [μm]	Channel width [μm]	Field-Effect mobility [$cm^2V^{-1}s^{-1}$]	Threshold voltage [V]	On/Off ratio
100	2000	$0\ 06 \pm 0\ 03$	$0\ 4 \pm 1\ 3$	$10^{-3} - 10^{-4}$
90	2000	$0\ 05 \pm 0\ 02$	$0\ 2 \pm 1\ 2$	$10^{-3} - 10^{-4}$
80	2000	$0\ 06 \pm 0\ 03$	$-0\ 2 \pm 1\ 3$	$10^{-3} - 10^{-4}$
70	2000	$0\ 05 \pm 0\ 03$	$0\ 0 \pm 1\ 2$	$10^{-3} - 10^{-4}$
60	2000	$0\ 05 \pm 0\ 02$	$-0\ 1 \pm 1\ 2$	$10^{-3} - 10^{-4}$
50	2000	$0\ 04 \pm 0\ 02$	$0\ 0 \pm 1\ 2$	$10^{-3} - 10^{-4}$
40	2000	$0\ 04 \pm 0\ 02$	$-0\ 1 \pm 1\ 2$	$10^{-3} - 10^{-4}$
30	2000	$0\ 04 \pm 0\ 02$	$0\ 0 \pm 1\ 1$	$10^{-3} - 10^{-4}$
20	2000	$0\ 04 \pm 0\ 02$	$0\ 1 \pm 1\ 2$	$10^{-3} - 10^{-4}$
10	2000	$0\ 04 \pm 0\ 02$	$0\ 1 \pm 1\ 4$	$10^{-3} - 10^{-4}$
8	1000	$0\ 11 \pm 0\ 02$	$3\ 6 \pm 0\ 6$	$10^{-3} - 10^{-4}$
5	1000	$0\ 10 \pm 0\ 006$	$1\ 9 \pm 0\ 6$	$10^{-3} - 10^{-4}$
3	1000	$0\ 12 \pm 0\ 007$	$5\ 4 \pm 1\ 8$	$10^{-3} - 10^{-4}$
2	1000	$0\ 10 \pm 0\ 005$	$5\ 6 \pm 1\ 4$	$10^{-3} - 10^{-4}$
1.5	1000	$0\ 14 \pm 0\ 01$	$3\ 6 \pm 1\ 2$	$10^{-3} - 10^{-4}$

The mobility is not the only parameter to be analysed in an organic field-effect transistor, the switch-on voltage (V_{SO})[42] is also to be noted. Comparing with data from literature with P3HT blends, Murphy et al.[11] reports a P3HT OFET measured in a nitrogen atmosphere a switch-on voltage of $+30V$ with the transistor driven at $-40V$ at the gate. Also Gofri et al.[10] report a $+10V$ switch-on voltage measured also in an inert atmosphere. Remarkably, in this study the switch-on voltage (see Figure 4.10(b)) is close to 0 V for a transistor driven at $-40V$ in gate voltage, emphasising also that the devices were measured and fabricated in ambient conditions (air, ambient humidity, etc.). Therefore, we can affirm that with this fabrication methodology the resulting P3HT films do not get doped and are stable in air.

4.4.3 Channel Length Dependency and Contact Resistance Calculation

After analysing data for channel lengths ranging from 100 μm down to 1 5 μm it is important to note that variation in mobility occurs. From Table 4.1, it is clear that devices with channel lengths below 8 μm exhibit higher mobilities. Therefore, the device reproducibility was assessed considering two groups of devices: 1) with L = 10 - 100 μm and W = 2000 μm, and 2) 1.5 μm < L < 8 μm and W = 1000 μm. The histograms with normal distribution fittings for both groups are depicted in Figures 4.13(a) and 4.13(b). One can clearly see a normal distribution tendency in both groups. The mean value for devices with channel length ranging from 100 μm down to 10 μm and constant channel width (W) of 2000 μm is 0 05 $cm^2V^{-1}s^{-1}$ with an standard deviation of 0 02 $cm^2V^{-1}s^{-1}$, while devices with channel lengths in the range of 1.5 μm < L < 8 μm and constant channel width (W) of 1000 μm exhibit a mean mobility value of 0 12 $cm^2V^{-1}s^{-1}$ with an standard deviation of 0 03 $cm^2V^{-1}s^{-1}$.

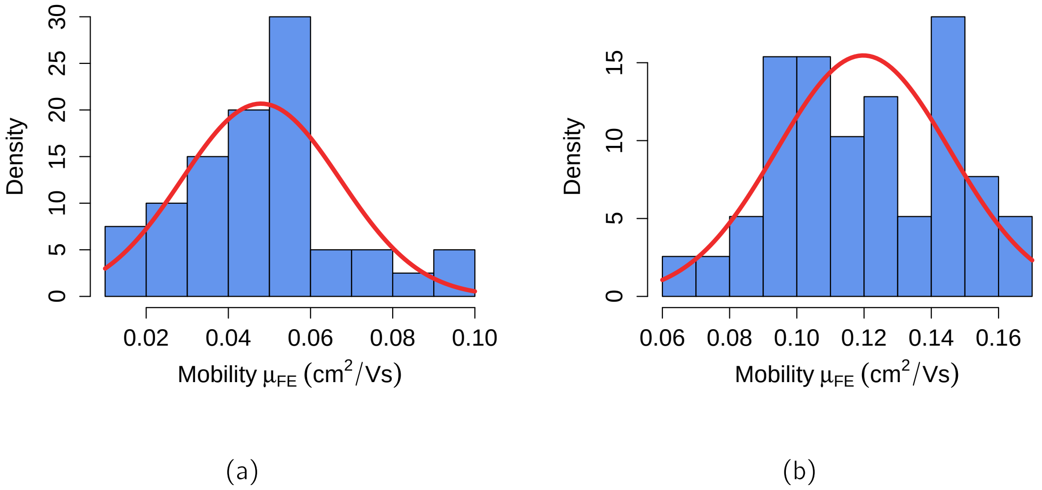

(a) (b)

Figure 4.13 *Histogram with fitted normal distribution for mobility in* $cm^2V^{-1}s^{-1}$ *(a) for devices with channel lengths from* $10\,\mu m$ *to* $100\,\mu m$ *with constant channel width equal to* $2000\,\mu m$ *and (b) devices with channel lengths 8,5,3,2 and 1.5* μm *and constant channel width 1000* μm*.*

Figure 4.14 shows the relationship between the saturation current ($V_{SG} = -40V$) and the width/length ratio for a number of OFETs with a fixed channel width equal to $2000\,\mu m$ and $L = 10-100\,\mu m$. The error bar reflects measurements over a set of data, and depicts that within the experimental error margin the saturation source -drain current is directly proportional to W/L, as predicted by Equation 1.3.

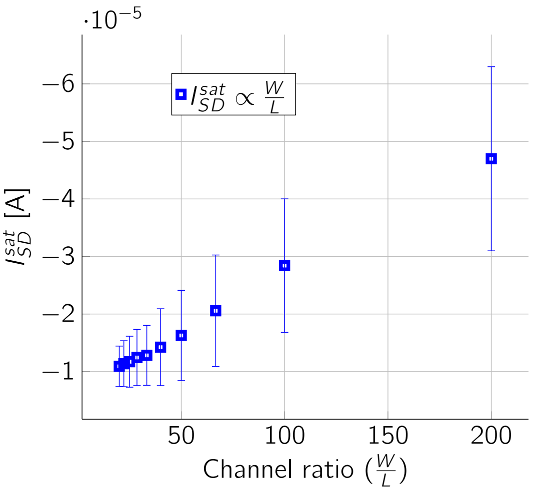

Figure 4.14 *Saturation current versus channel width/length ratio for P3HT:PS3000 (10:90) OTFTs.*

In order to assess the contact resistance which is strongly dependent on the nature of the electrode and strongly gate bias dependent as well, several devices with varying channel length while maintaining the channel width constant were measured. The output characteristics were recorded at several gate voltages ie. $-10V$, $-20V$, $-30V$ and $-40V$, then the linear regime was detected and source-drain current versus source-drain voltage were fitted into a straight line model. Since for small drain voltages it can be assumed that the total resistance is the sum of the channel resistance and the contact resistance, then the inverse of the slope for each line was calculated, assuming an ideal resistor operation. The procedure was repeated for each channel length and each gate voltage. Following equations 1.12 and 1.13 for the transfer-line method and the modified transfer-line method, respectively, the plots were constructed, which are shown in Figures 4.15(a) and 4.15(b) for both methods. In these figures each point is the average of four data points (error bars were removed for readability), and one can observe that all R-square values exceed 0.8 except the straight line at V_{SG} = -10 V for the modified transfer-line method which gives a 0.78 value for the R-square. Analysing the collected data in Table 4.2, one can see that the values reported for the contact resistance with the modified transfer-line are almost half of the values reported by the calculation out of the traditional transfer-line. One should note that it cannot be taken for granted that the contact and channel resistances do not fluctuate from one device to another, that is why the method requires measurements on several devices.

Park et al[13] and Singh et al[43] have previously reported contact resistance values for P3HT films and Au electrodes, which basically is the same system presented in this study despite the difference in the manufacturing process, in the order 0.4 - 0.6 MΩ with the OFET driven at gate voltage -40 V or -80 V. Also higher values were reported by Winter et al[14] for several types of functionalized electrodes which

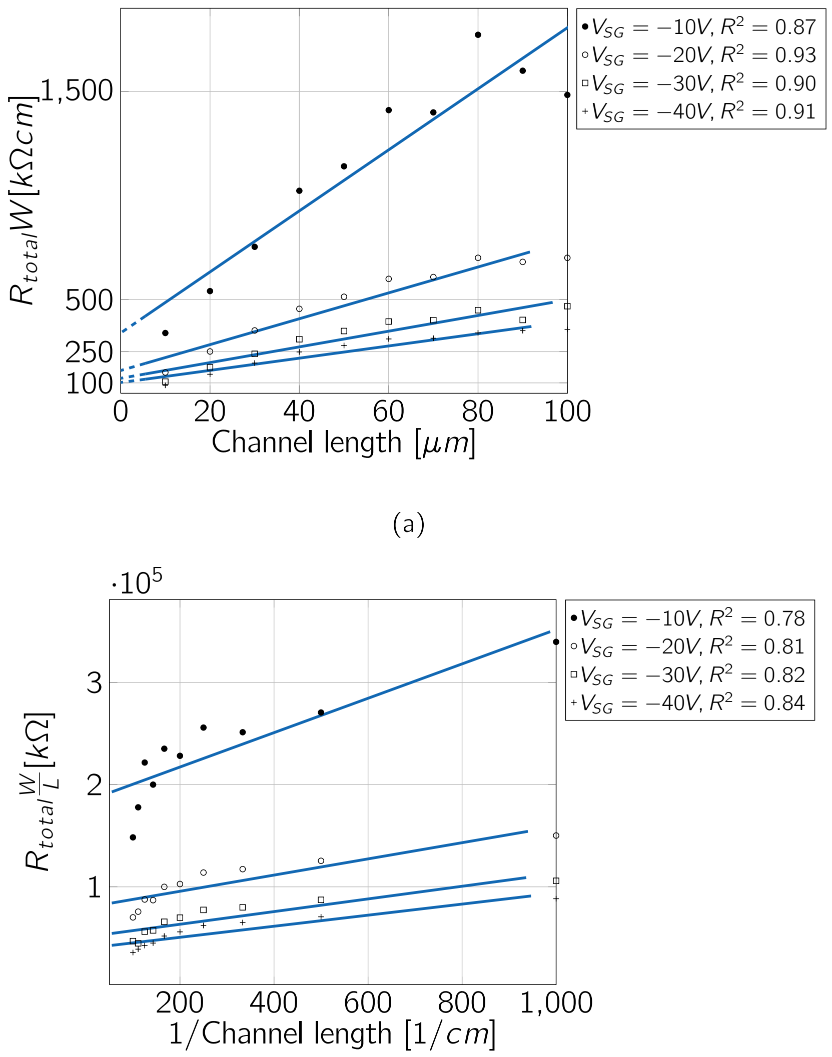

(a)

(b)

Figure 4.15 *(a) Transfer-line method for contact resistance extraction, and (b) Modified transfer-line method for contact resistance calculation.Error bars have been omitted for clarity.*

ranged from 80 down to 5 MΩ. It is well known the dependency of the contact resistance on the gate voltage. In order to assess the tendency of such dependence the values in MΩ and V_{SG} from Table 4.2 were fitted into a straight line model obtaining r-square values equals to 0.98 and 0.96 for the transfer-line method and the modified transfer-line method, respectively. In conclusion the contact resistance here reported are extremely well suited in comparison with those reported in the literature[44] and are inside the expected range for such systems.

Table 4.2 *Summary of the calculated contact resistances. For the transfer-line method (TLM) is the intercept of the fitting line as stated in equation 1.12, and for the modified transfer-line method (MTLM) the slope as in equation 1.13. All R-squared are represented in Figures 4.15(a) and 4.15(b).*

V_{SG} (V)	TLM (kΩ cm)	MTLM (kΩ cm)	TLM (MΩ)	MTLM (MΩ)
-10	349	168	1.75	0.84
-20	159	79	0.80	0.40
-30	122	62	0.61	0.31
-40	101	54	0.50	0.27

4.5 Summary

It has been shown that very smooth nanofilms of polystyrene with thickness around 80 nm down to 40 nm can be fabricated with the novel deposition technique BAMs described. The film formation relies on the efficient mass transfer (solvent evaporation) and the thickness of the final film is self-metered and dependent mainly on the concentration of the solution. The very low rms of these films make them good candidates for dielectrics.

Also demonstration of organic field-effect transistors were achieved employing P3HT blended with PS as organic semiconductor, with mobilities as high as $\approx 0\ 1 cm^2 V^{-1} s^{-1}$ in mean value and as high as $0\ 2 cm^2 V^{-1} s^{-1}$, which match the highest mobility reported in the literature[18]. It is also worth noting that the switch-on voltages are close to zero and always less than +5 V. The results shown here suggests that this deposition technique could be exploited for the fabrication of Organic Field-Effect Transistors in ambient conditions for a P3HT as semiconductor, proving to be a technique fairly robust while maintaining the low-cost, scalability and large are deposition that an organic layer formation technique should have.

Knowing that besides the excellent electrical characteristics shown it is imperative to design a method which can be further in the map for mass production, we believe that the scalability that this technology possess is a clear added value.

Bibliography

[1] P. Dontula. *Polymer Solutions in Coating Flows*. Ph.D. thesis, The University of Minnesota, **1999**.

[2] M. Pasquali. *Polymer Molecules in Free Surface Coating Flows*. Ph.D. thesis, The University of Minnesota, **2000**.

[3] A. D. Scaccabarozzi and N. Stingelin. "Semiconducting:insulating polymer blends for optoelectronic applications-a review of recent advances". *J. Mater. Chem. A*, **2014**, 2, 10818.

[4] Y. Yun. *Pentacene Based Organic Electronic Devices*. Ph.D. thesis, Durham University, **2010**.

[5] M.-H. Kim, C.-M. Keum and S.-D. Lee. "Tailoring and patterning of dielectric interfaces for the development of advanced organic field-effect transistors". *Liquid Crystals*, **2014**, 41, 310.

[6] J. F. Martínez Hardigree and H. E. Katz. "Through Thick and Thin: Tuning the Threshold Voltage in Organic Field-Effect Transistors". *Accounts of Chemical Research*, **2014**, 47, 1369.

[7] M. Jang, J. H. Park, S. Im, S. H. Kim and H. Yang. "Critical Factors to Achieve Low Voltage- and Capacitance-Based Organic Field-Effect Transistors". *Advanced Materials*, **2014**, 26, 288.

[8] J.-F. Chang, B. Sun, D. W. Breiby, M. M. Nielsen, T. I. Sölling, M. Giles, I. McCulloch and H. Sirringhaus. "Enhanced Mobility of Poly(3-hexylthiophene) Transistors by Spin-Coating from High-Boiling-Point Solvents". *Chemistry of Materials*, **2004**, 16, 4772.

[9] L. Fumagalli, M. Binda, D. Natali, M. Sampietro, E. Salmoiraghi and P. Di Gianvincenzo. "Dependence of the mobility on charge carrier density and electric field in poly(3-hexylthiophene) based thin film transistors: Effect of the molecular weight". *Journal of Applied Physics*, **2008**, 104 084513.

[10] S. Goffri, C. Muller, N. Stingelin-Stutzmann, D. W. Breiby, C. P. Radano, J. W. Andreasen, R. Thompson, R. A. J. Janssen, M. M. Nielsen, P. Smith and H. Sirringhaus. "Multicomponent semiconducting polymer systems with low crystallization-induced percolation threshold". *Nature Materials*, **2006**, 5, 950.

[11] C. E. Murphy, L. Yang, S. Ray, L. Yu, S. Knox and N. Stingelin. "Wire-bar coating of semiconducting polythiophene/insulating polyethylene blend thin films for organic transistors". *Journal of Applied Physics*, **2011**, 110 093523.

[12] M. Nicho, D. Pena-Salgado and P. Altuzar-Coello. "Morphological and physicochemical properties of spin-coated poly(3-octylthiophene)/polystyrene composite thin films". *Thin Solid Films*, **2010**, 518, 1799 . Photovoltaics, solar energy materials and thin films - IMRC 2008, Cancun, Mexico.

[13] B. Park, A. Aiyar, M. S. Park, M. Srinivasarao and E. Reichmanis. "Conducting Channel Formation in Poly(3-hexylthiophene) Field Effect Transistors: Bulk to Interface". *The Journal of Physical Chemistry C*, **2011**, 115, 11719.

[14] R. Winter, M. S. Hammer, C. Deibel and J. Pflaum. "Improvement of the

poly-3-hexylthiophene transistor performance using small molecule contact functionalization". *Applied Physics Letters*, **2009**, 95 263313.

[15] Y. Jeong, H. Lee, B.-S. Lee, S. Park, H. Yudistira, C.-L. Choong, J.-J. Park, C. Park and D. Byun. "Directly drawn poly(3-hexylthiophene) field-effect transistors by electrohydrodynamic jet printing: Improving performance with surface modification". *ACS Applied Materials and Interfaces*, **2014**, 6, 10736. Cited By (since 1996)0.

[16] L. Shi, X. Xu, M. Ma and L. Li. "High-performance, low-operating voltage, and solution-processable organic field-effect transistor with silk fibroin as the gate dielectric". *Applied Physics Letters*, **2014**, 104, 023302. Cited By (since 1996)0.

[17] K. Ali, U. Pietsch and S. Grigorian. "Enhancement of field-effect mobility due to structural ordering in poly(3-hexylthiophene) films by the dip-coating technique". *Journal of Applied Crystallography*, **2013**, 46, 908. Cited By (since 1996)1.

[18] H. Sirringhaus, N. Tessler and R. H. Friend. "Integrated Optoelectronic Devices Based on Conjugated Polymers". *Science*, **1998**, 280, 1741.

[19] J. Xiao and D. Attinger. "Simulations of Meniscus Motion and Evaporation for Convective Deposition Manufacturing". In "Proceedings of the COMSOL Conference 2010 Boston", , **2010**.

[20] K. Chen, S. V. Stoianov, J. Bangerter and H. D. Robinson. "Restricted meniscus convective self-assembly." *Journal of colloid and interface science*, **2010**, 344, 315.

[21] J. Cordeiro, O. Lecarme, G. Osvaldo Dias and D. Peyrade. "Three-dimensional

capillary force assembly: Fabrication of white light emitters". *Journal of Vacuum Science & Technology B*, **2012**, 30 06F203.

[22] Y. Cui, M. T. Börk, J. A. Liddle, C. Sönnichsen, B. Boussert and A. P. Alivisatos. "Integration of Colloidal Nanocrystals into Lithographically Patterned Devices". *Nano Letters*, **2004**, 4, 1093.

[23] P. A. Kralchevsky and N. D. Denkov. "Capillary forces and structuring in layers of colloid particles". *Current Opinion in Colloid & Interface Science*, **2001**, 6, 383 .

[24] O. Lecarme, T. Pinedo-Rivera, K. Berton, J. Berthier and D. Peyrade. "Plasmonic coupling in nondipolar gold colloidal dimers". *Applied Physics Letters*, **2011**, 98 083122.

[25] H. C. Mayer and R. Krechetnikov. "Landau-Levich flow visualization: Revealing the flow topology responsible for the film thickening phenomena". *Physics of Fluids (1994-present)*, **2012**, 24 052103.

[26] A. S. Dimitrov and K. Nagayama. "Steady-state unidirectional convective assembling of fine particles into two-dimensional arrays". *Chemical Physics Letters*, **1995**, 2614, 462.

[27] P. Kumnorkaew and J. F. Gilchrist. "Effect of nanoparticle concentration on the convective deposition of binary suspensions." *Langmuir*, **2009**, 25, 6070.

[28] B. G. Prevo, D. M. Kuncicky and O. D. Velev. "Engineered deposition of coatings from nano- and micro-particles: A brief review of convective assembly at high volume fraction". *Colloids and Surfaces A: Physicochemical and Engineering Aspects*, **2007**, 311, 2.

[29] B. G. Prevo and O. D. Velev. "Controlled, Rapid Deposition of Structured

Coatings from Micro- and Nanoparticle Suspensions". *Langmuir*, **2004**, 20, 2099.

[30] Y. Lu, Y. Yin, B. Gates and Y. Xia. "Growth of Large Crystals of Monodispersed Spherical Colloids in Fluidic Cells Fabricated Using Non-photolithographic Methods". *Langmuir*, **2001**, 17, 6344.

[31] L. Malaquin, T. Kraus, H. Schmid, E. Delamarche and H. Wolf. "Controlled Particle Placement through Convective and Capillary Assembly". *Langmuir*, **2007**, 23, 11513.

[32] D. Peyrade, M. Gordon, G. Hyvert, K. Berton and J. Tallal. "Direct observation and localization of colloidal nanoparticles on patterned surface by capillary forces". *Microelectronic Engineering*, **2006**, 83, 1521 .

[33] T. Pinedo Rivera, O. Lecarme, J. Hartmann, E. Rossitto, K. Berton and D. Peyrade. "Assisted convective-capillary force assembly of gold colloids in a microfluidic cell: Plasmonic properties of deterministic nanostructures". *Journal of Vacuum Science & Technology B*, **2008**, 26, 2513.

[34] T. P. Rivera, O. Lecarme, J. Hartmann, R. Inglebert and D. Peyrade. "Spectroscopic studies of plasmonic interactions in colloidal dimers fabricated by convective-capillary force assembly". *Microelectronic Engineering*, **2009**, 86, 1089 .

[35] S. E. Fritz, T. W. Kelley and C. D. Frisbie. "Effect of Dielectric Roughness on Performance of Pentacene TFTs and Restoration of Performance with a Polymeric Smoothing Layer". *The Journal of Physical Chemistry B*, **2005**, 109, 10574.

[36] K. Shin, C. Yang, S. Y. Yang, H. Jeon and C. E. Park. "Effects of polymer gate

dielectrics roughness on pentacene field-effect transistors". *Applied Physics Letters*, **2006**, 88 072109.

[37] Y. Yun, C. Pearson, D. H. Cadd, R. L. Thompson and M. C. Petty. "A cross-linked poly(methyl methacrylate) gate dielectric by ion-beam irradiation for organic thin-film transistors". *Organic Electronics*, **2009**, 10, 1596 .

[38] G. Nunes, S. G. Zane and J. S. Meth. "Styrenic polymers as gate dielectrics for pentacene field-effect transistors". *Journal of Applied Physics*, **2005**, 98 104503.

[39] A. Merari Masillamani, E. Orgiu and P. Samori. "Effect of the molecular weight of the polymer gate dielectric on the performances of solution-processed ambipolar OTFTs". *J. Mater. Chem. C*, **2013**, 1, 7725.

[40] H. Chang, P. Wang, H. Li, J. Zhang and D. Yan. "Solvent vapor assisted spin-coating: A simple method to directly achieve high mobility from P3HT based thin film transistors". *Synthetic Metals*, **2013**, 184, 1.

[41] X. Yifan. *Studies on Field-Effect Transistors with Conjugated Polymer and High Permitivity Gate Dielectrics using Pulsed Plasma Polymerization*. Ph.D. thesis, The Ohio State University, **2005**.

[42] E. J. Meijer. *Charge transport in disordered organic field-effect transistors*. Ph.D. thesis, Delft University of Technology, **2003**.

[43] K. a. Singh, T. Young, R. D. McCullough, T. Kowalewski and L. M. Porter. "Planarization of Polymeric Field-Effect Transistors: Improvement of Nanomorphology and Enhancement of Electrical Performance". *Advanced Functional Materials*, **2010**, 20, 2216.

[44] D. Natali and M. Caironi. "Charge Injection in Solution-Processed Organic

Field-Effect Transistors: Physics, Models and Characterization Methods". *Advanced Materials*, **2012**, 24, 1357.

Chapter 5

Large area processing of TTF derivatives for applications in organic field-effect transistors.

5.1 Introduction

Solution processed Organic Field-Effect Transistors (OFETs) exhibiting high performance have been reported in the last years. However, the limitations towards applications lie on finding low-cost deposition methods compatible with upscaling that permit to cover large areas with organic semiconductors. An additional challenge is to achieve stable devices. Then, amalgam the processability that polymers offer with high mobility of small-molecules is a plausible methodology. Further, blending polymers and small-molecules into composite materials, helps to satisfy the perspectives that OFETs need, namely low-cost, and processing from solution. Therefore, forming composites is an attractive methodology to improve the processing, and in some cases has also given rise to the improvement of the performance and the stability of the devices[1–5]. The here developed Bar Assisted Meniscus Sheering (BAMs) technique appends the large area and scalability to both low-cost and solution processing. Thus, this technique is promising to apply for the deposition of small molecule/polymer blends for OFETs.

In this thesis, as small molecule organic semiconductors three tetrathiafulvalene derivatives were chosen: dibenzo-tetrathiafulvalene (DB-TTF), dithiophene-tetrathiafulvalene (DT-TTF) and bis(ethylenethio)-tetrathiafulvalene (BET-TTF) (see Figure 5.1).

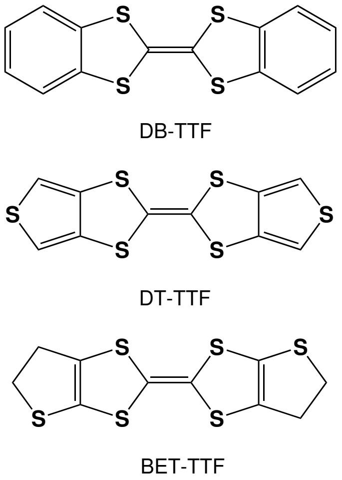

Figure 5.1 *Chemical structures of dibenzo-tetrathiafulvalene (DB-TTF), dithiophene-tetrathiafulvalene (DT-TTF) and bis(ethylenethio)-tetrathiafulvalene (BET-TTF).*

OFETs based on thermally evaporated DB-TTF have been studied by Naraso et al.[6] and Noda et al.[7] reporting mobilities in the range of 0.01 to 0 06 $cm^2V^{-1}s^{-1}$. However, for low-cost applications OFETs should be processed from solution in liquid phase. For this reason, OFETs based on DB-TTF single crystals were studied by Mas-Torrent et al.[8] reporting hole mobilities up to 1 $cm^2V^{-1}s^{-1}$. It should be highlighted that although this molecule is a promising and commercial organic semiconductor (OSC), it gets doped * very easily. Another well studied organic semiconductor is DT-TTF which was first synthetized by Rovira et al.[9,10]. Single crystal (SC) DT-TTF OFETs fabricated by drop casting with a maximum mobility of up to 3.6 $cm^2V^{-1}s^{-1}$ were reported by Mas-Torrent el at.[11–13]. Charge transport of DT-TTF SC-OFETs was also studied and reported as temperature activated transport[14]. Also OFETs fabricated by zone casting were published[15] reporting mobilities as high as 0 17 $cm^2V^{-1}s^{-1}$. Pfattner

---

*Doping in organic semiconductors, in this case particularly TTF derivatives, refers to the intrinsic property of such semiconductors to be extremely sensitive to oxygen and water. The OSCs are oxidised and charge carriers are formed in the material.

et al.[16] reports a crystalline phase which is only stable in a thin-film morphology the $\beta - phase$ DT-TTF giving mobilities of 0 13 $cm^2V^{-1}s^{-1}$. Further, evaporated thin film OFETs were reported[16] with mobilities values of 0 068 $cm^2V^{-1}s^{-1}$, and in such thin film the $\beta - phase$ was also found. So, DT-TTF has a stablished reputation to be a well suited candidate for OFETs, however the lack of processability technologies preclude it to be processed over large areas at higher speeds than those used in zone casting like the processing velocities that Bar Assisted Meniscus Sheering (BAMs) technique offer. But, the processability on large areas and processing velocity are not the only factors that hamper DT-TTF, also the amount of material required is an issue considering the expensive and complex synthetic routes that the material requires. So, blending with low cost materials forming composites could be an option to evade the later mentioned problems.

Besides, DB-TTF and DT-TTF, BET-TTF is yet another material well studied[17–28] with the ability to form molecular metals[29,30] and films with metal-like properties[31] and semiconducting characteristics[11,32]. In OFETs, this material was studied as single crystal with mobilities of the order of 1 $5x10^{-2}\,cm^2\;Vs$[11]. However, it was never studied as thin film OFET.

In this chapter, we searched for the most promising thin film for OFET applications based on a blend of a polymer matrix and one of the three above mentioned TTF derivatives as organic semiconductors. The first subject of study was DB-TTF. Then OFETs based on thermally evaporated thin films constituted the starting point, where their electrical performance and stability were addressed. Further, OFETs based on blends of DB-TTF and polymers have been prepared in order to find the most promising formulation that gives the best device performance. The blends were processed by spin coating and BAMs, giving the latter the better results. The second subject of study was DT-TTF, for which OFETs based on blends with insulating polymers in binary and ternary mixtures were prepared by

BAMs, and electrically characterised, in order to find the best case scenario for DT-TTF. Finally, the third subject of study was BET-TTF, for which thermally evaporated OFETs were electrically characterised and their stability under ambient conditions evaluated. Also, OFETs based on blends of BET-TTF and insulating polymers were prepared and electrically characterised to find the best performing formulation. Further, preliminary studies of doping the films based on BET-TTF blends point towards the possibility of fabricating organic electrodes with these films.

5.2 OFETs based on DB-TTF: from thermally evaporated to composite materials

5.2.1 Thermally Evaporated Films

Thermally evaporated thin-films of DB-TTF were prepared with a slow evaporation rate of about 0.5 Å/s on Si/SiO_x and octadecyltrichlorosilane (OTS) functionalized Si SiO_x substrates with pre-fabricated ITO/Au source and drain electrodes. Samples were fabricated and electrically characterised inside a glove box.

Topography

Figures 5.2(a) and 5.2(b) depicts AFM images of the films in which clearly defined micrometer sized crystal grains of DB-TTF are seen. In Figure 5.2(b) the grains exhibit less isle-like geometry than the grains observed in Figure 5.2(a) tentatively due to the influence of the self-assembled monolayer deposited for the sample seen in Figure 5.2(b). The thickness of the evaporated organic film was found to be 110 nm extracted from the AFM analysis.

[†] Work carried out in close collaboration with Dr. Sergio Galindo and Dr. Raphael Pfattner.

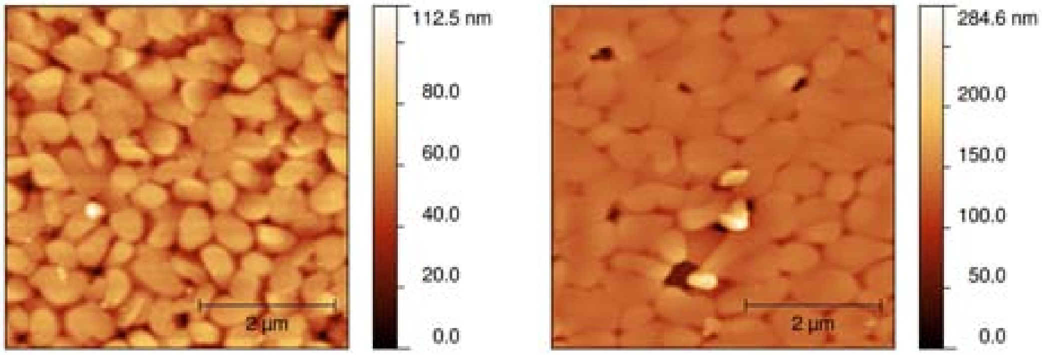

(a) (b)

Figure 5.2 *Atomic force microscope pictures for (a) evaporated DB-TTF film without surface treatment,(b) evaporated DB-TTF film with an OTS self-assembled monolayer on* SiO_x *surface.*

Electrical characterization

The electrical measurement of the devices was carried out under inert conditions with levels of oxygen and water below 2 and 3 ppm, respectively (Figure 5.3). The field-effect mobility of the freshly prepared devices was found to be $\mu_{FE}^{sat} = 0.023\ cm^2V^{-1}s^{-1}$, and did not exhibit a significant change after 66 h of storage. Despite the unchanged mobility value over this time, it should be noted that even at such low levels of O_2 and H_2O the devices exhibited a positive shift of V_{TH} of about 6.6 V and a shift of approximately 10 V in the switch-on voltage (V_{SO}). When the devices were taken out of the inert atmosphere and exposed to air at ambient conditions, a strong shift of V_{TH} to positive values (ΔV_{TH}= 80 V) within seconds was observed resulting in highly doped devices unable to be turned off by positive gate voltages.

Due to the clear environmental instability of this material in thermally evaporated thin films, it is of vital importance to devise composite materials to help to promote stability while maintaining good electrical characteristics, and equally important to be able to process such unstable semiconductor material in air.

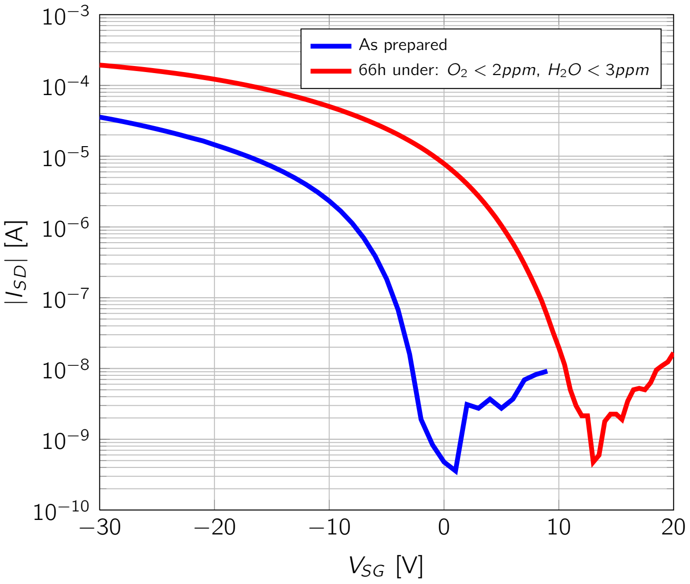

Figure 5.3 *Electrical characteristics and stability of OFETs based on evaporated DB-TTF film. Electrical transfer characteristics of a thermally evaporated DB-TTF thin film on Si SiO_2 as substrate measured as prepared under inert atmosphere and after 66 hours of storage under darkness inside a glove box; O_2 and H_2O were below 2 and 3 ppm, respectively. Both curves measured at V_{SD} = -30 V.*

5.2.2 OFETs based on spin-coated DB-TTF composites

In order to evaluate the possibility to fabricate OFETs based on composites comprised of DB-TTF and polymers, first several polymers were tested (i.e. Poly (bis(4-phenyl) (2,4,6-trimethylphenyl)amine) (PTAA), and polystyrene (PS280k) M_w = 280000 g/mol) blended with DB-TTF and processed by spin coating.

PTAA and DB-TTF composite OFETs

PTAA was selected due to its reported stability and good characteristics as a binder in composites[33–35]. This polymer is an amorphous organic semiconductor although exhibits a very low field-effect mobility. Spin coating was used to evaluate the potential of this blend. First, solutions of 2 mg/ml of PTAA and DB-TTF in chloroform in separated vials were prepared. From these solutions mixtures 1:1

Work carried out in close collaboration with Dr. Raphael Pfattner.

and 1:2 PTAA:DB-TTF were prepared. Then substrates were placed on the spin coater, and a drop of 100 μl of the PTAA:DB-TTF solution was deposited on the substrate, and spin coated at rpm 1500 for 1 min. As a reference, also pure PTAA films are prepared.

Figures 5.4(a) and 5.4(b) depicts typical output and transfer characteristics respectively, for pure PTAA OFETs. Output characteristics clearly shows two well defined regions linear and saturation. From transfer characteristics one can observe that the threshold voltage is located below zero volts ($V_{TH} =$ -40 V) which pictures an OFET non doped but 40 V away from an ideal state.

Figures 5.4(c) and 5.4(d) depicts a typical output and transfer characteristics, respectively for a film of 1:1 PTAA:DB-TTF. From the output characteristics one can observe that the OFET does not saturate even at high source-drain voltages ($V_{SD} >$ -100 V). Also is important to note that when comparing Figure 5.4(b), the transfer characteristics for pure PTAA, and Figure 5.4(d), the transfer characteristics for the composite PTAA:DB-TTF in a ratio 1:1, one can clearly see that the threshold voltage displacement is completely evident by at least 20 Volts positive and also it is observed how the current is increased by roughly one order of magnitude. Thus, the inclusion of DB-TTF into the PTAA matrix provokes the formation of a more doped film.

Figure 5.5 shows a resume of mobility for two composites and PTAA itself, using devices with different channel lengths. One can infer from the plot that increasing the amount of DB-TTF the mobility of the whole composite increases as well. Another way to interpret the Figure 5.5 is that by adding DB-TTF to PTAA one can invigorate its mobility by two orders of magnitude. For shorter channel lengths, the mobility tends to increase.

Despite the satisfactory results in terms of mobility, this type of composites were dropped due to the fact that the PTAA is an expensive material and in

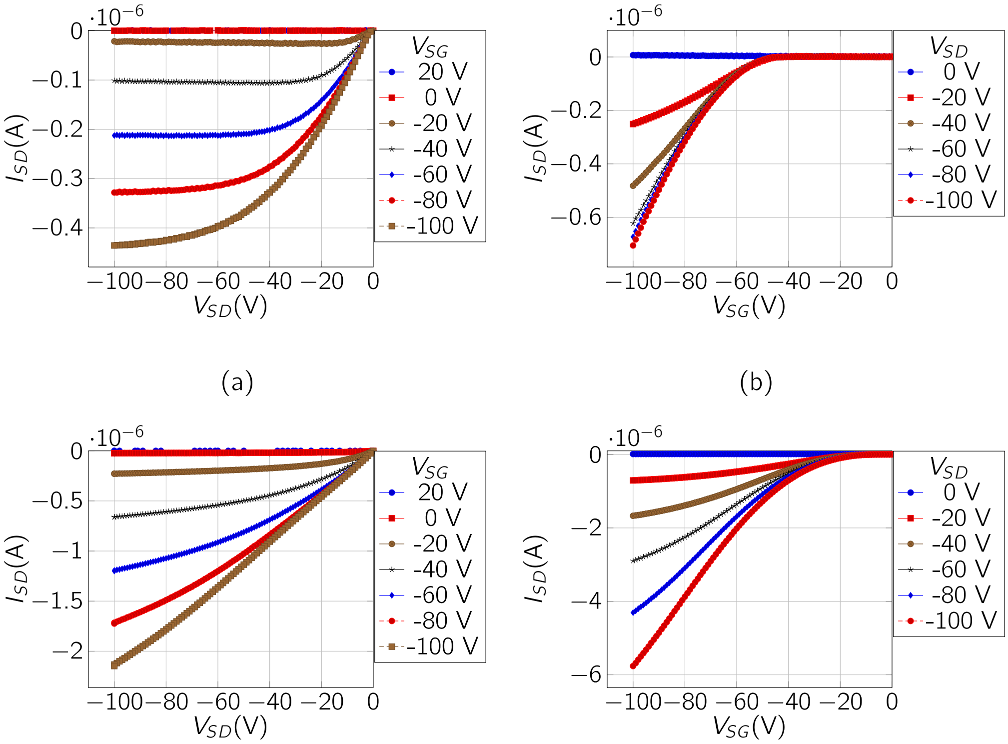

(a) (b)

(c) (d)

Figure 5.4 *Output characteristics for (a) PTAA and (c) PTAA:DB-TTF. Transfer characteristics for (b) PTAA and (d) PTAA:DB-TTF. Both cases devices with L = 20 µm W = 10000 µm. PTAA:DB-TTF blend ratio 1:1.*

conjunction with the DB-TFF itself the cost of the composite will increase substantially the cost of the final OFET. Moreover, although in terms of mobility the devices are interesting; the overall device performance is not ideal for applications. Additionally, the increase of DB-TTF in the composition will have a detrimental effect in the stability of the whole composite. So, composites with insulating materials were devised at this point.

Polystyrene (PS280k) and DB-TTF composite OFETs

In order to first evaluate the capabilities of composites based on insulating polymers in this case polystyrene (PS280k) as binder

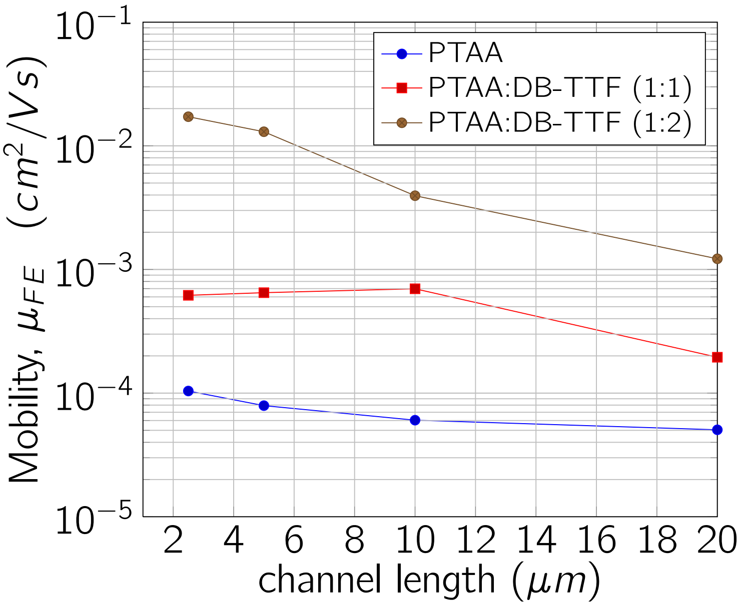

Figure 5.5 *Mobility of PTAA, and PTAA composites with DB-TTF as a function of channel length.*

and DB-TTF as active material was explored. First spin coated films were fabricated, following the same procedure explained before for the PTAA and DB-TTF composites. Spin coated films were fabricated in a ratio 1:1 PS280k:DB-TTF. Figures 5.6 show optical microscope pictures of the device fabricated, in which one can see a fairly homogeneous film over the entire area depicted (see Figure 5.6(a)). Small dots are randomly located in the film (see Figure 5.6(b)). These structures could be ascribed to small DB-TTF crystalline domains, that due to the centrifugal force and fast solvent evaporation applied during the spin coating process remained implanted in the PS matrix. Such structures seems to do not be interconnected inside the insulating polymeric matrix, which is in agreement with the fact that no field-effect characteristics were observed. Despite that spin coating is ubiquitous in research labs, the scalability and the failure to allow to set temperatures for coating are major drawback. At this point, the bar assisted meniscus shearing (BAMs) technique was applied for the fabrication of DB-TTF blends. This technique allows to coat from 1 cm per second up to 10 cm per second and to set the coating temperature from room temperature up to 150 ^oC, so BAMs covers a wide range of temperatures and coating velocities as well. Thus, fabrication of OFETs of DB-TTF and insulating polymers using spin coating was dropped.

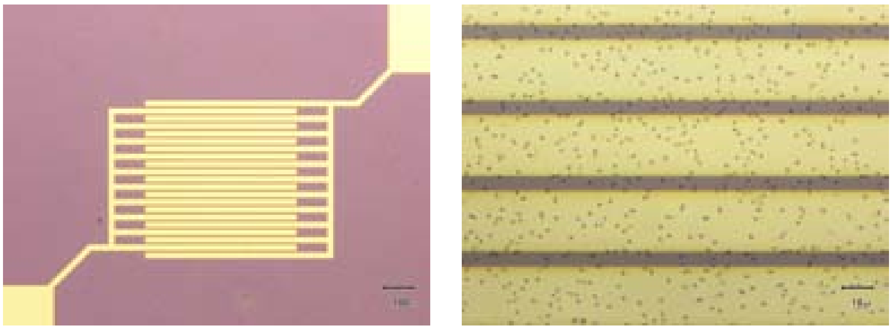

(a) (b)

Figure 5.6 *Optic microscope pictures for a spin coated film of a blend DB-TTF and Polystyrene. PS280k:DB-TTF 1:1 ratio.*

5.2.3 OFETs based on DB-TTF composites prepared by BAMs

PAMS and DB-TTF composite OFETs

To form the semiconducting layer, a 1% wt chlorobenzene solution of poly-(α-methyl styrene) (PAMS)[36–47]and 1% wt chlorobenzene solution of DB-TTF were mixed in ratios 50:50 and 40:60. Then 30 μl of the blend was dropped on a Fraunhoffer test chip, which was previously cleaned and subsequently placed on the machine held at 105^oC. After coating the test chip was removed immediately, and placed in a vacuum desiccator to remove any possible solvent trace that could remain trapped inside the film.

The best performing devices were obtained with the 1:1 ratio. Figure 5.7 depicts typical output and transfer characteristics obtained. Output characteristics depicts well defined linear and saturation regions, emulating textbook-like characteristics (see Figure 5.7(a)). It is important to note, by simple inspection from transfer characteristics that the threshold voltage is located below zero volts ($V_{TH} \approx$ -10 V), suggesting a non ideal OFET but importantly not doped. One must take into account that DB-TTF is a highly prone to doping material and that all fabrication and characterisations were carried out in air, a huge device improvement has been achieved with this method.

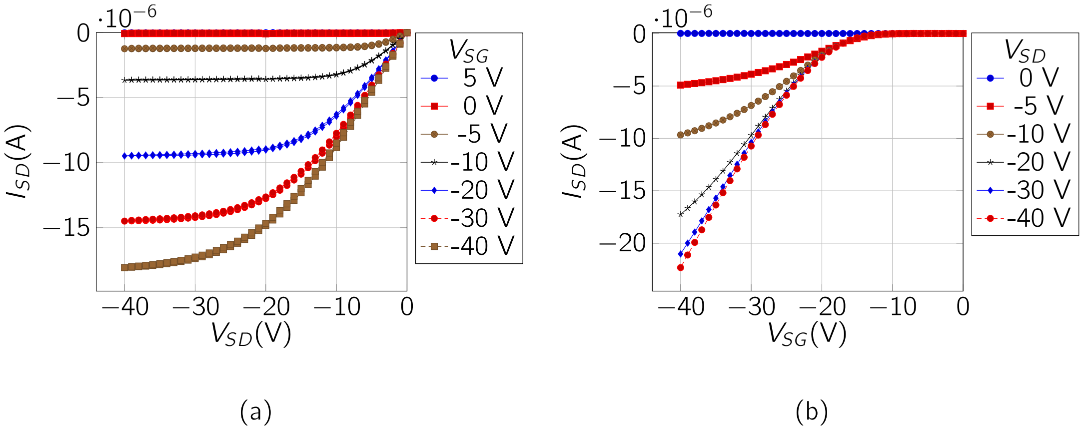

Figure 5.7 *(a) Output characteristics and (b) Transfer characteristics. Blend DB-TTF:PAMS at ratio 1:1. L = 20 μm and W = 10 mm.*

For this blend in which the amount of active material, DB-TTF, is reduced by 50% since a 1:1 ratio is used, the mobility is calculated in the range of $10^{-3}\,cm^2V^{-1}s^{-1}$. One can compare with the mobility values for the PTAA:DB-TTF blend (see Figure 5.5) with the same ratio polymer:small molecule, and it is clear that are in the same order of magnitude. However, one should highlight that the PAMS is an insulating material and at least one tenth of the cost of the PTAA, which implies that the final OFET will be less costly. Additionally, the electrical characteristics are much more closer with the ones reported in text-books than the one found for the PTAA:DB-TTF blend. One can wrap the found advantages into - OFETs were satisfactory fabricated in air, in one step, with only the 50% of active material, plus all samples were characterised in air while making the final OFETs less costly that the ones fabricated based on PTAA:DB-TTF composites.

iPS and DB-TTF composite OFETs

Despite the very satisfactory results found in PAMS:DB-TTF blends, it is well known that using more crystalline materials as binders in composites might enhance the charge transport in semiconductors[48]. So, an isotactic polystyrene (iPS) was used as replacement for PAMS in order to evaluate the results in OFETs in quantitative terms of mobility, and threshold voltage and qualitatively by the curve shapes for output and transfer, keeping constant the DB-TTF as an active material[48–59]. The same procedure for fabrication as in the previous case was followed, only changing the PAMS for iPS. Figure 5.8 depicts output and transfer characteristics. Output characteristics reveals hysteresis suggesting trapping, however the current is one order of magnitude higher than the previous case (see Figure 5.8(a) for iPS based blend and Figure 5.7(a) for the PAMS.). The calculated mobility for these devices is in the range on 10^{-2} $cm^2V^{-1}s^{-1}$, then is one order of magnitude higher than the one found for the PAMS:DB-TTF case for the same 1:1 ratio.

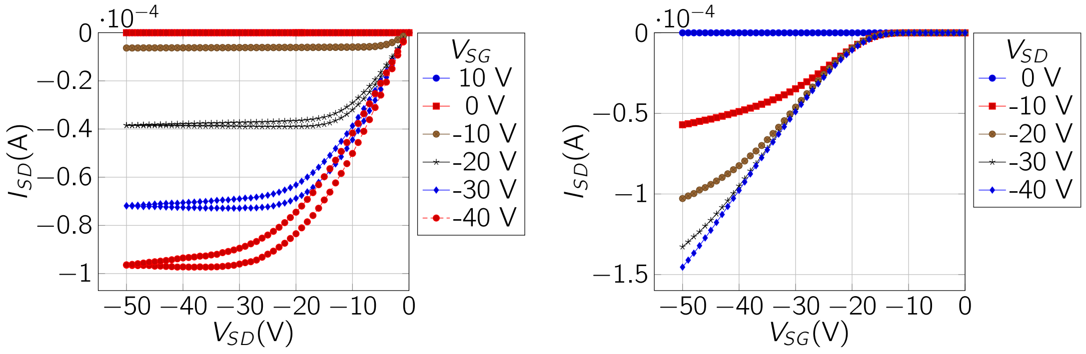

(a) (b)

Figure 5.8 *Output and Transfer DB-TTF and iPS composite, blend ratio (50:50). L = 20 µm and W = 10000 µm.*

Despite the high mobility found for this blend compared with previous ones found in this study, the drawback of this composite is its dynamic viscosity[56,60,61] which is high ($\approx 0\ 05 Pas$) even at such low concentration[49,51,52,54,55,57]. This makes difficult to work with this polymer and increases the error when the experimentalist tries to determine the exact volume that drops on the sample to form the film, causing reproducibility issues. The crystalline order of iPS[42,63] may contribute to a particular organisation of DB-TTF inside the composite[48]. However, the formation of metastable phases of crystalline materials during sheared depositions on substrates is also related to the shear field generated by the moving meniscus, the convective flow generated by solutes moving towards the meniscus and by the convective mass transfer from the meniscus to the surrounding air. The shear stress is small right at the air-liquid interface, but it increases while approaching the solid substrate[64,65]. Since the polystyrene gave highly performing devices, experiments were devised in order to reduce the shear stress[60,61,63] by reducing the viscosity of the the solution, simply by changing the molecular weight of the polymer used [¶].

Atactic PS and DB-TTF composite OFETs

Polystyrene for GPC 10000 (PS10000), polystyrene for GPC 30000 (PS3000), and polystyrene for GPC 1000 (PS1000), were each tested in several ratios blended with DB-TTF procuring always to decrease the amount of semiconductor used. Proportions with higher concentration of DB-TTF than PS were not tested and are out the scope of this thesis. So, the organic semiconductor DB-TTF and the insulating polymer PS10000 both were weighted and placed in separate vials. Solutions at $2\% wt$ were made using anhydrous chlorobenzene. Appropriate ratios DB-TTF:PS10000 ranging from 1:1, 1:2 to 1:3 all were mixed in separate vials with total volumes not exceeding 500 μl. Heavily doped n-type Silicon with a 200 nm thick SiO_x dielectric was used as substrate and gate electrode. The heating

---

[§] Water at 25 ^oC has a dynamic viscosity equal to 0.8937 x 10^{-3} Pa s[62]

[¶] atactic polystyrene with low molecular weights were tested instead of low molecular weight isotactic polystyrene due to availability and price.

bed of the coating machine was set at 105 ^{o}C before coating. Cleaned substrates with prefabricated electrodes were carefully placed on the coating machine where a small volume of the solution typically $\approx 30\,\mu l$ was used. The solution was casted at a constant velocity of 1 cm/s, during the process the substrate and the solution were held at 105 ^{o}C. Immediately, after casting the coated substrates were removed from the coating machine and placed in Petri dishes covered with aluminium foil and left to cure in vacuum ($P_{abs} = 7kPa$) at 60^{o}C for at least 2 h, in order to remove any residual solvent and to fully dry the sample. After curing, output and transfer characteristics were measured at room temperature under ambient conditions in darkness. Top contact devices were also fabricated. Film deposition were performed on bare Si/SiO_x substrates following the same procedure as described for bottom contact devices. Top contact electrodes were deposited by thermal evaporation trough a shadow mask, with a nominal Au thickness equivalent to 80 nm.

Electrical characterisation and ratio screening in DB-TTF: PS10000 blends

Table 5.1 collects the resume of mobility and threshold voltage for several DB-TTF:PS10000 ratios in bottom contact OFETs. It is known that the ratio among components strongly affects the electrical performance[66,67]. One of the main goals of blending was to use the minimal amount of semiconductor in the blend as possible, while not constricting electrical performance. Considering this, the blend ratio 1:3 for semiconductor:polymer (DB-TTF:PS10000), respectively, turns to be the most suitable, giving mobility values in the range of $10^{-2}\,cm^{2}V^{-1}s^{-1}$, which is on the same order of magnitude as that found for evaporated DB-TTF films. Also, one can observe that going from ratio 1:1 to 1:2 as the DB-TTF proportion decreases the mobility increases. This can be interpreted as the semiconductor material is reduced in the blend, better and perhaps, more efficient pathways for conduction are constructed inside the composite, probably due to a higher phase separation in the film that results in the formation of a more homogeneous DB-TTF layer. In 1:3 ratio the mobility remains constant and from that point drastic mobility drops can be observed when DB-TTF proportion diminishes, as observed in the 1:4 ratio where most devices measured produced no field-effect characteristics. One important feature to highlight from Table 5.1 is that no dependence on the channel length was observed for the range studied 25 μm < L < 100 μm.

Table 5.1 *Mobility and threshold voltage resume data table for bottom contact architecture devices for blends DB-TTF:PS10000 with ratios 1:1,1:2 and 1:3, from twin samples for repeatability.*

Bottom Contact Architecture/Blend of DB-TTF with PS10000						
	Blend Ratios - Semiconductor:Polymer					
	1:1		1:2		1:3	
Channel Length	μ	V_{TH}	μ	V_{TH}	μ	V_{TH}
[μm]	$\left[\frac{cm^2}{V s}\right]$	[V]	$\left[\frac{cm^2}{V s}\right]$	[V]	$\left[\frac{cm^2}{V s}\right]$	[V]
25	2.05e-3	-2.69	1.56e-2	-1.60	9.75e-3	-1.81
50	2.35e-3	-2.30	2.26e-2	1.48	1.42e-2	-0.38
75	6.25e-3	-2.77	1.67e-2	-0.01	1.02e-2	1.18
100	6.39e-4	-3.84	9.40e-3	0.19	1.27e-2	-1.11

Figure 5.9 depicts the Output and Transfer Characteristics [†] for a typical device based on DB-TTF:PS10000 ratio 1:3. The device show typical field-effect characteristics clearly observed in Figure 5.9(a) in which is seen how the gate voltage applied modulates the current measured as well as how the current tends to saturate as the source-drain voltage applied reaches the gate-voltage applied. It is also worth noting the negligible hysteresis shown in the output characteristics.

It is also important to highlight the reproducibility in fabrication. Forty devices

---

[†] Output and transfer characteristics for typical devices from each blend ratio can be found in Appendix F

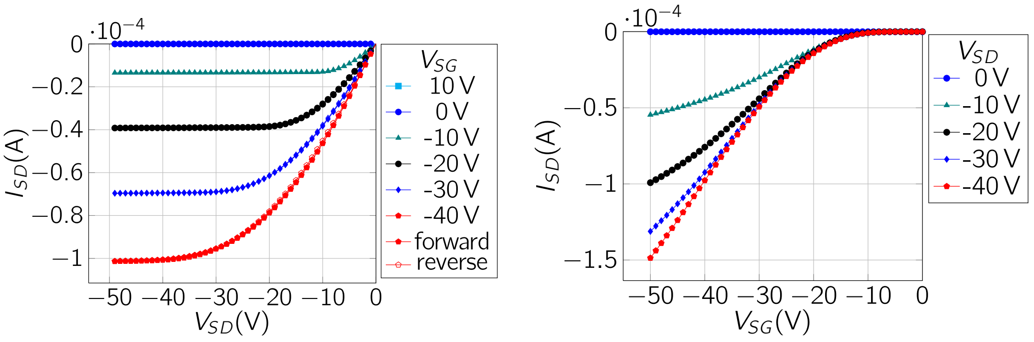

(a) (b)

Figure 5.9 *(a) Output characteristics, and (b) Transfer characteristics for DB-TTF:PS10000 blend ratio 1:3 in bottom contact architecture. Device with L = 75 µm W = 75000 µm. Measured in air and darkness.*

were analysed, generating a mean mobility equal to $1.8\text{x}10^{-2} \pm 2.0\text{x}10^{-3}$ $cm^2V^{-1}s^{-1}$. In order to evaluate if the casting direction is significant in order to produce anisotropy in the films, devices parallel to the casting direction and perpendicular to the casting direction were analysed statistically [**] . So it is concluded that the parallel and perpendicular directions reports the same mean value. So, the mean mobility value from the devices casted parallel is statistically equal to the mean mobility value from the devices casted perpendicularly.

Further, electrical characterisation was carried out on devices fabricated with top-contact bottom-gate architecture. Table 5.2 resumes the mobility and threshold voltage average values for all tested composition ratios, observing again that the ratio 1:3 is the most suitable to use in terms of performance and amount of organic semiconductor used, as found in the bottom contact devices. Figure 5.10 reveals the output and transfer characteristics for a typical top contact device fabricated from a blend of DB-TTF and PS10000 in a ratio semiconductor polymer

---

[**] Tested within a 5% significance level ($\alpha = 0\ 05$), and assuming equal deviations the calculated value was found equal to 0.1490, and from a t-student distribution table the critical value $t_{(0.025,17)} = 2\ 11$ was found.

Table 5.2 *Resume table for mobility and threshold voltage as a function of composition ratio for top contact devices. L in the range 20 - 100 μm*

ratio	μ_{FE}	V_{TH}	
OSC:Polymer	$[cm^2\ Vs]$	[V]	n devices
1:1	5.5x10^{-5}	-2.2	4
1:2	2.5x10^{-2}	3.0	10
1:3	5.5x10^{-2}	3.2	11

equal to 1:3. Figure 5.10(a) depicts typical output characteristics for a field-effect transistor showing clear zones of saturation and linear behaviour, while the hysteresis is negligible. Devices fabricated in top contact architecture exhibit mobility values in the order of magnitude of $10^{-2}\,cm^2V^{-1}s^{-1}$ and threshold voltage around zero volts.

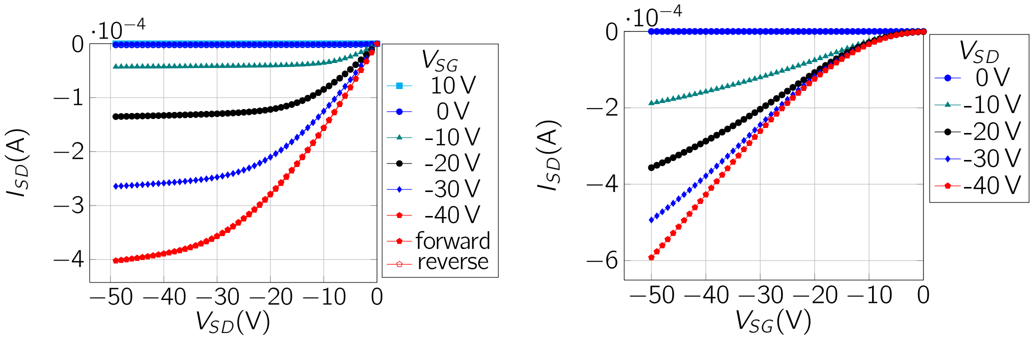

(a) (b)

Figure 5.10 *(a) Output characteristics, and (b) Transfer characteristics for DB-TTF PS10000 blend ratio 1:3 in top contact architecture, device L = 19.54 μm W = 4000 μm.*

Despite the textbook-like characteristics for both output and transfer, plus the high mobility achieved of the order as in the bottom contact devices. The overall variation device-to-device in mobility terms, exceeds one order of magnitude and is tentatively ascribed to film damage during evaporation of top contact electrodes. For this reason, bottom contact devices were selected from this point on.

Morphology, film thickness and crystal structure Figure 5.11 shows an optical microscope image of the film DB-TTF:PS10000 ratio 1:3 casted in an bottom contact architecture, which one clearly observe an even crack-free film over the whole area. It is important to note that even with interdigitated structures the film was casted on the top homogeneously. In Figure 5.11(b) the polarized optical microscope image is shown and elucidates the formation of crystalline structures which are embedded in the film forming pathways to hole transport between electrodes.

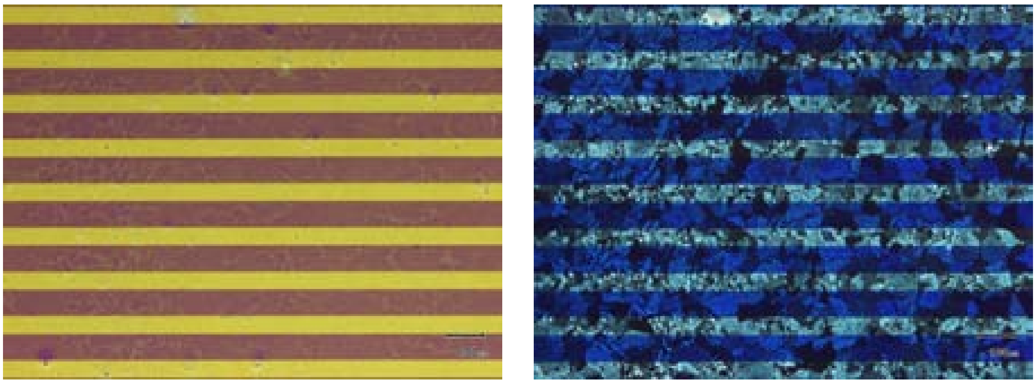

(a) (b)

Figure 5.11 *Polarized microscope images for bottom contact device, DB-TTF and PS10000 ratio: 1:3, (a),* $\Phi_{P\ A} = 0^o$ *between Polarizer and Analyzer and (b),* $\Phi_{P\ A} = 90^o$ *between Polarizer and Analyzer.*

Figure 5.12(a) depicts the topography measured by AFM for a particular zone on a film based on DB-TTF:PS10000 ratio 1:3, in which one can see different structures, non periodic nor structured, while Figure 5.12(b) reveals roughness values of around 2 nm taken from a diagonal profile, demonstrating a very smooth film. Neglecting the peak observed at x $\approx$ 1 μm the values oscillate around + 0.5 and -0.5 nm.

A FIB-SEM [††] system combines traditional thermal emission Scanning Elec-

---

[††] This work was carried out in collaboration with Dr. R. Pfattner, Dr. T. Trifonov and Prof. J. Puigdollers at the Center for Research in NanoEngineering (crne) at Universitat Politècnica de Catalunya (UPC).

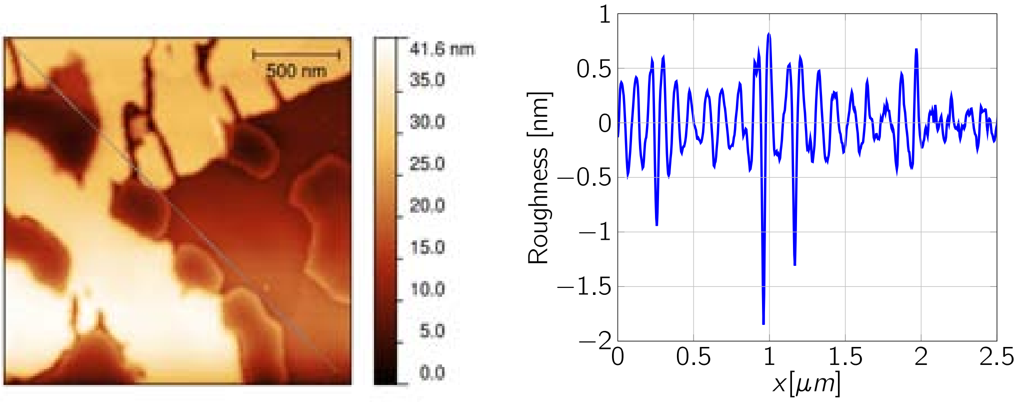

(a) (b)

Figure 5.12 *(a) Topographic Atomic Force Microscopy picture, and (b) roughness from the diagonal profile of figure (a), for a film based on DB-TTF:PS10000 ratio 1:3.*

tron Microscopy (SEM) with Focused Ion Beam (FIB) for 3D characterisation and nanoanalysis. This technique is suitable to study the cross section of devices and to analyse interfaces between materials, due to a focused ion beam of Ga^+ that can be used for nanostructuring and imaging. In order to calibrate the Ga^+ ion beam and to obtain a clean cut at the cross section, 100 nm of Pt was thermally evaporated on top of the sample. Figure 5.13(a) shows the hole in the sample in order to study the cross section of the device depicted in Figure 5.13(b), in which the full thickness of the film was found to be around 50 nm. It can be clearly distinguished the layers of Pt, film, SiO_2 and Si which constitutes the sample. Unfortunately, the resolution was not good enough to find out if vertical phase separation in the blend was taken place.

Also, X-ray diffraction were carried out in a BAMs casted film and in a thermally evaporated film of pure DB-TTF, both depicted in Figure 5.14. From such figure one can see that both films coincide in more than 3 peaks, and for both cases the γ crystalline phase is ascribed as reported by Brillante el al.[68].

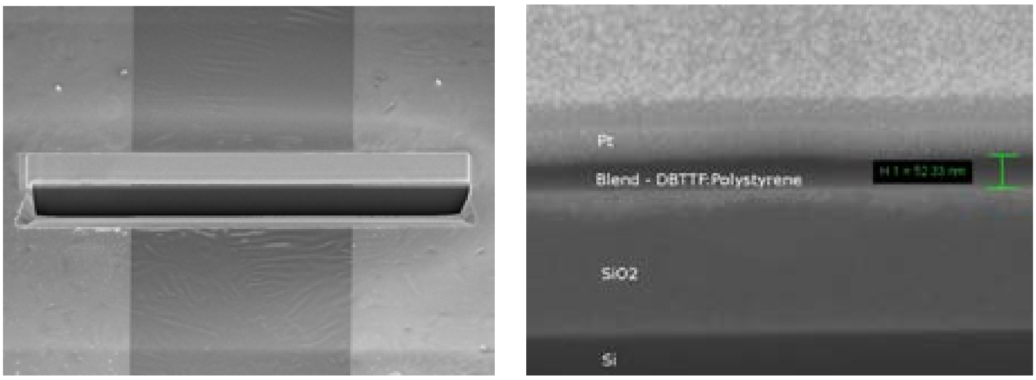

(a) (b)

Figure 5.13 *FIB-SEM analysis and image of the cross section found for a OFET based on DB-TTF:PS10000 (1:3 ratio).*

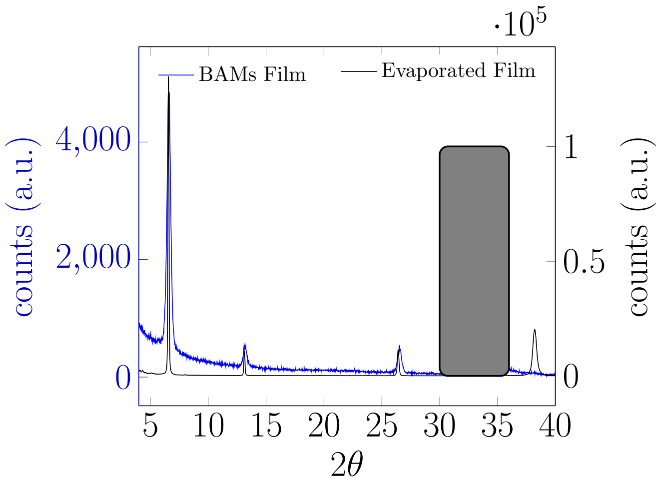

Figure 5.14 *XRD diffraction for pure thermally evaporated DB-TTF and a DB-TTF:PS10000 (1:3 ratio) composite film casted using BAMs.*

Stability test in air In order to evaluate the applicability in circuits and other applications, it is of imperative importance to evaluate how stable the OFET could be under ambient conditions. Thus, to evaluate the stability in air of the blend DB-TTF:PS10000 ratio 1:3, a particular device was wired and placed inside an incubator with controlled temperature ($T \approx 25^oC$) and measured continuously. Figure 5.15 shows the logarithmic transfer measured sequentially. A negligible shift in the switch-on voltage for 14 hours exposed to air but kept in darkness was observed, suggesting that the stability has been enhanced tremendously compared to DB-TTF evaporated films.

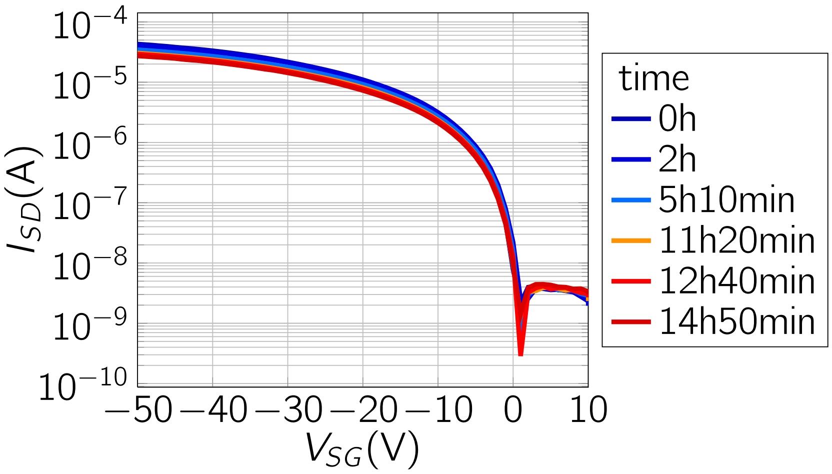

Figure 5.15 *Log transfer plot for DB-TTF:PS10000 ratio 1:3 blend OFET measured in air.*

Influence of the PS molecular weight Considering the promising results with DB-TTF and PS10000 blends, it was decided to explore the influence of modifying the molecular weight of the polymer binder in the final device performance. First, a very low molecular weight polymer was investigated: PS1000. However, no field-effect was observed in the films despite all the experimental conditions attempted. Next, a polymer with an intermediate weight was used, PS3000. Using PS3000 as binder several ratios DB-TTF:PS3000 were tested (1:1, 2:3, 1:2, and 1:3) for both architectures bottom and top contact. Table 5.3 compiles all the average mobilities and threshold voltages for all cases . One can observe that the maximum mobility value is 0.1 $cm^2V^{-1}s^{-1}$ found for the bottom contact architecture and 1:2 ratio. Also, one can observe that in the top contact configuration as the amount of semiconductor embedded in the polymeric matrix decreases the mobility prevails around the same order of magnitude, tentatively ascribed to a vertical phase separation. Further, as already observed for the blend of PS10000 the V_{TH}

Output and transfer characteristics for typical devices out of each ratio tested can be found in Appendix G is very low, ensuring that the film is not doped.

Table 5.3 *Mobility and threshold voltage resume data table for bottom and top contact architectures. Each point is the average of at least eight data points.*

	Bottom contact		Top contact	
ratio DB-TTF:Polymer	μ_{FE} $cm^2V^{-1}s^{-1}$	V_{TH} V	μ_{FE} $cm^2V^{-1}s^{-1}$	V_{TH} V
1:1	9.8e-5	-4.3	8.2e-3	-1.6
2:3	3.0e-2	-0.2	6.3e-2	-1.0
1:2	1.0e-1	-2.3	2.3e-2	-1.9
1:3	5.5e-3	-2.1	4.8e-2	-3.7

Therefore, lowering the polystyrene molecular weight from 10000 to 3000 has given rise to high performing OFETs with a mobility values one order of magnitude higher. Hence, the blend DB-TTF:PS3000 1:2 ratio was selected as the most promising one for fabricating OFETs. In Chapter 6 , a careful study on this blend and the resulting devices based on it, is carried out

5.3 OFETs based on DT-TTF composites prepared by BAMs

Composite thin films of DT-TTF and insulating polymers (PS10000, PS3000, PAMS, PS10000:PAMS and PAMS:poly-(methyl methacrylate) (PMMA) were fabricated using BAMs. DT-TTF was dissolved in chlorobenzene to a 2 % wt solution, in separate vials solutions of 2 %wt in chloroform of all polymers (PS10000, PS3000, PAMS, and PMMA) were prepared.

In two cases blends of polymers were prepared PAMS:PMMA ratio: 90:10 and PAMS:PS10000 ratio: 50:50. For all blends semiconductor:insulating polymer a ratio 1:1 is maintained. The same fabrication steps as the ones described previously for DB-TTF were followed. Table 5.4 contains a resume of all composite materials tested with average values for mobility and threshold voltage. It is worth noting that the highest average mobility recorded was 0 13 $cm^2V^{-1}s^{-1}$ for DT-TTF and (PAMS : PMMA (9:1)) ratio: 1:1 which matches that reported for OFETs based on films fabricated by zone casting and also those based on single crystal β-phase DT-TTF. Electrical characterisation for the best performing device was recorded and depicted in Figures 5.16(a) and 5.16(b) which depicts typical output and transfer characteristics for a best performing device. Both show little hysteresis suggesting some trapping and an interface semiconductor/insulator with defects, which also

Table 5.4 *Mean mobility and threshold voltage resume table for different blends, where always the ratio between semiconductor and polymer or polymeric blend is 1:1.*

	PS10000	PS10000:PAMS	PS3000	PAMS:PMMA	PAMS
	100 %	50 % :50 %	100 %	90 % : 10%	100 %
$\mu\ [cm^2\ V s]$	0.06	0.03	0.01	0.09	0.06
V_{TH} [V]	-25	-18	-20	-16	-20

is reflected in the threshold voltage values.

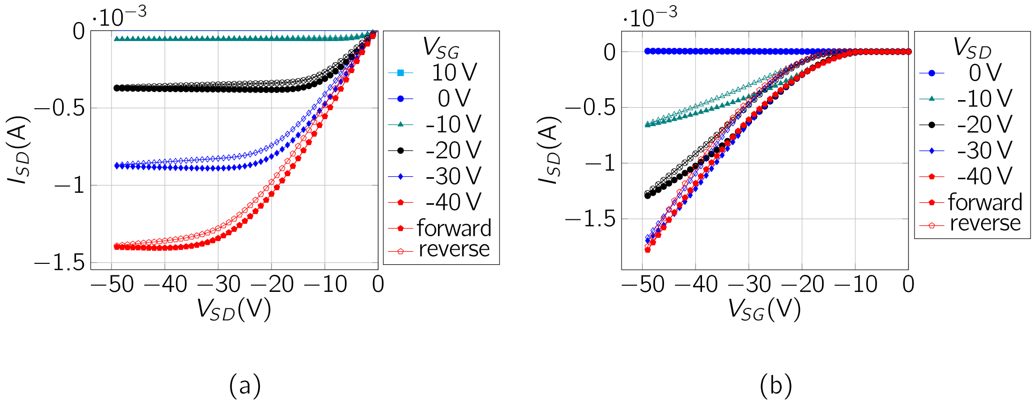

Figure 5.16 *(a) Output characteristics, and (b) Transfer characteristics for DT-TTF and (PAMS10k : PMMA (9:1)) ratio: 1:1 in bottom contact architecture. Device with L = 100 μm W = 100 mm. Measured in air and darkness.*

The best results in terms of V_{TH} were obtained when ternary blends[40,58] were used, tentatively ascribed to better film quality at the semiconductor/dielectric interface.

Figure 5.17(a) shows an optical microscope picture with 0^o angle between the polariser and analyser, showing a fairly homogeneous film across the whole sample despite the protruded electrodes over which the film was deposited. Figure 5.17(b) shows the same image with an angle of 90 ^{o} between polarizer and analyser showing crystalline structures embedded in the polymeric matrix across the entire interdigitated electrodes.

Figure 5.18(a) depicts the topography of a particular zone of the DT-TTF : (PAMS10k : PMMA) film which shows an homogeneous film with no evident pin holes or cracks down to the scale shown in the figure, while Figure 5.18(b) shows the roughness extracted diagonally which clearly implies a very low value since it fluctuates around ± 1 nm (rms ≈ 2 nm).

In order to gain information about the crystalline phase X-ray diffractograms (XRD) were recorded which are shown in Figures 5.19(a) 5.19(b). It is clear to ob-

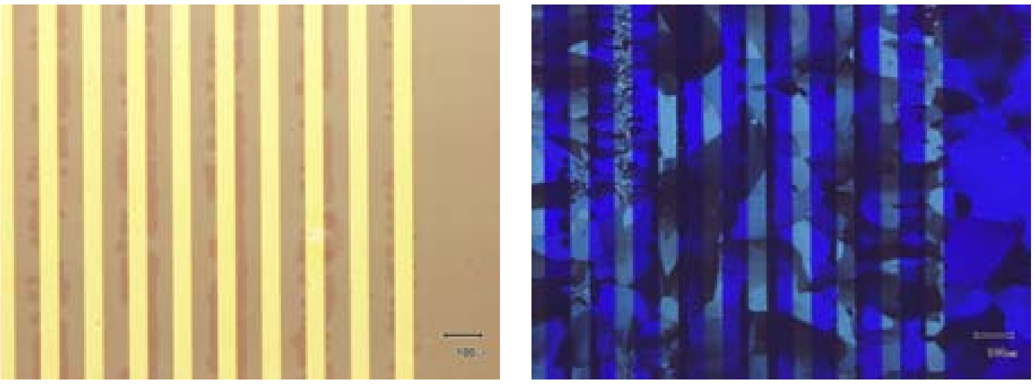

(a) (b)

Figure 5.17 *Polarized microscope images for bottom contact device, L = 75 µm W = 75000 µm, DT-TTF and (PAMS10k : PMMA (9:1)) ratio: 1:1 (a)* $\Phi_{P\ A}=0\ ^o$ *between Polarizer and Analyzer and (b)* $\Phi_{P\ A}= 90\ ^o$ *between Polarizer and Analyzer.*

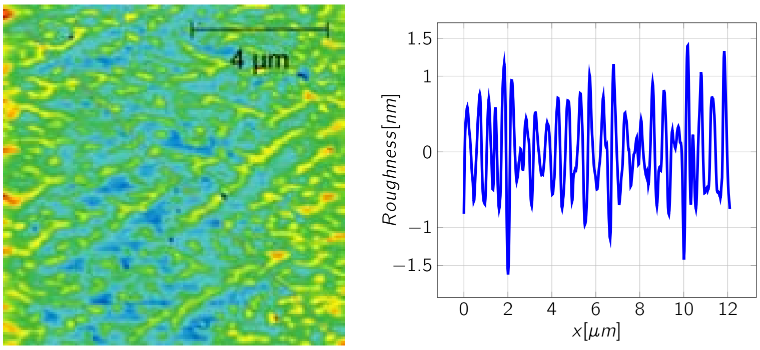

(a) (b)

Figure 5.18 *AFM - bar casted film of DT-TTF:PAMS/PMMA (1:1(9:1)) (a) Topography,(b) Roughness.*

serve that peaks are related to a periodicity which is estimated to be 13.18 Å , which suggests that DT-TTF molecules assemble on the surface with the long molecular axis aligned approximately parallel to the surface normal and coincides with the β-phase DT-TTF crystals reported by Pfattner et al.[16].

The best performing devices were found using a ternary blend of DT-TTF and (PAMS10k : PMMA (9:1)) in a ratio 1:1. OFETs exhibit excellent output and transfer characteristics, with mobility that match the mobility for a single crystal (β DT-TTF). Despite the high mobility found, one drawback is the moderate high

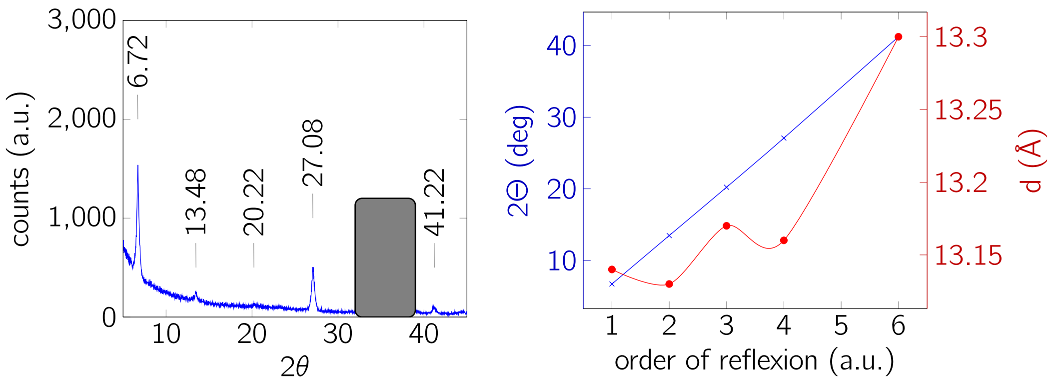

(a) (b)

Figure 5.19 *XRD diffraction for (a) bar casted film of DT-TTF and (PAMS10k : PMMA (9:1)) ratio: 1:1, (b) estimated d - spacing using reflection 1-4 and 6 as shown in (a)*

deviation from ideal state measured by the threshold voltage. However, important to highlight is that using the methodology here found, one can match the single crystal mobility, using a solution process technology while the material used has been reduced by a 50% which is fairly important since the DT-TTF is a difficult material to synthesise.

5.4 OFETs based on BET-TTF

5.4.1 Thermally evaporated films

Thermally evaporated thin films of BET-TTF were investigated as OFETs their stability in ambient conditions were tested. Films were evaporated at a rate of 0.5 Å/s and at 120 ^oC while the pressure of the chamber wast kept at $1x10^{-6}$ mbar. Fraunhoffer substrates were used. Figure 5.20 depicts the logarithmic transfer characteristics recorded when the OFET was measured in darkness and exposed to air. The colour gradient from blue to red represents increase in exposure to ambient conditions from zero to 3 hours. The very first curve in blue depicts the as prepared measurement, showing a switch on voltage close to + 20 V. Then the curve progresses to red in the picture, while the increase in current is evident. This increment is ascribed to dopping since the OFET is exposed to air. One should note that all these curves were recorded in darkness. However, when light is switch on the curve suffers a dramatic change depicted in the second block of curves from bottom to top. Such block of curves depicts how light degrades the OFET, clearly seen in the log transfer, in which one can see that the OFET will require more than + 20 V to switch off. The final block of curves from bottom to top, depicts the OFET reaction to a microscope light, in which one can clearly observe that the OFET is fully degraded and loses completely the FET characteristics, failing to switch-off. The calculated mobility fell in the 10^{-4} $cm^2V^{-1}s^{-1}$ range.

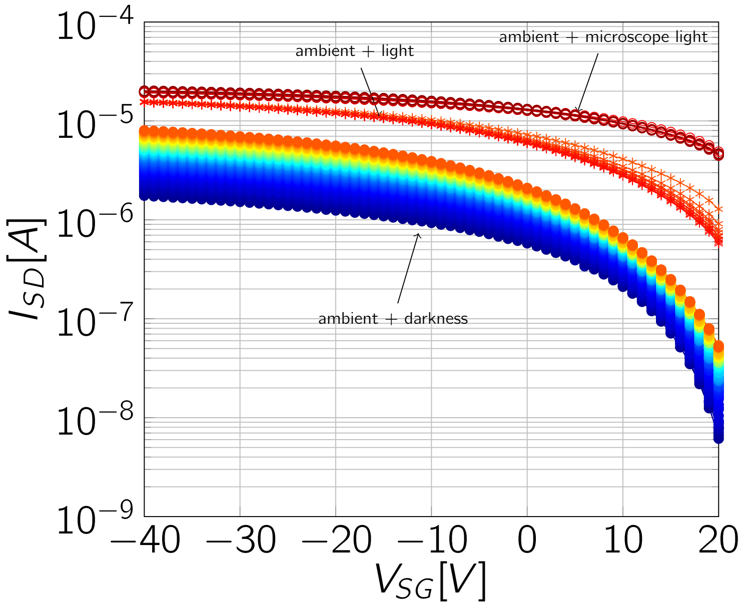

Figure 5.20 *Log transfer for a BET-TTF evaporated film as a function of time, exposed to ambient conditions and light.*

From Figure 5.20 one can infer that BET-TTF is a prone dopping material, which degrades rapidly in presence of oxygen, ambient humidity and light. However, blending could be an option to help to palliate, attenuate or eradicate doping.

5.4.2 OFETs based on BET-TTF composites prepared by BAMs

The polymers PS280k, PS10000, PS3000 and PAMS all were tested, however the ones that gave good results were PS280k, and PS10000. Figures 5.21(a) and 5.21(b) depicts output and transfer characteristics for a composite of BET-TTF and PS10000 in a ratio 2:1. The composite was formed from a starting solution of 2 %wt for both semiconductor and polystyrene and then they were mixed in the appropriate ratio. The output characteristics shows a region that the current tends to saturate at the end of the sampling for high V_{SD}, however it does not completely saturate. But, the field-effect induced by the gate voltage applied is clearly visible since the curves shows higher current as the gate voltage increases. The calculated mobility ranges between 10^{-5}- 10^{-4} $cm^2V^{-1}s^{-1}$, while the threshold voltage fluctuates around 1 V. Also, a composite was developed based on PS280k as binder an BET-TTF as semiconductor in a relationship (1:3) starting from solutions at 1% wt in chlorobenzene of both materials. Figures 5.21(c) and 5.21(d) shows typical output and transfer characteristics, with indeed very good OFET behaviour like negligible hysteresis. The mobility calculated is in range of 10^{-4} - 10^{-3} $cm^2V^{-1}s^{-1}$ and V_{TH} around 5 V. Despite the unstable character of the BET-TTF OFETs, composites based devices were fabricated and measured in air with no signs of apparent dopping by oxygen and/or water, keeping in mind that both evaporated and thin film composites have mobilities in the same order of magnitude.

5.4.3 Doping of BET-TTF:PS280k composites with I_2

Previously, it was demonstrated the preparation of thick films ($\approx 20\mu m$) of polycarbonate containing 2 % wt of BET-TTF by drop casting. Those after

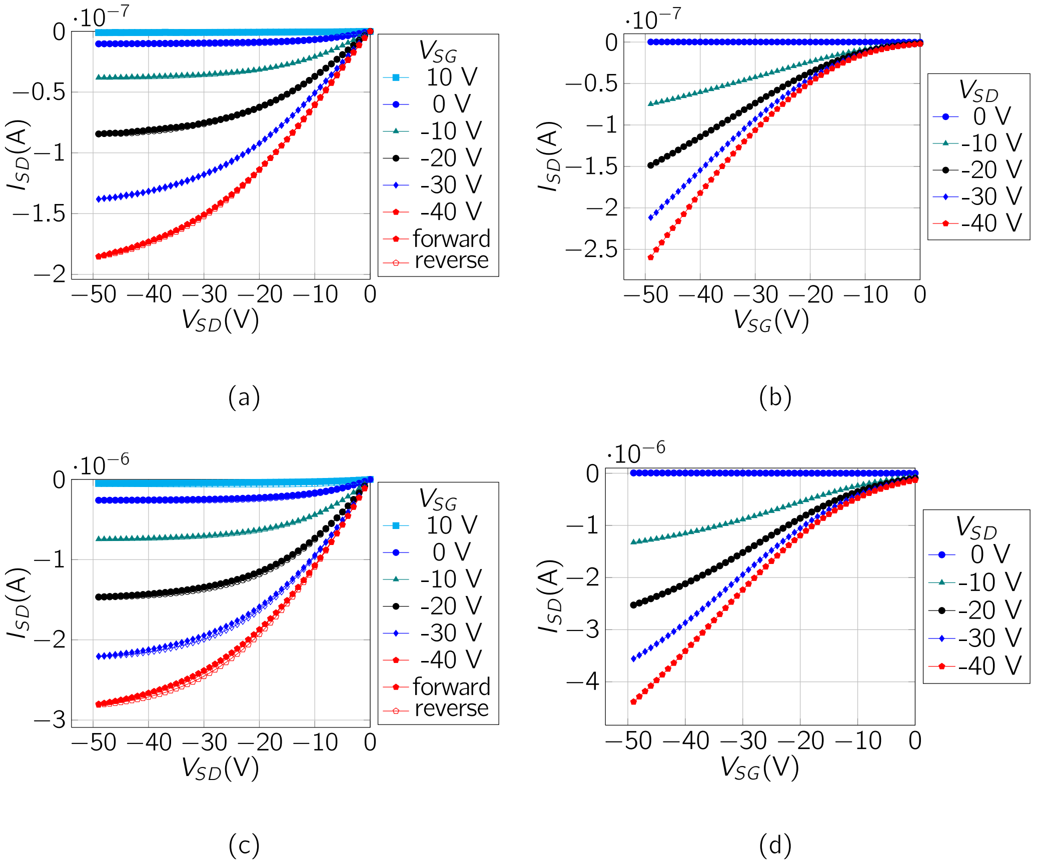

(a) (b)

(c) (d)

Figure 5.21 *Output characteristics (a) BET-TTF:PS10000 ratio 2:1 and (c) BET-TTF:PS280k ratio 3:1. Transfer characteristics (b) BET-TTF:PS10000 ratio 2:1 and (d) BET-TTF:PS280k blend ratio 1:3. (c) and (d) L = 20 μm and W = 20 mm. (c) and (d) L = 25μm W = 25 mm. Measured in air and darkness.*

doping with I_2 or Br_2 became metallic[31,69]. Preliminary studies were performed here in order to evaluate the possibility of fabricating organic electrodes directly on the organic semiconductor film. In this case the binder is polystyrene with a molecular weight equals to 280000 g/mol (PS280k). The proof of concept first consisted in developing a composite that works as a semiconductor. After the success in OFETs fabrication and knowing the semiconductor behaviour, the same procedure was carried on bare Si SiO_x, and using a very simple fabrication step depicted in Figure 5.22 in order to selective dope areas with I_2 vapours in order to obtain a metal-like conducting regions while areas not exposed may maintain the semiconductor behaviour.

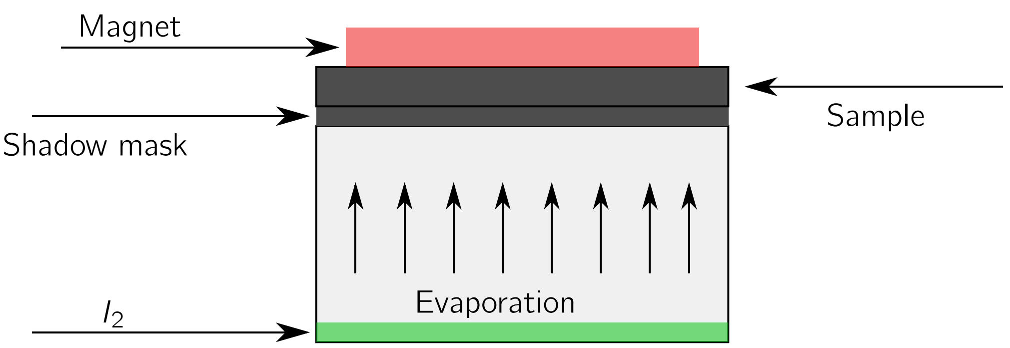

Figure 5.22 *Setup for patterning BET-TTF films using* I_2*.*

But, first a proof-of-concept was carried out when a typical BET-TTF:PS280k (ratio 3:1) OFET was exposed to a saturated solution of I_2 for 5 s in order to evaluate, how the intrinsic properties of the OFET changes. Figure 5.23(a) depicts the output for the non-doped transistor which one clearly observes the field-effect. However when the OFET is exposed to I_2 depicts now the absence of field-effect producing overlapping curves with all gate voltages tested was observed (see Figure 5.23(b)). Figures 5.24(a) and 5.24(b) shows the patterns obtained by the

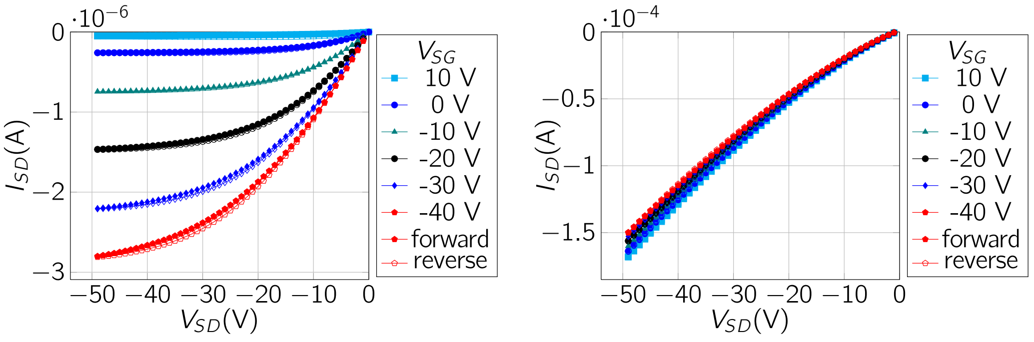

(a) (b)

Figure 5.23 *Output characteristics (a) before and (b) after* I_2 *exposure.*

process depicted in Figure 5.22, which are clearly seen contact like structures very well defined over the surface, and no cracks or pin holes were observed after the exposure to I_2. The rectangle-like zones were the zones exposed to I_2, while the path-like zones surrounding the exposed zones were the regions covered by the shadow mask.

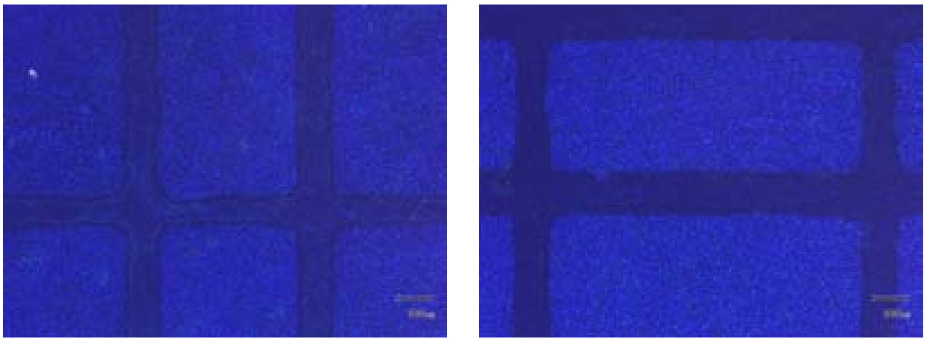

(a) (b)

Figure 5.24 *Optic microscope pictures with* $\Phi_{P\ A} = 90^{o}$ *between Polarizer and Analyzer for two different zones on the film.*

The SEM image in Figure 5.25 shows the crystalline domains formed by doping, which resembles the ones reported before for polycarbonate/BET-TTF conducting composites[31,69,70]. Analysis by EDX confirms the presence of iodine. The promising IV characteristics depicted in Figure 5.23(b) and patterning success depicted in Figure 5.24, are preliminary results which reveal that these materials and this methodology show potential to fabricate all-organic OFETs.

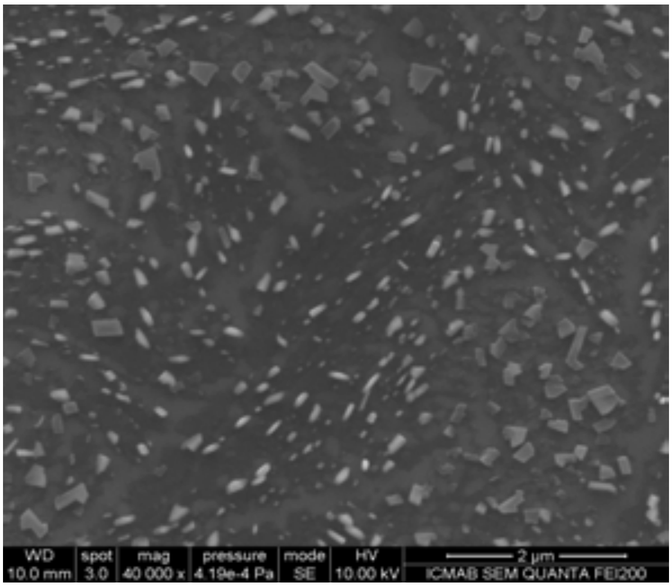

Figure 5.25 *SEM image of a* I_2 *doped thin film of BET-TTF:PS280k ratio 3:1.*

5.5 Summary

In this chapter three TTFs derivatives (DB-TTFF, DT-TTF and BET-TTF) blended with polymers were studied for their application in OFETs. For all three TTFs derivatives specific routes were found to assuage their instability relative to ambient conditions namely oxygen and water. Here it is demonstrated that DB-TTF OFETs based on thermally evaporated thin films were highly unstable in presence of oxygen and water even at ppm levels. A ratio screening was carried out for bottom and top contact architectures in order to determine the best case scenario. Using the Bar Assisted Meniscus Sheering (BAMs) technique a self-encapsulation in a PS matrix of DB-TTF is produced in one-step forming composites, invigorating the stability of the pure material, while making the DB-TTF processable on large-areas, from solution, while reducing the cost since more than 60 % of the whole material is a low cost polymer such as polystyrene. So, it is important to highlight that a highly unstable material is converted into an stable material just by finding an adequate manufacturing process. Further, by using composite materials and the BAMs technique the DT-TTF could be successfully processed over a large area while matching the mobility reported for single crystal OFETs as well for films fabricated by zone casting, and reducing the amount of material at least by 50% . For BET-TTF, a successful methodology was developed to migrate from highly unstable OFETs to stable OFETs. Also, a proof-of-concept study was carried out in order to pattern films of BET-TTF with I_2. Considering all the combinations of TTF/polymer blend studied, we selected as the most promising blend DB-TTF:PS3000 ratio 1:2 considering performance, price and applicability. Next chapter is devoted to peruse its behaviour in detail and evaluate its potential for applications (see Chapter 6).

Bibliography

[1] A. Arias, F. Endicott and R. Street. "Surface Induced Self Encapsulation of Polymer Thin Film Transistors". *Advanced Materials*, **2006**, 18, 2900.

[2] A. C. Arias, J. D. MacKenzie, I. McCulloch, J. Rivnay and A. Salleo. "Materials and Applications for Large Area Electronics: Solution-Based Approaches". *Chemical Reviews*, **2010**, 110, 3. PMID: 20070114.

[3] R. Hamilton, J. Smith, S. Ogier, M. Heeney, J. E. Anthony, I. McCulloch, J. Veres, D. D. C. Bradley and T. D. Anthopoulos. "High-Performance Polymer-Small Molecule Blend Organic Transistors". *Advanced Materials*, **2009**, 21, 1166.

[4] A. Facchetti. "Semiconductors for organic transistors". *materialstoday*, **2007**, 10, 28.

[5] T. Hasegawa and J. Takeya. "Organic field-effect transistors using single crystals". *Science and Technology of Advanced Materials*, **2009**, 10, 024314.

[6] Naraso, J.-i. Nishida, S. Ando, J. Yamaguchi, K. Itaka, H. Koinuma, H. Tada, S. Tokito and Y. Yamashita. "High-Performance Organic Field-Effect Transistors Based on pi-Extended Tetrathiafulvalene Derivatives". *Journal of the American Chemical Society*, **2005**, 127, 10142.

[7] B. Noda, H. Wada, K. Shibata, T. Yoshino, M. Katsuhara, I. Aoyagi, T. Mori, T. Taguchi, T. Kambayashi, K. Ishikawa and H. Takezoe. "Crystal structures and transistor properties of phenyl-substituted tetrathiafulvalene derivatives". *Nanotechnology*, **2007**, 18, 424009.

[8] M. Mas-Torrent, P. Hadley, S. T. Bromley, N. Crivillers, J. Veciana and

C. Rovira. "Single-crystal organic field-effect transistors based on dibenzo-tetrathiafulvalene". *Applied Physics Letters*, **2005**, 86 012110.

[9] C. Rovira, J. Veciana, N. Santalo, J. Tarres, J. Cirujeda, E. Molins, J. Llorca and E. Espinosa. "Synthesis of Several Isomeric Tetrathiafulvalene .pi.-Electron Donors with Peripheral Sulfur Atoms. A Study of Their Radical Cations". *The Journal of Organic Chemistry*, **1994**, 59, 3307.

[10] N. Crivillers, N. S. Oxtoby, M. Mas-Torrent, J. Veciana and C. Rovira. "Improved synthesis of the high-mobility organic semiconductor dithiophene-tetrathiafulvalene". *Synthesis*, **2007**, , 1621.

[11] M. Mas-Torrent, P. Hadley, S. T. Bromley, X. Ribas, J. Tarres, M. Mas, E. Molins, J. Veciana and C. Rovira. "Correlation between Crystal Structure and Mobility in Organic Field-Effect Transistors Based on Single Crystals of Tetrathiafulvalene Derivatives". *Journal of the American Chemical Society*, **2004**, 126, 8546.

[12] M. Mas-Torrent, M. Durkut, P. Hadley, X. Ribas and C. Rovira. "High Mobility of Dithiophene-Tetrathiafulvalene Single-Crystal Organic Field Effect Transistors". *Journal of the American Chemical Society*, **2004**, 126, 984.

[13] R. Pfattner, M. Mas-Torrent, C. Moreno, J. Puigdollers, R. Alcubilla, I. Bilotti, E. Venuti, A. Brillante, V. Laukhin, J. Veciana and C. Rovira. "Organic metal-organic semiconductor blended contacts in single crystal field-effect transistors". *Journal of Materials Chemistry*, **2012**, 22, 16011.

[14] M. Mas-Torrent, P. Hadley, X. Ribas and C. Rovira. "Temperature dependence of the electrical properties of single-crystals of dithiophene-tetrathiafulvalene (DT-TTF)". *Synthetic Metals*, **2004**, 146, 265.

[15] M. Mas-Torrent, S. Masirek, P. Hadley, N. Crivillers, N. S. Oxtoby, P. Reuter, J. Veciana, C. Rovira and A. Tracz. "Organic field-effect transistors (OFETs) of highly oriented films of dithiophene-tetrathiafulvalene prepared by zone casting". *Organic Electronics*, **2008**, 9, 143.

[16] R. Pfattner, M. Mas-Torrent, I. Bilotti, A. Brillante, S. Milita, F. Liscio, F. Biscarini, T. Marszalek, J. Ulanski, A. Nosal, M. Gazicki-Lipman, M. Leufgen, G. Schmidt, L. W. Molenkamp, V. Laukhin, J. Veciana and C. Rovira. "High-Performance Single Crystal Organic Field-Effect Transistors Based on Two Dithiophene-Tetrathiafulvalene (DT-TTF) Polymorphs". *Advanced Materials*, **2010**, 22, 4198.

[17] J. Tarres, N. Santalo, M. Mas, E. Molins, J. Veciana, C. Rovira, S. Yang, H. Lee, D. O. Cowan, M. . Doublet and E. Canadell. "A new family of molecular metals based on bis(ethylenethio)tetrathiafulvalene (BET-TTF) and octahedral counterions". *Chemistry of Materials*, **1995**, 7, 1558.

[18] E. Ribera, C. Rovira, J. Veciana, V. N. Laukhin, E. Canadell, J. Vidal-Gancedo and E. Molins. "Unusual transport and EPR properties of the (BET-TTF)-XF6 salts (X=P As)". *Synthetic Metals*, **1997**, 86, 1993.

[19] C. Rovira, J. Tarres, E. Ribera, J. Veciana, E. Canadell, E. Molins, M. Mas, V. Laukhin, M. . Doublet, D. O. Cowan and S. Yang. "Metallic conductivity in a disordered charge-transfer salt derived from cis-BET-TTF". *Synthetic Metals*, **1997**, 86, 2145.

[20] E. Ribera, C. Rovira, J. Veciana, V. N. Laukhin, E. Canadell, J. Vidal-Gancedo and E. Molins. "Unusual transport and EPR properties of the (BET-TTF)-XF6 salts (X=P, As)". *Synthetic Metals*, **1997**, 86, 1993.

[21] C. Rovira, J. Tarres, E. Ribera, J. Veciana, E. Canadell, E. Molins, M. Mas,

V. Laukhin, M. . Doublet, D. O. Cowan and S. Yang. “Metallic conductivity in a disordered charge-transfer salt derived from cis-BET-TTF”. *Synthetic Metals*, **1997**, 86, 2145.

[22] E. Coronado, J. R. Galan-Mascaros, C. Gimenez-Saiz, C. J. Gomez-Garcia, C. Rovira, J. Tarres, S. Triki and J. Veciana. “Radical salts of the organic donor BET-TTF with polyoxometalate clusters”. *Journal of Materials Chemistry*, **1998**, 8, 313.

[23] A. Perez-Benitez, J. Tarres, E. Ribera, J. Veciana and C. Rovira. “Improved synthesis of the -electron donor bis(ethylenethio)tetrathiafulvalene (BET-TTF)”. *Synthesis*, **1999**, , 577.

[24] E. Ribera, J. Veciana, E. Molins, I. Mata, K. Wurst and C. Rovira. “Novel dissymmetric tetrathiafulvalenes as precursors of organic metals: Synthesis, x-ray crystal structures, electrochemical properties and study of their radical cations”. *European Journal of Organic Chemistry*, **2000**, , 2867.

[25] M. Clemente-Leon, E. Coronado, J. R. Galan-Mascaros, C. Gimenez-Saiz, C. J. Gomez-Garcia, E. Ribera, J. Vidal-Gancedo, C. Rovira, E. Canadell and V. Laukhin. “Hybrid molecular materials based upon organic -electron donors and metal complexes. Radical salts of bis(ethylenethia)tetrathiafulvalene (BET-TTF) with the octahedral anions hexacyanoferrate(III) and nitroprusside. The first kappa phase in the BET-TTF family”. *Inorganic chemistry*, **2001**, 40, 3526.

[26] S. S. Khasanov, A. Perez-Benitez, B. Z. Narymbetov, L. V. Zorina, R. P. Shibaeva, J. Singleton, A. . Klehe, V. N. Laukhin, J. Vidal-Gancedo, J. Veciana, E. Canadell and C. Rovira. “Interesting transport and magnetic properties in a new family of molecular materials based on the organic donor

BET-TTF and the perrhenate anion". *Journal of Materials Chemistry*, **2002**, 12, 432.

[27] A. Kowalska, R. Wojciechowski, J. Ulanski, M. Mas-Torrent, E. Laukhina, C. Rovira and K. Yakushi. "Evaluation of charge transfer degree in the bis(ethylenethio) tetrathiafulvalene salts by Raman spectroscopy". *Synthetic Metals*, **2006**, 156, 75.

[28] A. A. Kowalska, J. . Savy, D. de Caro, L. Valade, L. Vendier, E. Laukhina, C. Rovira and J. Ulanski. "Thin layers of new salt, BET-TTF[Ni(dmit)2]2, electrodeposited on silicon wafers". *Solid State Sciences*, **2008**, 10, 1777.

[29] E. Laukhina, E. Ribera, J. Vidal-Gancedo, S. Khasanov, L. Zorina, R. Shibaeva, E. Canadell, V. Laukhin, M. Honold, M. . Nam, J. Singleton, J. Veciana and C. Rovira. "Halides of BET-TTF: Novel hydrated molecular metals". *Advanced Materials*, **2000**, 12, 54.

[30] C. Rovira, S. LeMoustarder, D. Belo, J. Veciana, M. Almeida, V. Gama and M. T. Duarte. "BET-TTF (bisethylenethio-tetrathiafulvalene) donor as a building block of organic metals". *Synthetic Metals*, **2001**, 120, 717.

[31] M. Mas-Torrent, E. Laukhina, C. Ravira, J. Veciana, V. Tkacheva, L. Zorina and S. Khasanov. "New transparent metal-like bilayer composite films with highly conducting layers of θ-(BET-TTF)2Brá3H2O nanocrystals". *Advanced Funtional Materials*, **2001**, 11, 299.

[32] C. Rovira. "Bis(ethylenethio)tetrathiafulvalene (BET-TTF) and related dissymmetrical electron donors: From the molecule to functional molecular materials and devices (OFETs)". *Chemical reviews*, **2004**, 104, 5289.

[33] D. Hwang, C. Fuentes-Hernandez, J. Kim, W. Potscavage and B. Kippelen.

"Flexible and stable solution-processed organic field effect transistors". *Organic Electronics*, **2011**, 12, 1108.

[34] T. Lau, E. Lorenz and M. Koyuncu. "Lifetime of Poly(triaryl amine) Based Organic Field Effect Transistors under Different Environmental Conditions". *Japanese Journal of Applied Physics*, **2013**, 52, 041601.

[35] I. D. V. Ingram, D. J. Tate, A. V. S. Parry, R. Sebastian Sprick and M. L. Turner. "A simple method for controllable solution doping of complete polymer fieldeffect transistors". *Applied Physics Letters*, **2014**, 104, 153304.

[36] L. A. Majewski, R. Schroeder and M. Grell. "One Volt Organic Transistor". *Advanced Materials*, **2005**, 17, 192.

[37] S. Saeki, J. M. G. Cowie and I. J. McEwen. "The effect of molecular weight and casting solvent on the miscibility of polystyrene-poly(a-methyl styrene) blends". *Polymer*, **1983**, 24, 60.

[38] B. W. Suk-fai Lau, Jaya Pathak. "Study of phase separation in blends of polystyrene and poly(alpha-methylstyrene) in the glass transition region using quantitative thermal analysis". *Macromolecules*, **1982**, 15, 1278.

[39] M.-B. Madec, J. J. Morrison, V. Sanchez-Romaguera, M. L. Turner and S. G. Yeates. "Organic field effect transistors from ambient solution processed poly(triarylamine)-insulator blends". *J. Mater. Chem.*, **2009**, 19, 6750.

[40] J. M. G. Cowie and S. Miachon. "Miscibility in binary blends of poly(alpha-methylstyrene) and poly(methyl methacrylate)". *Macromolecules*, **1992**, 25, 3295.

[41] J.-H. Kwon, S.-I. Shin, K.-H. Kim, M. J. Cho, K. N. Kim, D. H. Choi and B.-K. Ju. "Organic thin film transistors using 6,13-bis(tri-

isopropylsilylethynyl)pentacene embedded into polymer binders". *Applied Physics Letters*, **2009**, 94, 013506.

[42] B. A. Miller-Chou and J. L. Koenig. "A review of polymer dissolution". *Progress in Polymer Science*, **2003**, 28, 1223.

[43] J. M. G. Cowie and I. J. Mcewen. "The thermodynamics of mixing of polystyrene and poly(alpha-methylstyrene) from a calorimetric viewpoint". *Polymer*, **1994**, 35, 2893.

[44] A. Brunacci, E. Pedemonte, J. M. G. Cowie and I. J. McEwen. "The thermodynamics of mixing of polystyrene and poly(a-methylstyrene) from a calorimetric viewpoint". *Polymer*, **1994**, 35, 2893.

[45] M. Cowie. "Miscibility in Binary Blends of Poly(a-methylstyrene) and Poly(methy1 methacrylate)". *Macromolecules*, **1992**, 3, 1.

[46] J. M. G. Cowie and I. J. McEwen. "Predicted miscibility of polystyrene and poly(a-methyl styrene) and comparison with experiment". *Polymer*, **1985**, 26, 1662.

[47] J. C. McEwen and I. "Predicted miscibility of polystyrene and poly (alpha - methyl styrene) and comparison with experiment". *Polymer*, **1985**, 26, 1662.

[48] S. Goffri, C. Muller, N. Stingelin-stutzmann, D. A. G. W. Breiby, C. P. Radano, J. W. Andreasen, R. Thompson, R. A. J. Janssen, M. M. Nielsen, P. Smith, H. Sirringhaus, C. M. Uller, A. J. Janssen and E. Ren. "Multicomponent semiconducting polymer systems with low crystallization-induced percolation threshold". *Nature Materials*, **2006**, 5, 950.

[49] H. D. Keith, R. G. Vadiriisky and P. J. Padden. "Crystallization of Isotactic Polystyrene from Solution". *Polymer Science Part A-2: Polymer Physics*, **2000**, 8, 1687.

[50] H. D. Keith, R. G. Vadimsky and F. J. Padden. "Crystallization of isotactic polystyrene from solution". *Journal of Polymer Science Part A-2: Polymer Physics*, **1970**, 8, 1687.

[51] C. J. G. Plummer and H.-H. Kausch. "Deformation in thin films of amorphous and semicrystalline isotactic polystyrene". *Polymer*, **1993**, 34, 1972.

[52] G. S. Y. Yeh and S. L. Lambert. "Crystallization kinetics of isotactic polystyrene from isotactic-atactic polystyrene blends". *Journal of Polymer Science Part A-2: Polymer Physics*, **1972**, 10, 1183.

[53] P. Lemstra and G. Challa. "Crystallization of isotactic polystyrene from dilute solutions". *Journal of Polymer Science: Polymer . . .*, **1975**, 13, 1809.

[54] H. Beck. "Heterogeneous nucleating agents for the crystallization of isotactic polystyrene". *Journal of Applied Polymer Science*, **1975**, 19, .

[55] Y. Miyamoto, Y. Tanzawa, H. Miyaji and H. Kiho. "Growth rate of isotactic polystyrene crystals in concentrated solutions and in the melt". *Polymer*, **1992**, 33, 2496.

[56] J. H. Aubert, B. Macromolecules, J. A. Polymer, I. Conformation, S. N. Laboratories, R. Manuscript and R. May. "Isotactic polystyrene phase diagrams and physical gelation". *Macromolecules*, **1988**, 21, 3468.

[57] F. Danusso and G. Moraglio. "Some solution properties of isotactic and atactic polystyrenes". *Journal of Polymer Science*, **1957**, XXIV, 161.

[58] T. A. M. Ferenczi, C. Müller, D. D. C. Bradley, P. Smith, J. Nelson and N. Stingelin. "Organic Semiconductor : Insulator Polymer Ternary Blends for Photovoltaics". *Advanced Materials*, **2011**, 23, 4093.

[59] A. A. Virkar, S. Mannsfeld, Z. Bao and N. Stingelin. “Organic Semiconductor Growth and Morphology Considerations for Organic Thin-Film Transistors”. *Advanced Materials*, **2010**, 22, 3857.

[60] W. R. Krigbaum, D. K. Carpenter and S. Newman. “The Configuration of Polymer Molecules. II. Isotactic Polystyrene”. *The Journal of Physical Chemistry*, **1958**, 62, 1586.

[61] F. Danusso and G. Moraglio. “Some solution properties of isotactic and atactic polystyrenes”. *Journal of Polymer Science*, **1957**, 24, 161.

[62] F. A. Morrison. *An Introduction to Fluid Mechanics*. Cambridge University Press, **2013**.

[63] J. Boon and G. Challa. “Study of molten isotactic polystyrene. II. The kinetics of thermal degradation from melt viscosity data”. *Die Makromolekulare Chemie*, **1965**, 84, 25.

[64] F. A. Morrison. *Understanding Rheology*. Oxford University Press, **2001**.

[65] G. Giri. *Understanding and tuning organic semiconductor packing during solution processing*. Ph.D. thesis, Stanford, **2013**.

[66] H. Hoppe and N. S. Sariciftci. “Organic solar cells: An overview”. *Journal of Materials Research*, **2004**, 19, 1924.

[67] J. N. Smith, J. G. Labram and T. D. Anthopoulos. *Semiconducting Organic Molecule/Polymer Composites for Thin-Film Transistors*, pages 219 249. Wiley-VCH Verlag GmbH & Co. KGaA, **2012**.

[68] A. Brillante, I. Bilotti, R. G. Della Valle, E. Venuti, S. Milita, C. Dionigi, F. Borgatti, A. N. Lazar, F. Biscarini, M. Mas-Torrent, N. S. Oxtoby, N. Crivillers, J. Veciana, C. Rovira, M. Leufgen, G. Schmidt and L. W.

Molenkamp. “The four polymorphic modifications of the semiconductor dibenzo-tetrathiafulvalene”. *CrystEngComm*, **2008**, 10, 1899.

[69] M. Mas-Torrent, E. E. Laukhina, V. Laukhin, C. M. Creely, D. V. Petrov, C. Rovira and J. Veciana. “Direct micro-patterning of TTF-based organic conductors on flexible substrates”. *Journal of Materials Chemistry*, **2006**, 16, 543.

[70] R. Pfattner. *Organic Electronics based on Tetrathiafulvalene-Derivatives: Organic Field-Effect Transistors and Sensors*. Ph.D. thesis, Universitat Autónoma de Barcelona, **2011**.

Chapter 6

In-depth study of OFETs based on DB-TTF and PS3000

6.1 Introduction

Embedding a small-molecule in a polymeric matrix is a feasible approach to improve stability[1–8]. New emergent methods have been devised to satisfy the requirements of large-area electronics manufacturing[9,10] such as Bar Assisted Meniscus Sheering (BAMs) technique (see Figure 6.1). Despite the plethora of materials which has been tested as semiconductors in Organic Field-Effect Transistors (OFETs)[11–13], it is not enough an electrical characterization to extract the mobility and threshold voltage of such materials to consider them as good candidates for OFETs applications. Such candidates must pass other tests such as reproducibility, stability in air and possibly in

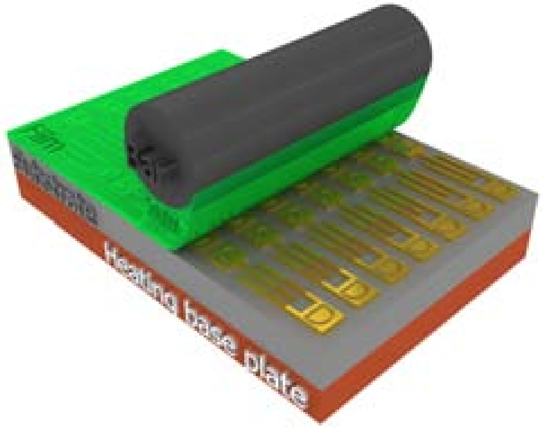

Figure 6.1 *Conceptual schematic of the Bar assisted meniscus shearing (BAMs) technique.*

aqueous media if sensors are the target application. Also the scalability of the desired manufacturing process must undergo feasibility analysis. The charge transport in the material has to be understood and finally circuits such as inverters in which discrete devices are combined to form a simple application should be demonstrated since it is the basic of all further electronic applications. Thus, in this chapter an in-depth study of the potential of the Organic Field-Effect Transistors prepared using BAMs with the most promising OSC/polymer blend among those studied here is carried out. The film characterization was carried out using techniques such as: optic microscope, contact angle, x-ray diffraction, time of flight secondary ion mass spectroscopy, and atomic force microscope, while the homogeneity of the film was characterized using a computational tool such as ImageJ software. Electrical characterization was also carried out in order to determine the most important device characteristics and also the reproducibility and stability of the devices produced were validated. Temperature dependence experiments were performed to evaluate the dependence of mobility as a function of temperature. Finally, inverters were fabricated and tested.

6.2 Film Characterization

As mentioned in the previous chapter, the most promising OFETs prepared here consisted in blends of DB-TTF and PS3000, ratio 1:2, respectively. Here, a more detailed characterization of the films fabricated were performed in order to better understand the material and device properties.

6.2.1 Optic microscope and crystallite size

In order to gather information about film integrity, optic microscope images were recorded and depicted in Figure 6.2, in which one can see an homogeneous film without major defects even when deposited on an interdigitated architecture. Figure 6.2(a), with an angle between Polarizer and Analyzer $\Phi_{P\ A} = 0^o$ shows a highly homogeneous film. Figure 6.2(b) with $\Phi_{P\ A} = 90^o$ elucidates that domains are formed by crystalline structures implanted in the film. Such structures are also depicted in Figure H.1 (see Appendix H) which shows several pictures for different channel lengths. From such pictures one can see that crystallites create connections between the electrodes.

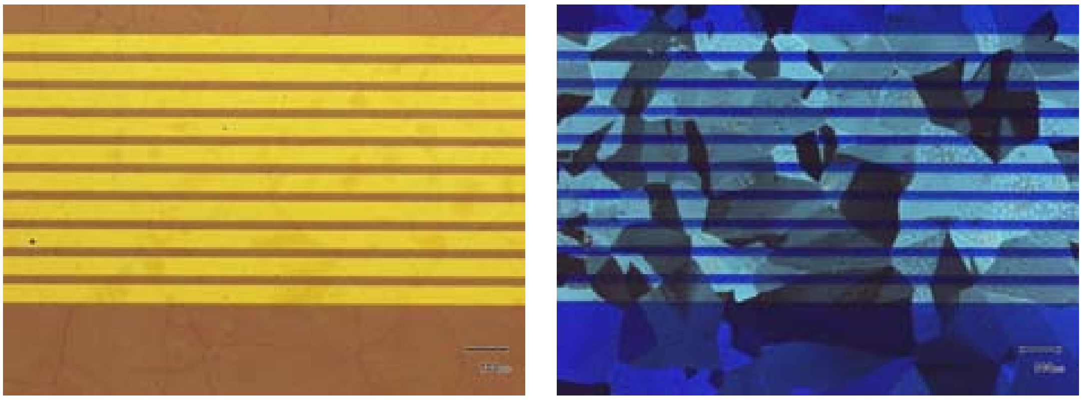

(a) (b)

Figure 6.2 *Polarized microscope images for bottom contact device, L = 25 μm W = 25000 μm, DB-TTF and PS3000 ratio: 1:2, (a) $\Phi_{P\ A} = 0^o$ between Polarizer and Analyzer and (b) $\Phi_{P\ A} = 90^o$ between Polarizer and Analyzer.*

It often appears that given an image processing task will have a simple solution, yet in practice, turns out to be a difficult task. This is especially true when the problem involves image analysis, where the goal is not only to enhance the appearance of a particular image but instead extract information about its contents, extract data for further studies[14,15]. Region labelling or region coloring is the search for binary regions with tasks like find out which pixel belong to which region, how many regions are in the image, and where the regions are located.

In order to assess the homogeneity of the film produced, an estimation of crystalline domains [*] is obtained using Image-J[16]. For all channel lengths more than 2000 domains were found and analysed. To do so, five pictures were analysed per channel length; pictures were taken on fully functional devices with the mean mobility $(cm^2V^{-1}s^{-1})$ located inside the statistical range depicted in the Figure 6.11(a). Figure 6.3(a) depicts a scatter of the whole analysis, in which a mean crystallite size assuming a square is found to be in the order of 180 x 180 μm (L_{CD} = length of crystalline domains). From the box plot [†] in Figure 6.3(b) it is clear to observe that the mean value is located at the same level for each channel length in the range of 10 -100 μm, indicating that the device dimensions do not influence on the film morphology.

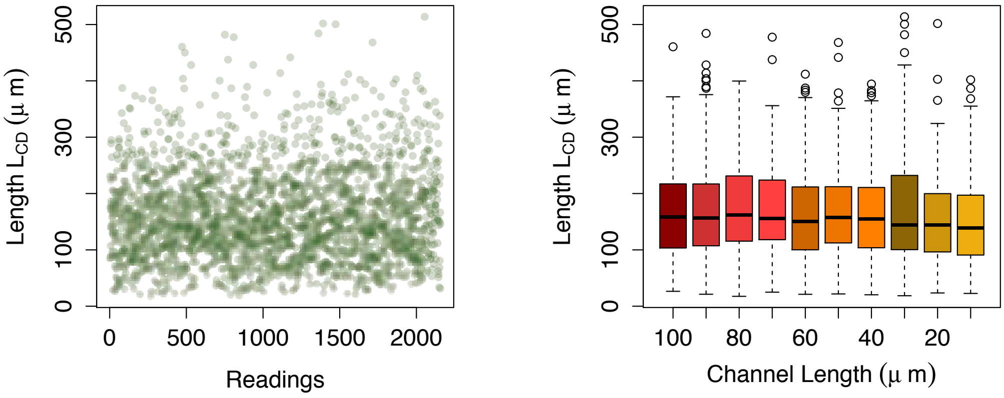

(a) (b)

Figure 6.3 *(a) Scatter plot for crystalline domains counted by ImageJ. (b) Crystalline domains quantification considering them square sized. Pictures taken with and Olympus Optical microscope with 90^o between polarizer and analyzer were analyzed.*

---

[*] Work carried out in collaboration with Witold Tatkiewicz.

[†] The top and bottom line of the whisker are first and third quartile respectively, while the band located inside the whisker is the second quartile. The extremes of the whiskers are the maxima and minima data found, and finally any data not included between the whiskers are plotted as an outlier with circles.

6.2.2 Atomic Force Microscopy (AFM) Analysis

In order to gather further information about the film morphology and the characteristics of the film itself regarding roughness and thickness, Atomic Force Microscopy (AFM) was used in tapping mode. Several samples and different regions on each one were analysed. Figure 6.4(a) depicts a particular zone on the film in which a profile was extracted from which the roughness of the film was calculated using Gwyddion software and is depicted in Figure 6.4(b). It was observed a fairly homogeneous profile in term of roughness since the values fluctuates around ±1.5 nm, and an rms of 1.05 was calculated. It is important to note that this value is one order of magnitude lower than that found for evaporated DB-TTF films (17.6 nm). One key parameter to analyse is the film thickness, which was measured by AFM giving a value of 29 nm ± 4.2 nm. This value is the average of seven different measurements taken from different zones and from different films. A typical topography and profile used to extract the film thickness are shown in Figures 6.5(a) and 6.5(b), respectively.

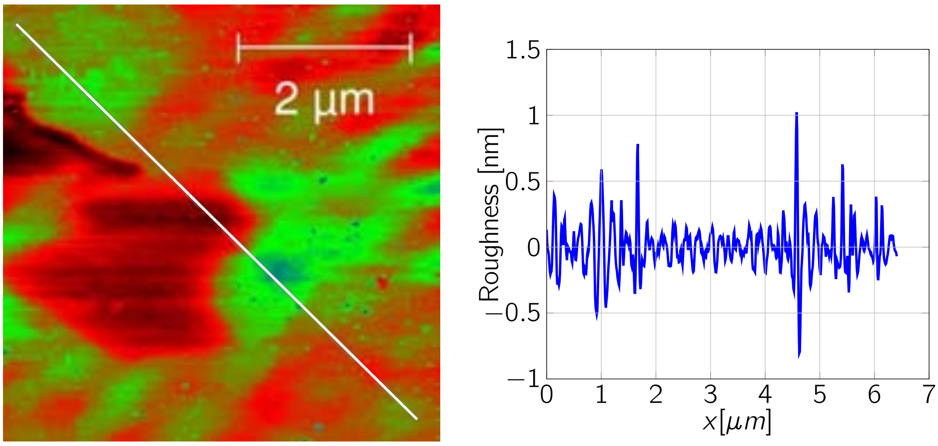

(a) (b)

Figure 6.4 *Atomic force microscope, (a) Topography and (b) Roughness in a diagonal profile extracted from Figure (a) with rms = 1.05 nm.*

An open-source software for scanning probe microscopy data analysis[17].

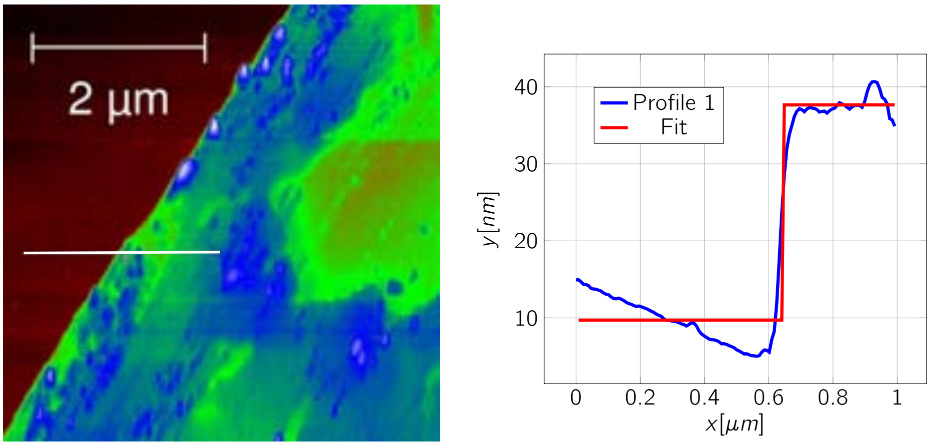

(a)

(b)

Figure 6.5 *Atomic force microscope, (a) Topography and (b) Profile extracted from Figure (a) and the fit with a step* $h = 27\ 9nm \pm 3\ 2nm$.

6.2.3 X-ray analysis

DB-TTF is known to crystallize forming different polymorphs[18]. X-ray diffraction (XRD) powder analysis were performed to better understand the nature of such crystalline structures forming the film. Further, for comparison XRD data were also gathered from thermally evaporated film. Both data are shown in Figure 6.6 exhibiting the same crystalline phase, γ-DB-TTF[18], for both preparation techniques. This is in agreement with previous studies that pointed that γ-phase is the most kinetically favourable polymorph and the most commonly found in thin films[18].

Further, it should be highlighted that the highest performance found for the BAMs processed films compared to the evaporated ones, cannot be accounted by the formation of a different polymorph but to a better quality thin film.

6.2.4 Contact Angle

Contact angle measurements are done to gain understanding on the nature of the interface air-film. By using a drop of water and measuring the angle that is formed with the surface, hydrophilic or hydrophobic nature can be assessed (see

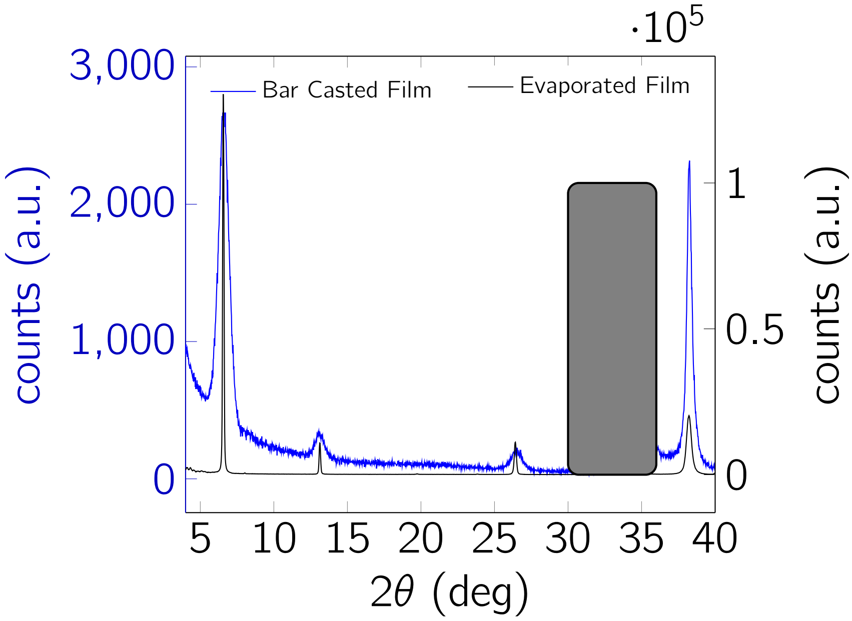

Figure 6.6 *XRD diffractogram of thermally evaporated thin films of DB-TTF on Si SiO_x (black, right y-axis) and DB-TTF/PS3000 blend prepared by the solution sheering technique (blue, left y-axis) exhibit reflections in agreement with the previously reported γ-phase of DB-TTF. A peak identified as a reflection of Si was found in the range $32^o < 2\theta < 36^o$ and is not shown in the figure.*

Section B.1). The contact angle value of a 5 μl mili-q water drop for a thin film of only PS3000 is 95^o (see Figure 6.7(a)), and the value for the film with DB-TTF/PS3000 blend is 91^o (See Figure 6.7(b)). The film of the blend exhibits a very hydrophobic surface, suggesting a rich polystyrene top surface.

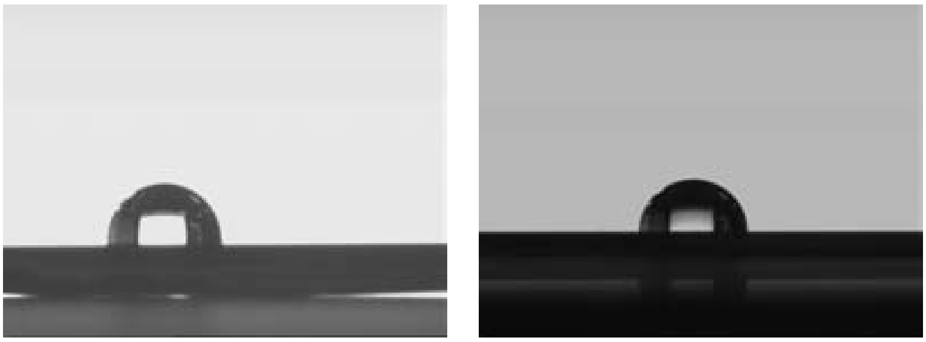

(a) (b)

Figure 6.7 *Water contact angle pictures for films of (a) PS3000,(b) DB-TTF:PS3000 1:2 blend.*

6.2.5 Time of Flight Ion Mass Spectroscopy

Important in this context is the investigation of a possible vertical phase separation, and film composition per-sé. In this particular case the analysis of the data gathered by a depth profile starting from the sample surface reaching the SiO_x/blend interface was performed by Time of Flight Ion Mass Spectroscopy (ToF-SIMS). So, Sulphur (S), Carbon (C) and Silicon dioxide (SiO_2) were investigated as function of depth. Clearly visible is the initial higher concentration of S which decays until the next $\approx$ 10 nm in depth and then reaches a plateau lasting $\approx$ 10 nanometers followed by a decay starting at $\approx 20\,nm$. This means that the small molecule semiconductor DB-TTF is mostly concentrated on the top layer of the film, indicating a clear vertical separation. Probably the crystalline DB-TTF layer is on the top part of the film but embedded in the polymeric matrix as suggested by the AFM and contact angle characterizations. Further studies performed regarding device stability to ambient conditions will also agree with this hypothesis (introduced later on, Figure 6.14) It should also be noticed that the thickness found by ToF-SIMS is also in agreement with the AFM studies.

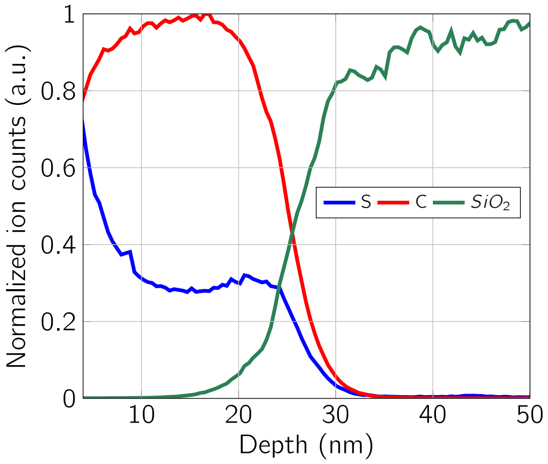

Figure 6.8 *Time of Flight Secondary Ion Mass Spectroscopy (ToF-SIMS) spectrum measured at 1 keV for a thin film made of dibenzo-tetrathiafulvalene and polystyrene 3000 ratio 1:2, where Sulphur (S), Carbon (C) and Silicon dioxide (SiO_2) were analysed.*

6.3 Electrical Characterization

6.3.1 Output and Transfer Characteristics

The output and transfer characteristics of a DB-TTF:PS3000 (ratio 1:2) film are shown in Figure 6.9. For the output measurement the drain voltages were forward and reverse swept from + 10 V down to -50 V with a step of - 1 V, while the gate voltage was swept from +10 V down to -40 V the step used was -10 V. Transfer curves were measured for linear and saturation regimes, the drain voltage for the linear regime was -5 V and - 50 V for the saturation regime, while the gate voltage was swept forwardly and reversely from +10 V to -50 V each -1V (see Figure 6.9(a)). Both device characteristics show that the device behaves very ideally with also negligible hysteresis, giving a high mobility of 0.4 $cm^2V^{-1}s^{-1}$. As observed in the transfer curve Figure 6.9(b) the device turns on at gate voltage $V_{SG} \approx 0V$ very abruptly and the channel current is enhanced by ≈ 5 orders of magnitude when the device is fully ON. Transfer curves at high V_{SG} shows excellent linear behaviour, implying a gate-independent mobility, that can be observed in the mobility profile depicted in Figure 6.10(a) suggesting efficient charge injection from gold electrodes to the semiconductor, and negligible carrier trapping. This is observed in eight devices whose mobility profiles are plotted in Figure 6.10(b). It is clear that almost all of them overlap with a flat profile over a wide V_{SG} scan suggesting high mobility reproducibility in its value but importantly in mobility independence with respect to gate voltage. Such type of gate voltage mobility independence is not common in OFETs and only in a few cases have been reported, like Zhang et al. in a Nature Communications[19]. Thus this is a clear evidence of the high quality of the films.

A key factor in the development of OTFTs besides mobility is the threshold voltage, the latest ultimately determines circuit functionality. Additionally the

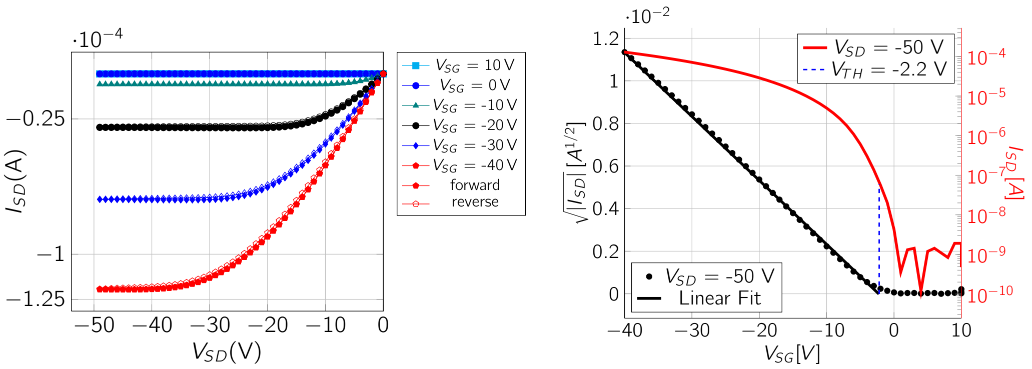

(a) (b)

Figure 6.9 *(a) Output Characteristics, (b) Log-transfer and Square root plot at saturation regime,device L = 70 μm, W = 2000 μm.* μ_{FE}^{sat} = 0.41 $\frac{cm^2}{Vs}$ and V_{TH} = -2.2 V.

understanding of threshold voltage enables a better understanding of transistor behaviour since, variations in threshold voltage suggests a dependency of gate dielectric material and is also related to their dependence on trap states at the semiconductor-dielectric interface or on doping. Figure 6.9(b) shows a negative threshold voltage V_{TH} = -2.2 V, which was extracted from the linear fit of the $\sqrt{I_{SD}}$ $f(V_{SG})$ linealized curve and subsequent extrapolation[20].

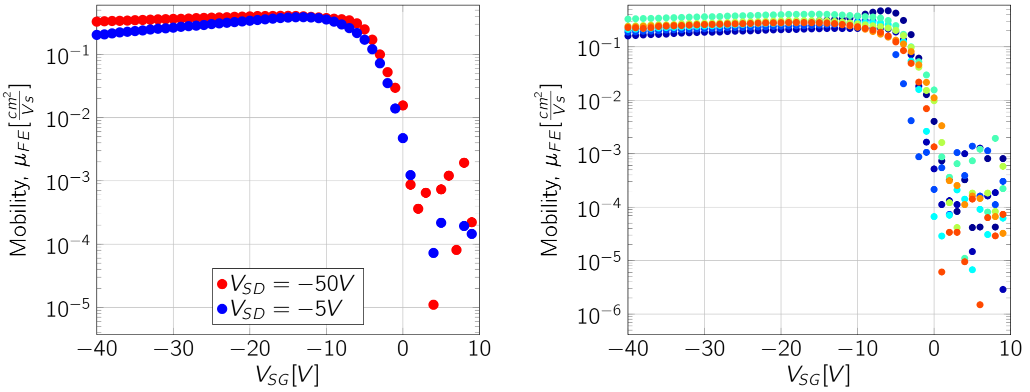

(a) (b)

Figure 6.10 *(a) Mobility profile at saturation and linear regimes as function of* V_{SG}*, device L = 70 μm, W = 2000 μm.* $\mu_{FE}^{sat} = 0\ 41 \frac{cm^2}{Vs}$ and V_{TH} = -2.2 V. *and (b) Mobility profiles at saturation regime* V_{SD} *= -50 V for eight different devices. Both plots are with the y-axis in logarithmic scale.*

In the output curve Figure 6.9(a) drain current saturates at high drain voltage (V_{SD}), and at the low-bias region the current-voltage relationship exhibits a approximate linear tendency which suggest and ohmic behaviour. The linear tendency is also observed between $\overline{I_{SD}}$ and V_{SG}, which suggests square-law type behaviour at the saturation regime, and is shown in Figure 6.9(b) (see Figure H.5,H.6, and H.7 for several devices and channel lengths). A parameter to estimate the breakdown voltage of a dielectric is the gate leakage. Typically in all measured transistors the gate leakage is in the range of nA (10^{-9}A), which is several orders of magnitude lower than the drain current, which was generally in the 10^{-4} A range.

6.3.2 Reproducibility

The reproducibility of the device fabrication and performance is a crucial issue to address in order to consider their potential in applications. Full statistics performance of devices is depicted in Figure 6.11(a), where $\approx$ 200 devices were analysed. Using R data was plotted in a histogram and fitted to a Gaussian curve, both are depicted in Figure 6.11(a) with the y-axis in density units. Since the mean mobility value 0.158 $cm^2V^{-1}s^{-1}$ and the median 0.157 $cm^2V^{-1}s^{-1}$ are quite close, a symmetrical data can be assumed. It should be noticed that mobility values higher than 0.4 $cm^2V^{-1}s^{-1}$ after applying the Chauvenet's criterion (see Appendix A) were dropped. However in Figure 6.12(a) these values are clearly visible as outliners. Figure 6.11(b) depicts the Q-Q plot or Quantile-Quantile plot for the sample data, where the observed values are drawn along the y-axis. Since the theoretical quantiles are previously known those are plotted in the x-axis[26]. One can observe that the trend of the data is to follow a straight line in the Q-Q plot, suggesting normally distributed data, despite the left skewed of the data.

[§] R is a GNU language and environment for statistical computing and graphics[21–25]

Also, it is important to highlight the yield of fabrication ($yield_f$) which is $90\ \% \leq yield_f < 100\ \%$.

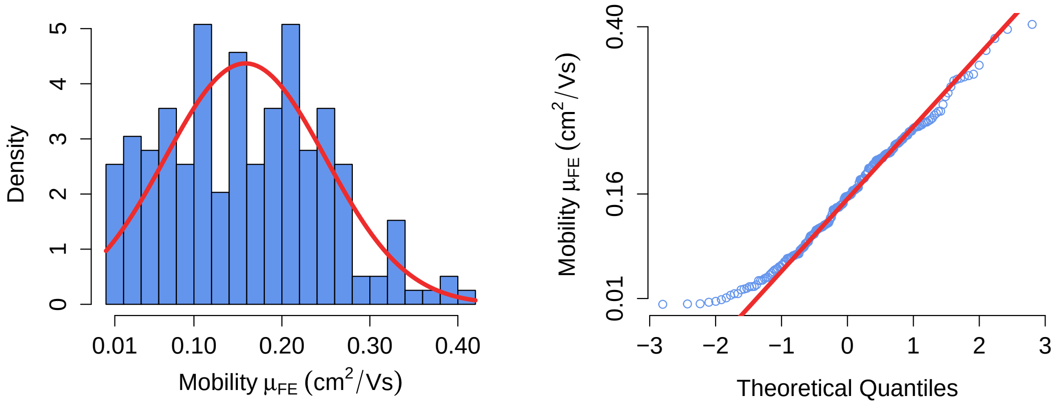

(a) (b)

Figure 6.11 *(a) Histogram for mobility extracted at saturation regime* $V_{SD} = -50V$ *where more than 200 samples analysed, (b) Quantile-Quantile plot for mobility values depicted in (a).*

Therefore, it can be affirmed that both the reproducibility of the devices and the yield of fabrication is succinct and satisfactory, making the BAMs technique and the DB-TTF/PS3000 (1:2 ratio) blend outstanding alternatives to more traditional ways to fabricate OFETs showing great potential for applications.

6.3.3 Mobility and threshold voltage dependence on channel length

Eight devices per channel length were electrically characterized obtaining the mobility in ($cm^2V^{-1}s^{-1}$) and threshold voltage in (V) and these data was used inside R-statistical software. Both mobility and threshold voltage are plotted against channel length using box plots, which allows to visually peruse the data obtained and to immediately get a rough estimate of how, and where data is fluctuating as changes in the independent variable are produced (see Figure 6.12). From Figure 6.12(a) one can see that the mobility values are located on the positive theoretical quantiles (see Figure 6.11(b)). Statistically equal mobility values for channel lengths 100 μm down to 20 μm were found calculated using a pairwise comparison inside R[¶], while mobility values for channel length equal to 10 μm gives the highest statistical difference (see Table H.2). Figure 6.12(b) depicts the boxplot for threshold voltage as a function of channel length. One can see a monotonic behaviour on the median values represented by the line inside each box per channel length over the range 20 $\mu m \leq$ L $\leq$ 100 μm, while at channel length equal to 10 μm a decrease in value is observed. Table H.1 is the output extracted from the statistical software R, where as the value deviates more from one means that are less equal. It is clearly seen that all values for the threshold voltage are statistically equal for 20 $\mu m \leq$ L $\leq$ 100 μm, and the deviation is present at channel length equal to 10 μm as said before.

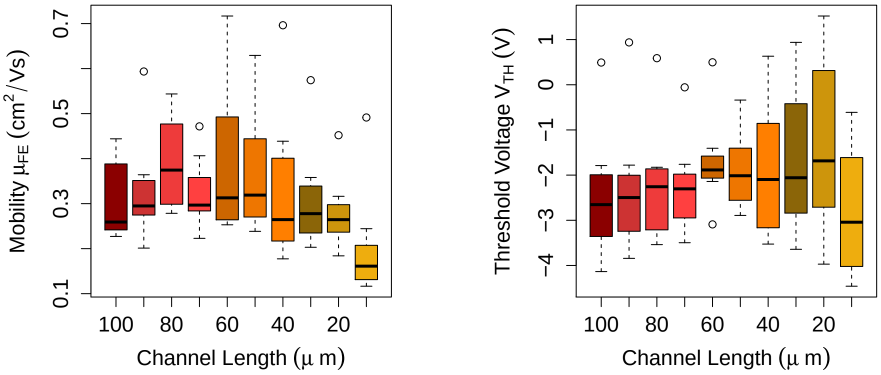

(a) (b)

Figure 6.12 *A total of 80 devices were measured, eight devices were measured per channel length.(a) Boxplot for Mobility (cm^2 Vs) as a function of channel length (μm), and (b) Boxplot for threshold voltage (V) as a function of channel length (μm). The line inside each box is the second quartile or the median per data set, the points located outside the box are outliners.*

[¶] `pairwise.t.test` function built into the `stats package`[27]

One can infer from the previous analysis that no significant differences in mobility and threshold voltage were present in the channel length range 20 $\mu m \leq$ L $\leq$ 100 μm.

6.3.4 Contact resistance

Contact resistance is a strong dependent function on the nature of the electrode and gate bias. To extract it, the channel length dependence resistance of the device was measured. Several devices with varying channel length and constant channel width were measured. The output characteristics for devices with L = 10 - 100 μm were measured and collected in Figures H.2, H.3, and H.4. In these figures only typical characteristics for each channel length devices are shown, and one can see that at lengths equals to 10 and 20 μm contact resistances are easily observed in the I-V curves, where depressions at the beginning of the I-V characteristics (low V_SD) are observed. Also for these L values hysteresis is present in the measurement, since the reverse sweep does not overlap completely the forward sweep, which is assumed to come from trapping effects on the devices.

The output characteristics were recorded at several gate voltages ie. -10 V, -20 V, -30 V and -40 V. Assuming an ideal resistor operation in the linear regime, source/drain current versus source/drain voltage are fitted into a straight line. Since for small drain voltages it can be assumed that the total resistance is the sum of the channel resistance and the contact resistance, then the inverse of the slope for each line is calculated, and the procedure is repeated for each channel length and each gate voltage. Following equations 1.12 and 1.13 for the transfer-line method (TLM) and the modified transfer-line method (MTLM), respectively. Figures 6.13(a) for the TLM method and 6.13(b) for the MTLM method were constructed. In Figures 6.13(a) and 6.13(b) each point is the average of eight data points, error bars were removed for readability. One can observe that all R-square

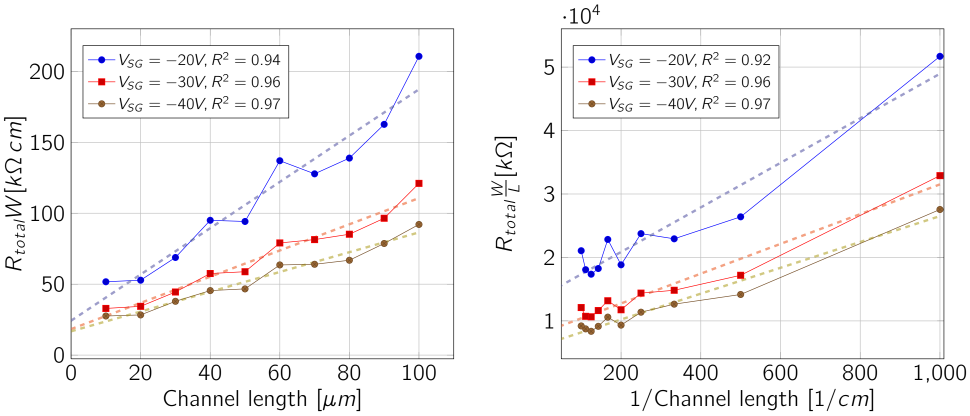

(a) (b)

Figure 6.13 *(a) Transfer-line method (TLM) and (b) Modified transfer-line method (MTLM), for OFETs fabricated in bottom contact architecture with semiconducting film made of a blend of DB-TTF and PS3000 in a ratio 1:2, for channel lengths from 10μm to 100μm each 10μm.Error bars have been omitted for clarity.*

values exceed 0.9, i.e in Figure 6.13(a) the straight line for $V_{SG} = -40V$ shows an R^2 equals to 0.97, which says that the 97% variation observed in $R_{total}W[k\Omega\, cm]$ is due to the Channel length variation $[\mu m]$ and only 3 % due to random sources present in the measurements.

Analysing the collected data in Table 6.1, one can see that the values reported for the modified transfer-line are slightly higher than the values reported by the calculation out of the traditional transfer-line. It should be kept in mind that both methods differ in how the data is plotted, in the traditional TLM the contact resistance is extracted from the intercept while from the MTLM is extracted out of the slope[28]; however, despite the slight difference, one can think that is agreeable said that both match in order of magnitude and both are in the lower range among the reported values of contact resistances for organic semiconductors and gold electrodes[29,30]. The values here reported can also be compared to the ones found for organic electrodes and TTFs reported by Pfattner in 2012[31].

Table 6.1 *Summary of the calculated contact resistances for blends of DB-TTF:PS3000, 1:2 ratio. For the transfer-line method is the intercept of the fitting line as stated in equation 1.12 and for the modified transfer-line method the slope from Equation 1.13. All R-squared are represented in Figures 6.13(a) and 6.13(b).*

V_{SG} (V)	TLM (kΩ cm)	MTLM (kΩ cm)	TLM (kΩ)	MTLM (kΩ)
-20	24	35	120	175
-30	18	23	90	115
-40	17	20	85	100

6.3.5 Anisotropy

Molecular crystals of organic semiconductors show in general anisotropic transport due to different intermolecular interactions present in all crystallographic directions[32]. This suggest that the field-effect mobility can vary significantly depending on the measurement direction, which is a drawback where large area coverage machinery is needed or used. The zone casting technique was reported for the fabrication of OFETs including TTF derivatives[33](see Figure 1.18). In this technique the substrate moves very slowly approximately 20 to 40 μm/s, the resulting film is a high quality crystalline film but exhibiting a large mobility anisotropy. On the other hand, the BAMs technique is very fast compared with zone casting, minimum coating speed 1 cm/s, where the crystalline film is formed right after the coating and thus, in principle should not very influenced by the casting direction. So, in order to test if the film is either isotropic or anisotropic, a substrate was designed with horizontal and vertical structures (L = 100 μm and W = 8 mm). After analysing 24 devices (12 with horizontal orientation and 12 in vertical orientation) with mobilities ranging from the mean to the left of the zero theoretical quantile in Figure 6.11(b), and using a t-Test to compare different samples (degrees of freedom = 21) is found that the t-calculated value (-0.0074) is much less than the reported in tables (t_{95} = 2.080) using a significance level of 5 percent (one-half of 10 percent). So it can be concluded that the material is isotropic. Also assuming the vertical devices mean mobility value as 100 % and calculating the percentage of the difference between the mean vertical mobility value and mean horizontal mobility devices, the difference represents only 0.21%. This is a very remarkable result since to achieve OSC films with isotropic mobility is highly desirable for applications, since it ensures a high device-to-device reproducibility.

6.4 Stability in Air and Water

Besides the statistical reproducibility of devices it is also important to study the stability as a function of time and shelf stability as well. In order to study its functionality over a period of time a device was prepared and first measured, as prepared, then measured over twelve hours straight with one measurement per minute. Only transfer characteristics were measured sweeping the gate voltage from positive 10 V down to negative 40 V each minus 1 V as step, while maintaining the drain voltage constant at - 40 V in order to record the saturation regime characteristics as a function of time. The mobility and threshold voltage were extracted using Equation 1.8 and from the intercept to the x-axis from the $\sqrt{I_{SD}}$ f(V_{SG}) respectively, and results are depicted in Figure 6.14(a). Despite the lack of controlled ambient conditions such as temperature and relative humidity, the OFET showed a fairly stable behavior over that period of time for mobility and threshold voltage with no appreciable threshold voltage shift from 2 hours up to 12 hours suggesting a stable operation over such period of time. This test constitutes a "real conditions" experiment in order to evaluate the performance where no control over the temperature or the ambient is held.

One important issue in organic electronics is to find materials stable in time. To evaluate the shelf stability, devices were prepared and measured as prepared, and then stored in a container for more than forty days. Figure 6.14(b) depicts the evolution of mobility and threshold voltage of 10 devices, and it is appreciably notably that the error bars shows small error among devices. In this figure one can see minimal reduction in mobility and threshold voltage. The small fluctuations observed in the threshold voltage can be mainly ascribed to humidity, or temperature fluctuations during storage. Therefore, it can be affirmed that the devices show and excellent shelf-stability without revealing any appreciable degradation for over 40 days. Due to the fact that DB-TTF is very unstable in air, this can be explained by the fact that DB-TTF is encapsulated by the hydrophobic PS.

Healthcare and environmental monitoring in recent decades demanded the use of field-effect transistors (FETs) targeting primarily portable and label-free sensing applications which received great attention[34], but organic semiconductors typically degrade rapidly under humid conditions[35]. Generally, H_2O and O_2 will be adsorbed by the organic film changing its morphology, increasing the concentration of traps or doping it, typically giving rise to an off current increase and a decrease in the on/off ratio[35]. Then, there is a high interest in developing water stable active materials in order to develop chemical or biological sensors[34,36,37], which is an area in which organic devices are promising since they would open a new field of applications.

So, besides the high stability in ambient conditions it is worth testing the aqueous stability of the devices by immersing a device in mq-water for a defined period of time. After the immersion in water the devices were dried with a N_2 stream and measured. Figure 6.15(a) depicts the log-transfer measured for several immersion times showing minimal shift in the switch on voltage as well as in the on/off ratio. The "shape" of the curve is conserved over a 12 hour immersion,

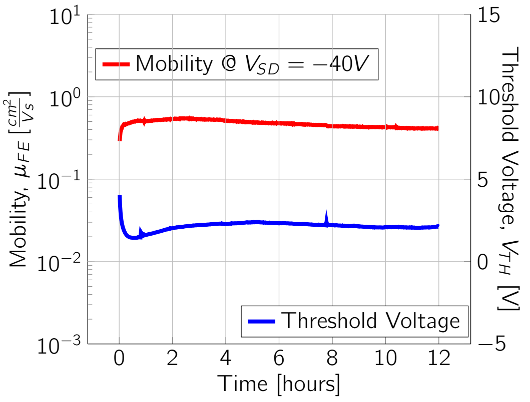

(a)

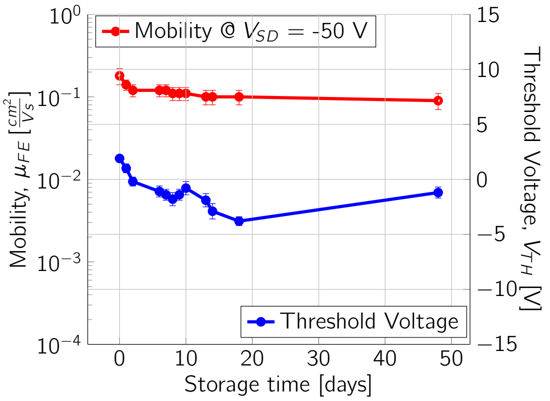

(b)

Figure 6.14 *(a) Mobility and threshold voltage values gathered over a period of 12 hours with one measurement per minute, and (b) Average mobility and threshold voltage values per 10 devices over a storage period equivalent to 50 days.*

which suggests high stability under aqueous media. The mobility and threshold voltage were studied as well and plotted in Figure 6.15(b). The mobility found for this device as starting value is located to the left of the mean value, on the negative side for the theoretical quantiles reported in Figure 6.11(b), however inside the statistic tolerable range. Such value only declines slightly as the immersion time progress, but most importantly the threshold voltage which is an indicator of doping does not shift to positive values over 12 hours ($\approx 10^4$ s), which is a further indication of the successful encapsulation of the semiconductor material.

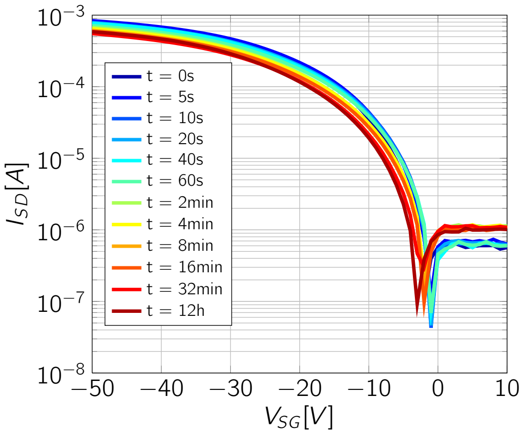

(a)

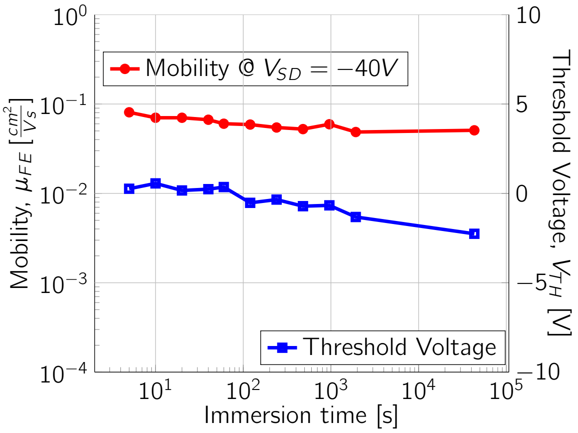

(b)

Figure 6.15 *(a) Log-transfer at V_{SD} = -40 V for sequentially immersion times and (b) mobility and threshold voltage as a function of immersion time. For a device with L = 75 µm, and W = 75 mm.*

6.5 Temperature dependence studies [†]

The transport mechanisms in organic semiconductors have been studied theoretically, modelled, and measured extensively during the past 50 years[38]. But, studies on the fundamentals of transport mechanisms have achieved substantial progress in the past decade due to the fabrication of excellent high-performance

---

[†] Work carried out in close collaboration with Dr. Simone Fabiano, Prof. Xavier Crispin and Prof. Magnus Berggren @ Linköping University.

single crystal organic field-effect transistors (SC-OFETs), such as rubrene single crystal OFET[39]. However, the exact conduction mechanism that holds for organic semiconductors, remains still open and has not been established yet[38], thus charge transport is experimentally unresolved and a theoretical challenge[39]. However, early models suggested that thermally activated small-polaron hopping explains the motion of carriers through and organic crystal[40–44]. Holstein assumed that successive carrier hops to neighboring sites were uncorrelated, giving a simple activated-type variation of carrier mobility with temperature down to some critical temperature, below which band transport would dominate. The assumption of independent hops applies if the hopping rate is low enough for the lattice to relax between hopping events. Further, a hopping mechanism involving tunneling between molecules has been also suggested, which mechanism would be temperature independent[38].

It is customary to describe OFETs by the model derived for MOSFETs, since MOSFETs are well studied and its behaviour at first glance is quite similar to OFETs. However, there are some features that are difficult to explain inside the MOSFET framework, and one of those things is temperature dependent charge transport which deserves extra attention. In MOSFET devices charge-carrier mobilities and currents are essentially independent of temperature, while in OFETs, as mentioned, typically thermally activated transport is found although complicated dependencies of temperature have also been observed and reported[45]. Recently Xie et al.[39] report a temperature independent mobility in a single crystal of dinaphtho-thieno-thiophene (DNTT), reinforcing the before stated that charge transport is still an open question. Furthermore, it is possible that traps or contact effects make a temperature independent transport look temperature dependent or exhibit unusual temperature dependency, but the reverse is simple not possible[38].

Surprisingly, the devices reported here were found to exhibit temperature independent mobility in wide range of temperatures $85K < \mathrm{T} < 295K$ (see Figures 6.16 and H.11) and to the best of our knowledge is the first solution processed material and thin film which exhibits such behaviour.

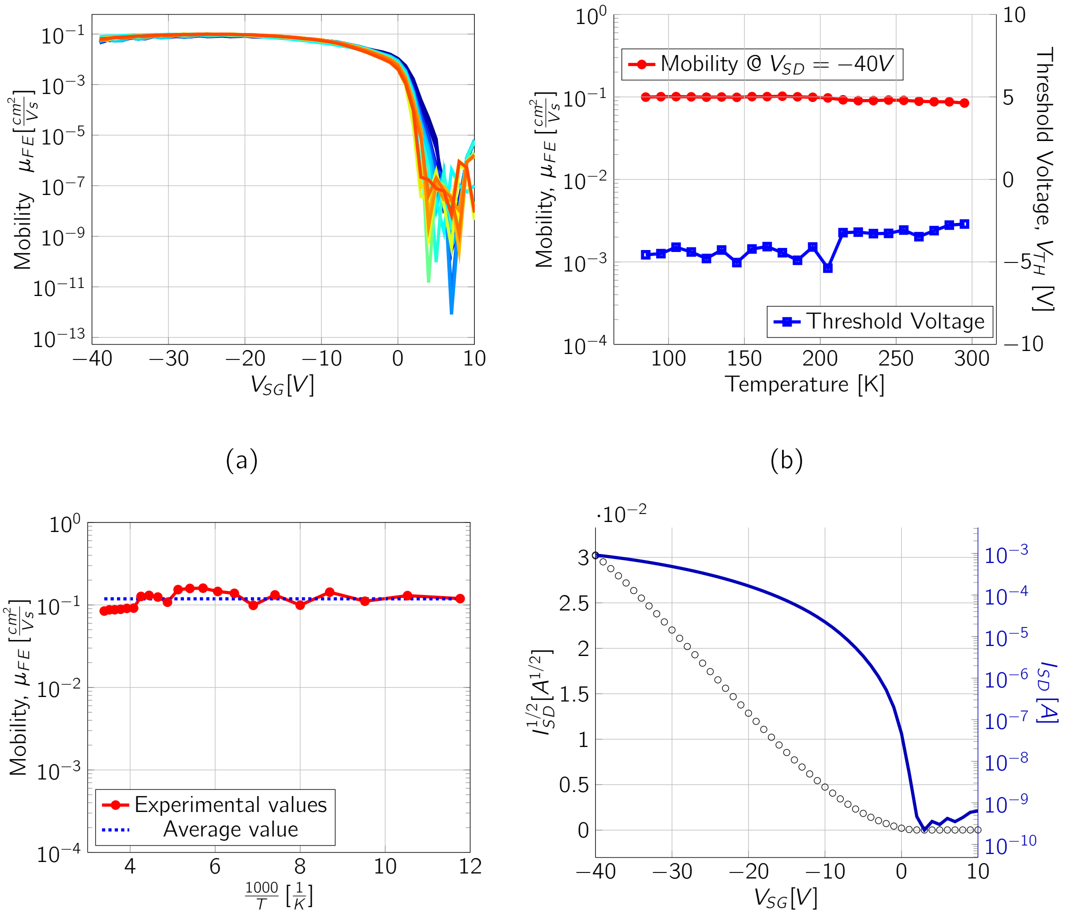

(a) (b)

(c) (d)

Figure 6.16 *(a) Mobility profiles over temperature variation $85K < T < 295K$ (b), Mobility and threshold voltage as function of temperature extracted at saturation regime $V_{SD} = -40V$ (c) Graphical representation of mobility in red the experimental values and in blue an average value as function of 1000/T. (d) $\sqrt{I_{SD}}\, f(V_{SG})$ and log-transfer recorded at 85 K.*

Figure 6.16(a) depicts the mobility profile as a function of temperature (85 K < T < 295 K, step = 15 K) in which one can see that the mobility profile shows a gate independent behaviour suggesting low contact resistance and efficient charge injection. Importantly, no variations as a function of temperature are noted since most of the curves overlap to each other, then suggesting a trap-free transport phenomena. Further the mobility is extracted and depicted in Figure 6.16(b) as a function of temperature plotted together with threshold voltage. The mobility fluctuation is inexistent while the threshold voltage fluctuates around 2 V. Figure 6.16(d) depicts $\sqrt{I_{SD}}\, f(V_{SG})$ and log-transfer recorded at 85 K (for all profiles see Figure H.11), which suggests that even at such low temperature the transistors maintain their characteristics. Moreover, one thing to note is the dramatic change in current that occurs below threshold voltage which corresponds approximately to four orders of magnitude, with a sub-threshold swing around 200 mv/decade which is very low for organic semiconductors.

Previously it has been demonstrated that the covering of dielectrics with polar hydroxyl groups, such as SiO_2 or Al_2O_3, with a thin layer of PS minimizes the number of interfacial charge carrier trap states enhancing the device performance[46,47]. Additionally, the higher mobility of small molecule/polymers blends was also previously attributed to a vertical phase separation of the materials that may exclude impurities from the critical charge-transporting region, while covering the dielectric with a thin layer of PS enhancing the device performance[46]. Thus, we believe that both effects might be coexisting here and being responsible for the high and temperature-independent mobility observed.

6.6 Applications - Inverters

OFETs are promising candidates for applications like displays, chemical sensors and radio frequency identification tags among many others[48]. One among many applications for OFETs is signal processing circuits. The basic element for digital circuit design is the logic inverter or the NOT gate, and it is used to con-

---

**Work carried out in close collaboration with Dr. Simone Fabiano, Prof. Xavier Crispin and Prof. Magnus Berggren @ Linköping University.

struct logic gates and more intricate digital circuits. Such basic element, the inverter, functions as a complementary switch where a low input signal results in a high output signal and vice versa.

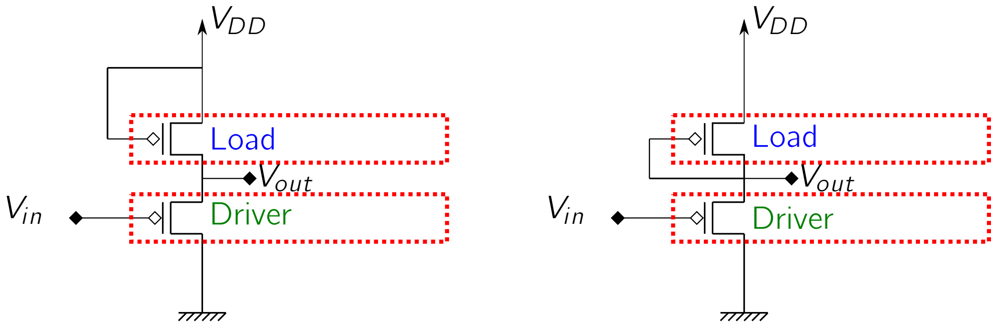

(a) Saturated Load. (b) Depleted Load.

Figure 6.17 *Equivalent electric circuit layout of a p-type unipolar inverter with (a) saturated load and (b) depleted load.* V_{in} *is the input voltage,* V_{out} *is the output voltage, and* V_{DD} *is the supply voltage. In each configuration the driver and the load transistors are denoted*[49].

Two technologies for the fabrication of organic integrated circuits are demonstrated up to date: the unipolar and the complementary technology. For the unipolar inverters either a pair of p-channel or n-channel transistors construct the inverter. While complementary inverter circuits are composed by both n-channel and p-channel transistors. While the latter type of inverters are more desirable own to high signal integrity and low power consumption, the lack of n-channel transistors exhibiting ambient stability drains the expansion of such devices.

The unipolar inverter circuit consists of a driver transistor and a load transistor connected in series. Two inverter configurations are commonly employed in a unipolar inverter which are depicted in Figure 6.17: the saturated and the depleted load. The supply voltage (V_{DD}) is connected to the drain electrode of the load transistor and the input and output signals (V_{in},V_{out}) are connected to the gate and the drain electrodes of the driver transistor, respectively. When the drain and the gate electrodes of the load transistor are connected together, the load transistor operates in the saturation regime and hence the inverter is in saturated load. On the other hand, when the gate and source electrodes of the load transistor are connected, the load transistor is always off thus the inverter is designated as a depleted load inverter[49].

The inverter configuration used in this work is the depleted load inverter, in which the gate of the load transistor is wired to its own source, so V_{SG} = 0 V at all times. Output characteristics [††] for typical devices which conform an inverter are depicted in Figure 6.18

Figure 6.19 shows a photo of one of the constructed inverters realized by connecting two transistors. In an inverter the typical parameters are: V_{out} = the output voltage, V_{DD} = the supply voltage,V_{in} = the input voltage. The working principle of a inverter is to control the voltage division through the input, thus tuning the driver OFET resistance through V_{in} controlling the inverter output voltage. Ideally, the voltage difference between V_{out} and V_{in} (voltage swing) should be equal to V_{DD} (supply voltage). The voltage transfer characteristics (VTC), the output voltage as a function of input voltage, are shown in Figure 6.20(a), which depicts that

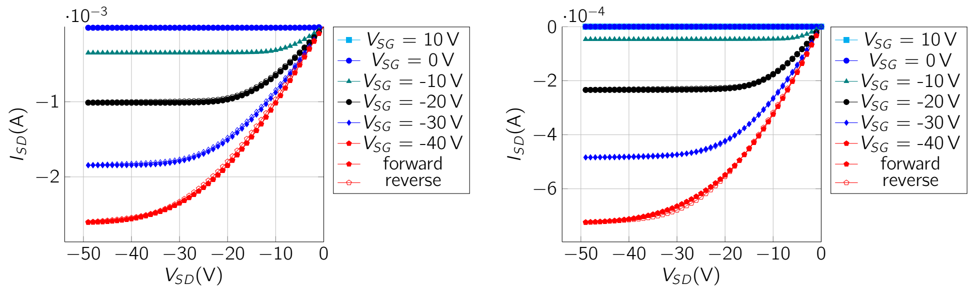

(a) (b)

Figure 6.18 *Output characteristics for typical devices that conforms an unipolar inverter wired in depleted mode (a) Load transistor L = 100 μm, W = 200 mm,* $\mu_{sat} = 0\ 15\,\frac{cm^2}{Vs}$ *and* $V_{TH} = -1\ 8V$*, and (b) Driver transistor L = 100 μm, W = 100 mm,* $\mu_{sat} = 0\ 09\,\frac{cm^2}{Vs}$ *and* $V_{TH} = -6\ 9V$.

[††] Output characteristic is almost universally presented as the qualitative proof that a transistor has been formed[50].

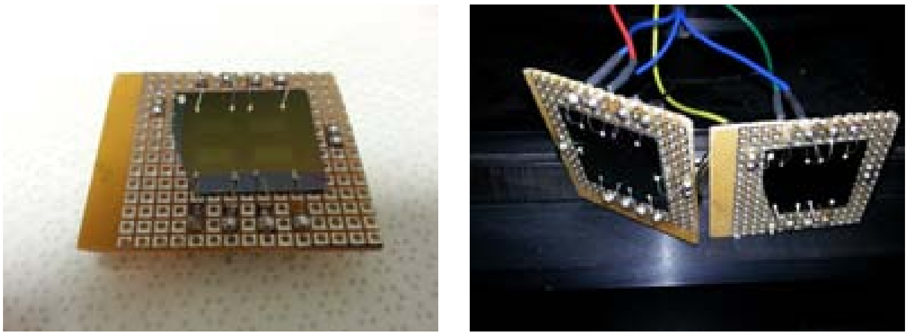

(a) (b)

Figure 6.19 *(a) Substrate with four transistors (L = 100 μm and W = 100 mm) mounted in a single side prototype board with pins and (b) Depleted load inverter constructed of two substrates wired and each substrate with four transistors, and inside (b) for the left plate four transistors with L = 100 μm and W = 200 mm and for the right plate four transistors L = 100 μm and W = 100 mm*

the highest voltage obtained at different supply voltages are quite similar, within a very small transition region of about 0.1 V. Another key parameter of an inverter is the gain, which is defined as the numerical derivative of the V_{out} versus V_{in}, and inverters that exhibit gains larger than one are candidates to drive other gates in logic circuits. The gain for a typical fabricated inverter is depicted in Figure 6.20(b) in which one can see a gain higher than 300. Such value, to the best of our knowledge, is the highest value for an organic unipolar inverter reported to date.

The switching threshold is ideally located at $V_{DD}/2$ and is defined as the switch voltage from high to low or vice versa. Figure 6.21 shows that the switching threshold when V_{DD} = -10 V is located at -6 V only 1 V deviation from the ideal position. In this case the width of the load is twice the width of the driver, since varying the width of the load and the driver is a well-known technique followed to move the switching threshold close or on the ideal value[51,52].

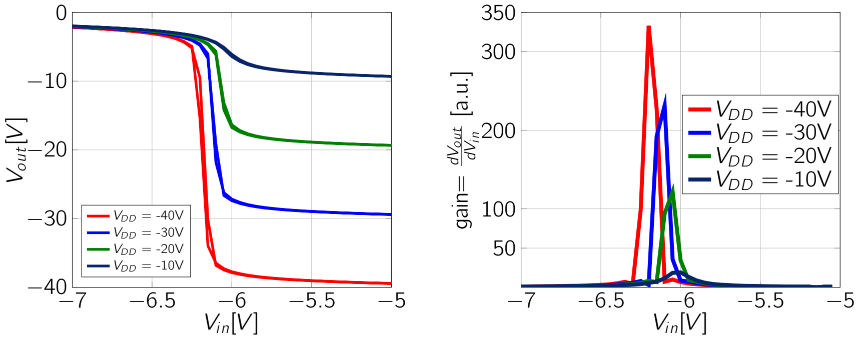

(a) (b)

Figure 6.20 *Characteristics of inverters based on OFETs fabricated in bottom contact/bottom gate architectures, with a semiconducting thin film made of a composite of DB-TTF:PS3000 in a ratio 1:2. (a) Output voltage (V_{out} in V) and (b) signal gain as a function of input voltage (V_{in} in V), both for supply voltages between -10V and -40 V (step -10 V).*

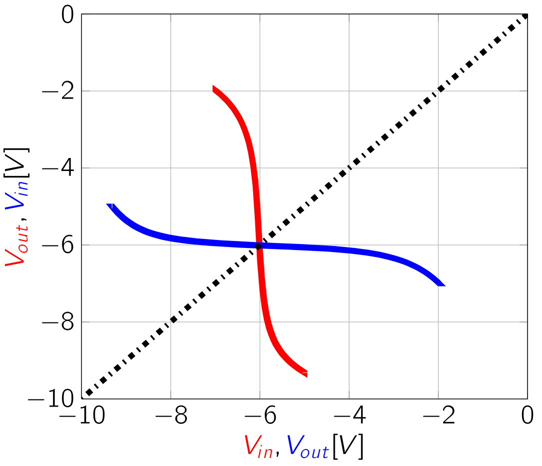

Figure 6.21 *Voltage transfer characteristics (VTC) for an unipolar inverter with a load transistor L = 100 μm and W = 200 mm, and a driver transistor L = 100 μm and W = 100 mm working in depleted mode at $V_{DD} = -10V$.*

6.7 Summary

High performing organic field-effect transistors based on DB-TTF and PS3000 in a ratio 1:2 were demonstrated, with mobility and threshold voltage independent of channel length in the range of 20μm to 100μm. The reproducibility in mobility and threshold voltage was proven after measuring ≈ 200 devices. Homogeneity in the film was studied by analysing the crystalline structures using a computational tool such as ImageJ confirming a mean value of a crystalline domain of 180 μm over a wide range of channel lengths. High stability was demonstrated for short term (12 hours) and long term stability for more than forty days. Also stability over a period of 12 hours in an aqueous media was demonstrated with no positive shift in threshold voltage observed. Low contact resistance values were extracted from linear regimes out of several devices, and according to the literature locating such values as one of the lowest for organic semiconductors and gold electrodes. Temperature independent mobility was demonstrated, suggesting for the first time a trap-free transport in solution processed thin films materials. The operation of inverter circuits based on DB-TTF:PS3000 composite have been demonstrated. The depleted load inverter worked very well, with an unprecedent gain as high as 300, and such devices working only at -10 V as supply voltage deviates only 1 V from the ideal. The results shown here demonstrate that DB-TTF/PS3000 transistors could be successfully exploited as components in integrated organic electronic circuits.

Bibliography

[1] S. Goffri, C. Muller, N. Stingelin-Stutzmann, D. W. Breiby, C. P. Radano, J. W. Andreasen, R. Thompson, R. A. J. Janssen, M. M. Nielsen, P. Smith and H. Sirringhaus. "Multicomponent semiconducting polymer systems with low crystallization-induced percolation threshold". *Nature Materials*, **2006**, 5, 950.

[2] R. Hamilton, J. Smith, S. Ogier, M. Heeney, J. E. Anthony, I. McCulloch, J. Veres, D. D. C. Bradley and T. D. Anthopoulos. "High-Performance

Polymer-Small Molecule Blend Organic Transistors". *Advanced Materials*, **2009**, 21, 1166.

[3] M.-B. Madec, D. Crouch, G. R. Llorente, T. J. Whittle, M. Geoghegan and S. G. Yeates. "Organic field effect transistors from ambient solution processed low molar mass semiconductor-insulator blends". *J. Mater. Chem.*, **2008**, 18, 3230.

[4] D. M. Russell, C. J. Newsome, S. P. Li, T. Kugler, M. Ishida and T. Shimoda. "Blends of semiconductor polymer and small molecular crystals for improved-performance thin-film transistors". *Appl. Phys. Lett.*, **2005**, 87, 222109.

[5] J. Smith, R. Hamilton, M. Heeney, D. M. de Leeuw, E. Cantatore, J. E. Anthony, I. McCulloch, D. D. C. Bradley and T. D. Anthopoulos. "High-performance organic integrated circuits based on solution processable polymer-small molecule blends". *Applied Physics Letters*, **2008**, 93 253301.

[6] J. Smith, R. Hamilton, I. McCulloch, N. Stingelin-Stutzmann, M. Heeney, D. D. C. Bradley and T. D. Anthopoulos. "Solution-processed organic transistors based on semiconducting blends". *J. Mater. Chem.*, **2010**, 20, 2562.

[7] N. Stingelin-Stutzmann, E. Smits, H. Wondergem, C. Tanase, P. Blom, P. Smith and D. de Leeuw. "Organic thin-film electronics from vitreous solution-processed rubrene hypereutectics". *Nature M*, **2005**, 8, 601.

[8] C. E. Murphy, L. Yang, S. Ray, L. Yu, S. Knox and N. Stingelin. "Wire-bar coating of semiconducting polythiophene/insulating polyethylene blend thin films for organic transistors". *Journal of Applied Physics*, **2011**, 110 093523.

[9] A. C. Arias, J. D. MacKenzie, I. McCulloch, J. Rivnay and A. Salleo. "Materials and Applications for Large Area Electronics: Solution-Based Approaches". *Chemical Reviews*, **2010**, 110, 3. PMID: 20070114.

[10] N. A. Azarova, J. W. Owen, C. A. McLellan, M. A. Grimminger, E. K. Chapman, J. E. Anthony and O. D. Jurchescu. “Fabrication of organic thin-film transistors by spray-deposition for low-cost, large-area electronics”. *Organic Electronics*, **2010**, 11, 1960 .

[11] A. Facchetti. “Semiconductors for organic transistors”. *materialstoday*, **2007**, 10, 28.

[12] M. Mas-Torrent and C. Rovira. “Novel small molecules for organic field-effect transistors: towards processability and high performance.” *Chemical Society Reviews*, **2008**, 37, 827.

[13] S. Holliday, J. E. Donaghey and I. McCulloch. “Advances in Charge Carrier Mobilities of Semiconducting Polymers Used in Organic Transistors”. *Chemistry of Materials*, **2014**, 26, 647.

[14] W. Burger and M. Burge. *Digital Image Processing: An Algorithmic Introduction Using Java*. Texts in Computer Science. Springer, **2009**.

[15] W. Burger and M. Burge. *Principles of Digital Image Processing: Core Algorithms*. Undergraduate Topics in Computer Science. Springer, **2010**.

[16] W. S. R. Caroline A Schneider and K. W. Eliceiri. “NIH Image to ImageJ: 25 years of image analysis”. *Nature Methods*, **2012**, 9, 671.

[17] D. Ne as and P. Klapetek. “Gwyddion: an open-source software for SPM data analysis”. *Central European Journal of Physics*, **2011**, 10, 181.

[18] A. Brillante, I. Bilotti, R. G. Della Valle, E. Venuti, S. Milita, C. Dionigi, F. Borgatti, A. N. Lazar, F. Biscarini, M. Mas-Torrent, N. S. Oxtoby, N. Crivillers, J. Veciana, C. Rovira, M. Leufgen, G. Schmidt and L. W. Molenkamp. “The four polymorphic modifications of the semiconductor dibenzo-tetrathiafulvalene”. *CrystEngComm*, **2008**, 10, 1899.

[19] X. Zhang, H. Bronstein, A. J. Kronemeijer, J. Smith, Y. Kim, R. J. Kline, L. J. Richter, T. D. Anthopoulos, H. Sirringhaus, K. Song, M. Heeney, W. Zhang, I. McCulloch and D. M. DeLongchamp. "Molecular origin of high field-effect mobility in an indacenodithiophene-benzothiadiazole copolymer." *Nature communications*, **2013**, 4, 2238.

[20] A. Wang. *Threshold voltage in pentacene field effect transistors with parylene dielectric*. Master's thesis, Massachusetts Institute of Technology, **2004**.

[21] B. Venables. "Programmer's Niche". *R News*, **2001**, 1, 27.

[22] U. Ligges. "R Help Desk: Automation of Mathematical Annotation in Plots". *R News*, **2002**, 2, 32.

[23] M. Schwartz. "The Decision To Use R". *R News*, **2004**, 4, 2.

[24] L. Komsta. "Processing data for outliers". *R News*, **2006**, 6, 10.

[25] R. Core Team. "What is R?" *R News*, **2001**, 1, 2.

[26] P. Dalgaard. *Introductory Statistics with R*. Statistics and Computing. Springer, **2008**.

[27] L. Pace. *Beginning R: An Introduction to Statistical Programming*. Apressus Series. Apress, **2012**.

[28] K. Ryu. *Characterization of Organic Field Effect Transistors for OLED Displays*. Master's thesis, Massachusetts Institute of Technology, **2005**.

[29] D. Natali and M. Caironi. "Charge Injection in Solution-Processed Organic Field-Effect Transistors: Physics, Models and Characterization Methods". *Advanced Materials*, **2012**, 24, 1357.

[30] R. Pfattner, M. Mas-Torrent, C. Moreno, J. Puigdollers, R. Alcubilla, I. Bilotti, E. Venuti, A. Brillante, V. Laukhin, J. Veciana and C. Rovira. "Organic metal-organic semiconductor blended contacts in single crystal field-effect transistors". *J. Mater. Chem.*, **2012**, 22, 16011.

[31] R. Pfattner, C. Moreno, C. Voz, R. Alcubilla, C. Rovira, J. Puigdollers and M. Mas-Torrent. "Restraints in low dimensional organic semiconductor devices at high current densities". *Organic Electronics*, **2014**, 15, 211 .

[32] M. Mas-Torrent and C. Rovira. "Role of molecular order and solid-state structure in organic field-effect transistors". *Chemical Reviews*, **2011**, 111, 4833.

[33] T. Marszalek, A. Nosal, R. Pfattner, J. Jung, S. Kotarba, M. Mas-Torrent, B. Krause, J. Veciana, M. Gazicki-Lipman, C. Crickert, G. Schmidt, C. Rovira and J. Ulanski. "Role of geometry, substrate and atmosphere on performance of OFETs based on TTF derivatives". *Organic Electronics: physics, materials, applications*, **2012**, 13, 121.

[34] O. Knopfmacher, M. L. Hammock, A. L. Appleton, G. Schwartz, J. Mei, T. Lei, J. Pei and Z. Bao. "Highly stable organic polymer field-effect transistor sensor for selective detection in the marine environment." *Nature communications*, **2014**, 5, 2954.

[35] Y. Qiu, Y. Hu, G. Dong, L. Wang, J. Xie and Y. Ma. "H[sub 2]O effect on the stability of organic thin-film field-effect transistors". *Applied Physics Letters*, **2003**, 83, 1644.

[36] M. D. Angione, S. Cotrone, M. Magliulo, A. Mallardi, D. Altamura, C. Giannini, N. Cioffi, L. Sabbatini, E. Fratini, P. Baglioni, G. Scamarcio, G. Palazzo and L. Torsi. "Interfacial electronic effects in functional biolayers integrated

into organic field-effect transistors." *Proceedings of the National Academy of Sciences of the United States of America*, **2012**, 109, 6429.

[37] K. Kuribara, H. Wang, N. Uchiyama, K. Fukuda, T. Yokota, U. Zschieschang, C. Jaye, D. Fischer, H. Klauk, T. Yamamoto, K. Takimiya, M. Ikeda, H. Kuwabara, T. Sekitani, Y.-L. Loo and T. Someya. "Organic transistors with high thermal stability for medical applications." *Nature communications*, **2012**, 3, 723.

[38] S. F. Nelson, Y.-Y. Lin, D. J. Gundlach and T. N. Jackson. "Temperature-independent transport in high-mobility pentacene transistors". *Applied Physics Letters*, **1998**, 72, 1854.

[39] W. Xie, K. Willa, Y. Wu, R. Hausermann, K. Takimiya, B. Batlogg and C. D. Frisbie. "Temperature Independent Transport in High Mobility Dinaphtho Thieno Thiophene (DNTT) Single Crystal Transistors". *Advanced Materials*, **2013**, 25, 3478.

[40] P. Stallinga. *Electrical Characterization of Organic Electronic Materials and Devices*. Wiley, **2009**.

[41] P. Stallinga and H. Gomes. "Trap states as an explanation for the Meyer Neldel rule in semiconductors". *Organic Electronics*, **2005**, 6, 137 .

[42] P. Stallinga and H. Gomes. "Modeling electrical characteristics of thin film field effect transistors: II: Effects of traps and impurities". *Synthetic Metals*, **2006**, 156, 1316 .

[43] P. Stallinga and H. Gomes. "Modeling electrical characteristics of thin-film field-effect transistors: I. Trap-free materials". *Synthetic Metals*, **2006**, 156, 1305 .

[44] P. Stallinga, H. L. Gomes, F. Biscarini, M. Murgia and D. M. de Leeuw. "Electronic transport in field-effect transistors of sexithiophene". *Journal of Applied Physics*, **2004**, 96, 5277.

[45] P. Stallinga and H. Gomes. "Thin film field-effect transistors: The effects of traps on the bias and temperature dependence of field-effect mobility, including the Meyer Neldel rule". *Organic Electronics*, **2006**, 7, 592 .

[46] B. Park, I. In, P. Gopalan, P. G. Evans, S. King and P. F. Lyman. "Enhanced hole mobility in ambipolar rubrene thin film transistors on polystyrene". *Appl. Phys. Lett.*, **2008**, 92, 133302.

[47] Y. Yuan, G. Giri, A. L. Ayzner, A. P. Zoombelt, S. C. B. Mannsfeld, J. Chen, D. Nordlund, M. F. Toney, J. Huang and Z. Bao. "Ultra-high mobility transparent organic thin film transistors grown by an off-centre spin-coating method." *Nature communications*, **2014**, 5, 3005.

[48] Y. Yun. *Pentacene Based Organic Electronic Devices*. Ph.D. thesis, Durham University, **2010**.

[49] H. Sinno. *Polyelectrolyte-Gated Organic Field Effect Transistors - Printing and Electrical Stability*. Ph.D. thesis, Linköping University, **2013**.

[50] I. Kymissis. *Organic Field Effect Transistors: Theory, Fabrication and Characterization*. Integrated Circuits and Systems. Springer, **2008**.

[51] H. Wang, P. Wei, Y. Li, J. Han, H. R. Lee, B. D. Naab, N. Liu, C. Wang, E. Adijanto, B. C.-K. Tee, S. Morishita, Q. Li, Y. Gao, Y. Cui and Z. Bao. "Tuning the threshold voltage of carbon nanotube transistors by n-type molecular doping for robust and flexible complementary circuits." *Proceedings of the National Academy of Sciences of the United States of America*, **2014**, 111, 4776.

[52] L. Kergoat, L. Herlogsson, B. Piro, M. C. Pham, G. Horowitz, X. Crispin and M. Berggren. “Tuning the threshold voltage in electrolyte-gated organic field-effect transistors”. *Proceedings of the National Academy of Sciences*, **2012**, 109, 8394.

Chapter 7

Conclusions

Organic electronics (OE) still have to face many challenges which prevents their widespread adoption. Challenges regarding charge transport and device to device variability, both are limits to the long term use and fabrication of complex circuits. However, the charge transport mobility and the stability during the past few years have seen huge improvements. Now, the potential for solution processed is exploited, in addition with low cost flexible and printable electronics is also possible , all ensuring a bright future for organic electronics.

1. The Bar Assisted Meniscus Sheering (BAMs) was developed as a new coating technique for the deposition of solutions of polymers for a broad range of target applications like deposition of dielectrics and semiconducting thin solid films. This technique gives rise to very smooth and homogeneous films.

2. The approach of blending organic semiconductors with insulating polymers shows great potential for applications since it lower the price of the device (i.e. less amount of the organic semiconductor is used) and helps to attain solution processability.

3. The application of BAMs to fabricate organic semiconductors films based on blends leads to, in one-step, the self-encapsulation of the organic semiconductor and the formation of highly crystalline and isotropic films due to the vertical phase separation procedures.

4. Organic Field-Effect Transistors based on blends of poly-(3 hexylthiophene) (P3HT) and polystyrene (PS) have been successfully fabricated using BAMs. Such devices equate the highest mobilities reported in literature (0.1 $cm^2V^{-1}s^{-1}$) while maintaining the threshold voltage close to zero volts. All devices were fabricated in air, with only the 10% of the whole composite material that comprises the thin film being P3HT. All fused have been an achievement to-date with no mate data reported in the literature.

5. TTF derivatives DB-TTF, DT-TTF and BET-TTF are well know to be good candidate semiconductors for OFETs applications. The application of BAMs in polymeric blends of these TTF derivatives has appended solution processing and large area coverage to the inherent high performance that the mentioned TTF derivatives possess. But, the achievement was not only to be able to process the materials from solution into large areas, the achievement has been to convert a highly unstable material such as BET-TTF and DB-TTF into an stable material. Several composites have been developed with unprecedented characteristics, like stability, reproducibly, high mobility and high on/off ratio. Importantly, the devices exhibited enhanced OFET performances compared to the ones found for evaporated thin films.

6. Preliminar proof-of-concept experiments have been developed towards organic electrodes fabricated on the same semiconducting film which shown the potential to fabricate all-organic devices.

7. After the screening of different TTF/polymeric blends to be applied in OFETs using BAMs. The most optimum combination found considering device performance and cost was the blend DB-TTF:PS3000 1:2 2 % wt. The resulting thin films gave average mobility values of 0.16 $cm^2V^{-1}s^{-1}$ although mobilities of up to 0.7 $cm^2V^{-1}s^{-1}$ were recorded.

8. The exceptionally high stability of OFETs based on DB-TTF:PS3000 films in environmental conditions and in water represents an important step forward in the field and indicates that theses materials could also find their place in other applications such as sensors.

9. Charge transport in organic semiconductors is still an unresolved issue and theoretical challenge. Most of the organic electronics community members have a strong believe that temperature independent charge transport is exclusive of highly purified materials processed under inert conditions and high vacuum, however here we successfully demonstrate, to the best of our knowledge, the first material processed from solution and fabricated entirely under ambient conditions that exhibits a temperature independent mobility. Then sculpt a new paradigm in organic electronics that even solution processed materials can exhibit a temperature independent charge transport. Also, when such devices became a part of an application like inverters, the latter behaves impressively well. So, we were able to record the highest gain $\approx$ 300 for an organic based inverter to-date and to the best of our knowledge.

To sum up, the work here developed contributes to the development of organic electronics for potential applications. Because, a new coating technique has been developed which is compatible with upscaling, highly unstable materials have been transformed into stable ones, high performing devices have been found, the first temperature independent processed entirely from solution material have been reported, inverters with record gain have been also reported, so we strongly believe that this work contributes to the organic electronics community in a plausible way.

Appendices

Appendix A

Chauvenet's Criterion

During experimentation is common that some measurements appear to disagree discordantly with all the others. The experimentalist is therefore encounter with the task of judging if these points are the result of some anomalous experimental behavior and thus be neglected or if they represent a new type of behavior of a physical phenomenon which is peculiar to a certain operating condition. However, the engineer must not just throw out those points that do not match with expected values - there must be some consistency for such exclusion.

Suppose n measurements of a quantity are taken, and n is large enough that the data taken expect to follow the gaussian error distribution, and such distribution is used to compute the probability that a given data point will deviate a certain amount from the mean[1,2]. First the ratio d_i/σ must be calculated, then in accordance with TableA.1 a reading can be excluded, finally a standard deviation and a new mean value must be computed.

$$
\begin{aligned}
x_m &= \frac{1}{n}\sum_{i=1}^{n} x_i \\
d_i &= x_i - x_m \\
\sigma &= \left[\frac{\sum_{i=1}^{n}\left(x_i - x_m\right)^2}{n-1}\right]^{1/2}
\end{aligned}
$$

Table A.1 *Chauvenet s criterion for rejecting a reading.*

Number of Readings **n**	Ratio of Maximum Acceptable Deviation to Standard Deviation, $d_{max}\ \sigma$
3	1.38
4	1.54
5	1.65
6	1.73
7	1.80
10	1.96
15	2.13
25	2.33
50	2.57
100	2.81
300	3.14
500	3.29
1000	3.48

where x_i is each reading, n are the number of readings, x_m is the arithmetic mean, d_i is the deviation for each reading and σ is the standard deviation.

Bibliography

[1] J. Holman. *Experimental methods for engineers*. McGraw-Hill series in mechanical engineering. McGraw-Hill, **2001**.

[2] J. Taylor. *An introduction to error analysis: the study of uncertainties in physical measurements*. Physics - chemistry - engineering. University Science Books, **1997**.

Appendix B

A brief description of techniques

B.1 Contact Angle

Consider a liquid drop on a solid surface surrounded by a gas B.1. At equilibrium, the contact angle is the angle the interface makes with the solid surface, as measured through the dense medium[1], then is the angle at which a liquid - vapor interface meets the solid surface, and it is specific for each system and corresponds to the interactions across the three interfaces. The shape of the droplet is determined by the Young-Laplace equation (see Equation B.1) and the angle plays the role of a boundary condition. The contact angle value is extracted using a goniometer, to characterize the wettability of a surface Figure B.1 by measuring the surface tension of a solvent droplet at its interface with a homogeneous surface[2,3].

(a) (b)

Figure B.1 *Difference in wettability. (a) a hydrophobic surface, and (b) a hydrophilic surface.*

$$P_1 - P_2 = \gamma_{12}\left(\frac{1}{R_1} + \frac{1}{R_2}\right) \tag{B.1}$$

One can imagine that measuring the radius of a bubble as well as the pressure difference will end up with the surface tension calculation, however this measurement is difficult. On the other hand, the contact angle does not give the surface tension of an interface directly because the surface tension is function of several variables as specified by Young's equation but the measurement of the contact angle is straight forward. The Young-Laplace equation states that any curved surface at equilibrium separation phase 1 from phase 2 maintains a pressure drop across the surface, then equilibrium relations at an interface dictate the shape of the interface and the forces at the interface[1]. In Equation B.1, R_1 and R_2 are the radii of curvature of the surface in two orthogonal directions, and γ the surface tension. Also the Young-Laplace equation can be expressed for a pressure drop across an isotropic curved interface (see Equation B.2) in which γ_{lg} is the surface tension between liquid and gas, and R is the radius of the bubble, the sign of the variation ΔP_{lg} is defined such the liquid is at less pressure than the bubble, and Equation B.3 is the result after equating forces at the triple point, since the surface tension can be considered as a force per unit length, can be simply show these forces all acting at the triple point, and at equilibrium such forces sum to zero.

$$\Delta P_{lg} = 2\frac{\gamma_{lg}}{R} \tag{B.2}$$

$$\cos\theta = \frac{\gamma_{sg} - \gamma_{sl}}{\gamma_{lg}} \tag{B.3}$$

B.2 Atomic Force Microscopy

The Atomic Force Microscope (AFM) is a high resolution type of scanning probe microscope, whose working principle is based on the deflection of a very sensitive cantilever, and its fundamental components are the probe and the scanner.

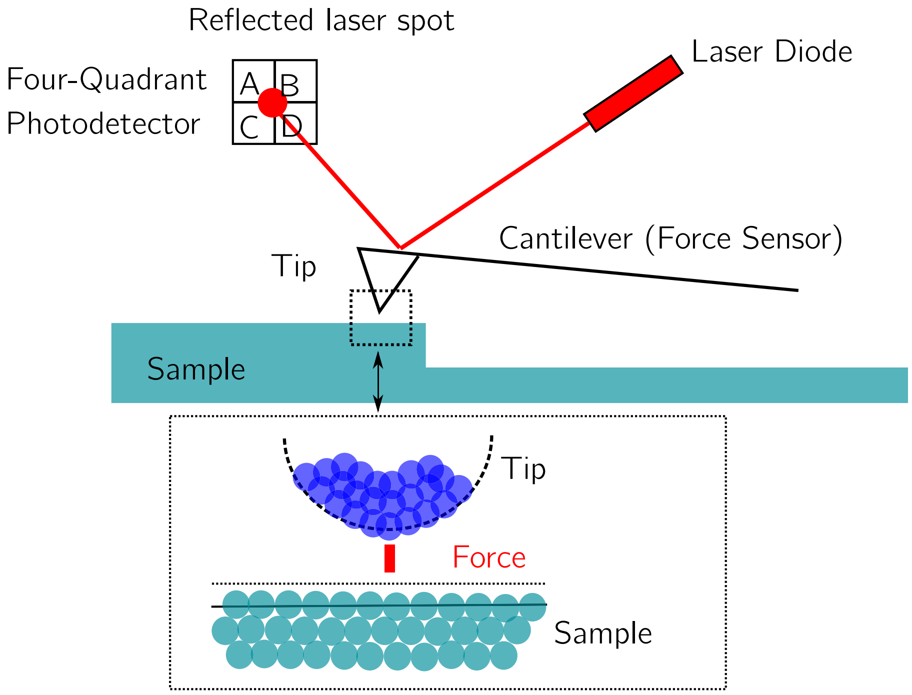

Figure B.2 *Atomic Force Microscopy (AFM) scheme.*

The probe is very sharp tip (usually sharp enough to end in one atom) which is located at the end of a cantilever. Due to forces between sample and tip the cantilever deflects, and such deflection is measured by a laser beam during the sample scanning, while a piezoelectric translator scans in x,y and z coordinates, the computer system controls the (x,y,z) translation and records the reflected laser beam signal, finally dedicated software constructs the data gathered into topological images[2,4].

B.3 X-Ray

X-rays were discovered in 1885 by a German physicist Wilhelm Conrad Röntgen. X-rays are electromagnetic radiation with a wavelength range of 0.01 - 100 Å, which correspond to frequencies in the range of 30PHz - 300 EHz. In order to reveal the nature of a crystal lattice only a short wavelength of about 0.5 - 2.5

Å is used, so the diffraction pattern produced by x-rays through a closely spaced lattice in the crystal is recorded and analyzed. Copper (Cu) $K\alpha$ radiation with a wavelength of 1.54 Å is the most common used radiation in diffraction analysis.
Bragg's law (Equation B.4), was introduced in 1913 by English physicists William Henry Bragg and his son William Lawrence Bragg, and since then has been one of the most important laws to interpret diffraction data.

$$2d\sin\theta = n\lambda \tag{B.4}$$

where d is the interplanar spacing, θ is incident wave angle, n indicates the reflection order and λ is the wavelength of incident waves.
X-rays interference is a direct evidence for the periodicity in the atomic structure inside a crystal. The diffraction pattern will evidence sharp peaks only if the atoms in a crystal structure are regularly arranged in a long range. Also, a diffraction peak shift and a change in interplanar distance are observed while the internal stress and its composition differ. So, diffraction patterns allow to make deductions on crystal structure, crystal size, internal stress, and composition[2].

B.4 Time of Flight Secondary Ion Mass Spectroscopy (TOF-SIMS)

Time-of-Flight Secondary Ion Mass Spectroscopy (TOF-SIMS) is a surface analytical technique used to analyse the composition of solid surfaces and thin films. Focusing a pulsed beam of primary ions (typically Cs or Ga) on the surface to be analysed, producing secondary ions in a sputtering process. These particles are accelerated into a time-of-flight tube and their mass is determined by measuring

---

[*] Analysis made at Plataforma de Nanotecnologia Institut de Bioenginyeria de Catalunya (IBEC) by Raúl Pérez, Principal TOF-SIMS technician

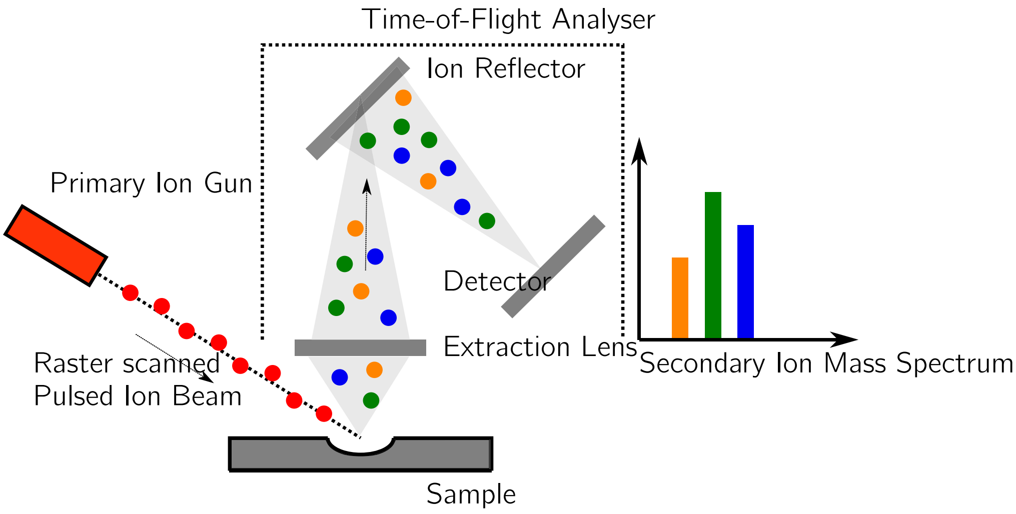

Figure B.3 *Time of Flight Secondary Ion Mass Spectroscopy (ToF-SIMS).*

the time at which reach the detector (Figure B.3). Analysing the secondary ions gives information about the molecular and elemental species present on the surface, despite the technique does not produce quantitative analysis, qualitative analysis can be acquired over the surface.

B.5 Electrical Characterization

The current, I, versus voltage, V, characteristics were measured in a Süss probe station under ambient conditions using a Keithley 2612AB. To measure the output characteristics of the field-effect transistors, a voltage was applied to the gate while the value of the drain-source voltage was swept in forward and reverse directions, during this the drain current was measured. The loop is performed several times according with the number of gate voltages to be measured.To measure the transfer characteristics, a constant voltage is applied to the drain and the drain current was measured at each point of a defined gate voltage swept in forward and reverse fashion. For both output and transfer measurement were performed using three probes. The transistors characterized in Section 4.4 were measured using

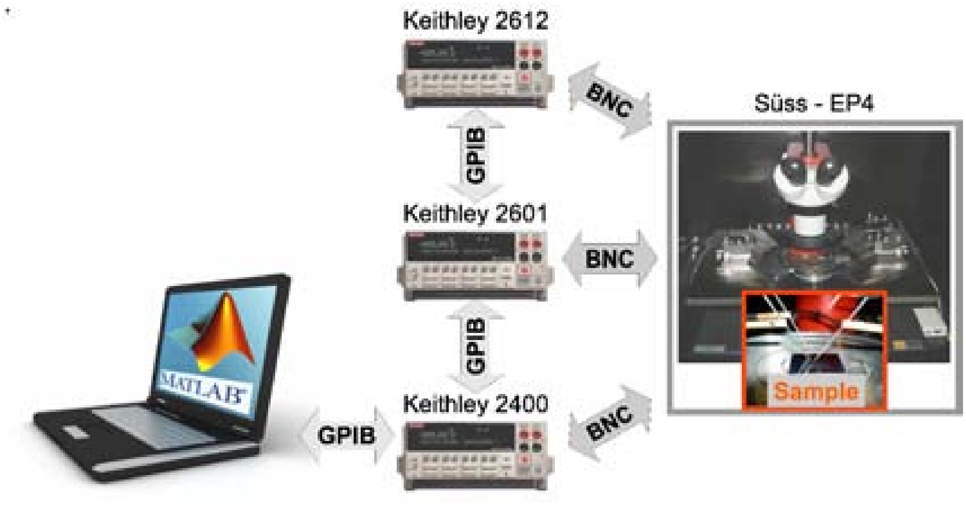

Figure B.4 *Electrical characterization measuring setup.*

two Keithleys a 2400 series and 2600 series.

The electrical characteristics of the transistors for temperature dependence measurements were measured using a Keithley 4200-SCS semiconductor parameter analyser , and a cryogenic chamber with temperature controller and Nitrogen atmosphere in vacuum, at Linköping University at the laboratory of organic electronics. The inverters were characterized using a Keithley 2612AB to record the Voltages and a Keithley 2400 to write the supply voltages, using a home-made software written in MATLAB.[†]

Bibliography

[1] B. Kirby. *Micro- and Nanoscale Fluid Mechanics: Transport in Microfluidic Devices*. Cambridge University Press, **2010**.

[2] S. Zhang, L. Li and A. Kumar. *Materials characterization techniques*. CRC Press, **2009**.

[3] J. Comelles. *Biochemical Gradients on Poly(methyl-methacrylate) Surfaces*. Ph.D. thesis, Universitat de Barcelona, **2010**.

[†] Software writen by Dr. Raphael Pfattner.

[4] Y. Yun. *Pentacene Based Organic Electronic Devices*. Ph.D. thesis, Durham University, **2010**.

Appendix C

Modification of Surface Properties using Self-Assembly

Self-assembly is a spontaneous formation of highly ordered and potentially convoluted structures via thermodinamically-controlled ordering of individual components such as molecules[1–3]. Self-assembly offers a "bottom-up" approach in contrast to the typical "top-down" approach of lithography[4]. Molecular self-assembly is responsible for the formation of biological structures, which are extremely complex and far from being replicated in a laboratory[2,4]. A simpler non-biological example of self-assembly is the spontaneous formation of an ordered monolayer of surfactant molecules on a solid surface[3]. Self-assembled monolayers (SAMs) have been well-studied and used in a variety of applications including lubrication, corrosion resistance, microfluidics, adhesion promotion[5].

SAMs on Gold are widely studied, other materials relevant to the fabrication of organic devices include oxides such as SiO_2. Like gold, the surfaces of such oxide materials can be modified with SAMs. Molecules that self-assemble on oxides include trichlorosilanes, trialkoxysilanes, phosphoric acids and carboxylic acids[3,6]. A hydroxylated surface (i.e. one with OH groups) is required for the self-assembly of organotrichlorosilanes[3]. The hydroxylation can be accomplished by immersing the substrates in a 3:1 mixture of sulphuric acid (H_2SO_4) and hydrogen peroxide

(H_2O_2, 30 % aqueous solution) for several minutes. After self-assembly of silanes, for example octadecyltrichlorosilane (OTS) which molecules make an angle of ≈ 10 degrees with respect to the substrate normal. The formation of high quality monolayers of OTS from solution is not as straightforward as the formation of high quality organothiolate SAMs on gold substrates, due to the nature of the reactions involved[3,5,7]. The amount of water present is precisely critical, as too little water results in incomplete SAM formation, while too much water leads to polymerisation in solution and further deposition of the polymer formed onto the substrate surface. Also other reaction conditions such as solvent temperature, and adsorption time are critical as well, making reproducibility a common issue[5].

Bibliography

[1] J. S. Moore. “Supramolecular Materials”. *MRS Bulletin*, **2011**, 25, 26.

[2] G. M. Whitesides, J. P. Mathias and C. T. Seto. “Molecular self-assembly and nanochemistry: a chemical strategy for the synthesis of nanostructures”. *Science*, **1991**, 254, 1312.

[3] A. Ulman. “Formation and Structure of Self-Assembled Monolayers”. *Chemical Reviews*, **1996**, 96, 1533.

[4] P. Kazmaier and N. Chopra. “Bridging Size Scales with Self-Assembling Supramolecular Materials”. *MRS Bulletin*, **2000**, 25, 30.

[5] D. J. L. Mascaro. *Formation of In-Plane Crystals of Molecular Organic Semiconductors*. Ph.D. thesis, Massachusetts Institute of Technology, **2004**.

[6] Y. Xia and G. M. Whitesides. “Soft Lithography”. *Angewandte Chemie International Edition*, **1998**, 37, 550.

[7] N. L. Jeon, K. Finnie, K. Branshaw and R. G. Nuzzo. “Structure and Stability of Patterned Self-Assembled Films of Octadecyltrichlorosilane Formed by Contact Printing”. *Langmuir*, **1997**, 13, 3382.

Appendix D

Thermal Evaporated thin film preparation

Solid materials will change its solid state to vapor state when heated at sufficiently high temperatures (Fig. D.1). When molecules leave its source travels a fixed distance in a vacuum chamber to impinge on the substrate, as a thin film deposit. This method has been used typically for the deposition of inorganic materials, such as metals and alloys. However, this technique has been extrapolated for the formation of layers of organic compounds. The rate of evaporation Γ ($kg\, m^{-2}s^{-1}$) from a surface is given by the Langmuir equation (Ec.D.1):

$$\Gamma = P\left(\frac{M}{2\pi RT}\right)^{\frac{1}{2}} \tag{D.1}$$

where P is the vapour pressure (Nm^{-2}) of the material, T is temperature (K), M is the molecular weight and R is the gas constant.

Even at high vacuum there are some remaining ambient gas atoms, which eventually collide with vapour atoms resulting in the last to be scattered. For a path that follows a straight line use of low pressures is necessary ($< 10^{-4}$ mbar), where the mean free path of the gas atoms λ is much greater than the source to substrate distance.

$$\lambda = \frac{k_B T}{P\pi d^2 \sqrt{2}} \tag{D.2}$$

where d is the diameter of the molecules and k_B is Boltzmann's constant. Important parameters of thin film growth are the evaporation rate, substrate temperature, and the chemical and physical natures of the substrate surface. Figure D.1 depicts a typical setup for a Physical Vapour Deposition Unit[1–4].

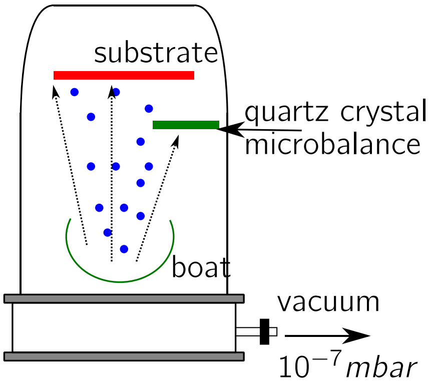

Figure D.1 *Thermal evaporation system for thin film deposition.*


(a)
(b)

Figure D.2 *Glove box and typical sample*

Bibliography

[1] H. Hoppe and N. S. Sariciftci. "Organic solar cells: An overview". *Journal of Materials Research*, **2004**, 19, 1924.

[2] I. Kymissis. *Organic Field Effect Transistors: Theory, Fabrication and Characterization*. Integrated Circuits and Systems. Springer, **2008**.

[3] F. C. Krebs. "Fabrication and processing of polymer solar cells: A review of printing and coating techniques". *Solar Energy Materials and Solar Cells*, **2009**, 93, 394.

[4] Y. Yun. *Pentacene Based Organic Electronic Devices*. Ph.D. thesis, Durham University, **2010**.

Appendix E

Mobility numerical extraction

The most commonly mathematical models encountered in engineering are in the form of differential equations[1,2] (see equations 1.7 and 1.8). Several types of ordinary differential equations, and a few partial differential equations, render themselves to analytical or the so-called closed-form solution. Taylor series provides a means to predict a function value at one point in terms of the function value and its derivatives at another point. In particular, the theorem states that any smooth function can be approximated as a polynomial[3,4].

Equation E.1 is a centered finite difference equation with error $O(h^2)$ while equation E.2 is a centered finite difference with error $O(h^4)$ lower error than the previous equation due to the use of more terms in the Taylor series[3,5,6].

$$\begin{aligned} f\left(x\right) &= \frac{f\left(x_{i+1}\right)-f\left(x_{i-1}\right)}{2h} && \text{(E.1)} \\ f\left(x\right) &= \frac{-f\left(x_{i+2}\right)+8f\left(x_{i+1}\right)-8f\left(x_{i-1}\right)+f\left(x_{i-2}\right)}{12h} && \text{(E.2)} \end{aligned}$$

Three different possibilities for the calculation of derivatives are basic and useful. One can choose a forward difference or a backward difference or a centered difference. In this study centered differences are chosen for all intermediate points, because centered or central finite differences are more accurate than one-sided finite differences[6,7]. Equations E.4 and E.6 are the result after plug-in the respective variables for mobility calculation.

Central finite difference approximations are not always usable. For example, consider the situation where the function is given at the n discrete points x_0 x_1 x_n.Because central differences use values of the function on each side of x, one would be unable to compute the derivatives at x_0 and x_n. Clearly, there is a need for finite difference expressions that require evaluations of the function on only one side of x. These expressions are called forward and backward finite difference approximations[8–10], and are handy to calculate derivatives at boundaries and equations E.3 and E.5 are used to calculate at x_0 and x_n respectively.

$$\left(\frac{d\sqrt{I_{SD}^{sat}}}{dV_{SG}}\right)_{n=1} = \frac{-3\left(\sqrt{I_{SD}^{sat}}\right)_n + 4\left(\sqrt{I_{SD}^{sat}}\right)_{n+1} - \left(\sqrt{I_{SD}^{sat}}\right)_{n+2}}{2\Delta V_{SG}} \tag{E.3}$$

$$\left(\frac{d\sqrt{I_{SD}^{sat}}}{dV_{SG}}\right)_{n=2 \quad (o-1)} = \frac{\sqrt{I_{SD}^{sat}}_{n+1} - \sqrt{I_{SD}^{sat}}_{n-1}}{2\Delta V_{SG}} \tag{E.4}$$

$$\left(\frac{d\sqrt{I_{SD}^{sat}}}{dV_{SG}}\right)_{n=o-1} = \frac{\sqrt{I_{SD}^{sat}}_{o-2} - 4\sqrt{I_{SD}^{sat}}_{o-1} + 3\sqrt{I_{SD}^{sat}}_{o}}{2\Delta V_{SG}} \tag{E.5}$$

$$\left(\frac{d\sqrt{I_{SD}^{sat}}}{dV_{SG}}\right)_{n=2 \quad (o-1)} = \frac{-\sqrt{I_{SD}^{sat}}_{n+2} + 8\sqrt{I_{SD}^{sat}}_{n+1} - 8\sqrt{I_{SD}^{sat}}_{n-1} + \sqrt{I_{SD}^{sat}}_{n-2}}{2\Delta V_{SG}} \tag{E.6}$$

Equation E.3 for the first point (n = 1), equation E.4 and E.6 for internal points, (n = 2,. . . , o-1, o = last data point. Eq. E.6 more accurate centered finite-difference equation) and equation E.5 for the last point.

Bibliography

[1] A. Constantinides and N. Mostoufi. *Numerical Methods for Chemical Engineers with MATLAB Applications*. Prentice Hall, **1999**.

[2] M. Jain, S. Iyengar and R. Jain. *Numerical Methods - Problems and Solutions*. New Age International (P) Ltd., second edition, **2007**.

[3] S. C. Chapra. *Applied Numerical Methods with MATLAB for Engineers and Scientists*. McGraw, thrid edition, **2012**.

[4] S. C. Chapra and R. P. Canale. *Numerical Methods for Engineers*. McGraw Hill, sixth edition, **2010**.

[5] J. Mathews and K. Fink. *Numerical methods using MATLAB.* Pearson Education. Prentice Hall, **1999**.

[6] W. H. Press, S. A. Teukolsky, W. T. Vetterling and B. P. Flannery. *Numerical Recipes: The Art of Scientific Computing*. Cambridge, third edition, **2007**.

[7] G. Strang. *Computational Science and Engineering*. Wellesley-Cambridge, **2007**.

[8] J. Kiusalaas. *Numerical Methods in Engineering with Python*. Cambridge University Press, **2010**.

[9] J. Kiusalaas. *Numerical Methods in Engineering with MATLAB*. Cambridge, second edition, **2010**.

[10] W. Y. Yang, W. Cao, T.-S. Chung and J. Morris. *Applied Numerical Methods using MATLAB*. Wiley Interscience, **2005**.

Appendix F

Optical microscope pictures and electrical characterization for DB-TTF:PS10000 blends

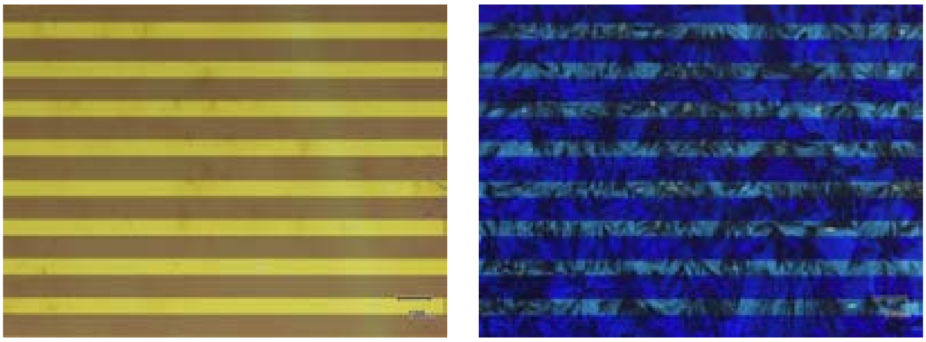
(a) (b)

Figure F.1 *Polarized microscope images for bottom contact device, DB-TTF and PS10000 ratio: 1:1, (a), $\Phi_{P\ A} = 0^o$ between Polarizer and Analyzer and (b), $\Phi_{P\ A} = 90^o$ between Polarizer and Analyzer.*

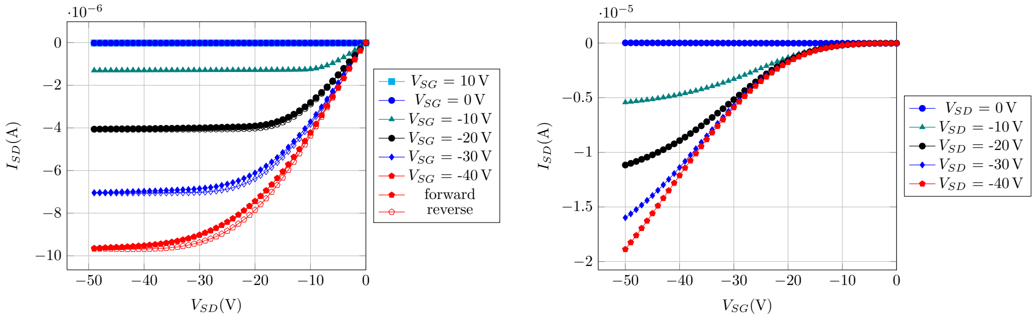

(a) (b)

Figure F.2 *(a) Output Characteristics, and (b) Transfer Characteristics for DB-TTF PS10000 blend ratio 1:1 in Bottom Contact Architecture, device L = 100µm W = 100000µm.*

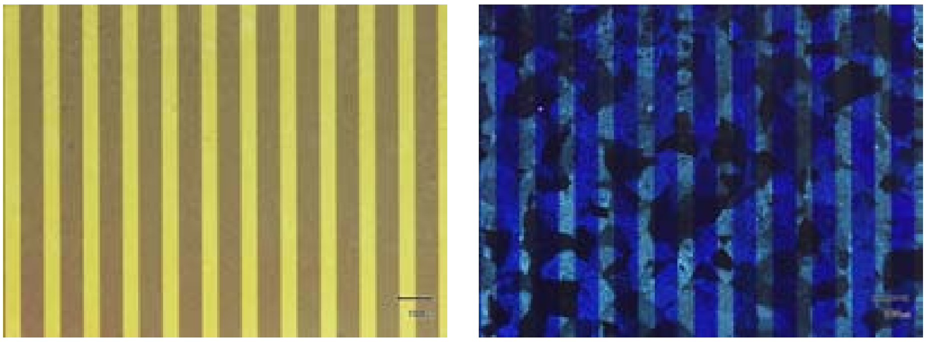

(a) (b)

Figure F.3 *Polarized microscope images for bottom contact device, DB-TTF and PS10000 ratio: 1:2, (a), $\Phi_{P\ A} = 0^o$ between Polarizer and Analyzer and (b), $\Phi_{P\ A} = 90^o$ between Polarizer and Analyzer.*

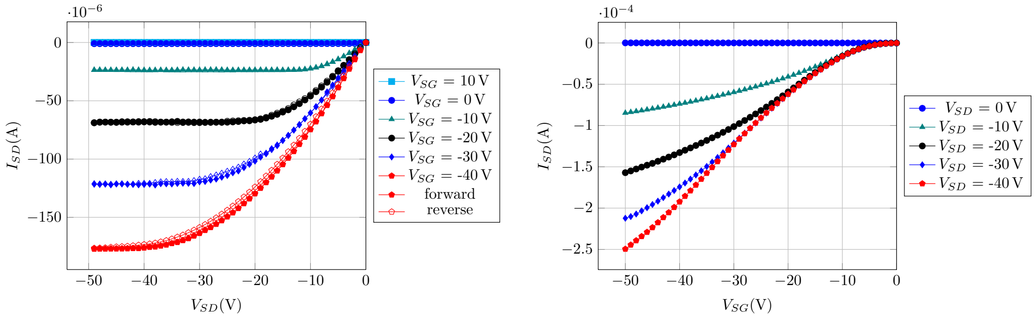

(a) (b)

Figure F.4 *(a) Output Characteristics, and (b) Transfer Characteristics for DB-TTF PS10000 blend ratio 1:2 in Bottom Contact Architecture, device L = 50µm W = 50000µm.*

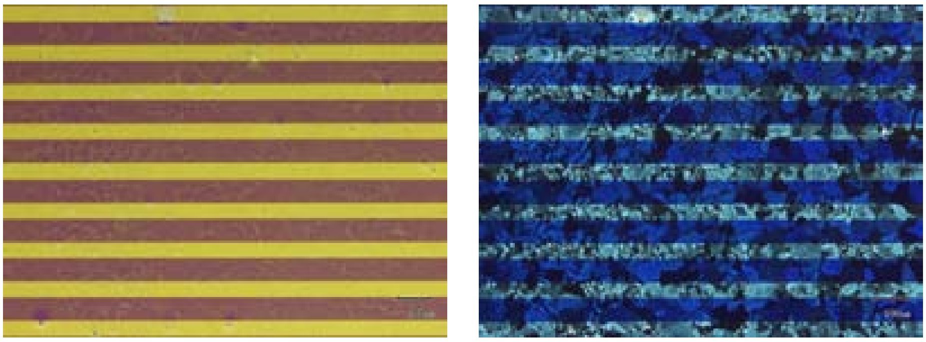

(a) (b)

Figure F.5 *Polarized microscope images for bottom contact device, DB-TTF and PS10000 ratio: 1:3, (a),* $\Phi_{P\ A} = 0^o$ *between Polarizer and Analyzer and (b),* $\Phi_{P\ A} = 90^o$ *between Polarizer and Analyzer.*

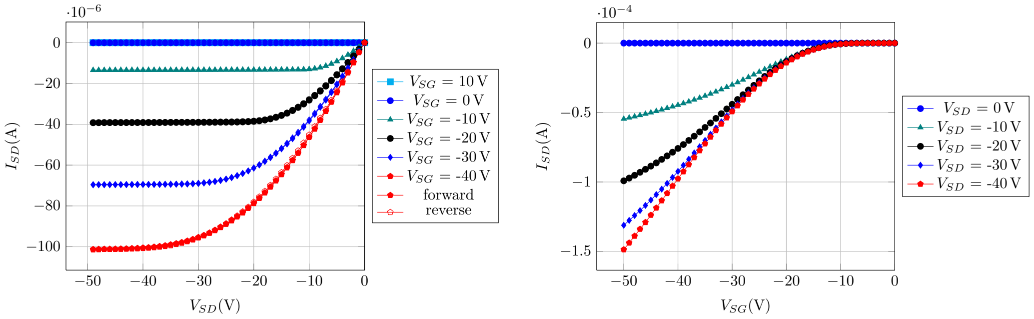

(a) (b)

Figure F.6 *(a) Output Characteristics, and (b) Transfer Characteristics for DB-TTF PS10000 blend ratio 1:3 in Bottom Contact Architecture, device L = 75µm W = 75000µm.*

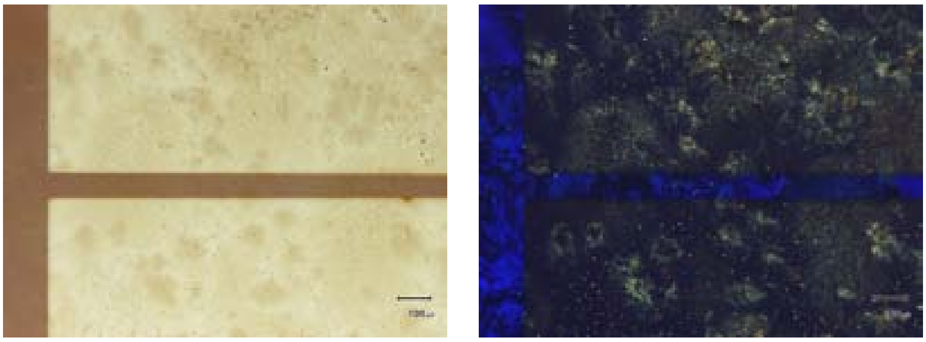

(a)

(b)

Figure F.7 *Polarized microscope images for top contact device, DB-TTF and PS10000 ratio: 1:1, (a), $\Phi_{P\ A} = 0^o$ between Polarizer and Analyzer and (b), $\Phi_{P\ A} = 90^o$ between Polarizer and Analyzer*

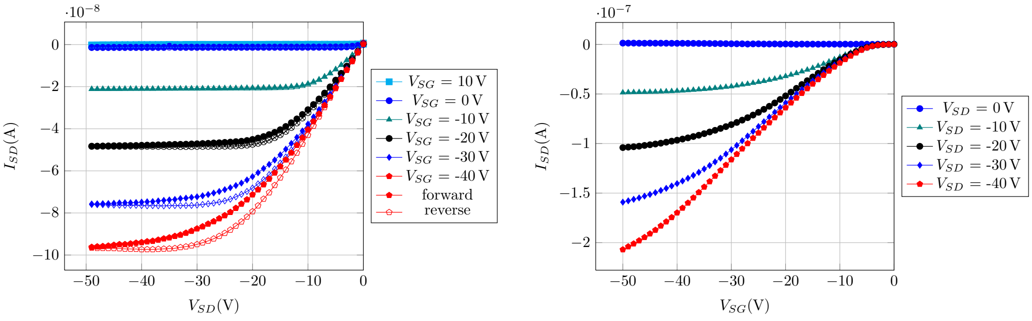

(a)

(b)

Figure F.8 *(a) Output Characteristics, and (b) Transfer Characteristics for DB-TTF PS10000 blend ratio 1:1 in Top Contact Architecture, device L = 38.72µm W = 4000µm.*

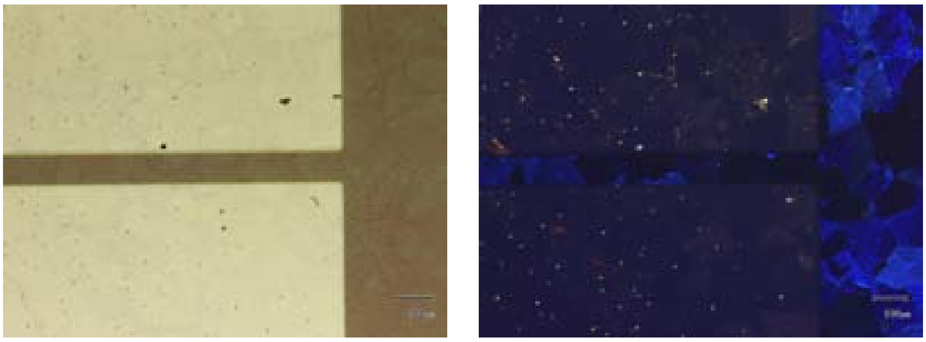

(a)　　　　(b)

Figure F.9 *Polarized microscope images for top contact device, DB-TTF and PS10000 ratio: 1:2, (a), $\Phi_{P\ A} = 0^o$ between Polarizer and Analyzer and (b), $\Phi_{P\ A} = 90^o$ between Polarizer and Analyzer*

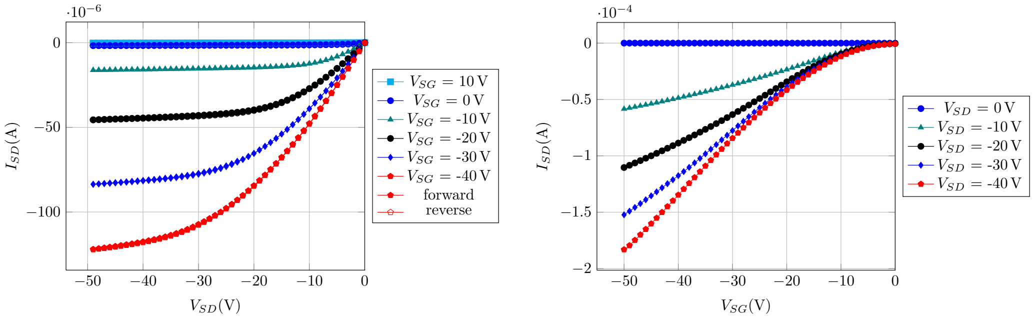

(a)　　　　(b)

Figure F.10 *(a) Output Characteristics, and (b) Transfer Characteristics for DB-TTF PS10000 blend ratio 1:2 in Top Contact Architecture, device L = 42.68μm W = 4000μm.*

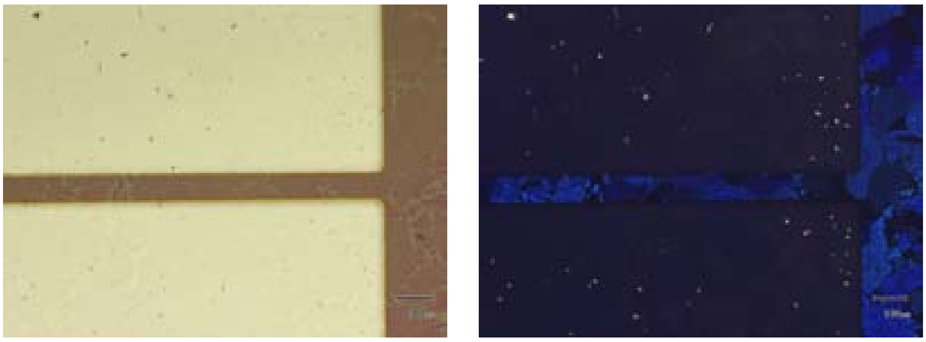

(a) (b)

Figure F.11 *Polarized microscope images for top contact device, DB-TTF and PS10000 ratio: 1:3, (a),* $\Phi_{P\ A} = 0^o$ *between Polarizer and Analyzer and (b),* $\Phi_{P\ A} = 90^o$ *between Polarizer and Analyzer*

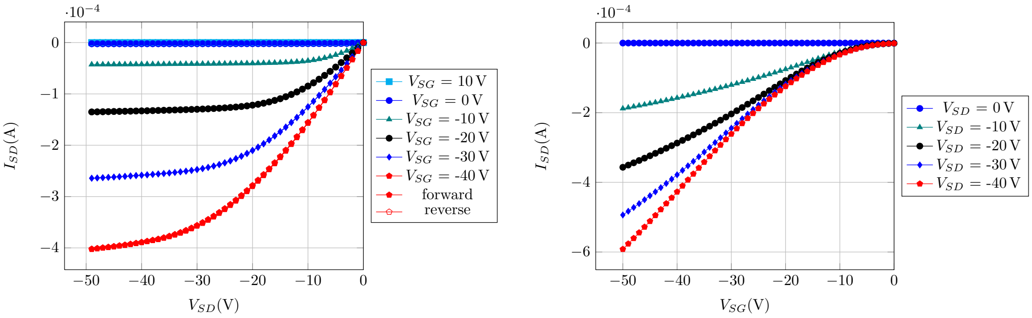

(a) (b)

Figure F.12 *(a) Output Characteristics, and (b) Transfer Characteristics for DB-TTF PS10000 blend ratio 1:3 in Top Contact Architecture, device L = 19.54µm W = 4000µm.*

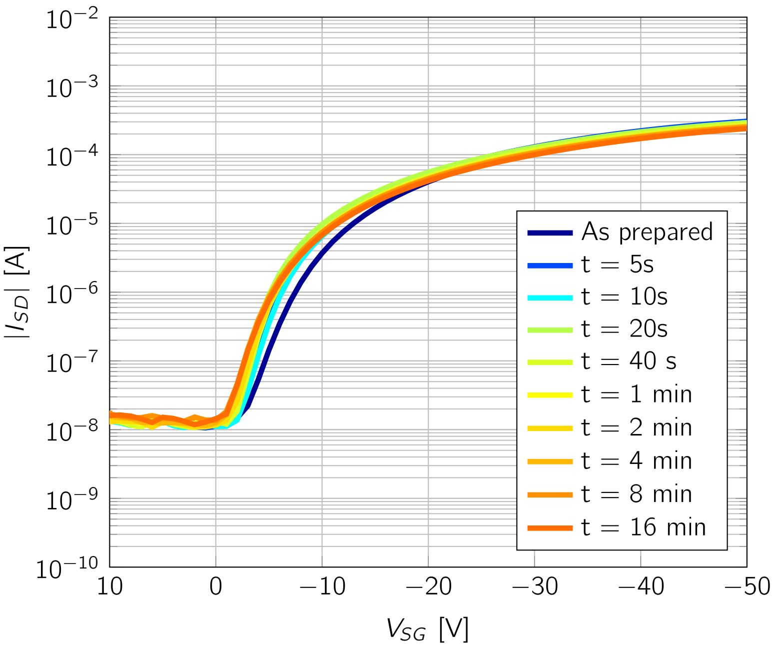

Figure F.13 *Log transfer for water immersion experiments for an OFET based on DB-TTF and PS10000 in a blend ratio 1:3, respectively.*

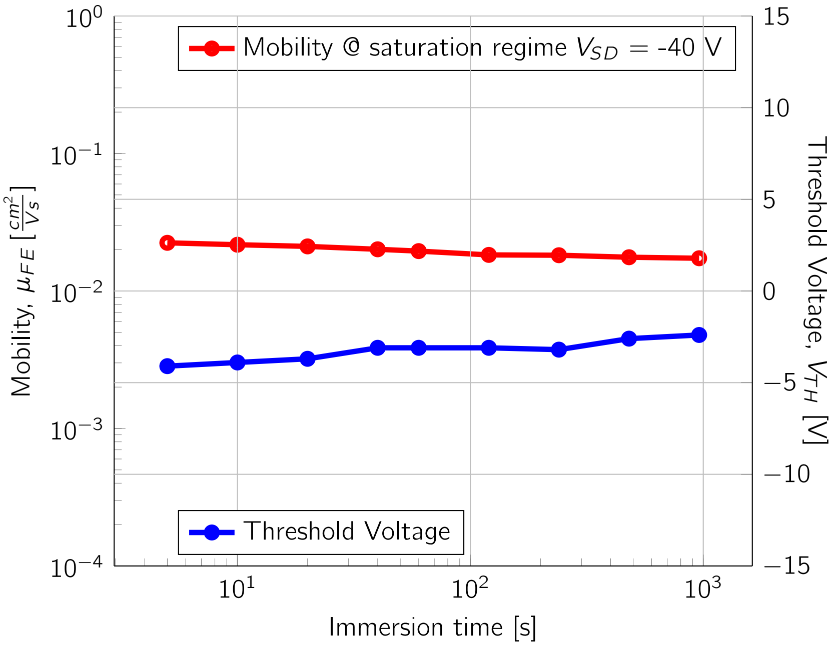

Figure F.14 *Mobility and threshold voltage for water immersion experiments for an OFET based on DB-TTF and PS10000 in a blend ratio 1:3, respectively.*

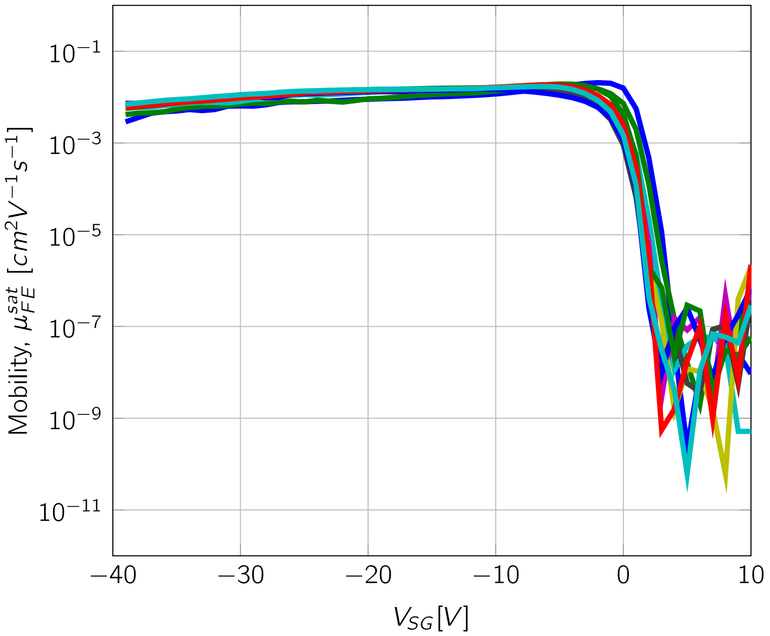

Figure F.15 *Mobility profile as a function of temperature 150 K < T < 300 K (step = 15 K) for an OFET based on DB-TTF and PS10000 in a blend ratio 1:3.*

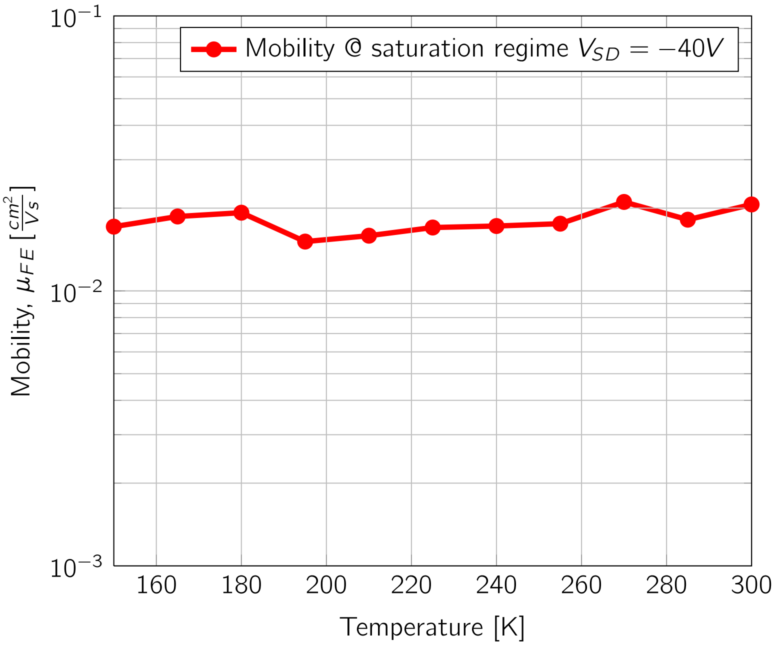

Figure F.16 *Mobility as a function of temperature. 150 K < T < 300 K (step = 15 K). L = 50 µm W = 50 mm.*

Appendix G

Optical microscope pictures and electrical characterization for DB-TTF:PS3000 blends

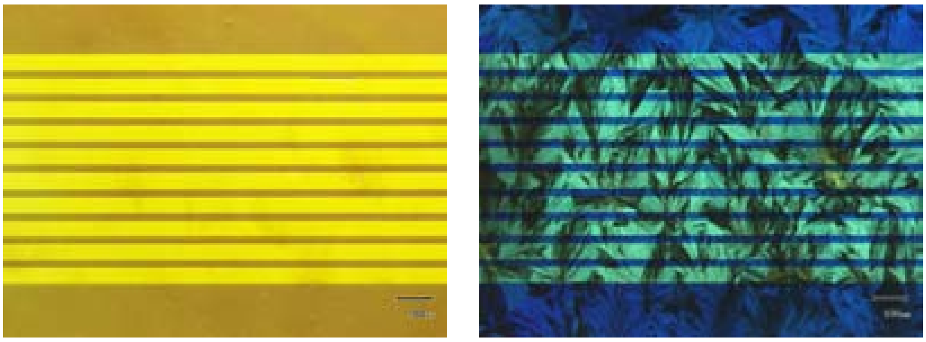

(a)

(b)

Figure G.1 *Polarized microscope images for bottom contact device,* $L = 25\mu m$ $W = 25000$ μm, *DBTTF and PS3000 ratio: 1:1 (a)* $\Phi_{P\ A} = 0^o$ *between Polarizer and Analyzer and (b)* $\Phi_{P\ A} = 90^o$ *between Polarizer and Analyzer.*

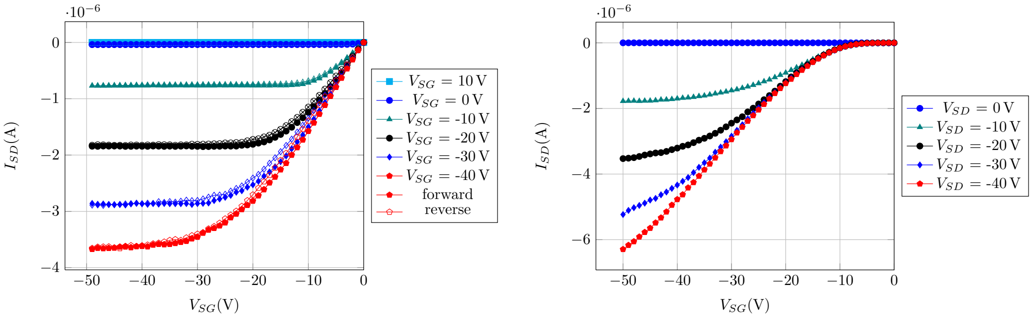

(a)   (b)

Figure G.2 *(a) Output Characteristics, and (b) Transfer Characteristics for DB-TTF PS3000 blend ratio 1:1 in Bottom Contact Architecture, device L = 50µm W = 50000µm.*

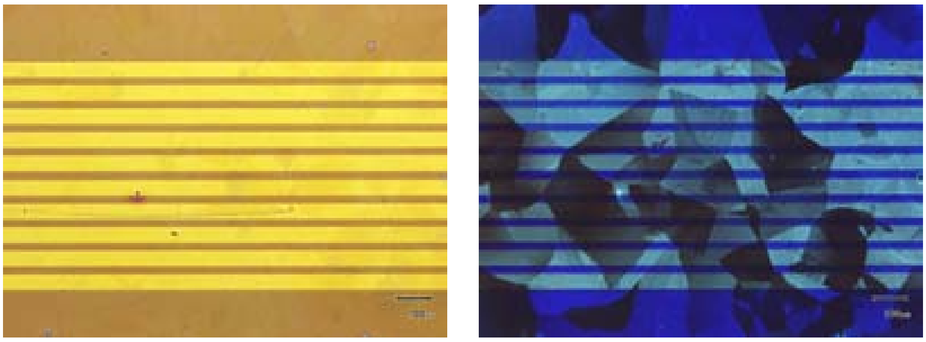

(a)   (b)

Figure G.3 *Polarized microscope images for bottom contact, device L = 25µm W = 25000 µm, DB-TTF and PS3000 ratio: 2:3, (a),* $\Phi_{P\ A} = 0^o$ *between Polarizer and Analyzer and (b),* $\Phi_{P\ A} = 90^o$ *between Polarizer and Analyzer.*

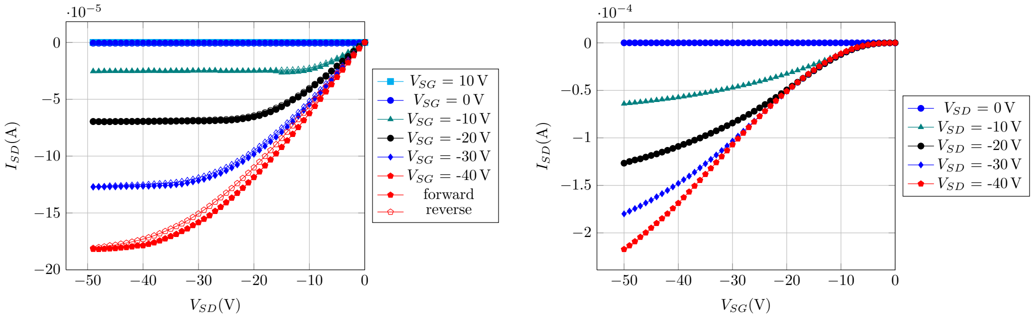

(a) (b)

Figure G.4 *(a) Output Characteristics, and (b) Transfer Characteristics for DB-TTF PS3000 blend ratio 2:3 in Bottom Contact Architecture, device L = 75µm W = 75000µm.*

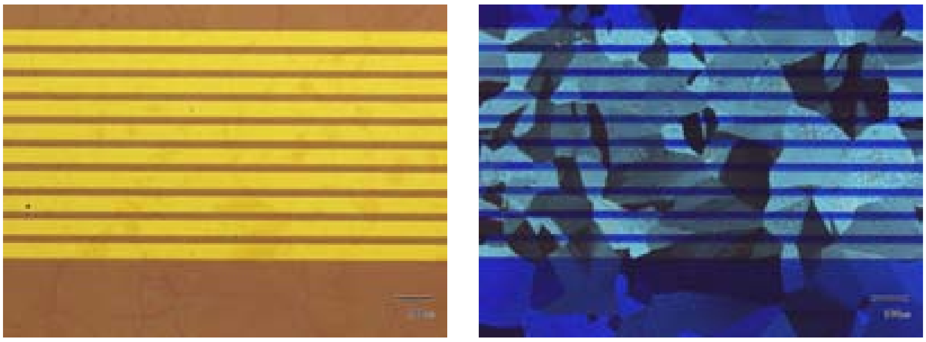

(a) (b)

Figure G.5 *Polarized microscope images for bottom contact device, L = 25µm W = 25000 µm, DB-TTF and PS3000 ratio: 1:2, (a),* $\Phi_{P\ A} = 0^o$ *between Polarizer and Analyzer and (b),* $\Phi_{P\ A} = 90^o$ *between Polarizer and Analyzer.*

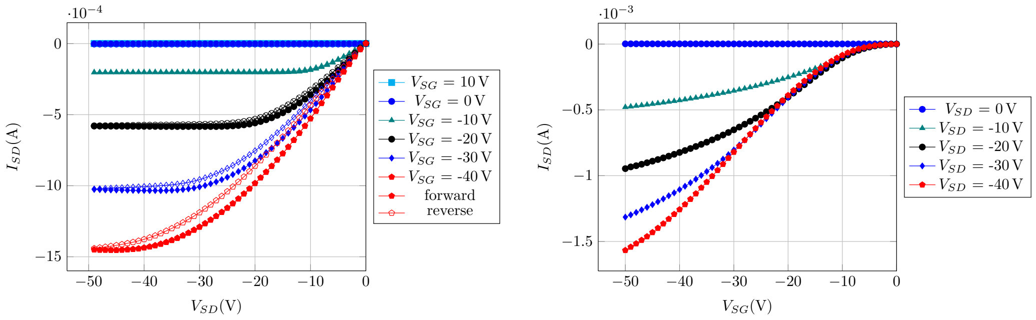

(a) (b)

Figure G.6 *(a) Output Characteristics, and (b) Transfer Characteristics for DB-TTF PS3000 blend ratio 1:2 in Bottom Contact Architecture, device $L = 75\mu m$ $W = 75000\mu m$.*

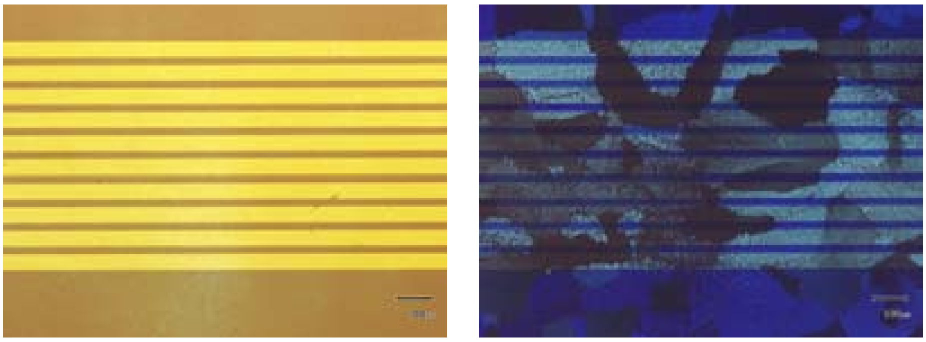

(a) (b)

Figure G.7 *Polarized microscope images for bottom contact device, $L = 25\mu m$ $W = 25000\ \mu m$, DB-TTF and PS3000 ratio: 1:3, (a), $\Phi_{P\ A} = 0^o$ between Polarizer and Analyzer and (b), $\Phi_{P\ A} = 90^o$ between Polarizer and Analyzer.*

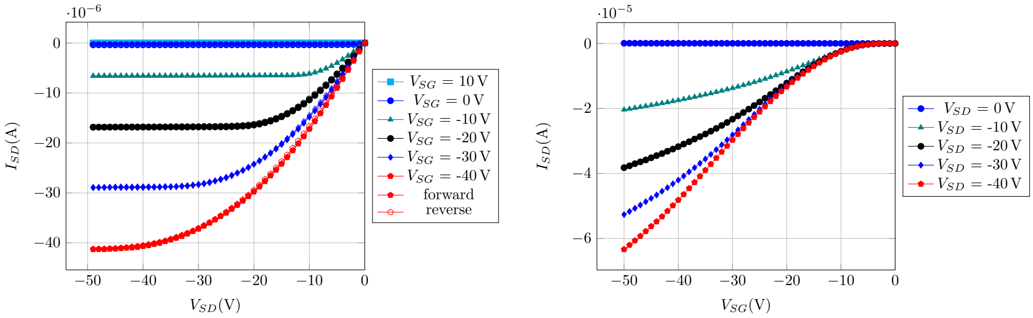

(a) (b)

Figure G.8 *(a) Output Characteristics, and (b) Transfer Characteristics for DB-TTF PS3000 blend ratio 1:3 in Bottom Contact Architecture, device L = 100µm W = 100000µm.*

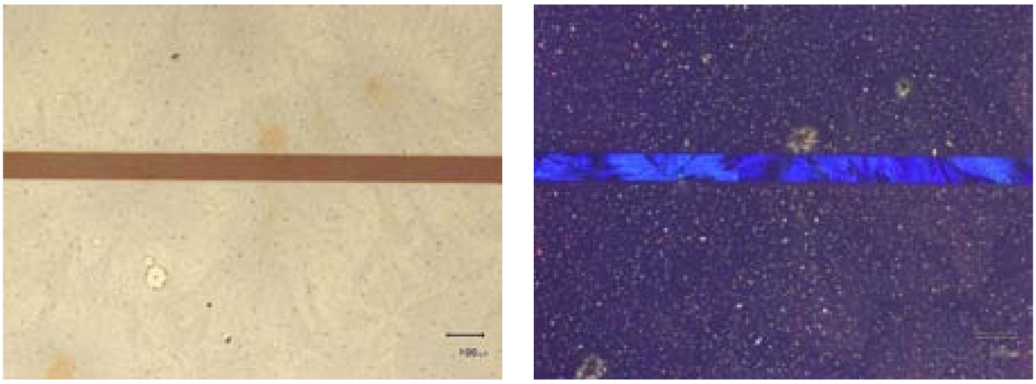

(a) (b)

Figure G.9 *Polarized microscope images for top contact device, DBTTF and PS3000 ratio: 1:1, (a), $\Phi_{P\ A} = 0^o$ between Polarizer and Analyzer and (b), $\Phi_{P\ A} = 90^o$ between Polarizer and Analyzer.*

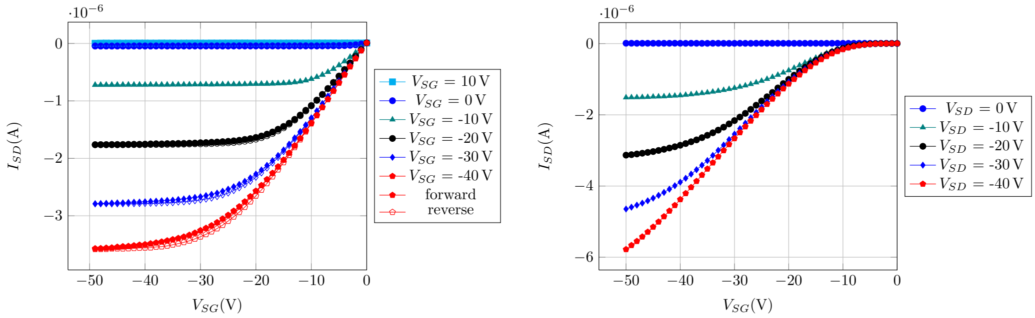

(a)

(b)

Figure G.10 *(a) Output Characteristics, and (b) Transfer Characteristics for DBTTF PS3000 blend ratio 1:1 in Top Contact Architecture, device L = 54.38µm W = 4000µm.*

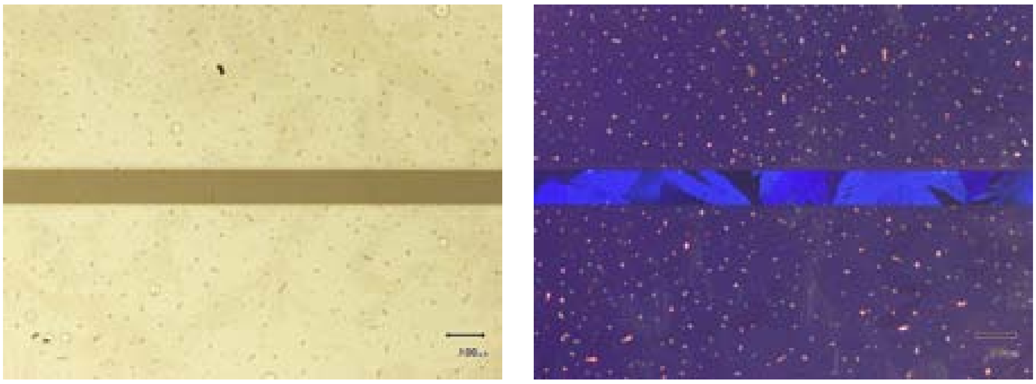

(a)

(b)

Figure G.11 *Polarized microscope images for top contact device, DBTTF and PS3000 ratio: 2:3, (a),* $\Phi_{P\ A} = 0^o$ *between Polarizer and Analyzer and (b),* $\Phi_{P\ A} = 90^o$ *between Polarizer and Analyzer.*

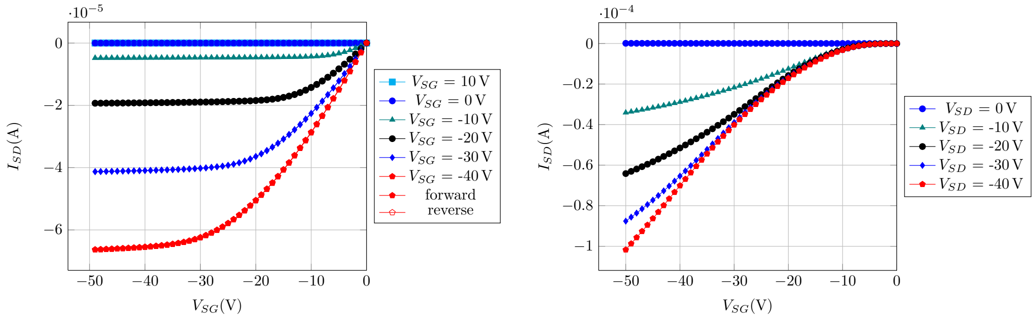

(a)

(b)

Figure G.12 *(a) Output Characteristics, and (b) Transfer Characteristics for DBTTF PS3000 blend ratio 2:3 in Top Contact Architecture, device* $L = 74.80\mu m$ $W = 4000\mu m$.

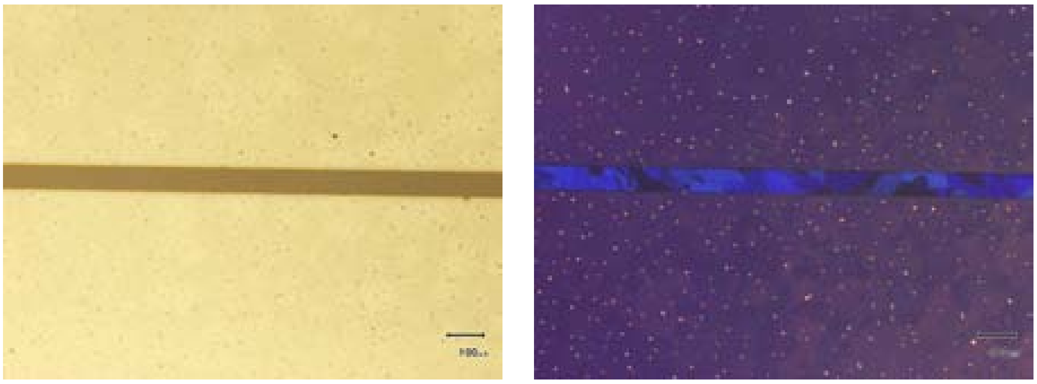

(a)

(b)

Figure G.13 *Polarized microscope images for top contact device, DBTTF and PS3000 ratio: 1:2, (a),* $\Phi_{P\ A} = 0^o$ *between Polarizer and Analyzer and (b),* $\Phi_{P\ A} = 90^o$ *between Polarizer and Analyzer.*

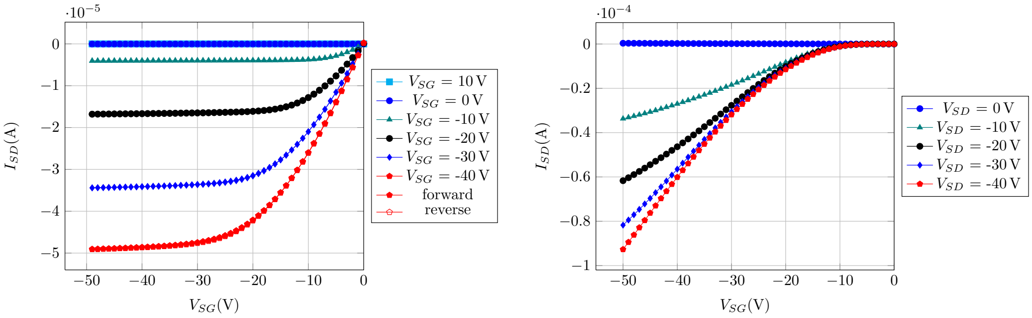

(a) (b)

Figure G.14 *(a) Output Characteristics, and (b) Transfer Characteristics for DBTTF PS3000 blend ratio 1:2 in Top Contact Architecture, device L = 84.04μm W = 4000μm.*

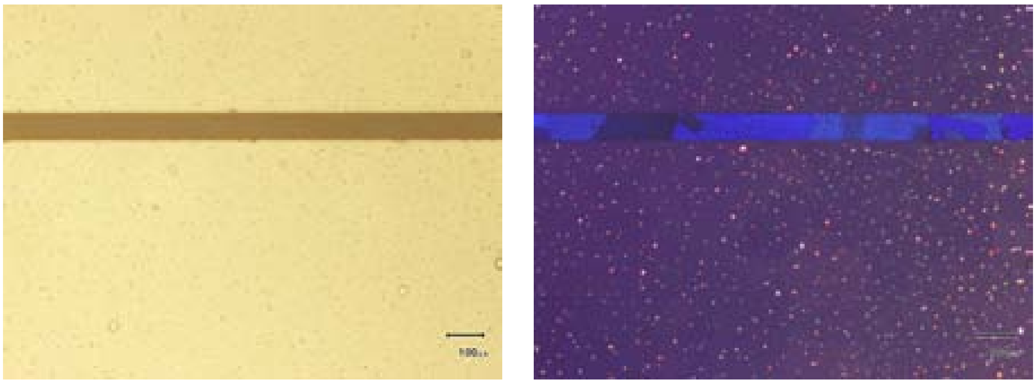

(a) (b)

Figure G.15 *Polarized microscope images for top contact device, DBTTF and PS3000 ratio: 1:3, (a), $\Phi_{P\ A} = 0^o$ between Polarizer and Analyzer and (b), $\Phi_{P\ A} = 90^o$ between Polarizer and Analyzer.*

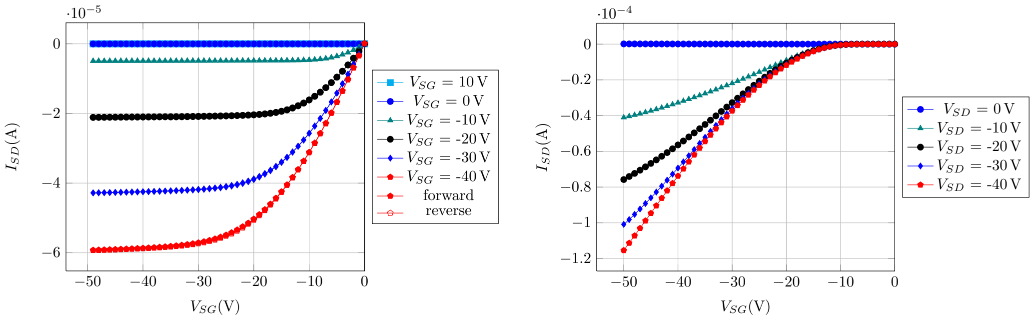

(a) (b)

Figure G.16 *(a) Output Characteristics, and (b) Transfer Characteristics for DBTTF PS3000 blend ratio 1:3 in Top Contact Architecture, device L = 51.48µm W = 4000µm.*

Appendix H

Supplementary information for Chapter 6

Table H.1 *Pairwise comparisons for threshold voltage [V] for DB-TTF:PS3000 blend 1:2 ratio.*

	100 μm	90 μm	80 μm	70 μm	60 μm	50 μm	40 μm	30 μm	20 μm
90 μm	1	-	-	-	-	-	-	-	-
80 μm	1	1	-	-	-	-	-	-	-
70 μm	1	1	1	-	-	-	-	-	-
60 μm	1	1	1	1	-	-	-	-	-
50 μm	1	1	1	1	1	-	-	-	-
40 μm	1	1	1	1	1	1	-	-	-
30 μm	1	1	1	1	1	1	1	-	-
20 μm	1	1	1	1	1	1	1	1	-
10 μm	1	1	1	1	1	1	1	1	0.34

Table H.2 *Pairwise comparisons for mobility $[cm^2V^{-1}s^{-1}]$ for DB-TTF:PS3000 blend 1:2 ratio.*

	100 μm	90 μm	80 μm	70 μm	60 μm	50 μm	40 μm	30 μm	20 μm
90 μm	1	-	-	-	-	-	-	-	-
80 μm	1	1	-	-	-	-	-	-	-
70 μm	1	1	1	-	-	-	-	-	-
60 μm	1	1	1	1	-	-	-	-	-
50 μm	1	1	1	1	1	-	-	-	-
40 μm	1	1	0.3	1	1	1	-	-	-
30 μm	1	1	1.8e-2	1	1	1	1	-	-
20 μm	0.3	0.1	3.63-4	8.4e-2	0.4	0.4	1	1	-
10 μm	1.7e-3	4.9e-4	5.1e-07	2.9e-4	1.8e-3	2.2e-3	2.3e-3	0.3	1

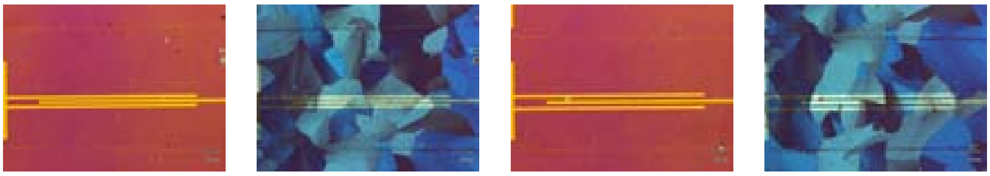

(a) L=10μm (b) L=10μm (c) L=20μm (d) L=20μm

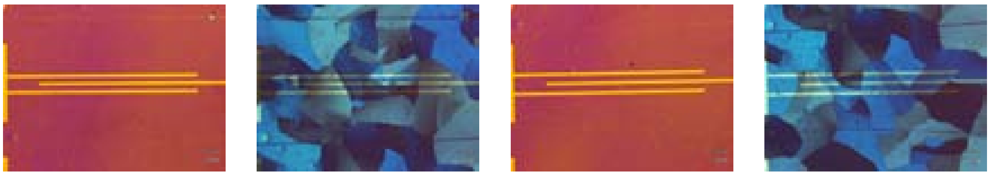

(e) L=30μm (f) L=30μm (g) L=40μm (h) L=40μm

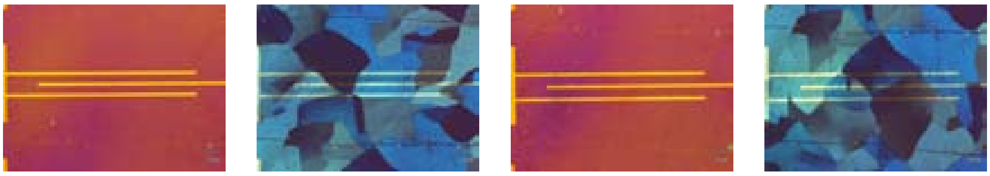

(i) L=50μm (j) L=50μm (k) L=60μm (l) L=60μm

(m) L=70μm (n) L=70μm (o) L=80μm (p) L=80μm

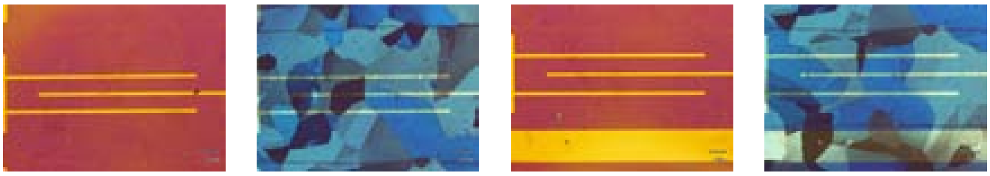

(q) L=90μm (r) L=90μm (s) L=100μm (t) L=100μm

Figure H.1 *Polarized microscope images for bottom contact devices with W = 2000 µm, DBTTF and PS3000 ratio: 1:2 (a), (c), (e), (g), (i), (k), (m), (o), (q), (s)* $\Phi_{P\ A} = 0^o$ *between Polarizer and Analyzer and (b), (d), (f), (h), (j), (l), (n), (p), (r), (t),* $\Phi_{P\ A} = 90^o$ *between Polarizer and Analyzer.*

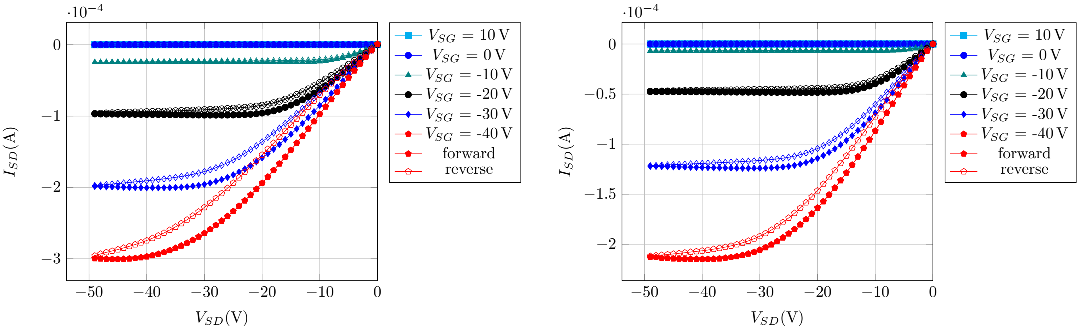

(a) L = 10 μm

(b) L = 20 μm

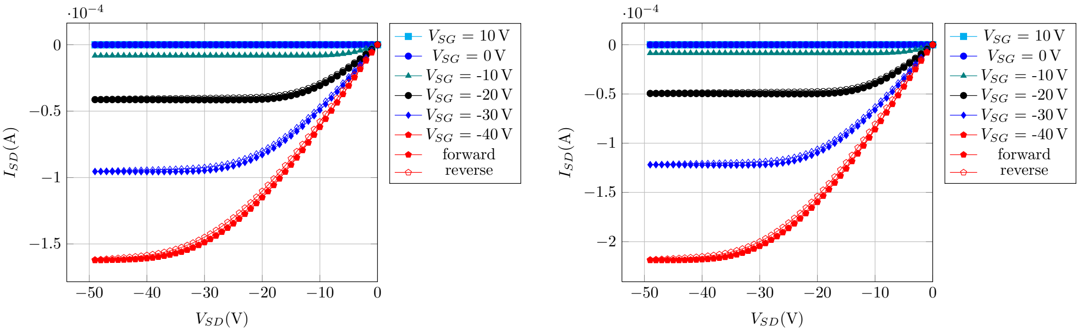

(c) L = 30 μm

(d) L = 40 μm

Figure H.2 *(a),(b),(c),(d),Typical Output Characteristics for DBTTF PS3000 blend ratio 1:2 in Bottom Contact Architecture,with a constant W = 2000μm.*

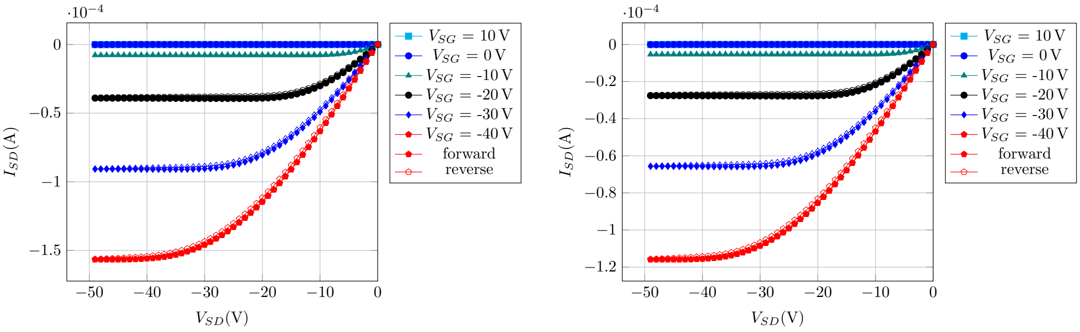

(a) L = 50 μm

(b) L = 60 μm

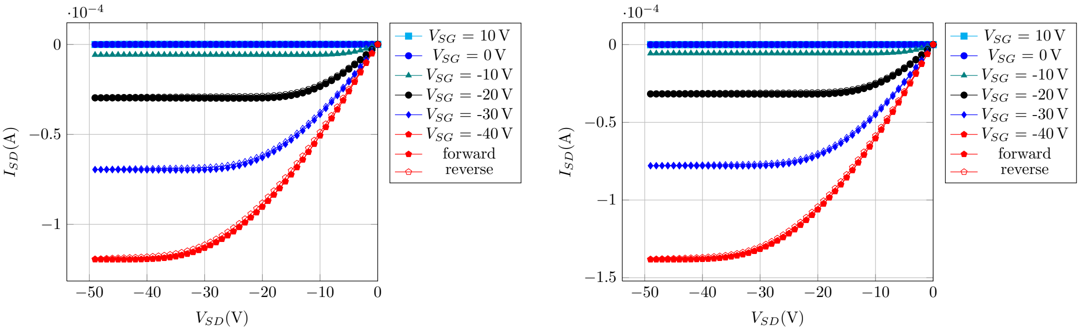

(c) L = 70 μm

(d) L = 80 μm

Figure H.3 *(a),(b),(c),(d),(a),(b), Typical Output Characteristics for DBTTF PS3000 blend ratio 1:2 in Bottom Contact Architecture,with a constant W = 2000μm.*

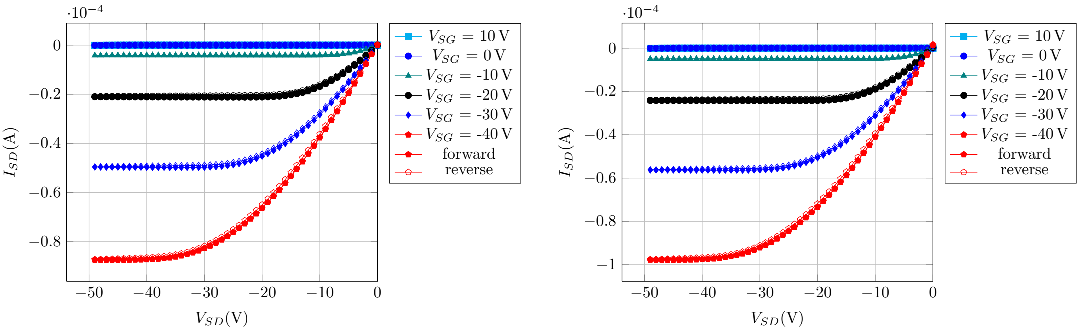

(a) L = 90 μm

(b) L = 100 μm

Figure H.4 *(a),(b), Typical Output Characteristics for DBTTF PS3000 blend ratio 1:2 in Bottom Contact Architecture,with a constant W = 2000μm and L varying from 10 μm to 100 μm each 10 μm.*

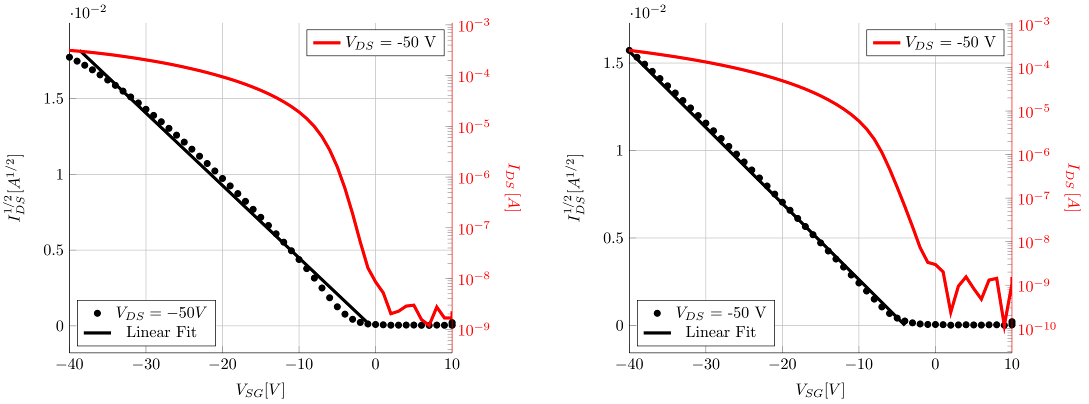

(a) L = 10 μm

(b) L = 20 μm

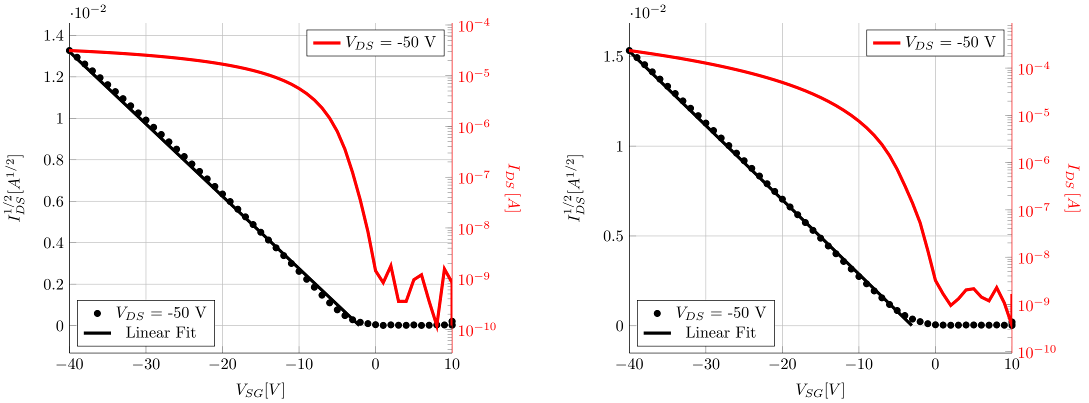

(c) L = 30 μm

(d) L = 40 μm

Figure H.5 *(a),(b),(c),(d), Transfer Characteristics for DBTTF PS3000 blend ratio 1:2 in Bottom Contact Architecture, with W = 2000µm constant.*

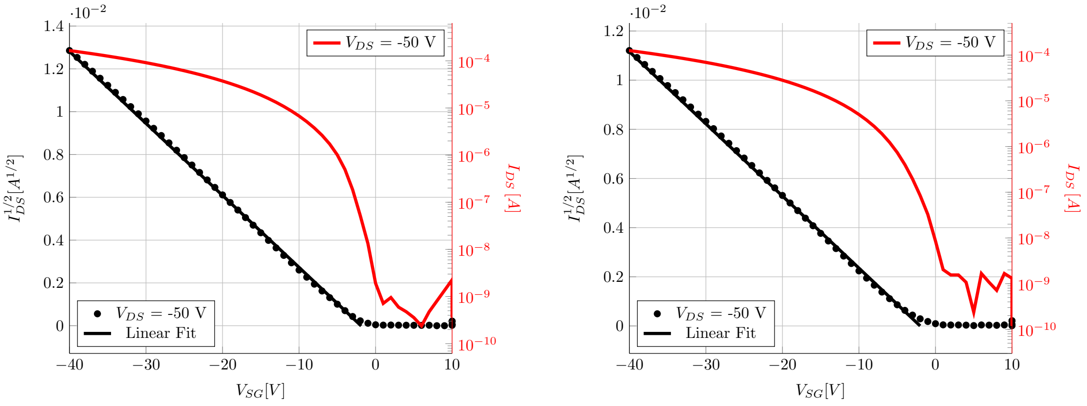

(a) L = 50 μm

(b) L = 60 μm

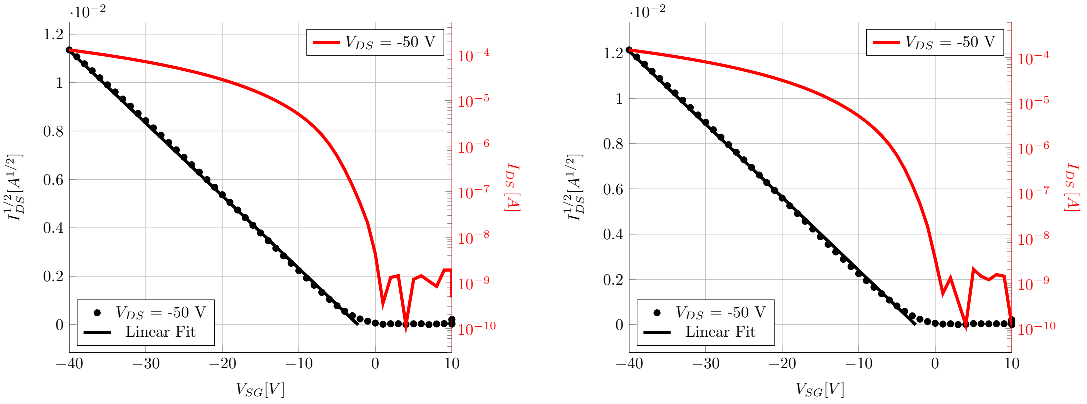

(c) L = 70 μm

(d) L = 80 μm

Figure H.6 *(a),(b),(c),(d), Transfer Characteristics for DBTTF PS3000 blend ratio 1:2 in Bottom Contact Architecture, with W = 2000μm constant.*

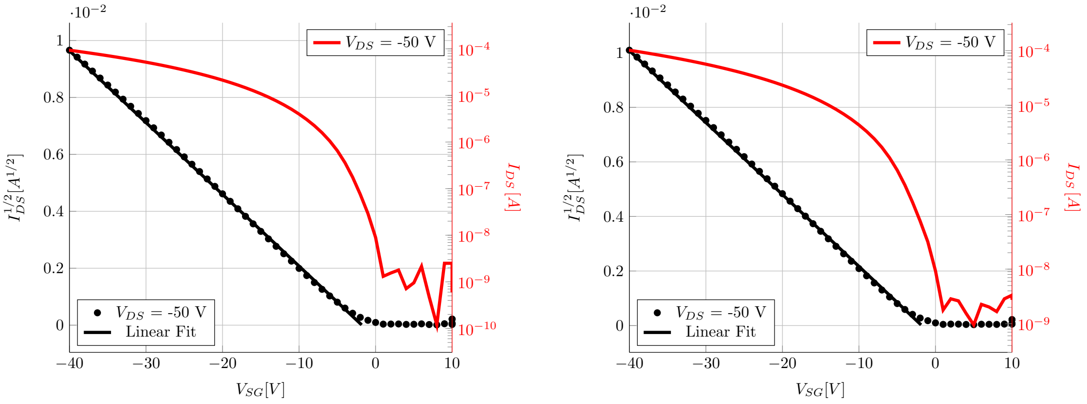

(a) L = 90 μm

(b) L = 100 μm

Figure H.7 *(a),(b) Transfer Characteristics for DBTTF PS3000 blend ratio 1:2 in Bottom Contact Architecture, with W = 2000μm constant.*

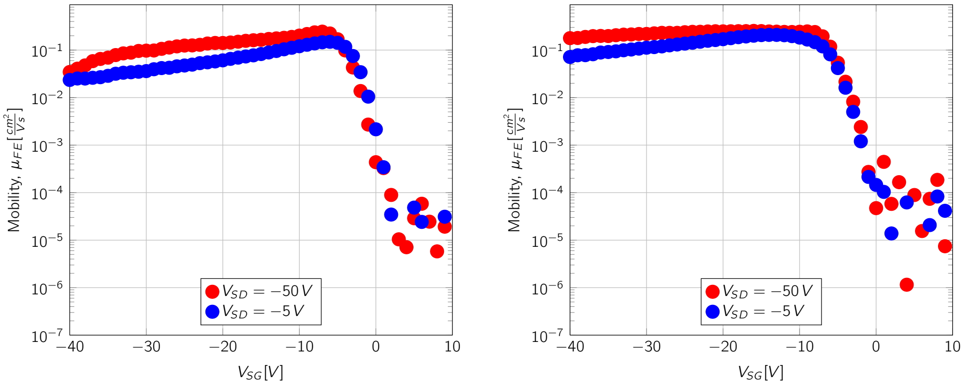

(a) L = 10 μm (b) L = 20 μm

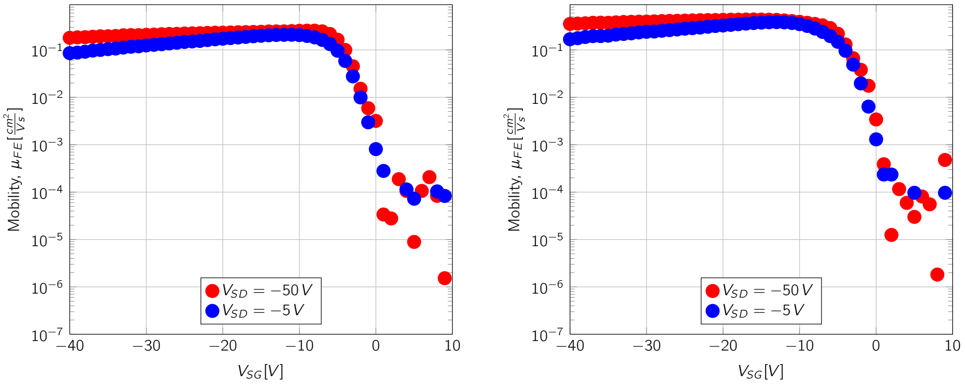

(c) L = 30 μm (d) L = 40 μm

Figure H.8 *(a),(b),(c),(d), Peak mobility plots for DBTTF PS3000 blend ratio 1:2 in Bottom Contact Architecture, and constant W = 2000μm.*

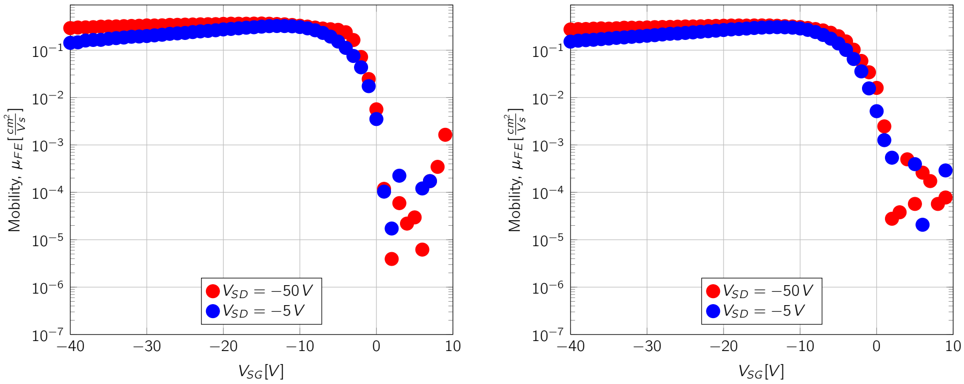

(a) L = 50 μm

(b) L = 60 μm

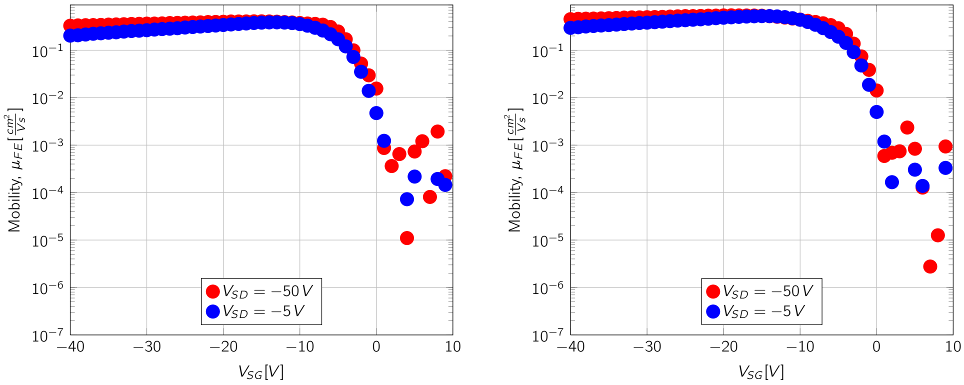

(c) L = 70 μm

(d) L = 80 μm

Figure H.9 *(a),(b),(c),(d),Peak mobility plots for DBTTF PS3000 blend ratio 1:2 in Bottom Contact Architecture, and constant W = 2000μm.*

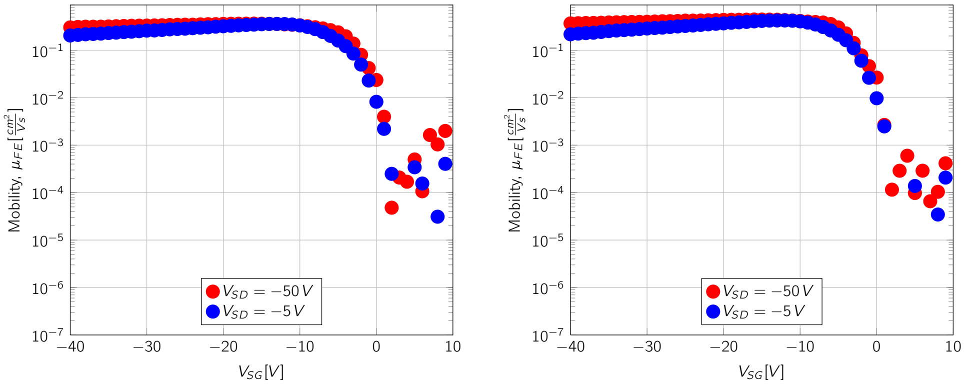

(a) L = 90 μm

(b) L = 100 μm

Figure H.10 *(a),(b), Peak mobility plots for DBTTF PS3000 blend ratio 1:2 in Bottom Contact Architecture, and constant W = 2000μm.*

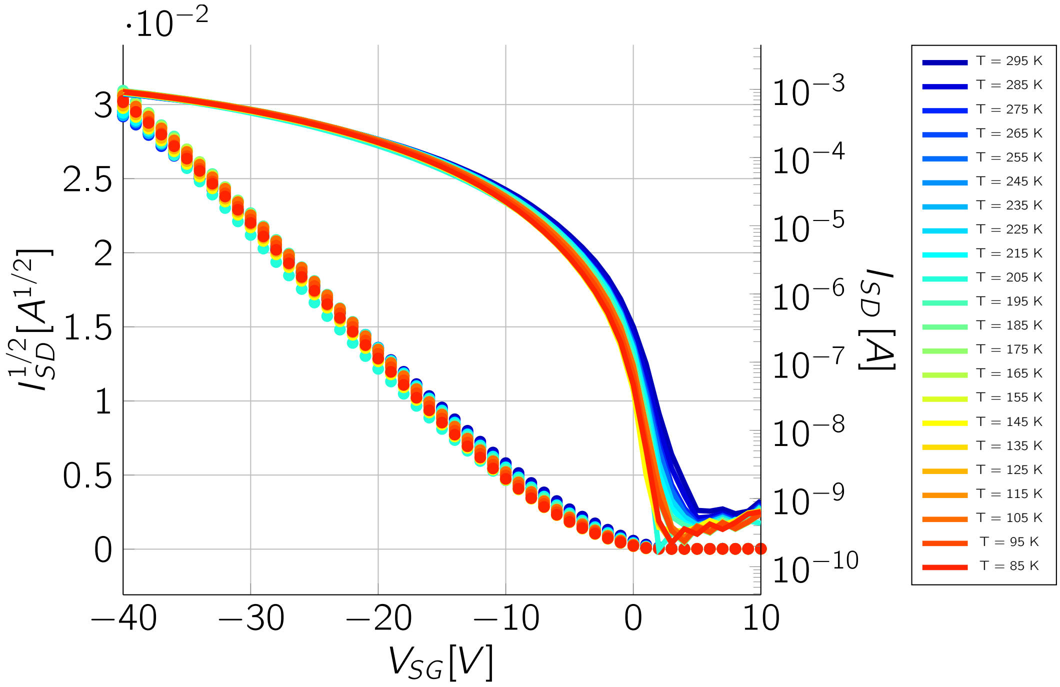

Figure H.11 *Logarithmic* I_{SD} *in the right y-axis and* $\sqrt{I_{SD}}$ *in the left y-axis, both as a function of* V_{SG}

Index